2015

Distribution protection in a modern grid embedded with renewable energy resources

Joel Kennedy
University of Wollongong

University of Wollongong

Doctoral Thesis

Distribution Protection in a Modern Grid Embedded with Renewable Energy Resources

Author:
Joel Kennedy, BE (hons)

Supervisors:
Dr Phil Ciufo and
Dr Ashish Agalgaonkar

A thesis submitted in fulfilment of the requirements for the award of the degree of Doctor of Philosophy

in the

School of Electrical, Computer and Telecommunications Engineering

June 2015

Declaration of Authorship

I, Joel KENNEDY, BE (hons), declare that this thesis titled, 'Distribution Protection in a Modern Grid Embedded with Renewable Energy Resources' and the work presented in it are my own. I confirm that:

- This work was done wholly or mainly while in candidature for a research degree at this University.
- This thesis has not been submitted for qualifications at any other academic institution.
- Where I have consulted the published work of others, this is always clearly attributed.
- Where I have quoted from the work of others, the source is always given. With the exception of such quotations, this thesis is entirely my own work.
- I have acknowledged all main sources of help.
- Where the thesis is based on work done by myself jointly with others, I have made clear exactly what was done by others and what I have contributed myself.

Signed: _____

Date: 27/03/2015

"It depends. . . "

Any Academic Ever

Abstract

The advent of inverter-interfaced, decentralised generation has incited a paradigm shift in distribution network design philosophy. Accordingly, the effects of decentralised generation on distribution network power quality, stability and protection have become important topics within research. Whilst the focus of this Thesis is protection design philosophy amidst increasing decentralised generation, protection efficacy is indelibly linked to power quality and stability. Ergo, it is prudent that all three areas of research interest are examined.

The motivation for this Thesis is to overcome some of the technical constraints that prevent the continued proliferation of decentralised energy resources. Further, this Thesis provides simulation tools that will aid in understanding the effects of decentralised generation on the protection adequacy of distribution networks. Generally speaking, there exists no consensus on how much embedded generation is permissible before traditional distribution network design philosophy becomes ineffective in maintaining protection, stability and power quality adequacy. Hence, the work conducted in this Thesis will provide utilities with the knowledge and tools required to cope with the continued proliferation of decentralised generation.

Currently, the embedded generation penetration levels in Australia reportedly cause instances of over voltage compromising the power quality in distribution networks. This Thesis proposes an over voltage mitigation scheme, which utilises a controller capable of indirectly regulating the voltage magnitude at the terminals of an embedded generator through reactive power absorption and apparent power curtailment. The scheme maximises the remuneration received by the embedded generator proprietor whilst adhering to voltage standards and does not require an off-line sensitivity analysis or communications infrastructure. The results indicate a proof of concept; however, there exists many concerns regarding how such a scheme could be incentivised – or, if necessary, enforced. The scheme operates best when all decentralised generators employ the proposed controller.

Instances of protection failure due to decentralised generation are non-existent in Australian distribution networks and requires a much more significant penetration of embedded generation than present. A small-signal analysis tool is required to determine whether the connection of an embedded generator will cause fault discrimination issues. Small-signal analysis is time-intensive and requires a large amount of information to accurately model the fault response of an embedded generator. This Thesis provides an alternative to small-signal analysis via an iterative solver that predicts the prefault, fault-instant and

steady-state fault data. Utilisation of the proposed solver allows a thorough protection analysis study of a distribution network for every fault type and location. A report is then generated containing the specific information relevant to a protection engineer. The strengths and limitations of the proposed solver are detailed and compared with small-signal analysis. The proposed solver is capable of greatly improving the productivity of protection engineers when dealing with large penetrations of embedded generation.

This Thesis extends into the natural evolution of embedded generation proliferation, namely, the microgrid concept. Some alterations to contemporaneous microgrid design philosophies are proffered with the intention of improving the ability of islanded embedded generation protection devices to discern the presence of high impedance single-phase to earth fault. An iterative solver is also developed to calculate the fault response of islanded embedded generation when employing conventional droop control developed for microgrid applications. The solver is capable of identifying the prefault, fault-instant and steady-state fault data including the island frequency. A key contribution of this Thesis is the introduction of a voltage sequence protection scheme. Results indicate that the voltage sequence protection scheme possesses excellent fault discrimination capabilities for islanded networks rich in inverter-interfaced generators.

The findings of this Thesis contain conceptual significance with numerous possible applications in future networks should the proliferation of inverter-interfaced generation be sustained. The ability to easily discern the impacts of increased decentralised generation on protection adequacy is a major strength of this Thesis. Furthermore, the over voltage mitigation scheme and microgrid design philosophy, including voltage sequence protection, represent new techniques that address obstacles in perpetual energy resource decentralisation: over voltage in grid-connected applications and protection discrimination in intentional islanding applications.

All contributions within this Thesis have been simulated within the MATLAB environment using an innovative simulation platform. Verification of simulation results are presented where validation against other published results has been possible. However, in order to fully examine the performance of the contributions developed in this Thesis, further research is required to prototype and rigorously test the concepts that have been developed using real-world networks.

Acknowledgements

To my family whom gave me the constitution to commence this Thesis, to my supervisors whom provided the direction and encouragement to complete this Thesis and to my wife whom distracted me from this Thesis...

Contents

List of Figures

List of Tables

Abbreviations

AC	**A**lternating **C**urrent
AS	**A**ustralian **S**tandard
CB	**C**ircuit **B**reaker
CERTS	**C**onsortium for **E**lectric **R**eliability **T**echnology **S**olutions
CSIRO	**C**ommonwealth **S**cientific and **I**ndustry **R**esearch **O**rganisation
CT	**C**urrent **T**ransformer
DC	**D**irect **C**urrent
DN	**D**istribution **N**etwork
dq	**d**irect-**q**uadrature
EF	**E**arth **F**ault
EG	**E**mbedded **G**eneration
EIT	**E**ffective **I**nstantaneous **T**rip
EOZ	**E**nd **O**f **Z**one
FAT	**F**ault **A**nalysis **T**ool
FATM	**F**ault **A**nalysis **T**ool: **M**icrogrid Version
FCL	**F**ault **C**urrent **L**imiter
HV	**H**igh **V**oltage
IDMT	**I**nverse **D**efinite **M**inimum **T**ime
IEEE	**I**nstitute of **E**lectrical and **E**lectronic **E**ngineers
IGBT	**I**nsulated **G**ate **B**ipolar **T**ransistor
IIEG	**I**nverter-**I**nterfaced **E**mbedded **G**eneration
KCL	**K**irchhoff's **C**urrent **L**aw
KVL	**K**irchhoff's **V**oltage **L**aw

LOM	**L**oss **O**f **M**ains
LPF	**L**ow **P**ass **F**ilter
LV	**L**ow **V**oltage
mmf	**M**agneto **M**otive **F**orce
MPPT	**M**aximum **P**ower **P**oint **T**racker
NDZ	**N**on **D**etection **Z**one
OC	**O**ver **C**urrent
OOZ	**O**ut **O**f **Z**one
OV	**O**ver **V**oltage
PAT	**P**rotection **A**nalysis **T**ool
PCC	**P**oint of **C**ommon **C**oupling
PLL	**P**hase **L**ocked **L**oop
PI	**P**roportional **I**ntegral
PR	**P**roportional **R**esonant
PV	**P**hoto**V**oltaic
RET	**R**enewable **E**nergy **T**arget
rms	**r**oot **m**ean **s**quared
ROCOF	**R**ate **O**f **C**hange **O**f **F**requency
SC	**S**attelite **C**entre
SCADA	**S**ystem **C**ontrol **A**nd **D**ata **A**cquisition
SCC	**S**hort **C**ircuit **C**apacity
SEF	**S**ensitive **E**arth **F**ault
SEL	**S**chweitzer **E**ngineering **L**aboratories
SOZ	**S**tart **O**f **Z**one
STS	**S**tatic **T**ransfer **S**witch
THD	**T**otal **H**armonic **D**istortion
UOF	**U**nder **O**ver **F**requency
UOV	**U**nder **O**ver **V**oltage
VT	**V**oltage **T**ransformer
VROC	**V**oltage **R**estrained **O**ver **C**urrent

Symbols

V	Voltage	Volts (V)
I	Current	Amperes (A)
P	Real Power	Watts (W)
Q	Reactive Power	Volt-Amperes-Reactive (VAR)
S	Complex Power	Volt-Amperes (VA)
t	Time	seconds (s)
R	Resistance	Ohms (Ω)
L	Inductance	Henries (H)
C	Capacitance	Farads (F)
X	Reactance	Ohms (Ω)
Z	Impedance	Ohms (Ω)
f	Frequency	Hertz (Hz)
E	Energy	Watt-hours (Wh)
ω	Angular Frequency	rads^{-1}

Publications

J. Kennedy, P. Ciufo, and A. Agalgaonkar. Intelligent load management in Microgrids. In *2012 IEEE Power and Energy Society General Meeting*, pages 1-8, 2012, DOI: 10.1109/PESGM.2012.6345729

J. Kennedy, P. Ciufo, and A. Agalgaonkar. Over-voltage mitigation within distribution networks with a high renewable distributed generation penetration. In *2014 IEEE International Energy Conference (ENERGYCON)*, pages 1107-1114, 2014, DOI: 10.1109/ENERGYCON.2014.6850562

J. Kennedy, P. Ciufo, and A. Agalgaonkar. Fault approximation tool for grid-connected inverter-interfaced distributed generators. In *2014 Australasian Universities Power Engineering Conference (AUPEC)*, pages 1-6, 2014, DOI: 10.1109/AUPEC.2014.6966578

Chapter 1

Introduction

1.1 Background

Since the Industrial Revolution, carbon dioxide concentrations have increased to be 26% higher than the maximum carbon dioxide concentrations over the previous 650 000 years [5]. The causal link between human behaviour since the early 19th century and the rise in carbon concentrations is a topic of some debate and is often heavily politicised. According to a study conducted by the Commonwealth Scientific and Industrial Research Organisation (CSIRO), about as many Australians believe that humans are causing climate change as those who believe climate change is occurring naturally [6]. However, within Australia there exists a general consensus that it is our population's responsibility to curtail carbon emissions where possible, despite relatively little being done of late in Australian politics.

The Renewable Energy Target (RET) scheme introduced by the Australian government in 2001 is still in effect. The RET scheme was designed to ensure 20% of Australia's electricity is generated by renewable energy resources (henceforth known as renewables) by 2020. The CSIRO found that most Australians agree that "responding to climate change will cost a lot of money" [6]. However, a RET policy analysis undertaken by ROAM Consulting in 2014 found that repealing the RET would increase electricity prices in the medium to long term [7]. Hence, it is likely that the RET scheme will not be

repealed despite the prevalence of climate change scepticism within the Australian Federal Government and population [8].

The RET scheme provides financial incentives for both large-scale and small-scale renewables. State governments have developed various schemes to encourage industrial, commercial and residential proprietors to invest in renewables, particularly solar photovoltaics (PV). It is well established that PV cells are carbon negative over their lifespan and PV systems are becoming increasingly affordable [9]. Contemporaneously, electricity prices have increased dramatically within Australia. An international comparison found that Australia's electricity prices were some of the highest in the world in 2012 and prices had grown by more than 40% between 2007 and 2012 [10]. The coupling of increased electricity prices and financial incentives provided by the RET scheme has led to a significant increase in small-scale generation investment; the Australian PV Institute reports an exponential growth in PV installations since 2010 [11].

While PV is popular, technical concerns over the widespread use of grid-connected renewables have risen. Instances of over voltage (OV) have reportedly caused nuisance trips of grid-connected energy resources which represents a loss of income for the proprietor [12]. Several utilities have reacted by imposing limits on renewable energy resource size or penetration within a feeder or substation. However, the limits imposed by utilities in Australia are non-uniform, suggesting that renewable energy connection policy is based more on empirical evidence than definitive analysis and the application of Australian Standards [13]. The potential impacts of increasingly high penetrations of grid-connected renewable energy resources on distribution systems are poorly understood and are a topic of increasing amounts of research. Through a better understanding of the impacts of grid-connected renewables, measures may be developed that allow the proliferation of small-scale renewables to continue at the distribution level, reducing carbon emissions and permitting an increased investment in small-scale generation in Australia and abroad.

1.2 Embedded Generation

Renewable embedded generation (EG) manifests in various forms. There are a wide variety of energy resource types, including solar PV, solar thermal, wind, hydroelectric, geothermal, tidal, fuel cells and biofuels. However, there are only three types of interfaces used in grid-connected EG: synchronous machines, induction machines and power electronic devices, most commonly, inverters. Often, there is also a transformer providing galvanic isolation from the mains supply. A transformer can provide a series inductance capable of filtering the voltage waveform provided by power electronic devices.

The advantages of EG include:

- reduced transmission and distribution losses.
- the ability for utilities to defer infrastructure upgrades.
- peak shaving.
- the possibility of intentional islanding to increase reliability.
- providing reactive power and/or voltage support [14].
- in some cases, improved fault ride-through [15].
- cogeneration applications (the ability to harness wasted energy available at the customer level where available).

EG has many distinct advantages over conventional large-scale generation. However, a large penetration of EG can impact the normal operation of contemporary distribution networks (DNs) significantly. Issues associated with the connection of small-scale EG (¡30 kW) to Australian DNs are minimised through the application of Australian Standards [16]. Applications for small-scale EG generally require only a very basic technical analysis before connection approval can be granted. Medium-scale EG (¡5 MW) requires a far more in-depth technical analysis before connection can be granted. Some potential issues include:

- Voltage fluctuations.
- Poor regulation of the steady state voltage magnitude.
- Changes to DN fault current characteristics.
- Generator stability [17].

Problems that may arise with EG connection are case dependent. The location of an EG site may have a significant impact on the severity of encountered problems. Hence, a custom detailed analysis of each prospective connection is vital in ensuring a new installation shall not compromise the expected operation of the grid.

There exists no universal standard for medium-scale EG integration in Australia; various utilities employ separate guidelines and a wide list of technical standards. However, all standards require protection coordination with DN devices. Anti-islanding protection is fundamental for protection coordination, which will be explored in more detail in Chapter 2.

The scope of the work contained within this Thesis is predicated on the continued proliferation of inverters as the most common energy resource to grid interface. There are many reasons why inverters are preferable to synchronous and induction machines in small-scale grid-connected generation applications, including:

- Many renewables produce direct current (DC) electricity which requires an inverter interface in order to be converted into an appropriate alternating current (AC) waveform, an operation that cannot be achieved efficiently using other interfaces.
- From a control perspective, inverters are the most flexible grid interface.
- Inverters have no moving parts and require little maintenance.
- Inverters are becoming increasingly affordable.
- Inverter interfaces enable the separation of the dynamics of the energy resource from the grid [18]. This means that the transient response of an embedded generator connected through an inverter to the grid is not dependent on the physical characteristics of the energy source.

Inverters are ubiquitous and increasing in popularity [13]. Inverters are a well established technology with which consumers are familiar; hence, the assumption of the continued proliferation of inverter-interfaced embedded generation (IIEG) is not unfounded. For these reasons, inverters are chosen to be the dominant EG interface and indeed the only acceptable interface as the shift toward autonomous grids becomes realisable.

1.3 Protection

The protection schemes implemented in Australian DNs employ over current (OC), earth fault (EF) and sensitive earth fault (SEF) techniques for fault detection. DN protection devices include reclosers, sectionalisers and fuses. Protection settings are chosen such that adequate protection discrimination and selectivity can be achieved across all protection devices.

The key objective of a DN protection scheme philosophy is to minimise customer disconnection within the scope of ensuring all faulted segments of a network are promptly isolated. Fast and effective fault detection is pivotal to reducing the risk of the electrocution of civilians and utility personnel, as well as minimising network infrastructure damage. The correct operation and coordination of protection devices is a critically important characteristic of any DN. Hence, the accurate selection of protection settings is crucial.

DN protection settings are determined through analysing the normal load behaviour and fault behaviour of the DN, both of which are impacted by the connection of EG. The ability to discern the anticipated effects of EG connection in DNs in a core focus of this Thesis and an important contribution to the field assuming the proliferation of EG continues.

1.4 The Microgrid Concept

There exists no unified definition of a microgrid; indeed, the definition and constitution of a microgrid has evolved in recent years. However, there are many similarities amongst contemporary definitions. A microgrid is modular composite of a larger power network. A

microgrid contains clusters of grid-connected energy resources and loads that are controlled and protected such that a microgrid can operate as a segment of a larger network or autonomously as an intentionally island. Historically, microgrids have been much simpler systems, often with a single back-up generator and one customer. However, these archaic designs, whilst they still exist, have been superseded from the microgrid label; they have specifically been excluded from the modern microgrid definition [19]. The IEEE Guide [20] introduces a new term, distributed resources island systems, in order to further abate the confusion that is presently, inextricably linked with the term microgrid. Distributed resources island systems are defined as electric power systems that:

- contain EG and load.
- can disconnect and reconnect to the grid.
- include low voltage segments and can possibly extend to medium voltage segments of the grid.
- are intentionally planned [20].

This definition is consistent with the scope of the microgrid covered within this Thesis.

Within the scope of contemporary definition of microgrids, each embedded generator should operate in a plug-and-play fashion and ideally not require the use of communications infrastructure. Autonomous operation of segments within DNs is currently prohibited by IEEE and Australian Standards [16, 21]. There are various technical obstacles preventing microgrid operation, which can be broadly categorised into four different groups: power quality, control, stability and protection. There has been a considerable amount of research investigating the plausibility of the microgrid concept, but there is no consensus on microgrid protection design philosophy.

1.5 The Problem Statement

At the core of DN design philosophy is the premise of radial power flow [22–26]. Within the context of DNs, radial power flow implies that the flow of electricity can be sourced

only from upstream of the zone substation. The connection of EG to DNs directly violates the premise of radial power flow and compromises the efficaciousness of DN protection, stability and power quality regulation. Instances of poor power quality, especially OV, have reportedly already occurred [12]; yet envisaged errors in protective response and stability have not yet become a problem in Australian DNs, as well as other DNs abroad.

For issues of stability or poor protective response to arise, the EG would have to constitute a significant portion of the total available generation. A search through extensive literature suggests that there is no evidence that significant stability or OC protection issues have occurred in Australian DNs on account of EG. However, the inclusion of EG in DNs does have an effect on the how OC protective devices respond to faults. The determination of the necessary penetration levels of EG before existing protection failure becomes a strong likelihood is still an unsolved problem. The variability of the structure and composition of Australian DNs suggests that a generalised penetration level where protection failure shall occur is non-deterministic and a tool that can analyse DNs on a case-by-case basis would be more useful. The development of such a tool is an important contribution of this Thesis and is a topic of increasing importance for power distribution utilities as the growth of EG continues.

A hierarchical view of the research problem explored within this Thesis is illustrated in Fig. 1.1. The research problem can be considered in two key sections: grid-connected only and the microgrid concept. While these sections are often explored independently, it is essential to recognise that the protection philosophy applied to the microgrid in grid-connected mode should be equivalent to the protection philosophy applied in any DN with a very high EG penetration.

1.5.1 Impacts of a High EG Penetration on OC Protection Schemes

EG can provide a fault current, which implies that EG can contribute to the fault current measured by protective devices. The extra fault current could cause the ratings of a circuit breaker (CB) to be exceeded which can damage the CB and also potentially prevent the CB from extinguishing the fault current. Hence, the inclusion of EG might require an expensive upgrade of protection devices, unless a fault current limiting device

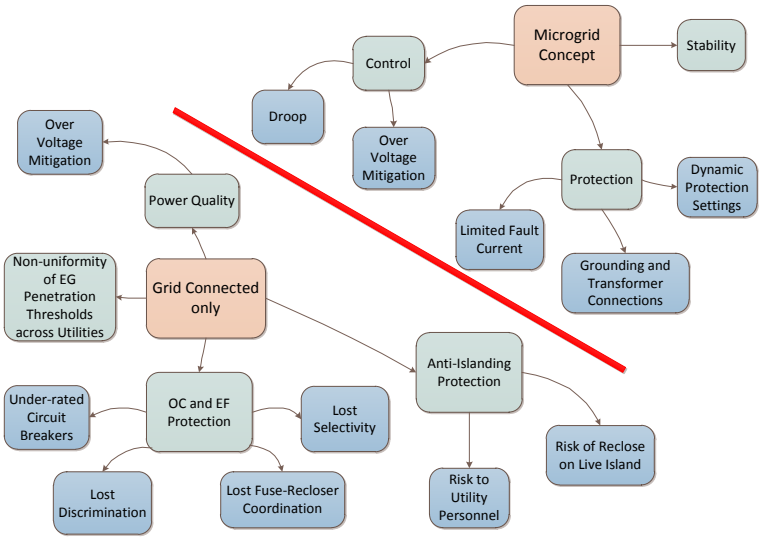

FIGURE 1.1: Problem Statement Diagram

is implemented [24]. In some circumstances, the extra fault current supplied from EG will increase the apparent fault impedance from the perspective of an OC protection device. The increased apparent impedance will reduce the fault current measured by the OC protection device which can cause fault under-reach. The inclusion of EG can complicate fault discrimination, particularly in segments of a network with a high short circuit impedance. EG units might also cause unnecessary tripping when a fault occurs in adjacent feeders. Furthermore, the grading process of inverse definite minimum time (IDMT) curves across protection devices is predicated on radial power flow in DNs. The introduction of multiple sources will have an effect on the selectivity in OC protection schemes designed for DNs [24].

Some DNs contain fuses which are coordinated with reclosers to prevent the fuse from blowing during a temporary fault. The recloser is programmed such that the recloser's IDMT curve will isolate the fault before the fuse blows. After the first reclose, the recloser will operate using a slower IDMT curve, allowing the fuse to burn out if the fault remains. Such an operation allows the fuse to remain intact if the fault is temporary. If a significant EG penetration were to exist in the isolated segment of a network, the EG fault current may cause the fuse to burn out on the first instance, irrespective of the temporary nature of the fault. Such an event would have a significant impact on the reliability of the network [23].

The impacts of EG on OC protection are further complicated through the diversity of EG unit interfaces. Synchronous machines are capable of providing a significant fault current, which implies that OC protection technology could be adapted to protect non-radial DNs containing synchronous machine-interfaced EG in much the same way as transmission networks are protected using directional OC and distance protection [27]. However, IIEG is current limited due to the power electronic switches within the inverter. Over-rating of inverters is expensive but may offer some advantages such as fault ride-through for sensitive loads [28]. The maximum current that can be provided by an inverter is generally stated in literature to be about twice the rated current, but is shown to be approximately five times the rated current experimentally in [29] lasting for one-tenth of a cycle. An inverter's fault current waveform is volatile, stochastic and short-lived; the authors of [29] compared their findings with manufacturer data and confirmed that the fault current contribution of IIEG units is much smaller than an equivalent sized synchronous machine. The implication of fault current contributions must be taken into consideration when assessing the efficaciousness of traditional protection techniques.

1.5.2 Impacts of a High EG Penetration on Anti-Islanding Protection

Passive anti-islanding protection will operate if a significant voltage or frequency deviation occurs. Deviations in voltage and frequency are created through the control response of EG units to disparities in real or reactive power generation and absorption within an island. Active anti-islanding protection reduces the non-detection zone (NDZ) of an island. However, with the exception of communications based active anti-islanding technology, there still exists a point or region of metastability that in theory will prevent anti-islanding protection from operating under certain conditions [30]. The likelihood of anti-islanding protection failure increases with the increased penetration of EG in DNs.

Consider the case where an isolated segment of a network maintains supply through EG support and anti-islanding protection fails to detect loss of mains (LOM). Generally, the isolated network will shift out of phase with the mains supply. In such as case, a reclosure attempt could cause significant damage to network infrastructure as well as EG

technology. It is also possible that a fault arc may not be extinguished as a result of a failure of anti-islanding protection to operate [24, 31].

A failure of anti-islanding protection to operate could cause utility personnel to incorrectly assume that a section of the grid isolated from the mains supply is dead. Even after connecting grounding leads on the upstream side of a maintenance site, there is still a risk of electrocution. The perceived risk of such events occurring is considered to be acceptably small with present EG penetration levels and modern anti-islanding technology [32]. However, the higher the penetration of EG, the higher the risk of protection failure. If the use of grid-connected renewables continues to grow as expected, the increased likelihood of protection failure will require reform of DN and EG protection design philosophy.

1.5.3 Moving Towards the Microgrid

As the penetration of EG approaches 100% of peak load within a DN, an opportunity to establish self-standing segments of a network arises. There are many technical concerns which have prevented international standards from allowing intentional islanding. Issues such as control and stability have been addressed through droop control and through decoupling machine dynamics via inverter interfaces. The protection of a microgrid is a topic of greater contention; traditional protection schemes are inappropriate due to the lack of radial fault current flow and the inherent fault current restrictions imposed by the power electronic interfaces of each EG unit. The connections of transformers and the grounding configurations of EG units and network infrastructure have a significant impact on the zero sequence current and zero sequence voltage observable during fault conditions, which are important for fault discrimination during earth faults.

1.5.4 Conclusion

The proliferation of small-scale grid-connected renewables cannot continue indefinitely when employing contemporary standards due to various technical concerns. In addition to utilities imposing limits on the connection of renewables, Australian state governments have eased incentive programs to curb new connection applications. In order for the

continued growth of small-scale renewables, these technical concerns must be addressed. Furthermore, there may be reliability improvements made possible through the implementation of the microgrid concept. By tackling the technical issues concerned with increased renewable EG penetration, carbon emissions will be reduced, utility infrastructure upgrades can be deferred, locally available energy can be harnessed and the reliability of DNs can be improved.

1.6 Objectives and Contributions

The purpose of this Thesis is to provide tools that aid the understanding and alleviation of the negative impacts of high EG penetration with a focus on protection adequacy in DNs. This Thesis extends from the continuation of contemporary grid-connected EG connection procedures to more experimental DN configurations such as intentional islanding applications.

The first major objective and contribution is the development of an extensive literature review examining the proposed protection schemes of DNs with a high EG penetration. Each method is critically analysed and assessed for appropriateness from a technical and economic point of view. The literature review encompasses both grid-connected and autonomous modes of operation.

Secondly, a platform for simulating the fault response of DNs with a high EG has been developed. The assumptions and underlying equations which define the behaviour of the models are outlined. The model includes IIEG with a variety of control types, including conventional constant power control and droop control. The control schemes are modified in order to aid the identification of high impedance single-phase to earth faults. A justification and verification of the models are provided. The contribution includes a critical analysis on modelling EG units from a protection perspective, meaning that the models are designed such that a realistic simulation of the expected fault response is achieved.

Thirdly, this Thesis contributes an OV mitigation scheme which is used to ensure that the voltage profile of a DN does not exceed given limits. The scheme requires only a minor modification to contemporary control schemes of grid-connected EG. The scheme does

not require a communications system nor an off-line sensitivity analysis. Furthermore, the remuneration received by each proprietor is maximised through use of reactive power absorption. The scheme naturally favours EG proprietors connected to segments of a DN with a lower short circuit impedance or in a close proximity to a load.

Fourthly, a tool is proposed that allows a protection engineer to quickly capture the expected fault responses of a DN with a high level of EG penetration. The tool is based on Newton's method of finding the roots of an equation by iterative techniques. The results are compared with the small-signal models also developed in this Thesis. The tool provides a fast alternative to small signal modelling; a very desirable quality when an intricate DN requires hundreds of simulations to verify the efficacy of a protection scheme. Further, the comparison of the proposed tool with small signal analysis provides a verification for the tool and validation of the results presented in this Thesis.

Fifthly, an automated protection scheme analysis tool is developed that generates a report informing the user of the impacts of the connection of EG from the DN protection perspective. The report can be used to identify if a CB's rating may be exceeded or if the fault reach of a protection unit is insufficient. This Thesis proposes plausible alterations that may be made in order to maintain an adequate protective response. The proposed tool can be used in a case-by-case basis that could be adopted by utilities to assess whether a prospective EG installation is acceptable. The contribution of the proposed protection analysis tool is significant as currently there exists no automated methodology for determining the maximum allowable EG penetration before protection efficaciousness is compromised.

The remainder of the contributions within this Thesis are focused on the application of the microgrid concept to future DNs. One of the major contributions is the proposal of a new microgrid design philosophy that aids in the fault identification process. The effects of earthing and transformer connection are taken into account and a sequence component voltage-based protection scheme is adopted as the preferred autonomous mode protection scheme. A tool is also developed to predict the fault response of an intentional island when droop control is employed. The results are compared to a small-signal model for verification purposes.

1.7 Significance of Research

This Thesis contributes to the body of research that allows the increased proliferation of renewable energy resources. The first frontier is assessing when the alteration of protection settings of contemporary DN OC protection devices are necessary. Coupled with OV mitigation technology, the capacity for EG penetration within a DN can be better defined. Through understanding the fault behaviour of DNs embedded with renewables, utilities will likely be able to permit the installation of more grid-connected renewables and continue to provide adequate protection.

The microgrid concept requires a much more dramatic paradigm shift in DN design philosophy. This Thesis will proffer a microgrid design philosophy that will ensure adequate protection discrimination for fault current limited IIEG. The microgrid concept is the culmination of energy decentralisation; EG units will increase in value due to the extra reliability they will provide in a deregulated market.

1.8 Scope

While stability and control are not the focus of this Thesis, protection design philosophies are indelibly linked to the underlying characteristics of the power system technology. The assumption that the commonly accepted constant power control of EG units is sustainable for future grids with a large penetration of EG is imprudent. Hence, this Thesis proposes an amendment to constant-power control which mitigates the risk of OV instances whilst ensuring power flow is allocated in a manner commensurate with the size of the EG and the short circuit impedance between the EG unit and closest upstream voltage regulated point.

The networks considered in this Thesis extend from zone substations down to the customer level. The voltage ranges of concern within this Thesis are 11 kV (henceforth known as high voltage (HV)) and 400 V (henceforth known as low voltage (LV)) as commensurate with most Australian DNs. This Thesis assumes that large EG connections are three-phase. This research also assumes that medium-scale EG units are likely to be

implemented in a microgrid rather than only small-scale EG due to the need for reliable, dispatchable power and the aggregate reduced cost of using medium-scale EG. Medium-scale is defined to be over 30 kW in size with significant reliability, whether through energy storage or through the innate availability of the primary energy resource. It is envisaged most medium-scale EG units are connected on strong segments of a DN with a low short circuit impedance. To simplify simulation studies, balanced loads are assumed (which is often not the case in LV networks). However, the envisaged worst case unbalance is considered when sequence component protection discrimination efficaciousness is evaluated.

1.9 Report Layout

The remainder of this Thesis is structured as follows.

Chapter 2 – A literature review with a focus on proposed protection schemes for DNs with a high EG. The literature review encompasses grid-connected only as well as microgrid applications.

Chapter 3 – The development of a modelling tool capable of simulating EG units, DNs and protection systems. The modelling tool is designed to realistically simulate the small-signal response of EG units to disturbances in a DN. The proposed controllers for grid-connected and autonomous EG are designed to aid in the protection prediction process. A partial verification and examples are included.

Chapter 4 – A control scheme is proposed that is capable of mitigating instances of OV that have occurred where EG is connected to segments of a DN with low local load and a high short circuit impedance. The proposed OV mitigation scheme does not require a significant amendment to contemporary grid-connected EG controllers and does not require communications between EG units or an off-line sensitivity analyses of the DN.

Chapter 5 – A fault analysis tool is proposed as an alternative to time-intensive small-signal modelling of fault conditions. The fault analysis tool is also capable of considering the impact of fault current limiters and IIEG with a limited thermal inertia.

Chapter 6 – The impacts of high levels of grid-connected EG are explored from the protection perspective. A tool is introduced that is capable of analysing the efficacy of a DN line protection scheme. The tool generates a report with the key information necessary for understanding the impacts of EG on CB ratings and protection discrimination.

Chapter 7 – The protection analysis tool is extended to apply to microgrid applications. A novel microgrid philosophy is presented with a focus on ensuring protection adequacy. A voltage sequence protection scheme capable complete fault discrimination during autonomous operation of a microgrid is introduced. Autonomous connection requires use of a communications medium. If communications systems fail, the microgrid will operate identically to contemporary networks with a high EG penetration. The protection scheme is outlined and tested within the simulation platform.

Chapter 8 – The final chapter gives the conclusion and recommendations for future work.

Chapter 2

Literature Review

2.1 Introduction

The increasing pressure for renewable or 'green' energy coupled with government funded economic incentives has caused a paradigm shift in the way residential, commercial and governmental bodies approach energy investment. The shift has predominantly manifested through the dramatic increase in the presence of grid-connected EG in sub-transmission and DNs.

DNs were designed under the premise of radial power flow [22–26]. The introduction of small-scale EG introduces the possibility of bi-directional power flow, rendering the network non-radial. The integrity of DN design philosophy is compromised by EG connection and a detailed analysis is required to ascertain the implications of various levels of EG penetration.

2.2 Contemporary DN Protection Systems

2.2.1 OC and EF Protection

The DN encompasses the electrical infrastructure between the zone substation and a customer's point of common coupling (PCC). The PCC is the point where the utility and

the customer interface. Typically, the PCC is on the customer side of the utility revenue meter [33]. Protective devices in DNs consist of reclosers, sectionalisers and fuses. To coordinate protective devices, traditional DN protection schemes implement graded OC protection and EF protection. OC and EF protection gradings are achieved using IDMT curves as shown in Fig. 2.1.

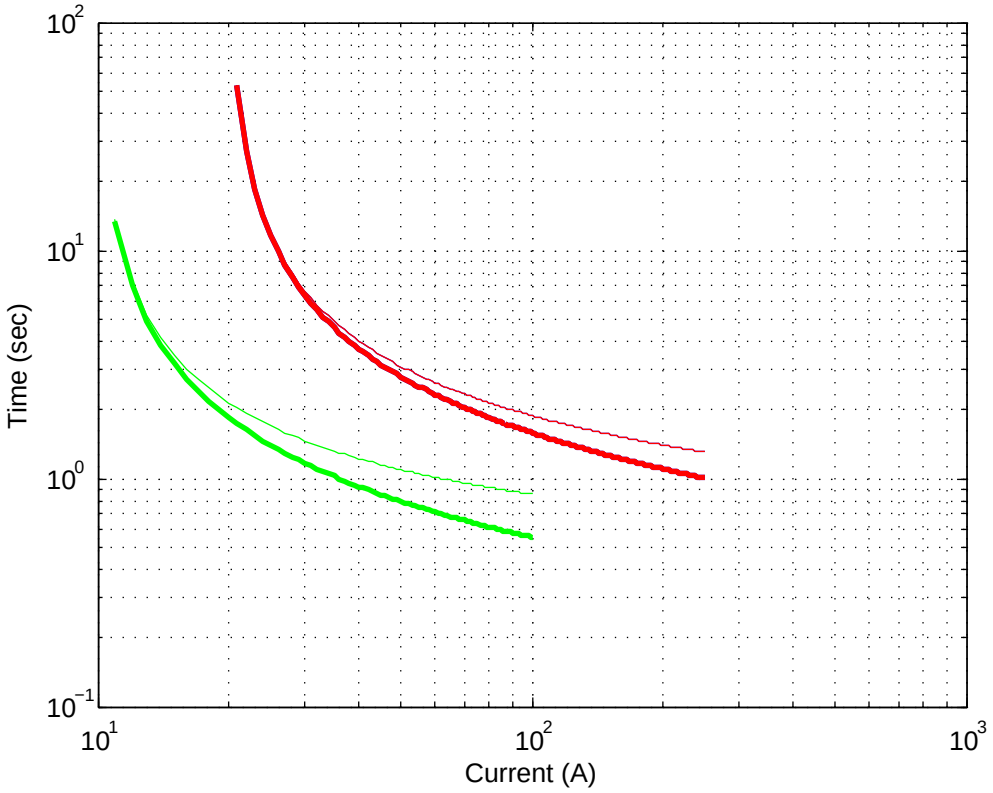

FIGURE 2.1: IDMT Curves

Each curve incorporates an error margin (the corresponding thin line) in order to account for delays in signal processing, signal transmission and the time for the relevant CB to open and extinguish the fault. A radial network has only one source of fault current. Therefore, any protective devices located between the fault source and the fault will observe (almost) the same fault current. Using the IDMT curves shown in Fig 2.1 as an example, the protection device programmed with the green curve is connected downstream of the protection device programmed with the red curve. A downstream device shall have a lower pick-up current and an upstream device has a higher maximum fault current; the IDMT curves are chosen accordingly. The protection device programmed with the green curve must always operate before the protection device programmed with the red curve

for any fault downstream of both protection devices. Hence, the green curve is placed below the red curve (taking into account tolerances shown by the thin lines), satisfying the protection selectivity criteria. To put it another way, IDMT curves must be arranged to ensure that the minimum number of customers are disconnected when a fault is isolated.

The design process of choosing appropriate IDMT curves does not incorporate the effects of EG. In fact, the Institute of Electrical and Electronics Engineers (IEEE) Standard 1547-2003 states that [21]:

> "Any distributed resource installation connected to a spot network shall not cause operation or prevent reclosing of any network protectors installed on the spot network. This coordination shall be accomplished without requiring any changes to prevailing network protector clearing time practices of the area electric power system."

Experimentally, OC and EF protection have been shown to be susceptible to poor discrimination in networks with a high EG penetration [34, 35]. Hence, a threshold of EG penetration must exist that defines the boundary where a network does not comply with the protection requirements stipulated within the IEEE Standard 1547-2003. The determination of such a boundary has not been ascertained, largely due to other limiting factors of EG connection such as OV; empirically, OV instances precede protection failure. However, there are control mechanisms, such as reactive power absorption and real power curtailment, capable of eliminating OV occurrences which are discussed in Chapter 3. The EG threshold before DN protection failure is poorly defined and is an area of research that requires further investigation.

Failure of OC and EF protection discrimination can be achieved in two ways. Firstly, a protection device can trip unnecessarily for a fault outside of that protection device's zone of protection. Secondly, a protection device can fail to trip when a fault occurs within that protection device's zone of protection. These protection failures are referred to as a nuisance trip and fail-to-trip respectively. Consider the circuit shown in Fig. 2.2. The star designates a fault which is located in CB2's zone of protection. Fault current will flow through all CBs; however, CB1 and CB3 will experience a fault current in the

opposite direction to normal power flow. OC and EF devices are typically not equipped with directional elements in DNs; the trip time of CB1 and CB3 can be expressed through each CB's respective IDMT curve.

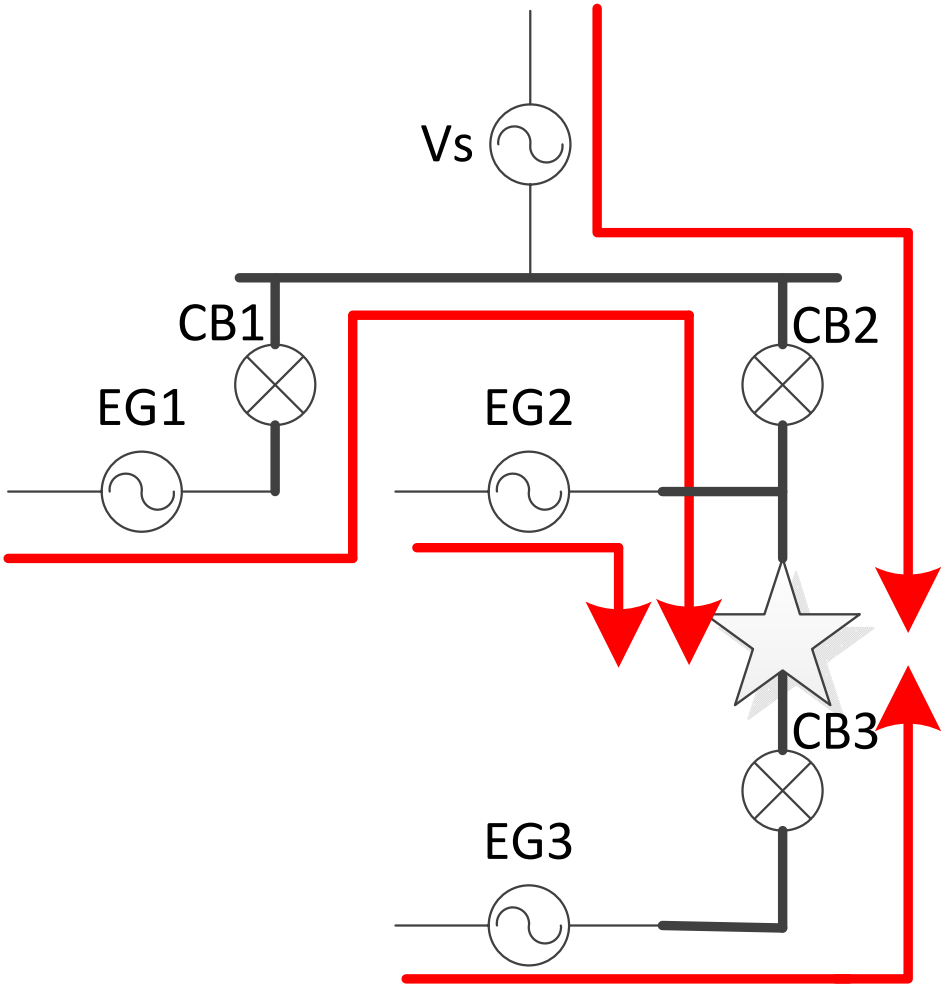

FIGURE 2.2: Protection Discrimination Example

The IDMT curves of CB1 and CB2 are not graded in the protection planning process due to the assumption of radial power flow – no reverse fault current will flow through CB1 during a fault in CB2's zone of protection if the DN is radial. While it is unlikely that CB1 would trip before CB2 isolates the fault, a CB1 nuisance trip may occur if the pick-up current of CB1 is significantly lower than CB2. The result would be the unnecessary loss of all customers on CB1's corresponding feeder. Customers will likely be reconnected

after an auto-reclosure once CB2 isolates the fault. However, the reliability of the overall network is compromised.

Similarly, CB3 would observe fault current in the opposite direction of radial power flow during the fault in CB2's zone of protection. In the unlikely event that the reverse fault current is sufficient to trip CB3, no extra customers are lost. A trip at CB2 isolates all customers downstream of CB2 which includes all customers downstream of CB3. All islanded EG units will isolate themselves via anti-islanding protection and reclosure attempts of CB2 and CB3 will ensure that the final operational state of each CB is identical to an equivalent network condition with no EG connection. However, the operation of CB3 violates the IEEE Standard 1547-2003 as normal protection behaviour has been impacted by EG connection [21].

The fault current provided by EG2 will increase the voltage drop between EG2 and the fault, reducing the fault current passing through CB2. Thus, the presence of EG may cause the fault current flowing through a protection device to be below the pick-up current, especially during a high impedance end of zone fault. In such a case, a fail-to-trip would occur, increasing the likelihood of bushfires and the electrocution risk to customers and utility personnel. Fault discrimination problems caused by high penetrations of EG can pose a significant threat to DN reliability and safety.

Contrary to discrimination, protection selectivity between reclosers can be improved through EG connection. Consider the circuit shown in Fig. 2.3.

CB2 and CB3 are graded to ensure that CB3 will operate before CB2 for a fault in CB3's zone of protection. Due to the presence of an EG unit (EG2) between CB2 and CB3, the current observed by CB3 is greater than CB2. Hence, the time difference between a CB3 trip and a CB2 trip will be greater than the graded IDMT curves would suggest. Hence, the selectivity of an OC/EF protection scheme can be improved through EG connection. However, there are further complications that must be considered concerning auto-reclosure.

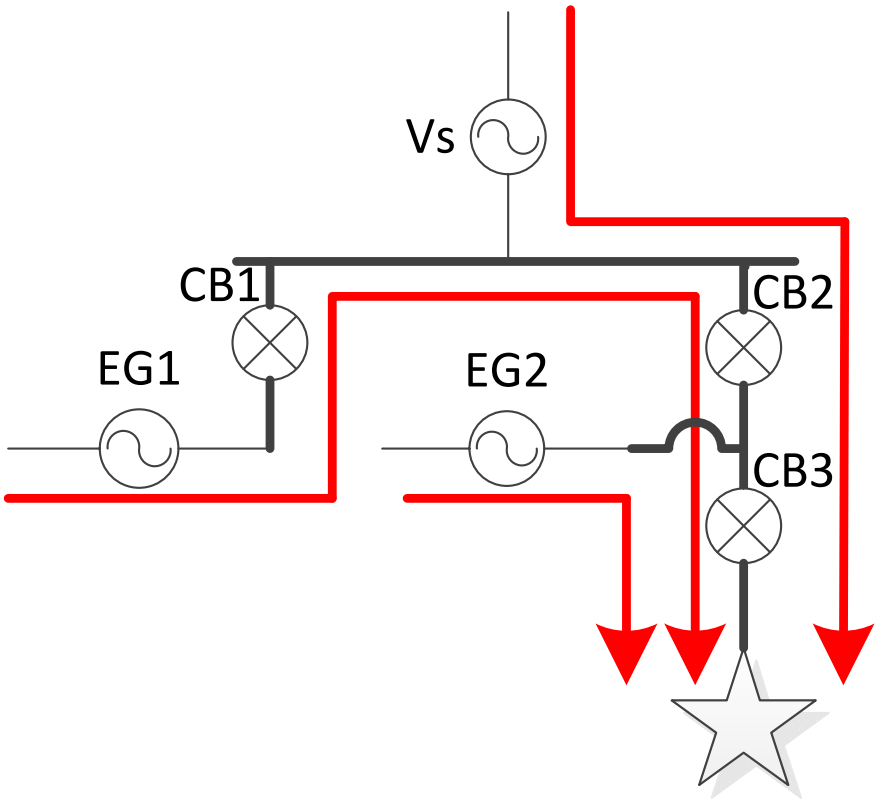

FIGURE 2.3: Protection Selectivity Example

2.2.2 Recloser-EG Coordination

Reclosers will typically trip before an EG unit's anti-islanding protection will detect LOM. The maximum allowable time it should take for passive anti-islanding protection to operate is two seconds according to Australian Standard (AS) 4777.3 and IEEE Standard 1547 [16, 21]. Reclosers will often remain open in the range of hundreds of milliseconds up to seconds before a reclosure attempt [31]. The time that a recloser remains open before a reclosure attempt is referred to as the recloser dead time. After the formation of an island, it is likely that a phase difference of the voltage waveforms across the open recloser will occur. Thus, an out-of-phase reclosure would create a large disturbance in the network, possibly damaging network infrastructure and EG. IEEE 1547-2003 states that an EG must cease to energise a network prior to a reclosure by the DN protection system [21]. Hence, it is important to consider the impact of EG anti-islanding operation when selecting reclosure times.

Further, it is possible for an EG unit to sustain an arc even after a recloser has isolated the fault from the main supply [31]. The purpose of the recloser dead time is to allow the arc path to de-ionise, thus removing the fault, assuming the fault is temporary. If the arc is sustained by EG, a temporary fault may become permanent, reducing the reliability of the network.

A trade-off is necessary when coordinating reclosers with EG units. The recloser must be open for long enough to ensure that anti-islanding protection can operate, but short enough such that the interruption experienced by customers is minimised. The coordination is further complicated when fuses and sectionalisers are installed within the DN.

2.2.3 Recloser-Fuse-EG Coordination

Reclosers are essential to maintain high reliability levels as most faults on DNs are temporary [26]. Spurs, off the backbone of a feeder, are normally protected by a fuse. Whenever a fuse isolates a fault, that fuse has to be replaced by utility personnel before supply is regained to customers downstream of the blown fuse. In order to further increase the reliability of DNs, reclosers are coordinated with fuses such that the recloser will isolate before the fuse will blow on the first detection of a fault. If the fault is temporary, the fault will usually be cleared before the first reclose and no more protection operations will be necessary. If the fault is still present, the fault is considered permanent; the fuse will blow faster than the recloser trip time. Hence, two separate IDMT curves are used for reclosers which are coordinated with fuses: a fast IDMT curve that will trip the recloser before the fuse blows and a slow IDMT curve that will allow the fuse to blow if the fault is still present (and downstream of that fuse). The inclusion of EG in DNs increases the likelihood of a fuse blowing out on a temporary fault before the recloser with a fast IDMT curve trips as the fuse may be exposed to more fault current than the recloser [23, 36].

In contemporary DNs, EG penetration levels are low and do not provide sufficient fault current to interfere with protection grading nor selectivity. However, as EG penetration rises, the aggregate fault current supplied by EG units may cause fuses to blow unnecessarily. Fig. 2.4 shows an example DN where a fuse has been coordinated with an upstream recloser (CB2) programmed with both a fast and slow IMDT curve. The additional fault

current supplied by the local EG implies that the fault current measured by the recloser is smaller than the fault current flowing through the fuse. If the difference in fault current is significant enough, the fuse may blow before the fast IDMT curve programmed within the recloser will send a trip signal. The overall reliability of the network will be significantly reduced as most faults within DNs are temporary in nature [26].

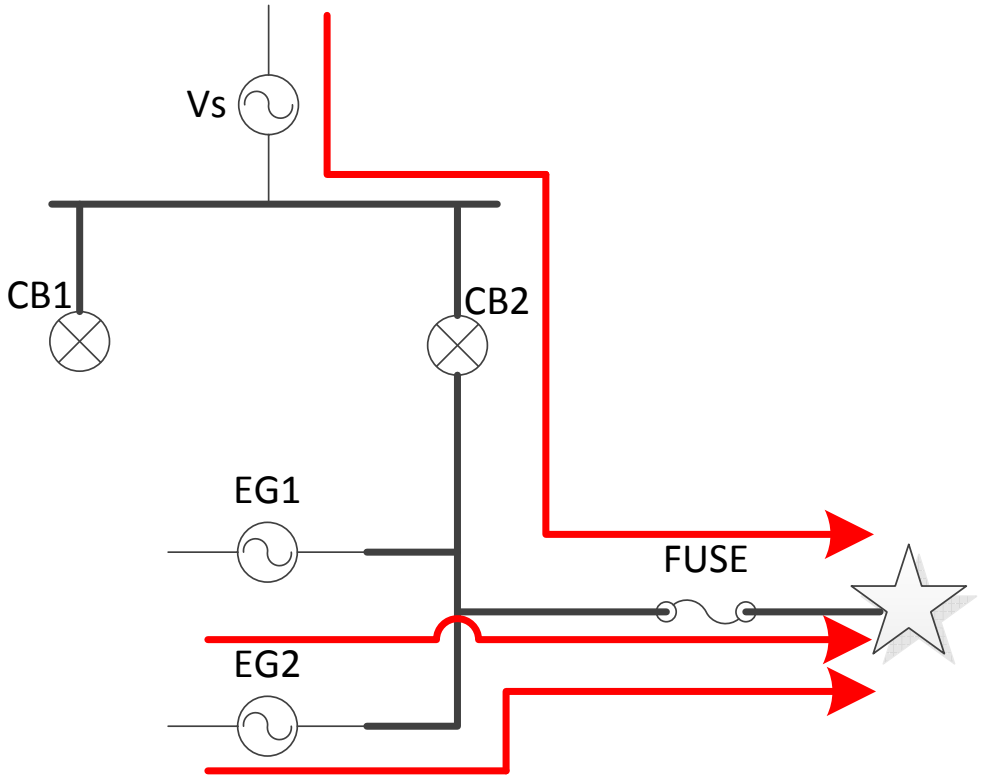

FIGURE 2.4: Effects of EG on Recloser-Fuse Coordination

2.2.4 Recloser-Sectionaliser-EG Coordination

Sectionalisers are incapable of extinguishing fault current levels associated with that sectionaliser's zone of protection. Hence, sectionalisers are only useful when coordinated with reclosers. Sectionalisers will open after a set number of identified reclosures and when the fault current has been extinguished by an upstream CB. The sectionaliser in Fig. 2.5 trips after the first reclosure: when the fault has been extinguished for the second time.

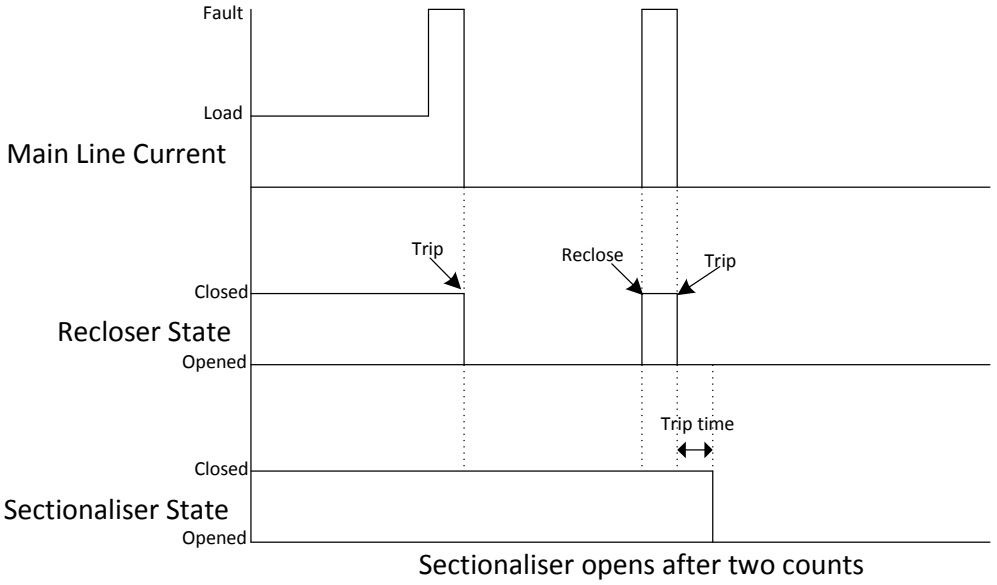

FIGURE 2.5: Sectionaliser Operation

However, if the fault current is sustained by the local EG, the current rating of the sectionaliser may be exceeded. Either the sectionaliser would be damaged upon trying to open with a sustained fault current or the sectionaliser may fail to detect an upstream CB operation. In either case, the overall reliability of the DN would be compromised.

2.2.5 Anti-Islanding Protection

Anti-islanding protection is responsible for preventing instances of unintentional islanding in DNs. Unintentional islanding is any situation where EG continues to supply a subsection of a network that has been isolated from the main grid. There are significant technical and safety issues that might arise from an islanding situation. Consequently, intentional islanding is forbidden by Australian and international standards [16, 21]. Anti-islanding protection can be broadly classified into three different types: passive, active and communications based. In contemporary applications, anti-islanding protection is limited to passive and active types.

According to comprehensive reports on anti-islanding technology, there is no form of non-communications or utility based anti-islanding protection without a non-detection zone

(NDZ) [30, 37]. In practice, however, the risks of most NDZs being realised are very small. However, as EG penetration rises, the risk of anti-islanding protection failure increases. Anti-islanding protection failure can lead to out-of-phase reclosure, decreased reliability and risk of electrocution to utility personnel.

Anti-islanding protection design is not a focus within this Thesis. A plethora of different anti-islanding methods have been proposed and assessed [30, 37]. The operational characteristics of an island that are required to prevent LOM detection within two seconds cannot be achieved with contemporary EG penetration sizes and limitations stipulated by utilities [13]. However, if EG restrictions are lifted and EG penetration levels can approach 100% within DNs, the likelihood of anti-islanding protection failure to detect LOM increases significantly. In such a case, traditional DN line protection would be completely inadequate. A significant protection design philosophy reform would be necessary, including the protection of EG units.

If EG penetration levels exceed 100% of DN capacity, a logical evolution of DN operation is the microgrid concept. Within a microgrid, anti-islanding protection is unnecessary, yet the detection of LOM is still vital such that the control and protection schemes employed by an EG unit can change as required. For instance, the control scheme of EG units may change from constant-power control to droop control to ensure proper load following as the microgrid transitions into autonomous mode. It is important to recognise that the protection techniques implemented in microgrids are also valid for grid-connected only operation as a microgrid must be capable of isolating a fault during both grid-connected and autonomous modes of operation. Conversely, grid-connected only protection techniques can be implemented in a microgrid during grid-connected operation.

2.3 Proposed Protection Schemes for DN Grid-Connected only Applications

The introduction of EG in DNs subverts the premise of radiality that is central to traditional DN protection philosophy. The non-radiality of DNs can be likened to the power

flow observed in transmission networks. The protection philosophy for transmission networks implements distance and directional protection elements to detect and locate faults despite the presence of multiple fault current sources. However, the energy resources connected to transmission networks are typically large-scale synchronous machines that are capable of delivering large fault currents. Hence, the principles used in transmission networks could, in theory, be utilised in DNs with a high EG penetration if EG units were interfaced through synchronous machines and the extra expense of directional and/or distance protection can be justified.

The implementation of directional OC relays is proposed by Bhalja et al. in [22]. All EG units midway through a distribution feeder have two separate protection devices with directional elements connected on each side of that EG unit's PCC. All other DN protective devices are non-directional. There are many concerns with such a protection scheme. There is a significant extra cost: two current transformers (CTs), two relays and two CBs are necessary for each EG unit connected midway through a feeder. The scheme also assumes that EG units are interfaced through synchronous machines which is often not the case. IIEG units would likely be unable to provide enough fault current for adequate protection discrimination due to the limited thermal inertia of power electronics switches. Finally, non-directional relays connected at the upstream end of each feeder could trip due to EG feeding faults on adjacent feeders. Hence, it may be appropriate for all OC protective devices to be equipped with directional elements with an EG unit downstream of that protective device.

An adaptive protection scheme that incorporates protection against voltage sag is proposed by Choi et al. in [38]. A single end-of-line synchronous generator is the adopted EG interface for Choi et al.'s case study. The proposed protection scheme includes both OC and voltage-based methods of fault detection. Protection thresholds of 'critical current' and 'critical voltage' are proposed and can be defined as the expected fault current and voltage at an EG unit's PCC during a zero-impedance fault at the nearest upstream protection device. These 'critical values' are thresholds used to determine if a fault is within the inter-tie CB's zone of protection. An instantaneous trip is implemented for any fault current above the critical current, otherwise IDMT curves are implemented if the measured current at the EG unit is above the pre-determined pick-up current. The

proposed protection scheme also uses IDMT curves to determine whether the recorded voltage magnitude is indicative of a fault and, upon detection, will trip the inter-tie CB. The protection scheme proposed by Choi et al. may be inappropriate for schemes with IIEG, particularly during high-impedance faults as the fault current would be minimal. Furthermore, many Australian DNs cover large distances and substantial voltage drops are frequent. Voltage regulation is commonly found in rural feeders which may affect the integrity of the proposed scheme. Hence, EG protection using voltage magnitude at the EG unit's PCC will likely encounter discrimination issues. Complications for detecting single-phase to earth faults would also arise as the earthing connection and transformer connection can prevent the flow of zero sequence fault current from EG units. There are also unanswered questions regarding the coordination of multiple EG units.

An alternative to OC protection in DNs using distance protection is proposed by Chilvers et al. in [39]. Distance protection is directional in nature and, hence, is appropriate for non-radial networks. A disadvantage of using distance protection is the required connection of a voltage transformer (VT) with each EG unit which represents a significant extra cost compared with traditional OC protection. It could be argued that the addition of a VT may be unnecessary as the voltage sensor can be connected on the LV side of the distribution transformer. However, the connection of a distribution transformer may restrict the ability of the distance protection to determine the zero sequence impedance of a fault. A significant complication arises due to delta-wye connected distribution transformers incapable of passing zero sequence current or voltage. For a fault on the HV side of the distribution transformer, there will be no zero sequence voltage on the LV side of such a transformer. The protection scheme attempts to compensate for the lack of measurable zero-sequence voltage data using a preset estimate of the impedance behind the distance relay during single-phase to earth faults, including the impedance of the earth return path. The determination of protection settings for distance protection may be a more rigorous process than traditional OC protection to prevent fault under-reach or over-reach during single-phase to earth faults.

Contemporary DNs are often separated by normally-open switches or reclosers which can be used to reroute supply during maintenance. In theory, normally-open points could be closed and the network could be protected using distance protection in much the same way

as transmission networks are protected [27]. The non-radiality of a DN would increase the reliability of that DN if protection selectivity and discrimination can be achieved. In addition to protection considerations, the voltage profile and thermal loading of the line must also be considered before a normally-open point should be closed. Distance protection also has the advantage of a faster operation time which is important for the overall stability of the DN. While preliminary research is promising, more research is necessary to assess the efficaciousness of distance protection in DNs with a high EG penetration.

2.4 Proposed Protection Schemes for Microgrid Applications

An effective, robust and experimentally verified protection design philosophy for intentional islanding has not yet been developed. Many protection schemes have been proffered by a variety of authors. Arguably, protection is the least understood topic within the realm of microgrid design philosophy largely due to the unusual fault response of IIEG units, which are an integral component of typical microgrid structures. Traditional OC protection alone has been shown to be insufficient for microgrids containing IIEG units [40]. Coordinating protection devices across both grid-connected and autonomous modes of operation to maintain adequate redundancy, discrimination and selectivity is a key focus in contemporary protection research.

The simplest method of maintaining a significant fault current during islanded operation is through connection of machines with a significant inherent inertia. The authors of [41] propose the inclusion of a flywheel system to complement IIEG in order to supply a significant current when a fault occurs in an islanded microgrid. Flywheel systems are very useful in applications containing critical load, especially when coupled with dispatchable power such as a diesel generators [42]. However, flywheels are expensive and require a sophisticated control scheme for coordination with IIEG in a microgrid. Due to the high cost of such a scheme, it is unlikely that every IIEG unit will be equipped with a flywheel system. Thus it is envisaged that a communications medium would be necessary

to instigate an inter-trip to isolate all non-inertial IIEG when a relay located at an inertial EG unit detects a fault. There is also no consideration for back-up protection for cases of communications or flywheel failure.

An alternative solution to maintaining a significant fault current in an inverter dominated microgrid is the installation of a fault current source as prototyped by [43]. The fault current source consists of a storage device, power electronics converter, a triggering circuit and a charging module. Fault current sources are similar to some power conditioning devices such as dynamic voltage restorers and static VAR compensators, but have an enhanced capability of exporting significant fault current that will aid in the fault detection process. The ratings of the power electronics must be chosen according to the maximum expected fault current export. Furthermore, a back-up fault current source may be necessary to ensure a significant redundancy is present within the microgrid. Otherwise, inter-tripping may be necessary and reliability will be compromised.

Three protection design schemes for microgrids are proffered by Conti et al. [1]. Each scheme assumes the presence of a microgrid central controller and thus communications which is a subversion of the desirable and well established plug-and-play microgrid design philosophy [44–46]. Each scheme also employs OC protection and, hence, cannot be considered appropriate for IIEG.

The first scheme proposed in [1] uses conventional OC protection to isolate the fault at the protection device adjacent to the 'satellite centre' (SC) (the circuit breaker (CB1) immediately downstream of SC in Fig. 2.6) of the microgrid. The SC contains a central controller that is capable of gathering fault data from microgrid protection devices and disseminating trip instructions in order to isolate faults within the microgrid as necessary. Before the satellite centre CB (CB1) trips, each protective device determines the direction of the fault. In the example of a single-phase to earth fault, the zero sequence current direction is determined using the zero sequence voltage as a reference. A lagging zero sequence current indicates a forward direction fault and vice versa. The central controller then determines the location of the fault using the information gathered by each relay transmitted over a communications channel and switches in and out the appropriate circuit breakers to ensure fault isolation and maximum customer connection. The central

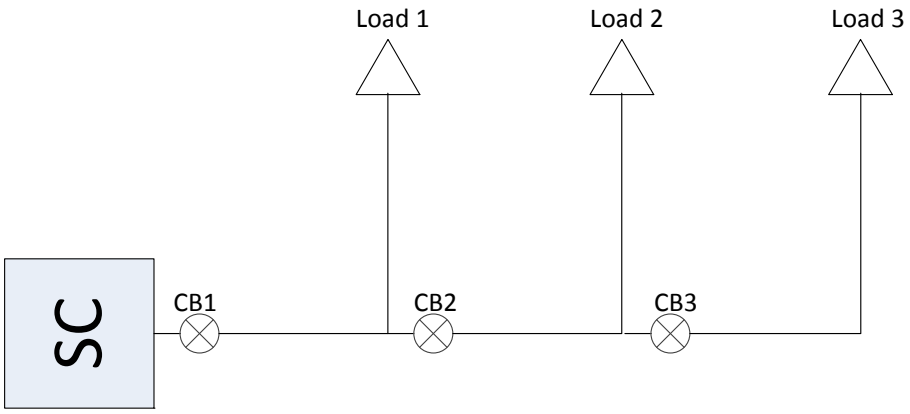

FIGURE 2.6: Microgrid Example (adapted from [1])

controller must be given a data set containing the network topology and protective device locations and identifiers. Any modification of the microgrid requires significant alterations and reprogramming of the protection devices. There is also a significant loss of reliability due to unnecessary tripping of upstream protective devices and the abandonment of recloser operation. Reclosures are essential in maintaining DN reliability (though reclosers can be problematic if EG isolation does not occur before the first reclose). It is important to note that for the first proposed scheme, the isolation of a fault is not dependent on communications; only the appropriate selectivity of the protection scheme is dependent on communications.

The second scheme proposed in [1] uses OC and zero sequence current relays to determine the presence and direction of a fault to identify the fault location, much like the first proposed scheme. The difference is that the CB immediately downstream of the satellite centre (CB1) no longer necessarily trips first. Upon detecting a fault, each protection device communicates with any adjacent protection devices through a pilot wire. If the OC or zero sequence current direction is the same, no protection trip is necessary. If the directions are different, the relevant CBs will isolate the fault. The advantage of the second proposed scheme is the short duration trip time, reducing the impact of fault current on existing infrastructure and minimising the risk of igniting a bushfire. The disadvantage of the second proposed scheme is the extra cost of the pilot wire and control logic, as well as the lack of contingent protection if communications are to fail. The absence of

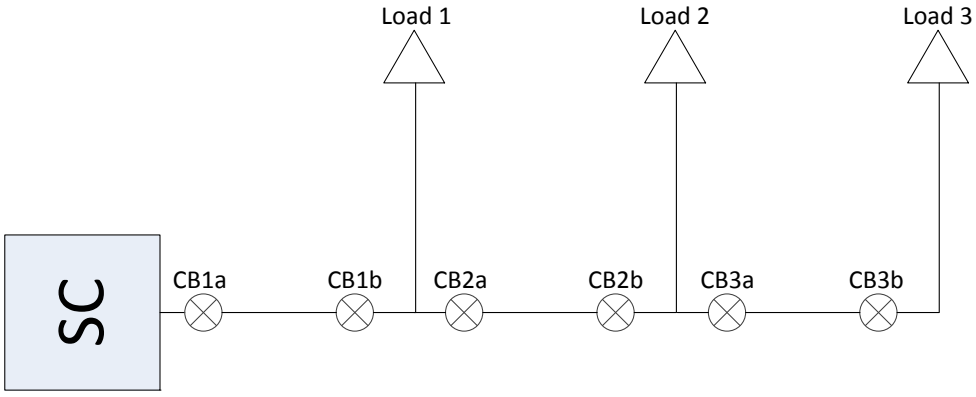

FIGURE 2.7: Final Protection Scheme Example (adapted from [1])

communication response and the detection of an OC would necessitate a trip signal which would compromise the selectivity and reliability of the protection scheme.

The final scheme proposed in [1] contains two sets of CTs, CBs and relays adjacent to every load and EG unit, except at the end of the line where only one set is necessary. Each protective device is directional in nature and 'looks' away from that protective device's load or EG unit as shown in Fig. 2.7. When a fault current is detected, the protective devices at the ends of each line segment (CB1a and CB1b, CB2a and CB2b, CB3a and CB3b) compare the measured direction of the fault. If the paired protection devices observe the same forward fault direction, those protection devices will trip, isolating the fault. A communications medium is required for the protection scheme to operate as expected; hence, a back-up protection is necessary in the case of communications failure. The extra protection infrastructure represents a significant cost and could only be deemed appropriate for large-scale EG such as those found in sub-transmission networks.

All three protection schemes rely on the presence of OC during fault response; a premise which is unreasonable in the case of microgrids dominated by IIEG. Conti et al. in [1] discuss the protection issues concerned with IIEG and recommend use of differential protection which also requires a communications medium. The reliance on a communications medium for adequate protection compromises the reliability of the microgrid. It is also preferable for the microgrid to operate in a plug-and-play manner as much as possible in

order to reduce DN planning complexity and to eliminate the need for the reconfiguration of protection settings each time a modification is made to the DN.

Zamani et al. in [47] use directional OC, negative sequence current and zero sequence current protection to detect faults within a microgrid. For high impedance faults, an energy level based protection proposed by [48] is adopted. However, there exists some 'noisy' loads in DNs that behave similarly to a high impedance fault [48]; hence, discrimination problems may arise. The proposed control scheme includes the provision of blocking signals between protective elements to preclude false trips due to faults in adjacent zones of protection. There are several advantages to using blocking signals to ensure selectivity and redundancy in DNs. Firstly, the use of blocking signals provides back-up protection for CB failure. Blocking signals will only be transmitted long enough for the fault to be isolated according to the IDMT curve programmed within each relay. If a CB has failed to isolate the fault, the blocking signal will be removed and the adjacent CB will trip, providing adequate back-up protection. Secondly, assuming communications infrastructure is healthy, selectivity can be achieved in tandem with fast tripping times, improving the stability of the network. Protective devices no longer have to wait until each upstream device has the opportunity to isolate a fault before tripping. Finally, in the event of communications failure, the protection scheme will still isolate the fault. The disadvantage of communications failure is that selectivity will be compromised, which will result in an unnecessary disconnection of supply to some customers. Such a disadvantage can be considered acceptable within the context of safe microgrid operation.

The use of differential protection in microgrids has been proposed by Zeineldin et al. for microgrid applications in [49] similar to Conti et al. in [1]. To accomplish differential protection, the end of each line must be equipped with a CT, relay and CB. A communications link will be necessary between devices at the end of each line such that the end of line currents can be compared. A relay will send a trip signal if the difference in current exceeds a predetermined level. In Zeineldin et al.'s proposed scheme, each EG unit is assumed to contain contemporary anti-islanding protection that will inform the central controller and EG unit whether an island has formed. Constant current control is used for grid-connected operation and P-V control is used for autonomous control. The proposed protection scheme offers very effective protection discrimination and selectivity, assuming

all components are working properly. However, no provision for back-up protection during communications or CB failure is given. The proposed protection scheme is also very expensive and only appropriate for sub-transmission level microgrids with limited spurs and loads.

Instantaneous communication-based differential protection is proposed as an effective protection scheme for microgrids in [50]. In the event of a CB failure, adjacent relays would receive an inter-trip signal to isolate a fault. However, provision for communication failure is not given. The authors in [51] investigate the efficacy of differential protection, but only consider three-phase bolted faults which are uncommon. Regardless, differential protection would theoretically provide adequate discrimination and selectivity for any type of fault given the fault current exceeds 10% of nominal current flow [50].

An interesting approach towards identifying high impedance single-phase to earth faults is proposed in [50]. The authors use the stochastic nature of single-phase to earth faults to identify the fault. A crude model of a high impedance fault is given, yet further work is needed to capture the scope of high impedance fault behaviour before the proposed fault scheme can be considered reliable.

The use of voltage-restrained over-current (VROC) in inverter dominated microgrids is proposed by Tumilty et al. in [52]. Tumilty et al. first explore the feasibility of using solely voltage-based protection techniques for protection adequacy in a network. The paper concludes that topological selectivity is problematic and impractical for complex microgrids. VROC relays can provide separate OC protection settings depending on the locally measurable voltage. The use of VROC reduces tripping times and reduces the risk of nuisance tripping if protection settings are chosen correctly. However, there still exists complications in coordinating protection devices using VROC; general selectivity for every microgrid configuration cannot be achieved without communications.

Al-Nasseri et al. in [53, 54] provide a sequence component voltage-based protection scheme for islanded operation. The three-phase voltage waveforms are converted into the direct-quadrature (dq) axes by (2.1) using a rotating reference frame as shown in (2.2). The difference between the reference dq voltages and the measured dq voltages is calculated and analysed to determine the fault type and location. Al-Nasseri et al.'s model of EG

units assumes an outer voltage regulation loop and an inner current regulation loop to control the gating signals transmitted to the inverter. Such a control scheme does not allow for load following and, hence, is inappropriate for use within microgrids using commonly accepted droop controllers [53, 55–57]. However, this Thesis will provide an alternative droop controller which will ensure fault discrimination is possible even during high impedance single-phase to earth faults.

$$\begin{bmatrix} V_{ds} \\ V_{qs} \\ V_0 \end{bmatrix} = \frac{2}{3} \begin{bmatrix} 1 & -\frac{1}{2} & -\frac{1}{2} \\ 0 & -\frac{\sqrt{3}}{2} & \frac{\sqrt{3}}{2} \\ \frac{1}{2} & \frac{1}{2} & \frac{1}{2} \end{bmatrix} \begin{bmatrix} V_a \\ V_b \\ V_c \end{bmatrix} \tag{2.1}$$

$$\begin{bmatrix} V_{dr} \\ V_{qr} \end{bmatrix} = \begin{bmatrix} \cos\omega t & -\sin\omega t \\ \sin\omega t & \cos\omega t \end{bmatrix} \begin{bmatrix} V_{ds} \\ V_{qs} \end{bmatrix} \tag{2.2}$$

The sequence component voltage-based protection scheme relies on communications infrastructure to provide fault discrimination. The authors of [51] found that if a significant voltage drop existed during normal operation, fault discrimination could not be achieved even with healthy communications. Fault discrimination is further complicated through the prevalence of very high impedance single-phase to earth faults in DN, particularly when control schemes such as droop control maintain the voltage within normal bounds of operation. Hence, voltage-based protection schemes are deemed inadequate as primary protection within microgrids with EG employing contemporary droop control methods.

A similar protection scheme is proposed by Voima et al. in [58]. The scheme observes the voltage drop throughout the network to identify the fault in a microgrid with fault current limited EG. The voltage vector is then compared with the current vector to identify the direction of the fault. A telecommunications link is subsequently used to exchange information, identifying the location of the fault with respect to all protection devices and promptly isolating the fault. This scheme is only suitable for three-phase bolted faulted which are rare in DNs and, hence, has limited practical applications.

Another protection scheme proposed by Al-Nasseri et al. in [25] involves the use of harmonic content of voltage waveforms in IIEG dominated microgrids. A protection relay

monitors the total harmonic distortion (THD) of the IIEG unit's PCC voltage and will trip the local CB if the THD exceeds a predetermined threshold and the fault is proven to be within that protection relay's zone of protection. A communications link is used to compare the THD at various EG units' terminals. There are no considerations for distribution transformer connection which are common in DNs. A delta-wye connected distribution transformer will have a significant impact on the fault current and voltage waveform at an EG unit's PCC. In some cases, protection discrimination through THD may be impossible. The proposed scheme is also inappropriate for high impedance faults which may only provide a voltage drop similar to significant unbalanced operation. There might also exist complications caused by dynamic loads which could cause nuisance tripping [25]. By the author's admission, protection using THD could only be implmented as a back-up or complementary form of protection [25].

Li et al. proffer a protection scheme for inverter dominated networks in [2] using transient fault information. Travelling waves are analysed to determine the location of the fault using a Rogowski Sensor [59]. If the first two wavefronts detected by a protective device have the same polarity, the fault is located within the relay's zone of protection as shown in Fig. 2.8. If the fault can be located, selectivity is assured and the fault will be isolated much quicker than traditional protection devices. The shortcoming of using wavefronts for protection analysis is the ambiguity of the fault inception angle. If the fault occurs when the voltage is not near peak, the protection performance will be inadequate. A rate of change of current back-up protection is proposed; however, the discrimination between fault events and acceptable disturbances has not been assessed and requires further research to determine the efficacy of the proposed protection scheme.

Distance protection is proposed for microgrid protection in [60] as the recommended form of primary protection. Directional OC and EF elements are used as local back-up protection. Distance protection requires measurement of the local voltage as well as current. The voltage is measured at the LV winding of the distribution transformer to avoid the need for a VT. It is assumed that a delta-wye connected distribution transformer is used. The distance protection relay must incorporate compensation for the voltage drop across the transformer. Detection of earth faults can be particularly challenging as the zero sequence voltage cannot be measured directly due to the connection of the voltage sensor

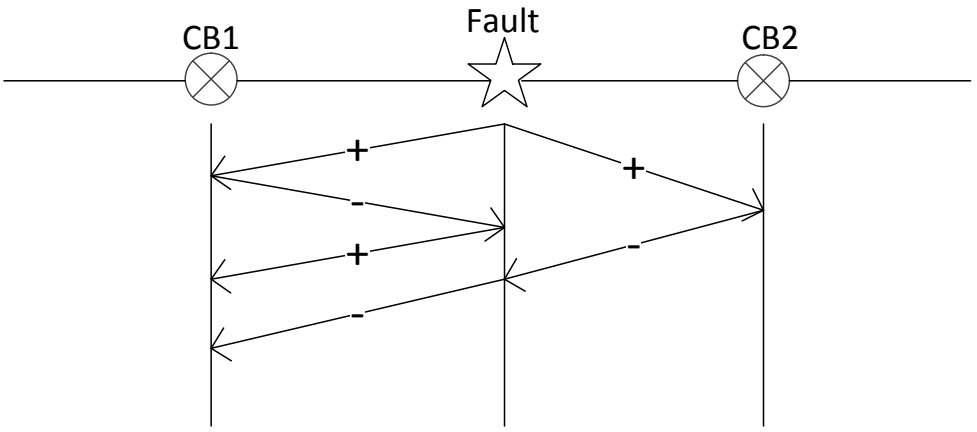

FIGURE 2.8: Protection using Travelling Waves (adapted from [2])

at the LV winding; the zero sequence voltage has to be estimated using an approximate fault impedance behind the distance relay and the measured line zero sequence current. Similarly to most proposed protection schemes, distance protection may have discrimination issues when high impedance single-phase to earth faults occur. However, if adequate impedance compensation and protection discrimination can be achieved, distance protection may be an effective means of microgrid protection.

A similar approach is adopted by Dewadasa et al. in [61] using an admittance-based protection scheme for application in inverter dominated microgrids. Each DN line protection device implements IDMT curves and expresses the tripping time as a function of normalised admittance Y_r, as shown in (2.3).

$$Y_r = |\frac{Y_m}{Y_t}| \tag{2.3}$$

Where Y_m is the measured admittance of the relay and Y_t is the admittance for a zero impedance fault at the end of the zone of protection. The scheme is shown to work for a three-phase bolted fault when the microgrid is operating in islanded mode. Further research is needed to identify whether admittance protection is effective for high impedance single-phase to earth faults.

A differential energy based scheme is proposed by Samantaray et al. in [62]. An S-transform is used to analyse the current waveform. The S-transform is a time-frequency

transform that is an aggregate wavelet and short-time Fourier transform. The current is measured and modified using the S-transform to find the spectral energy content at each protective device. The spectral energy is then compared with the data gathered at the other end of each zone of protection to find the differential spectral energy. The proposed protection scheme is inherently communication based and thus requires some form of back-up protection for instances of communication failure. Case studies carried out in [62] reveal that, in theory, differential energy based schemes are effective for both grid-connected and islanded modes of operation for a variety of fault types. Doubly-fed induction generator wind farms were implemented within the case study as the EG type. No provisions for energy storage were made which is impractical for microgrid applications. It is likely energy storage would be connected through an inverter interface. Further research is required to assess whether protection discrimination is possible for more complicated networks, particularly in the presence of unbalanced loading and significant IIEG.

A microgrid protection scheme based on symmetrical and differential current components is presented by Nikkhajoei and Lasseter in [63]. The authors assume that the microgrid can be separated from the main grid by means of a static transfer switch. The adopted protection design philosophy states that the static transfer switch shall be opened for any fault detection within the microgrid. In [63], Nikkhajoei and Lasseter assume that microgrid sources are inverter-interfaced and, hence, limited to 2.0 p.u. of rated current; traditional OC protection is deemed inappropriate for islanded modes of operation.

In [63], Nikkhajoei and Lasseter discuss the plausibility of detecting single-phase to earth faults using the differential components of phase currents as shown in (2.4).

$$I_d = \sum_{k=a,b,c,n} |I_k| \tag{2.4}$$

The differential phase current scheme proved effective for detection of single-phase to earth faults if the fault is located downstream of a protection device. All EG units are interfaced with the microgrid through a wye(neutral)-delta transformer which does not align with Australian DN transformer connections. All loads are also neutral connected

and a single earthing point is connected to the neutral upstream of the static transfer switch. The earthing and neutral connection of the proposed microgrid does not allow earth current to flow through a relay downstream of a single-phase to earth fault. Hence, bi-directional fault current detection cannot be achieved unless multiple earth points are available throughout the network. However, a multi-earthed system would introduce the possibility of nuisance trips and compromised fault discrimination as zero sequence current would flow from each earthing point during a single-phase to earth fault. Loads are usually unbalanced in DNs, providing earth current during normal operation if an earthing path is supplied, further complicating protection discrimination. A protection scheme based on differential components of phase currents would also be incapable of detecting line-to-line faults and, hence, cannot be implemented as a complete protection system.

In order to better identify the presence of single-phase to earth and line-to-line faults, Nikkhajoei and Lasseter propose a protection scheme that makes use of zero sequence and negative sequence currents, respectively [63]. Nikkhajoei and Lasseter acknowledge the presence of unbalanced loading conditions, which are considered when selecting protection settings for relays within the microgrid. Essentially, protection settings should be chosen such that a nuisance trip will not occur during the extremes of unbalanced loading and a trip should occur for a high impedance fault within a relay's zone of protection. The results of the proposed protection scheme are shown to be very promising within [63]. The main advantage of a sequence component based protection scheme is the absence of the requirement of communications. Time delays are used to ensure selectivity of the protection scheme.

The major complications of sequence-based protection are unfounded assumptions regarding the connection of distribution transformers and earthing points. Australian HV networks are three wire, meaning that there is no neutral return. Neutral points of the customer are earthed at each switchboard in Australia by the multiple earth neutral system stipulated in AS/NZS 3000:2007 [64]. The connection of transformer windings and EG unit earthing also dictates the flow of zero sequence current which must be taken into consideration if sequence-based protection is to be implemented in microgrids.

2.5 Conclusion

The protection of DNs with a high EG penetration is a very complex and poorly understood concept. There are many degrees of entropy including network topology, grid-connected or autonomous modes of operation, EG size and type, transformer connections, earthing connections and protective device locations which have a significant impact on the efficaciousness of the proposed protection schemes. Furthermore, there is a heightened desire for cost effectiveness for EG proprietors on the DN level due to the auxiliary costs of protection and control constituting a much higher percentage of the overall cost. Many protection schemes presume the existence of a communications medium which incurs transmission delays and an increased risk of poor reliability within networks. A back-up protection system using only locally available data is required.

This Thesis will offer a protection scheme that uses communications to improve the speed and selectivity of the protection response, but does not rely on communications for execution of the trip sequence. The protection scheme will ensure the DN is adequately protected for any mode of operation with N-1 redundancy including the possibility of communications failure. If an autonomous network is deemed to be unprotectable, the protection scheme will apply anti-islanding protection to isolate all EG units.

Chapter 3

Simulation Platform Development

3.1 Introduction

The small-signal simulator implemented in this Thesis is the central tool that was developed for validation of the proposed OV mitigation scheme, fault analysis tool and voltage sequence protection relay, which are presented later in this Thesis. The small-signal simulator could potentially be replaced with DIgSILENT, PSCAD or similar time domain simulation packages; however, significant manipulations of control and protection devices would be necessary. Many commercially available power simulation platforms contain components with limited flexibility of operation. This Thesis contains novel controllers and protection relays; hence, the ability to incorporate new components within a simulation is essential. Furthermore, direct juxtaposition of small-signal analysis with the fault analysis tools developed by the author in this Thesis would be impossible with other simulation platforms. Hence, the author found it pertinent to develop a flexible small-signal simulator within the MATLAB environment using m-script.

There are two types of solvers developed for this Thesis to perform small-signal analysis. Firstly, a novel Newtonian solver is used to capture a vectorised snapshot of a network during: the initial prefault condition, the fault-instant and the steady-state fault response. Secondly, a linearised solver provides a time domain plot of the network behaviour. The small-signal model requires an initial operating point to function, which is calculated using

a novel Newtonian iterative solver technique. The proposed Newtonian solver is presented in Chapter 5. The small-signal model converts differential equations into difference equations, linearising the system. The control and protection systems are solved separately to the circuit elements to reduce the complexity of each solve and more closely emulate the digitised approach of modern control and protection systems.

The strength of the presented simulation platform is a heightened level of flexibility where all presented components can be very easily manipulated. Furthermore, the small signal platform is indelibly linked to the proposed fault analysis and protection analysis tools explored in Chapters 5 and 6.

3.2 The Kirchhoff's Current Law (KCL) and Kirchhoff's Voltage Law (KVL) Algorithms

Most circuit analysis tools employ a manipulation of KCL to describe the topology of a circuit, most commonly a Y-bus matrix. The circuit can then be solved by nodal analysis. The benefit of employing both a KVL and KCL algorithm is the ability to have unearthed and galvanically isolated circuitry. Solvers that employ nodal analysis require a universal reference voltage. The lack of reference voltage can generally be solved by asserting on arbitrary reference point before solving. However, when iterative techniques are required to find a solution (such as in a load flow solver), floating neutral points of a network can prevent convergence of the solver, particularly in networks with a large number of floating neutral points. The benefits of using KCL and KVL in the proposed solver include:

- there is no need to reduce a circuit to a single line diagram or sequence components;
- effects of transformer windings are inherently included;
- earthed and unearthed systems can be solved without an arbitrary reference frame;
- voltages and currents are calculated simultaneously and;
- convergence complications are reduced, especially for fault studies.

The KVL and KCL algorithms within this Thesis are designed for fast performance but are limited to three wire systems. The algorithm can be altered to include more complicated systems at some computational expense. One, two and four wire systems were not included as the scope of this Thesis extends to 11 kV DNs which are primarily three-wire in Australia, especially in high-density load areas where medium-scale grid-connected EG penetration is most useful.

The KVL and KCL algorithm begins by identifying all node adjacencies. The node adjacencies are used to form paths. Subsequently, all elements are sorted into shunt and series components. Series devices include: lines, CTs, CBs and any fault not connected to earth. All shunt elements must be incorporated into a loop only once; series components can be incorporated as many times as necessary.

The path formation begins with a reference element which expands to an adjacent node. The path is then assessed to see if the path should be pursued, accepted or rejected through a series of testing. If pursued, further adjacencies will be identified and re-tested. If rejected, the last path addition will be deleted and the next path will be tested.

During the first iteration of loop formations, the shunt reference element must be connected to earth. The purpose of investigating earth connected paths first is to identify galvanic isolation from earth due to transformer connection.

The algorithm will reject a path if any of the following tests fail:

- Given the path traverses more than one phase, the path must follow one of the following phase combinations: depart A and return B; depart B and return C, or; depart C and return A.
- Further, given the path traverses more than one phase, the occupied phase paths must be a direct reflection of one another. For example, a path begins with phase A of the shunt element reference, proceeds through the phase A of a line element to a delta connected shunt element. The return path must solely traverse phase B of the same line element and shunt element reference.
- The path must not return to a node already occupied by that path.

- The path must not include a shunt element that is already part of a previously accepted path.

Given that all tests have passed but a complete loop has not been identified, the path will be extended and re-tested. If all tests have passed and a complete loop is found, the path will be accepted and be used in the KVL matrix derivation. Finally, if a test fails, the next path will be tested. All possible paths stemming from an earthed shunt element reference will be tested before shunt elements galvanically isolated from earth are tested. Galvanic isolation must also be noted for formation of the KCL matrix.

The path testing process is similar when a galvanically isolated element is used as a reference. Two more tests are included to aid detection of unwanted situations caused through delta connections.

- The path may pass through at most one winding of any delta connected three-phase element.
- In the case of three-phase faults, the path must not pass through more than one fault element.

The algorithm continues until all possible paths are tested, all galvanically isolated segments of the network are identified and the complete set of acceptable loops is compiled. The KCL and KVL matrices can then be determined.

KCL algorithms are simple to employ and are ubiquitous. The assumed direction of all elements is asserted upon data entry by selecting 'to' and 'from' nodes. All elements with a connection to earth or neutral point are asserted as coming from the neutral/earth point to an A, B or C phase node. The direction of all other elements can be chosen at the discretion of the user. Each row of the KCL matrix corresponds to a node within the circuit. If an element is coming from the relevant node, a coefficient of -1 is used; otherwise, a coefficient of 1 is used.

Once all nodes are allocated a row within the KCL matrix, one row per galvanic island is deleted. A network with n nodes requires $n-1$ rows for every branch current to be deterministic: the extra row offers no extra information. The deletion is necessary as a square

matrix is required when the characteristic, KCL and KVL matrices are concatenated for the linearised system to be solvable.

If no acceptable loops have been identified, the KVL algorithm will set all non-source voltages to zero. Furthermore, if a non-source element is not included in any identified loop, the voltage of that element will also be set to zero.

A row is added to the KVL matrix for all acceptable loops. A coefficient of -1 is allocated to source element; a coefficient of 1 is allocated to all other elements. The coefficient is then multiplied by -1 if the direction asserted by the user does not match the direction of the identified loop.

An extra loop is allocated to any galvanic island. The original earth-connected island is excluded. The loop consists of the delta winding that was used as the reference for the galvanic island. The extra loops are required to make the entire system solvable; thus ensuring the concatenated matrix in square.

3.2.1 Kirchhoff's Current Law and Kirchhoff's Voltage Law Solver Example

Consider the circuit shown in Fig. 3.1. Each box represents three elements that can be connected in either a wye or delta configuration. All sets of three elements are numbered in the bottom right-hand corner of each box. Within the given example, every wye-connected element is earthed at the star point. The earth is always allocated as node 1. All other nodes (black lines between elements) are allocated node numbers. The upper segment of the network is completely galvanically isolated from earth.

The red lines show the formation of acceptable loops according to the requirements stipulated in Section 3.2. The direction of each loop begins at the element designated the lowest number and traverses phases: from A to B, from B to C or from C to A. The output matrices of the KCL algorithm for the circuit given in Fig. 3.1 are shown in (3.1), (3.2) and (3.3).

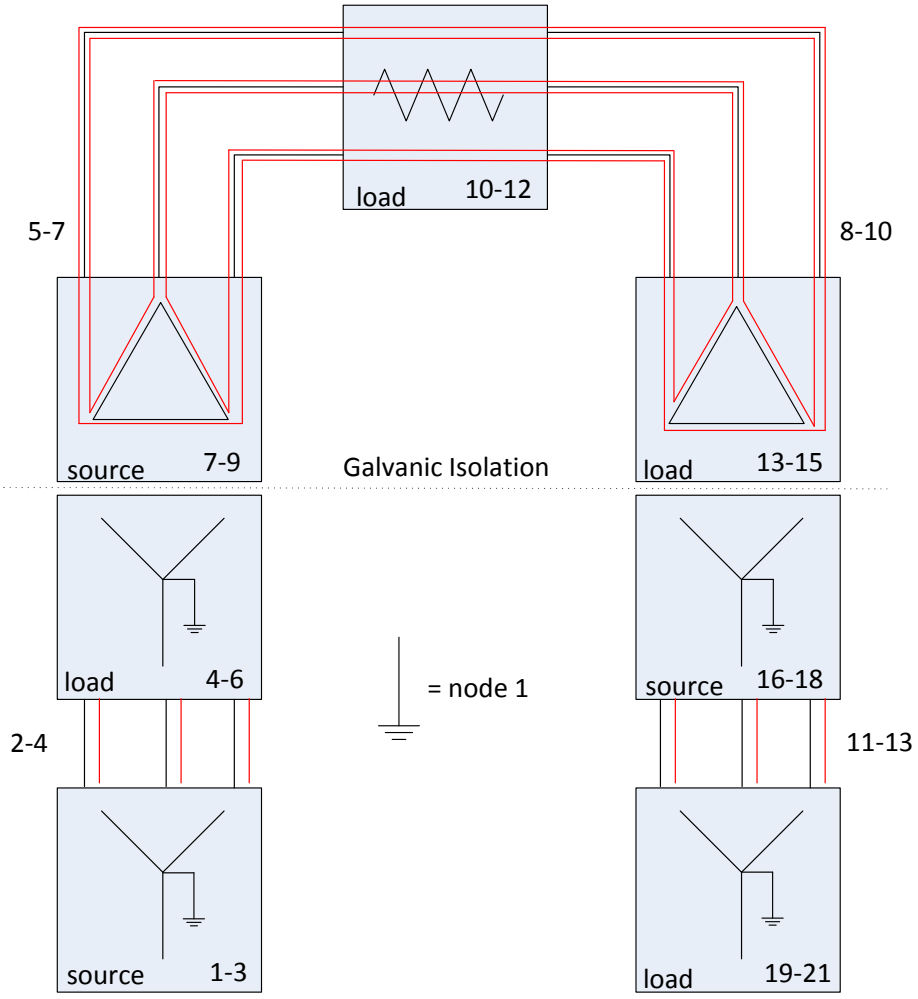

FIGURE 3.1: KCL/KVL Example

$$\begin{bmatrix} -1 & 0 & 0 & -1 & 0 & 0 \\ 0 & -1 & 0 & 0 & -1 & 0 \\ 0 & 0 & -1 & 0 & 0 & -1 \end{bmatrix} \begin{bmatrix} I_1 \\ I_2 \\ \vdots \\ I_6 \end{bmatrix} \tag{3.1}$$

$$\begin{bmatrix} 1 & -1 & 0 & 0 & 1 & 0 & 0 & 0 & 0 \\ 0 & 1 & -1 & 0 & 0 & 1 & 0 & 0 & 0 \\ 0 & 0 & 0 & -1 & 0 & 0 & -1 & 0 & 1 \\ 0 & 0 & 0 & 0 & -1 & 0 & 1 & -1 & 0 \\ 0 & 0 & 0 & 0 & 0 & -1 & 0 & 1 & -1 \end{bmatrix} \begin{bmatrix} I_7 \\ I_8 \\ \vdots \\ I_{15} \end{bmatrix} \tag{3.2}$$

$$\begin{bmatrix} -1 & 0 & 0 & -1 & 0 & 0 \\ 0 & -1 & 0 & 0 & -1 & 0 \\ 0 & 0 & -1 & 0 & 0 & -1 \end{bmatrix} \begin{bmatrix} I_{16} \\ I_{17} \\ \vdots \\ I_{21} \end{bmatrix} \tag{3.3}$$

Within the program, all three matrices shown in (3.1), (3.2) and (3.3) are concatenated, but are presented separately in this Thesis for clarity. Each row corresponds to a node within the circuit, minus one for the earth node and minus another for each galvanic island in the network. The row corresponding to node number 5 within the galvanic island was deleted in this case. The sign of each non-zero coefficient reflects the assumed orientation of each element. If an element is coming from the relevant node, a coefficient of -1 is used; otherwise, a coefficient of 1 is used.

The output matrices of the KVL algorithm for the circuit given in Fig. 3.1 are shown in (3.4), (3.5) and (3.6).

$$\begin{bmatrix} 1 & 0 & 0 & 1 & 0 & 0 \\ 0 & 1 & 0 & 0 & 1 & 0 \\ 0 & 0 & 1 & 0 & 0 & 1 \end{bmatrix} \begin{bmatrix} V_1 \\ V_2 \\ \vdots \\ V_6 \end{bmatrix} \tag{3.4}$$

$$\begin{bmatrix} 1 & 0 & 0 & 1 & 0 & 0 \\ 0 & 1 & 0 & 0 & 1 & 0 \\ 0 & 0 & 1 & 0 & 0 & 1 \end{bmatrix} \begin{bmatrix} V_{16} \\ V_{17} \\ \vdots \\ V_{21} \end{bmatrix} \tag{3.5}$$

$$\begin{bmatrix} 1 & 0 & 0 & -1 & 1 & 0 & 1 & 0 & 0 \\ 0 & 1 & 0 & 0 & -1 & 1 & 0 & 1 & 0 \\ 0 & 0 & 1 & 1 & 0 & -1 & 0 & 0 & 1 \\ 1 & 1 & 1 & 0 & 0 & 0 & 0 & 0 & 0 \end{bmatrix} \begin{bmatrix} V_7 \\ V_8 \\ \vdots \\ V_{15} \end{bmatrix} \tag{3.6}$$

Once again, the matrix has been split for clarity. The earth-connected loops were identified first as expected. Secondly, the loops of the galvanic island were detected. Finally, a delta winding KVL loop was added as required for each galvanic island. Again, every non-zero coefficient reflects the assumed orientation of each element. Furthermore, in the KVL algorithm, the sign is also reflective of the element type; the type may be allocated source or load. A coefficient of -1 is allocated to source element; a coefficient of 1 is allocated to all other elements. The coefficient is then multiplied by -1 if the direction asserted by the user does not match the direction of the identified loop.

3.3 Characteristic Equations of DN Elements

A characteristic equation is defined for each network element. Network elements comprise of: lines, loads, transformer windings, CBs, sources and faults. Generally, there is one element per phase with the exception of power transformers that possess two elements per phase: one element for the primary winding and one element for the secondary winding. In cases where an element contains an inductive component that does not share the total current of the element, or a capacitive component that does not share the potential difference of the element, another parameter is necessary to store the extra current or voltage parameter. An additional characteristic equation must then be employed to relate the extra parameter to the element current and/or voltage. The element current is simply the total current flowing in and out of the element. The element voltage is the potential difference across the element; not necessarily the potential difference between the positive node and earth as employed by some solvers.

The characteristic equations are concatenated with the KCL and KVL equations to form the total linearised representation of the power network as shown in (3.7). The network

is then solved for every nominated time step τ and stored for analysis upon completion. The time step can be altered, but is chosen to be 10 μs for the work presented in this Thesis. 10 μs is considerably less than the switching period of any analysed IIEG systems and is thus considered to be sufficiently small; a time step of 10 μs is also considered to be of reasonable computational expense for simulations with under 100 elements.

$$Ax = B \tag{3.7}$$

Where:

$$A = \begin{bmatrix} \text{characteristic} \\ \text{KCL} \\ \text{KVL} \end{bmatrix}$$

$$x = \begin{bmatrix} \text{parameters} \end{bmatrix}$$

$$B = \begin{bmatrix} \text{constants} \end{bmatrix}$$

The characteristic equations contain several differential operators, denoted s. Consider a parameter F with a coefficient s. The variable n represents the iteration of the simulation where $n \in \mathbb{N} : n \geq 2$. In order to linearise the system, parameters multiplied by s are redefined as a difference across a time step divided by that time step τ as shown in (3.8). The result is a difference equation.

$$sF \rightarrow \frac{F(n) - F(n-1)}{\tau} \tag{3.8}$$

In order to satisfy the format shown in (3.7), the differential operator s in matrix A becomes $1/\tau$ and the $F(n-1)/\tau$ is moved to the relevant B matrix element. Consider the example of an inductor with the characteristic equation shown in (3.9).

$$\begin{bmatrix} 1 & -sL \end{bmatrix} \begin{bmatrix} V \\ I \end{bmatrix} = \begin{bmatrix} 0 \end{bmatrix} \tag{3.9}$$

The s operator is converted into a difference equation. The resulting linearised system becomes (3.10).

$$\begin{bmatrix} 1 & -\frac{1}{\tau} \end{bmatrix} \begin{bmatrix} V \\ I \end{bmatrix} = \begin{bmatrix} -\frac{I[n-1]}{\tau} \end{bmatrix} \tag{3.10}$$

The inductor current must be stored each iteration to provide the constant matrix data for the following iteration. The linearised system is easily solvable within the MATLAB environment, if an initial condition is available.

The linearisations of all differential equations are implemented within the simulation platform, but are not explicitly given within this Chapter. The models for each component are not chosen to provide maximum accuracy, rather a reasonable approximation for how a component will behave during healthy and faulted operation. A more detailed simulation can be easily implemented if required, but represents an extra computational expense.

3.3.1 Constant Voltage Source Modelling

Fault events in DNs generally have enough electrical distance from the transmission network such that the dynamic response of large-scale generation can be ignored; the behaviour of the network upstream of the distribution domain can be approximated as an ideal voltage source and series impedance. The ideal voltage source can be modelled as (3.11).

$$\begin{bmatrix} 1 \end{bmatrix} \begin{bmatrix} V \end{bmatrix} = \begin{bmatrix} |V| \cos(\omega t + \phi) \end{bmatrix} \tag{3.11}$$

3.3.2 Line Modelling

The focus of this Thesis is Australian distribution level networks: generally 11 kV and 400 V. The line distances of DNs with enough load and prospective generation to warrant an investigation of the effects of EG on protection are typically only a few kilometres long. Ergo, shunt impedances of the modelled lines are generally very large and draw very little current. Hence, the assumption that lines can be modelled as a series connected resistor and inductor (as shown in (3.12)) can be considered reasonable. However, shunt elements can be easily included for future simulations if required.

$$\begin{bmatrix} -1 & R + sL \end{bmatrix} \begin{bmatrix} V \\ I \end{bmatrix} = \begin{bmatrix} 0 \end{bmatrix} \tag{3.12}$$

3.3.3 Load Modelling

Loads are modelled as constant impedances by (3.13). Loads can have an effect on fault response and protection adequacy, particularly in networks with a high EG penetration and in unbalanced networks. Each load is modelled as a parallel connected resistor, inductor and capacitor (if needed). The parameters are calculated using the power absorbed under nominal conditions. The current flowing through the inductor I_l must be stored each iteration due to the differential operator s and divergence of current due to the inherent parallel connection of the load elements.

$$\begin{bmatrix} \frac{1}{R} + sC & -1 & 1 \\ -1 & 0 & sL \end{bmatrix} \begin{bmatrix} V \\ I \\ I_l \end{bmatrix} = \begin{bmatrix} 0 \\ 0 \end{bmatrix} \tag{3.13}$$

3.3.4 Transformer Modelling

Each transformer phase is modelled as two separate elements. The equivalent circuit of the transformer is shown in Fig. 3.2. The equation is given in (3.14), where R_m represents the core loss, L_m represents the magnetising loss, R_1 and R_2 represent the respective

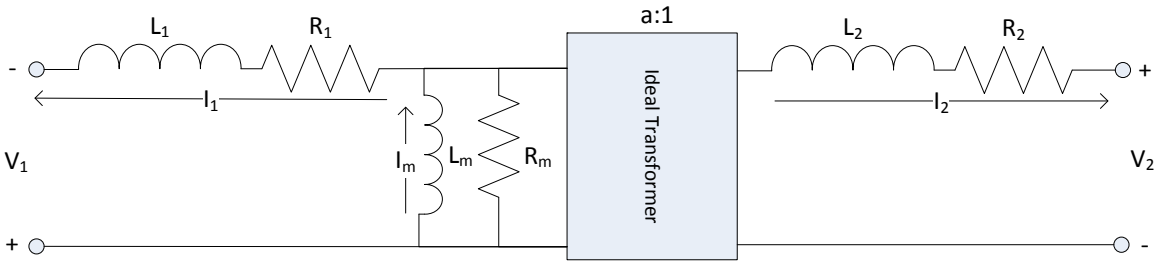

FIGURE 3.2: Transformer Equivalent Circuit

primary and secondary winding losses and X_1 and X_2 represent the respective primary and secondary winding leakage reactances. The magnetising inductance I_m must be stored, again as a consequence of the differential operator s and diverging current through parallel connected elements.

$$\begin{bmatrix} 1 & -R_1 - sL_1 & 0 & a & a(R_2 + sL_2) \\ 0 & 1 & -1 & \frac{a}{R_m} & \frac{1}{a} + \frac{a(R_2+sL_2)}{R_m} \\ 0 & 0 & 1 & \frac{a}{sL_m} & \frac{a(R_2+sL_2)}{sL_m} \end{bmatrix} \begin{bmatrix} V_1 \\ I_1 \\ I_m \\ V_2 \\ I_2 \end{bmatrix} = \begin{bmatrix} 0 \\ 0 \\ 0 \end{bmatrix} \tag{3.14}$$

3.3.5 Circuit Breakers

CBs are programmed with two characteristic equations: one for each operating state. For the 'on' state, the CB is modelled in exactly the same manner as a line as shown in (3.15).

$$\begin{bmatrix} -1 & R + sL \end{bmatrix} \begin{bmatrix} V \\ I \end{bmatrix} = \begin{bmatrix} 0 \end{bmatrix} \tag{3.15}$$

During the 'off' state, the CB is simulated as an ideal current source exporting no current. A current source exporting zero currently is effectively identical to an open circuit. Hence, (3.16) is implemented.

$$\begin{bmatrix} 0 & 1 \end{bmatrix} \begin{bmatrix} V \\ I \end{bmatrix} = \begin{bmatrix} 0 \end{bmatrix} \tag{3.16}$$

3.3.6 Current Transformers and Voltage Transformers

CTs are also represented in exactly the same way as a line element (3.17).

$$\begin{bmatrix} -1 & R + sL \end{bmatrix} \begin{bmatrix} V \\ I \end{bmatrix} = \begin{bmatrix} 0 \end{bmatrix} \tag{3.17}$$

Voltage or potential transformers are shunt elements and are assumed to draw zero current. Hence, the VT is modelled as an ideal current source exporting no current. Ergo, (3.18) is implemented.

$$\begin{bmatrix} 0 & 1 \end{bmatrix} \begin{bmatrix} V \\ I \end{bmatrix} = \begin{bmatrix} 0 \end{bmatrix} \tag{3.18}$$

3.4 IIEG Unit Modelling

3.4.1 DC-Side Modelling

The DC side of an inverter interface usually consists of an energy resource, a DC-DC converter to ensure maximum power export from the energy resource and a DC link capacitor to maintain a reasonably constant voltage on the DC side of the inverter. There may also exist a long term energy storage unit such as a battery bank coupled to the DC bus through another DC-DC converter.

When a fault occurs in a DN, the transient response of an inverter is largely governed by the inverter controller and the capabilities of the power electronics [65]. Ergo, the dynamics of the DC side of an inverter can be omitted from the simulation platform without significantly compromising the fault and protection response of a simulation.

The DC link capacitor between the energy resource and inverter ensures that the DC voltage at the inverter input will remain almost constant during short transients. In particular, if a storage such as a battery is coupled with the DC bus, it is reasonable to assume that the DC link capacitor will always be charged to provide energy for short term transients within the network. In the case of low impedance faults where the DC link voltage would not be sustained for a lengthy period of time, it is assumed that the protection will isolate the EG before a significant voltage drop is incurred on the DC-side of the inverter. Hence, the DC-side of an IIEG system can be modelled as a constant DC source.

The DC link capacitor has been divided into two capacitors with a centre tap and a solid earth connection is provided at the centre tap. The earth connection ensures that the average DC voltage midpoint does not float significantly above or below the earth potential. Without the split DC link capacitors and earth connection, the AC side voltage and current waveforms can possess a non-zero DC value.

The DC voltage must be chosen appropriately such that over-modulation does not occur during normal operation of the IIEG unit. As a rule, the DC voltage V_{dc} must be larger than that defined in (3.19) where $V_{rms_{l-l}}$ is the nominal line-to-line rms (root-mean squared) voltage at the AC side. The DC voltage must be greater than the line-to-neutral peak-to-peak AC voltage.

$$V_{\mathrm{dc}} > \sqrt{8/3} V_{\mathrm{rms_{l\text{-}l}}} \tag{3.19}$$

3.4.2 Inverter Modelling

The adopted inverter topology consists of a simple three-leg, three-phase system as shown in Fig 3.3. All inverters are assumed to be three-phase within the proposed simulation platform. The EG penetration levels required to adversely affect protection coordination require medium-scale generators (greater than 30 kW) which must be three-phase systems to prevent a significant voltage unbalance.

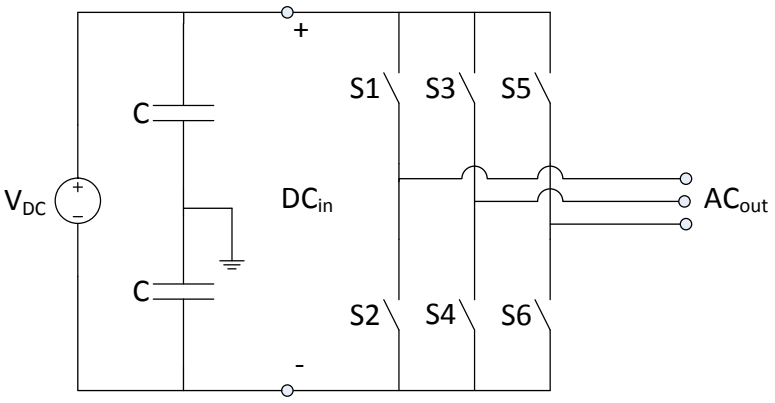

FIGURE 3.3: Inverter Topology

Most modern IIEG units export at least 1 kW and operate at switching frequencies of a few kHz. The EG power electronics operational characteristics are commensurate with the capabilities of insulated gate bipolar transistor (IGBT) [66]. According to a survey conducted by [67], IGBTs are the most common power electronics switch used in industry. Hence, IGBTs will be the adopted switch for inverter-interface models within this Thesis.

IGBTs have a very low on-state resistance and a wide safe operating area. When operating within rated voltages and currents, the IGBT can be modelled as an ideal switch (either a short or open circuit depending on the state) providing sufficient accuracy for the purposes of this Thesis.

The transient responses during switching of IGBTs generally only last in the order of hundreds of nanoseconds [68]. The switching period of the gate signals is in the order of hundreds of microseconds. The sampling of waveforms for protection response can be as low as sixteen samples per cycle in modern OC relays such as the Schweitzer Engineering Laboratories (SEL) relays [69]. The transient response as a direct result of switching and IGBT behaviour is largely attenuated by the anti-aliasing filters within relays signal processing systems; hence, the transient behaviour of the power electronics within inverters can be ignored when simulating protection adequacy.

The failure of IGBTs can be categorised as either catastrophic failure or wear out failure [70]. Wear our failure occurs as a result of accumulated degradation of components over time. Catastrophic failure is a result of a single high stress event. Protection devices are

essential to minimise the risk of failure of power electronic switches. If the voltage across the IGBTs exceeds rated voltage, the IGBT may break down and continue to conduct during the off-state. The leakage current and temperature will rise, usually destroying the IGBT after several microseconds during the on-state [70]. If the current flowing through the IGBT during on-state exceeds the rated current, a high power dissipation within the IGBT will cause a failure within a few microseconds.

The process of modelling the destruction of power electronic switches is difficult and unnecessary if an inverter unit is equipped with adequate OV and I^2t protection. It is assumed in this Thesis that fault current limiters and protection systems will eliminate the risk of catastrophic failure of power electronics switches; hence, the extremes of IGBT behaviour do not require consideration within the simulation platform given inverter protection and/or fault current limiters have been adequately modelled. Furthermore, within the microgrid scope, it is assumed that IIEG units are over-rated and capable of providing sustained OV which is necessary for the proposed voltage sequence protection scheme (which is presented in Chapter 7) to operate. Hence, the ideal model of IGBT switches is considered reasonable as extreme operation is precluded via protection, fault current limitation and over-rating of inverter interfaces.

Wear out failure is generally a result of long term recurring stresses on IGBTs and is often mechanical in nature. Long term failure of devices is outside of the scope of this Thesis.

3.4.3 AC-Side Modelling

The AC-side of an IIEG unit consists of a filter before the PCC, metering technology and usually a distribution transformer. An LCL configuration is the adopted filter within this design. LCL filters are capable of attenuating both voltage and current waveform distortion. The L_1 and C components are configured as shown in Figure 3.4. The inductance L_2 is supplied by the distribution transformer.

The selection of filter components is achieved using (3.20) and (3.21) [71, 72]. The choice of filter inductance L_1 and capacitance C ensures that ripple current and reactive power

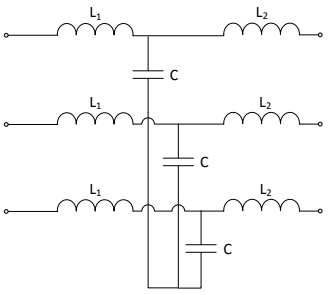

FIGURE 3.4: LCL Filter

consumption remains within acceptable bounds. A maximum current ripple of 20% and maximum reactive consumption of 5% are chosen.

$$L_1 = \frac{5V_{dc}V_{\text{base}}}{\sqrt{6}F_s S_{\text{base}}} \tag{3.20}$$

$$C = \frac{S_{\text{base}}}{20\omega_{\text{ref}}V_{\text{base}}^2} \tag{3.21}$$

V_{base} and S_{base} are the base voltages and apparent powers on the AC side of the inverter in Volts and Volt-Amperes. F_s is the switching frequency of the inverter gating signals in Hertz and ω_{ref} is the reference angular frequency in radians per second.

3.4.4 Grid-Connected Inverter Control Modelling

Contemporary IIEG control units employ a constant current or constant power control strategy. Many well-established control schemes involve an inner current control loop within an outer power control loop [73–75]. These control schemes are preferred by proprietors as maximum monetary compensation is achieved through exporting the maximum Watt-hours (Wh). Hence, constant power control with an inner current controlled loop is the adopted control scheme for grid-connected IIEG as shown in Fig. 3.5.

All measured parameters are converted into the *dq* rotating reference frame to reduce the complexity of the controller. All parameters are then passed through a low pass filter

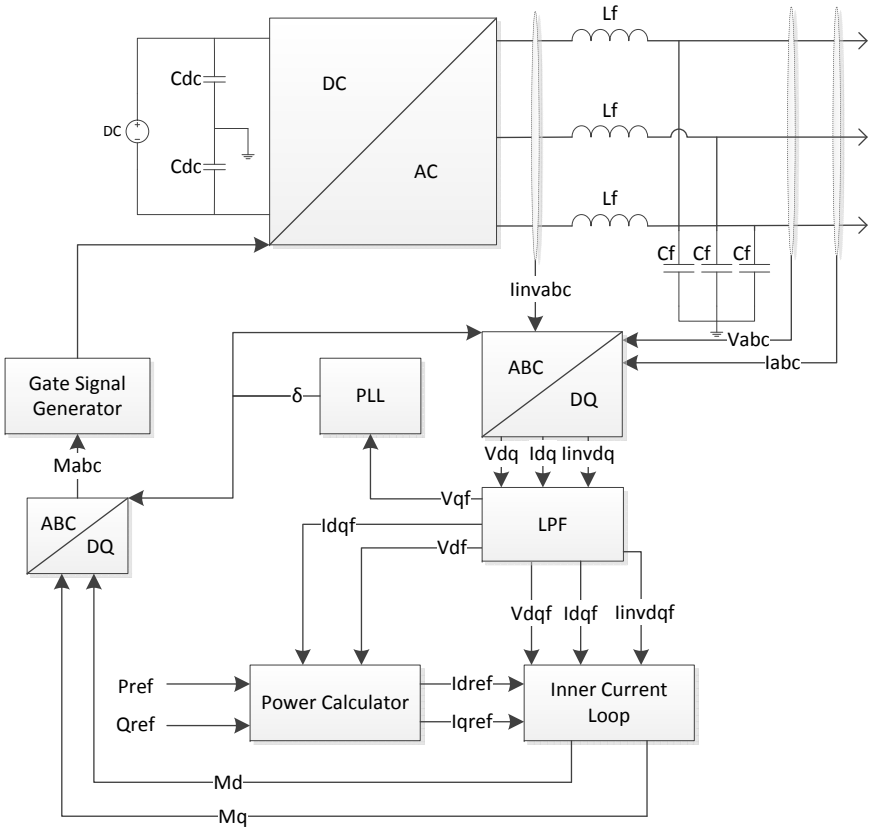

FIGURE 3.5: Constant Power Control of IIEG

(LPF) to attenuate short term disturbances. The cut-off angular frequency ω_c is chosen to be five times the fundamental angular frequency. A phase locked loop (PLL) is used to converge upon the rotating reference angle necessary to ensure that the quadrature voltage is equal to zero. The design of the PLL can be sourced in [74]. The power calculator determines the direct and quadrature current references via (3.22) and (3.23).

$$I_{d_{\text{ref}}} = 2/3 \frac{V_{df} P_{\text{ref}} + V_{qf} Q_{\text{ref}}}{V_{df}^2 + V_{qf}^2} \tag{3.22}$$

$$I_{q_{\text{ref}}} = 2/3 \frac{V_{qf} P_{\text{ref}} - V_{df} Q_{\text{ref}}}{V_{df}^2 + V_{qf}^2} \tag{3.23}$$

The current controller block diagram is given in Fig. 3.6. Note that the controller is duplicated for the dq axes components.

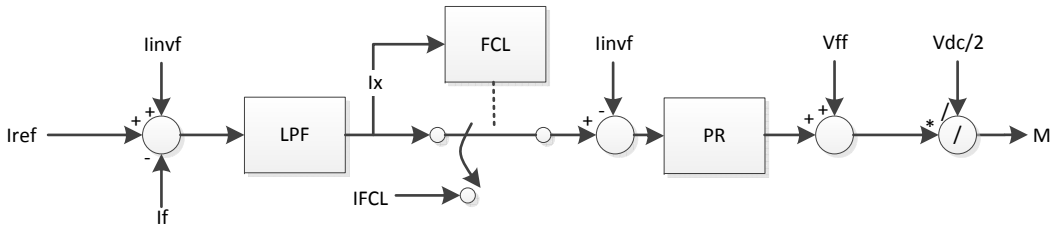

FIGURE 3.6: Current Controller

The current controller also contains an LPF to slow the current response; the cut off frequency ω_c is chosen to be one-fifth of the fundamental angular frequency. The LPF slows the transient response of the inverter, reducing the impact of short-term disturbances. A feed-forward voltage signal, V_{ff}, is implemented for fast voltage following capability. The output direct and quadrature voltages of the first LPF are used for the feed-forward voltage signal in the proposed controller. Separating the voltage and current response times improves the overall stability of the system by decoupling the dynamics of the control scheme from the network [74]. The use of an LPF also aids in the fault response prediction process, which is elaborated upon in Chapter 5. An optional FCL is installed within each inverter control system to allow IIEG to provide fault ride-through without exceeding the I^2t capabilities of the power electronic switches. If the fault current limit is exceeded (meeting the condition represented by (3.24)), the multiplexer selects constant values for I_{FCL} which are chosen as shown in (3.25) and (3.26).

$$\sqrt{I_{dx}^2 + I_{qx}^2} > \frac{k_1\sqrt{2}S_{\text{base}}}{\sqrt{3}V_{\text{base}}} \tag{3.24}$$

$$I_{d_{FCL}} = 0 \tag{3.25}$$

$$I_{q_{FCL}} = \frac{k_2\sqrt{2}S_{\text{base}}}{\sqrt{3}V_{\text{base}}} \tag{3.26}$$

Where k_1 and k_2 are constants and $k_1 < k_2$. The constants k_1 and k_2 are chosen such that, when the FCL is implemented, the fixed output current is greater than the FCL's

threshold. Correct selections of these constants shall prevent an oscillation between the fixed output current and constant power control.

The PR controller is used to replace conventional proportional-integral (PI) controllers. A PR controller has two important advantages over PI controllers: PR controllers have zero steady state error and do not require knowledge of the AC side filter circuit parameters of the IIEG unit [76]. Finally, the gate signal generator synthesises the AC waveform using pulse width modulation which is then smoothed using the LCL filter.

The grid-connected IIEG unit controller presented in this Chapter is a composite of several control schemes [74, 76, 77]. The advantages of the presented control scheme include: zero steady-state error, fault current limitation for fault ride-through support, a feed-forward voltage loop to decouple grid and controller response during disturbances. Furthermore, the grid-connected control scheme has been selected such that only minor alterations are required for autonomous control during microgrid operation.

3.4.5 Grid-Connected Inverter Control Verification

A thorough experimental verification of the grid connected controller is not within the scope of this Thesis. To the best knowledge of the author, there exists no experimental data of the adopted grid-connected inverter controller. Hence, a partial verification will be supplied by considering the theoretical steady-state and transient behaviour of the grid connected inverter.

A load shedding algorithm developed by the author in [78] yielded the theoretical steady-state condition of an islanded IIEG implementing the grid-connected controller. The circuit shown in Fig. 3.7 represents an equivalent circuit for an island. All IIEG units are condensed into one IIEG unit and all lines and loads are condensed into a parallel connected RLC load. The power convention for the IIEG unit is a positive real and reactive power indicates a real and capacitive power export, respectively. The network data is given in Table 3.1.

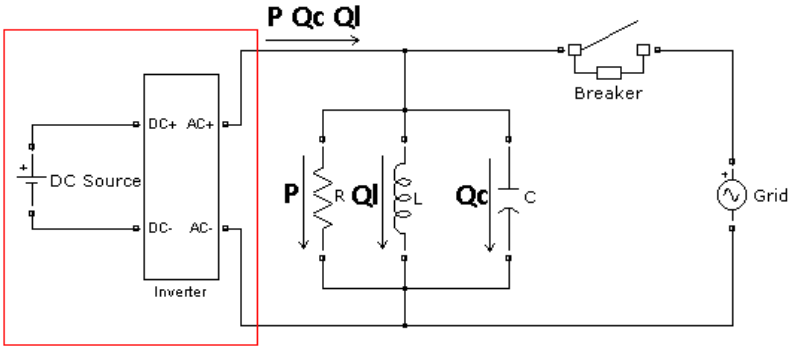

FIGURE 3.7: Equivalent Circuit for Island

TABLE 3.1: Equivalent Circuit Data

Line Data	
Line No.	1
Resistance (Ω)	0.1
Inductance (mH)	1
Load Data	
Load No.	1
Resistance (Ω)	200
Inductance (H)	5.093
Capacitance (uF)	2
Note: Impedance are connected in parallel.	
IIEG Data	
IIEG No.	12
DC Voltage (V)	8002
Switching Frequency (kHz)	4
Filter Inductance (mH)	163.3
Filter Capacitance (μF)	0.3316
S_{base} (kVA)	10
V_{base} (V)	400
P_{sp} (p.u.)	1
Q_{sp} (p.u.)	0
Low Pass Filter Cut-Off Frequency (Hz)	10
CB Data	
Operation No.	1
Operation time (s)	0.05
Fault type	Open

The voltage and frequency are line commutated and no longer regulated by the mains supply. Hence, the resultant voltage magnitude $|V|$ and island frequency ω are governed by the load and power set points of an inverter as shown in (3.27) and (3.28).

$$|V| = \sqrt{\frac{P_{sp}}{P}} \tag{3.27}$$

$$\omega = \frac{-Q_{sp} + \sqrt{Q_{sp}^2 + 4Q_c|V|^4 Q_l}}{2Q_c|V|^2} \tag{3.28}$$

P_{sp} and Q_{sp} are the real and reactive power set points of the IIEG unit. P, Q_l and Q_c are the rated real power, inductive and capacitive powers of the equivalent load impedance, respectively. All values are expressed as per unit. The derivation in given in Appendix A.

The equivalent circuit shown in Fig. 3.7 was simulated within the small-signal analysis platform. The CB is opened after 0.05 seconds of simulation, thereby creating an island. The small-signal plots showing the transient response of the island are shown in Figs. 3.8, 3.9, 3.10 and 3.11.

Before the formation of the island, the IIEG unit exports the real and reactive power at the designated set points as required. Note that the real and reactive powers diverge from the power set points after the island is formed. The steady-state error is due to the IIEG unit controller's response to the non-nominal frequency of the grid. The proportional-resonant (PR) controller is designed to provide accurate control at a fixed frequency only. Taking into account the power set point errors, the predicted voltage magnitude and angular frequency based on (3.27) and (3.28) are $|V_{IIEG}| = 264.7$ V and $\omega = 348.7388$ radians/second. The results of the simulation are $|V_{IIEG}| = 264.94 \pm 0.54$ V and $\omega = 349.2 \pm 1$ radians/second incorporating the ripple. The results are acceptably close; the discrepancies are attributable to the non-nominal frequency of the island which induces an error in the steady state response of the IIEG unit.

The transient response time of the voltage and current waveforms are dominated by the LPF and feed-forward voltage signal. The voltage magnitude changes instantaneously when the CB trips, then both waveforms decay to the steady-state values. The voltage

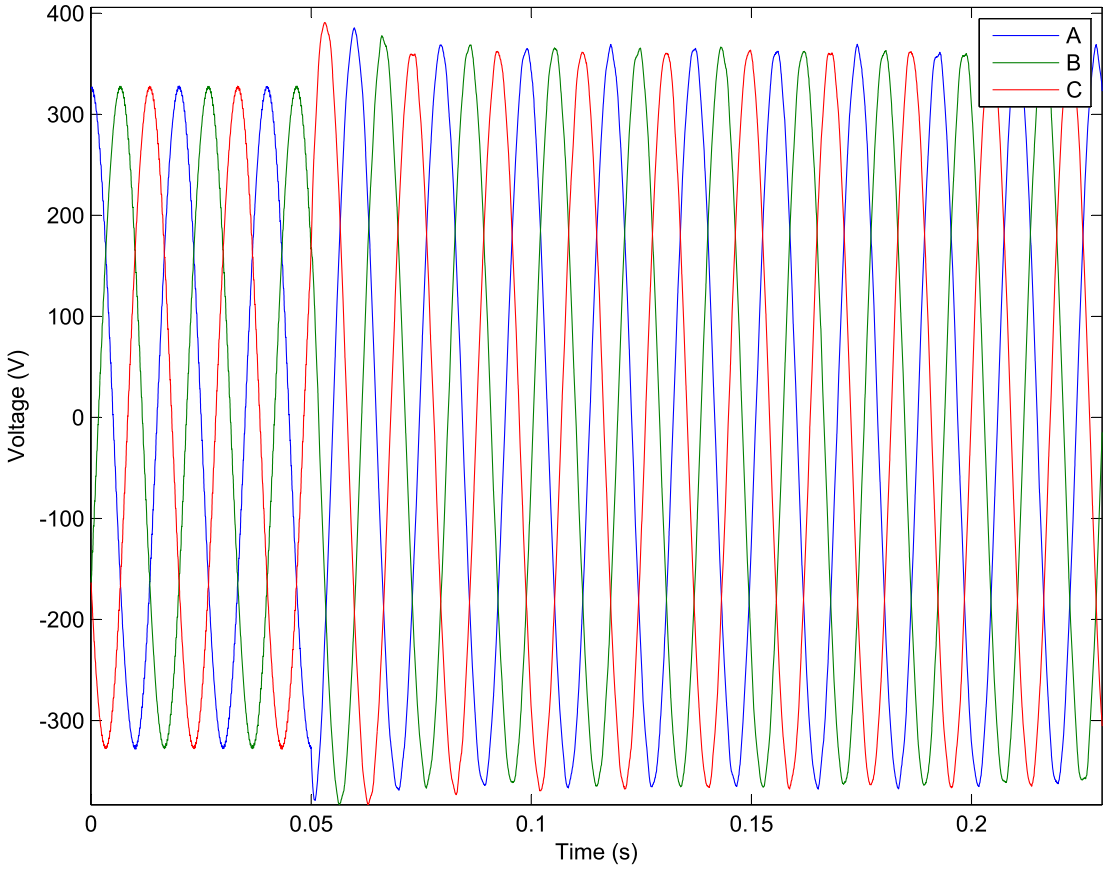

FIGURE 3.8: Islanded IIEG Voltage Waveform

and current waveforms then continue to transition slowly as the frequency is regulated. The response of the frequency waveform is governed by the PLL. In practice, passive anti-islanding protection will observe the voltage and frequency shift, isolating the IIEG as intentional islanding is forbidden by AS 4777.3 [16]. The transient response behaviour of the demonstrated example is arbitrary and does not represent a generalised nor required response time. The transient response of an island is dependent on the natural resonance of the island as well as the control characteristics of any EG within the island. Since the control requirements of IEEE 1547 are satisfied, the arbitrary response time of the island may be considered acceptable, but may be manipulated as required in future applications [21].

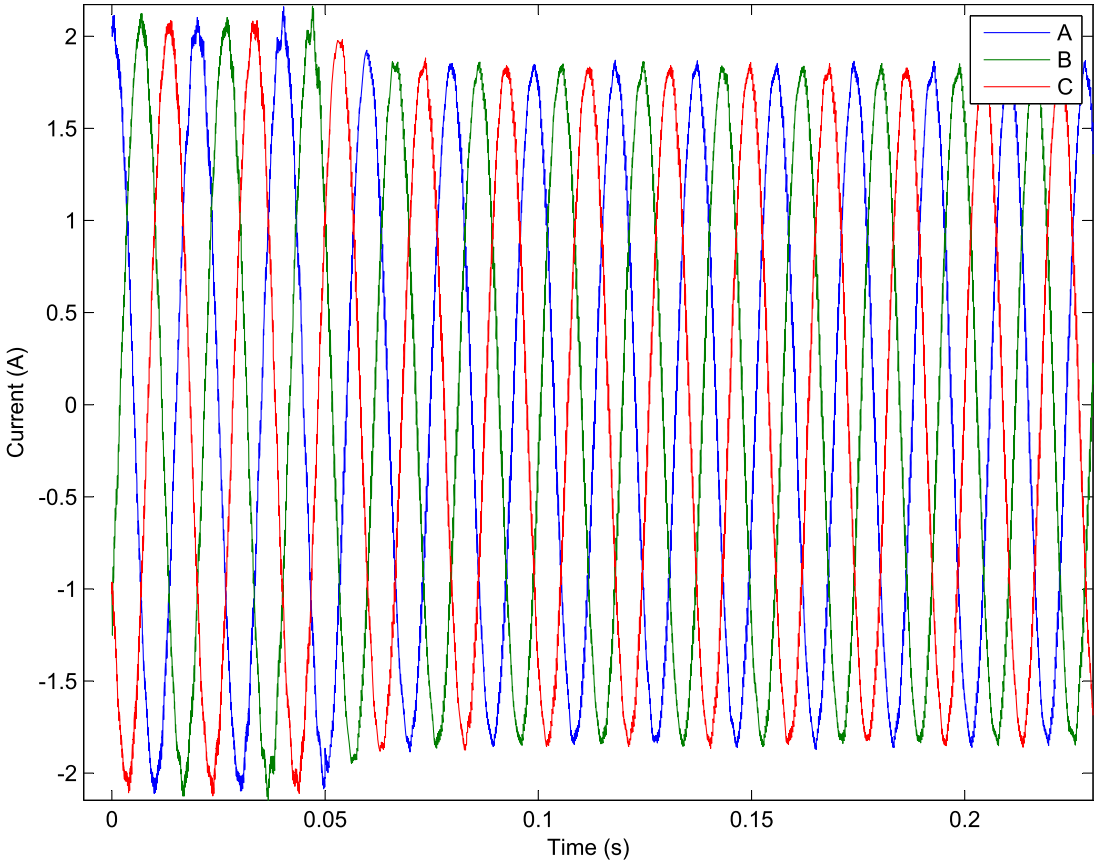

FIGURE 3.9: Islanded IIEG Current Waveform

3.4.6 Autonomous Inverter Control Modelling

Constant power control is inappropriate for autonomous operation of DNs as there is no mechanism for voltage and frequency regulation; the voltage and frequency are line-commutated. Currently, international standards forbid voltage regulation within EG unit control, mostly due to the need for anti-islanding protection to detect a fault passively [21]. The standards do not permit intentional autonomous operation of subsections of DNs due to various technical restraints including protection, power quality, control and stability issues. Subsequently, modelling autonomous subsections of the network requires a subversion of many assertions stipulated within international standards, including the regulation of voltage by EG unit control systems to 'path the way' to international standard reform.

Isochronous control is also inappropriate for autonomous operation. Similarly to large

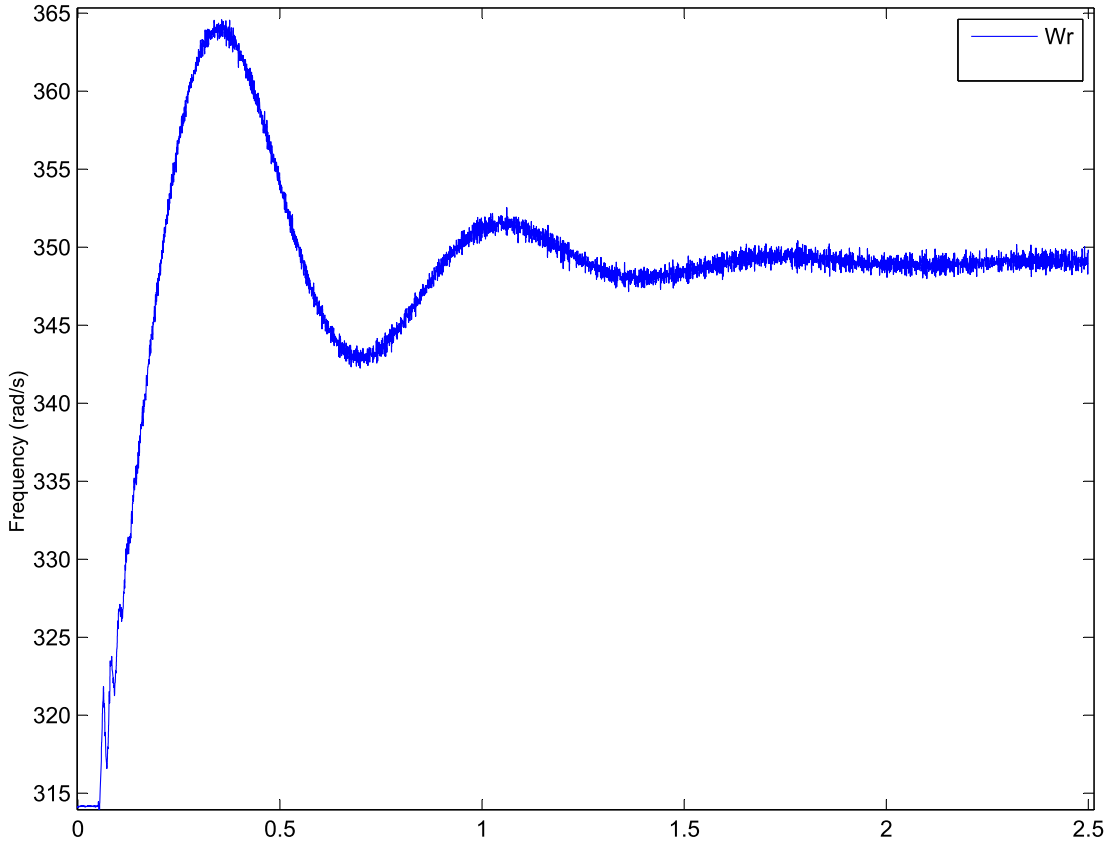

FIGURE 3.10: Islanded IIEG Frequency Response

scale generation, if voltage and/or frequency set points of EG control units are slightly different, circulating currents between EG units may result within an island. In a large-scale grid, there is typically a significant impedance between sources and circulated currents are acceptably small. However, the impedance in microgrids may be insufficient to prevent circulating currents from exceeding the ratings of network infrastructure and EG units [55]. Also, a load sharing algorithm will be necessary to prevent disproportionate power flow. Problems involving circulating current and load flow can be resolved using droop control. Droop control is well established in large-scale generation and is adopted as the preferred method by many authors for use during autonomous operation of a microgrid [44, 46, 55, 61, 79, 80]. The block diagram for the proposed autonomous control is given in Fig. 3.12.

The autonomous controller has been designed to behave in a similar fashion to the grid-connected controller to simplify the overall design of an IIEG unit within a microgrid.

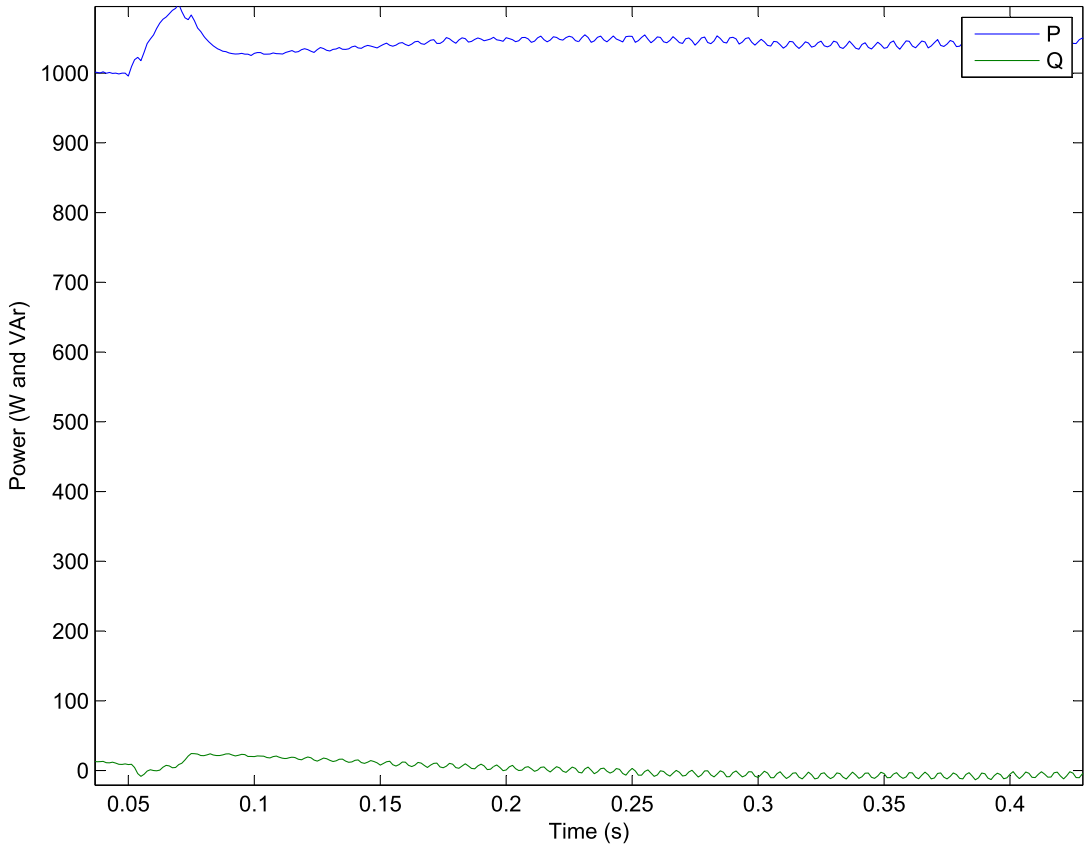

FIGURE 3.11: Islanded IIEG Power Response

Again, all measured voltage and current waveforms are converter to the dq axis and passed through an LPF. The droop controller block diagram is shown in Fig. 3.13.

The power calculator shown in Fig. 3.13 is identical to the power calculator in the grid-connected controller, which was shown in Fig. 3.5. The voltage calculator in Fig. 3.13 determines the magnitude of the voltage waveform for comparison with the voltage reference generated by the Q/V droop block. The magnitude is expressed in per unit and can be calculated by (3.29).

$$E = \sqrt{\frac{3}{2}} \frac{\sqrt{V_{df}^2 + V_{qf}^2}}{V_{\text{base}}} \tag{3.29}$$

The equations for the P/ω and Q/V droop blocks can be are given in (3.30) and (3.31) respectively.

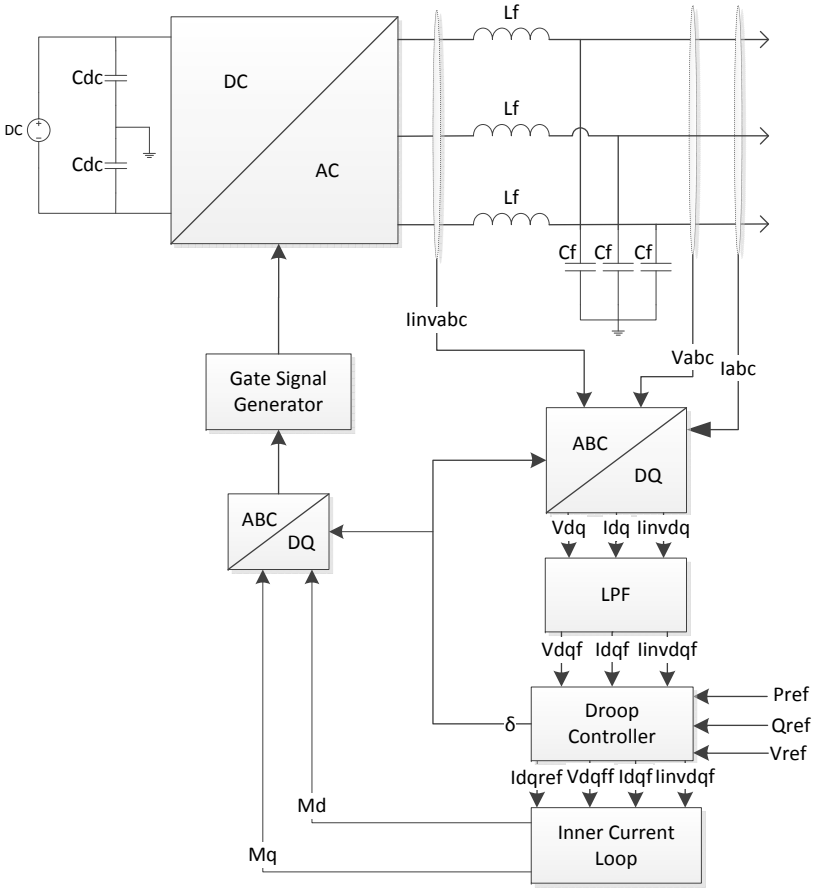

FIGURE 3.12: Autonomous Control of IIEG

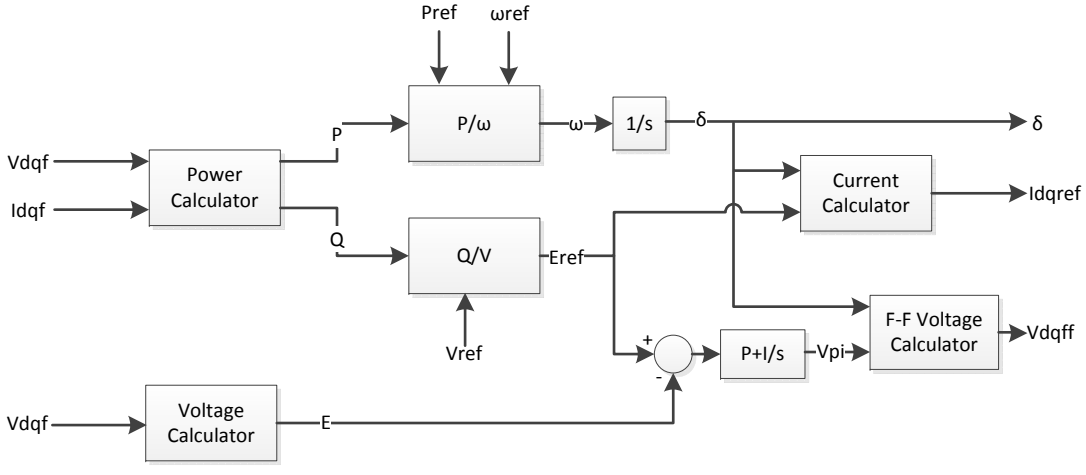

FIGURE 3.13: Droop Control Block

$$\omega = \frac{P_{\text{ref}} - P}{m_P} + \omega_{\text{ref}} \tag{3.30}$$

$$E_{\text{ref}} = V_{\text{ref}} - \frac{Q}{m_Q} \tag{3.31}$$

P and Q are the exported real and reactive power respectively. P_{ref}, ω_{ref} and V_{ref} are the power export, angular frequency and voltage references respectively. m_P and m_Q are the droop constants which can be calculated by (3.32) and (3.33).

$$m_P = \frac{\omega_{\text{ref}} - \omega_{\text{min}}}{P_{\text{max}} - P_{\text{min}}} \tag{3.32}$$

$$m_Q = \frac{V_{\text{max}} - V_{\text{ref}}}{Q_{\text{max}}} \tag{3.33}$$

The current calculator provides a reference for the inner current loop. The current calculator assumes that the impedance of the grid will remain constant for a shift in output current as shown in (3.34). Let I_1 be the desirable current and I_0 be the present current.

$$Z_{I_1} = Z_{I_0} \tag{3.34}$$

Z_{I_1} and Z_{I_0} are the equivalent impedances at an EG unit's PCC when currents I_1 and I_0 are exported respectively. Ohm's law yields (3.35).

$$\frac{V_{I_1}}{I_1} = \frac{V_{I_0}}{I_0} \tag{3.35}$$

Where V_{I_1} and V_{I_0} are the desirable and present voltages. The current references can then be expressed as in (3.36) and (3.37).

$$I_{d_{\text{ref}}} = \frac{I_{df}\sqrt{2/3}E\cos\delta}{V_{df}} \tag{3.36}$$

$$I_{q_{\text{ref}}} = \frac{I_{df}\sqrt{2/3}E\sin\delta}{V_{qf}} \tag{3.37}$$

The output of the Q/V droop block E_{ref} and the calculated voltage magnitude E are compared and then passed through a PI controller. The output of the PI controller V_{PI} and the phase angle δ are used to determine the feed-forward voltage signal via (3.38) and (3.39).

$$V_{dff} = \sqrt{\frac{2}{3}}V_{\text{base}}V_{PI}\cos\delta \tag{3.38}$$

$$V_{qff} = \sqrt{\frac{2}{3}}V_{\text{base}}V_{PI}\sin\delta \tag{3.39}$$

The inner current loops of the autonomous and grid-connected controllers are identical. The only differences between the two controllers are the use of a PLL and droop controller. A PLL is not essential for autonomous control as the phase angle is not directly regulated in the proposed controller and the angular frequency is only a function of the exported real power. The concept of phase angle regulation in an autonomous controller was explored by [81] and proved to reduce oscillations after a disturbance in the network. Hence, phase regulation may be incorporated in future controllers, but has not been deemed essential for understanding the fault behaviour of autonomously controlled IIEG units.

3.4.7 Autonomous Inverter Control Verification

Consider the small microgrid shown in Fig. 3.14. The network data is given in Table 3.2.

The CB is originally closed, opens at 0.2 seconds and closes again at 0.4 seconds. The expected response of the network to each disturbance compromises of:

- balanced load sharing where load dispatch is proportional according to the power base of each IIEG;
- an inverse relationship between real power and frequency as defined in (3.30);

TABLE 3.2: Autonomous Microgrid Data

Line Data		
Line No.	1	2
Resistance (Ω)	0.1	0.2
Inductance (mH)	1	2
Transformer Data		
Transformer No.	1	2
Primary Voltage l-l rms (V)	11000	11000
Primary Winding Resistance (Ω)	0.001	0.001
Primary Winding Inductance (mH)	0.1	0.1
Primary Connection	Wye-earthed	Wye-earthed
Secondary Voltage l-l rms (V)	400	400
Secondary Winding Resistance (Ω)	0.001	0.001
Secondary Winding Inductance (mH)	0.1	0.1
Secondary Connection	Wye-earthed	Wye-earthed
Load Data		
Load No.	1	2
Real Power (kW)	15	10
Reactive Power (kVAr)	0.5	0.5
Note: The equivalent resistance and inductance of the load are connected in parallel.		
IIEG Data		
IIEG No.	1	2
DC Voltage (V)	800	800
Switching Frequency (kHz)	4	4
Filter Inductance (mH)	8.165	16.33
Filter Capacitance (μF)	6.631	3.316
S_{base} (kVA)	20	10
V_{base} (V)	400	400
P_{ref} (p.u.)	1	1
P_{max} (p.u.)	1.05	1.05
P_{min} (p.u.)	0	0
$P = Q_{\text{max}}$ (p.u.)	0.4	0.4
V_{ref} (p.u.)	1	1
ω_{ref} (rad/sec)	$2\pi 50$	$2\pi 50$
ω_{min} (rad/sec)	$2\pi 49.5$	$2\pi 49.5$
Low Pass Filter Cut-Off Frequency (Hz)	10	10
CB Data		
Operation No.	1	2
Operation time (s)	0.2	0.4
Fault type	Open	Close

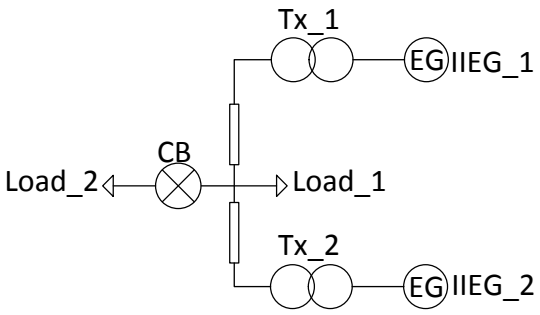

FIGURE 3.14: Autonomous Microgrid Example

- an inverse relationship between reactive power and voltage as defined in (3.31) and;
- a transient response time of approximately five time constants as in (3.40).

$$5\tau = \frac{5}{\omega_c} = \frac{5}{2\pi 10} \approx 0.08s \tag{3.40}$$

The voltage and current waveforms of IIEG_1 and IIEG_2 of the small-signal model are shown in Figures 3.15, 3.16, 3.17 and 3.18. Figures 3.19 and 3.20 show the real power, reactive power, voltage and angular frequency responses. All figures show a transient response consistent with the in-built LPF with a cut-off frequency of $\omega_c = 2\pi 10$ radians/second as the settling time was approximately 0.08 seconds. A clear inverse relationship between the real power and angular frequency as well as reactive power and voltage magnitude is apparent as observed in Figures 3.19 and 3.20. Furthermore, the per unit power export of each IIEG match with significant accuracy during steady state and the transient response.

The results indicate that the proposed control scheme satisfies the droop control requirements of autonomous operation. The results can also be considered as a partial verification of the simulation platform for steady-state and transient conditions of an intentional island.

The most significant operational difference between the proposed microgrid controller and controllers published by other authors [44, 81–83] is the slow current regulation that maintains the same current across all three phases. However, the current references may

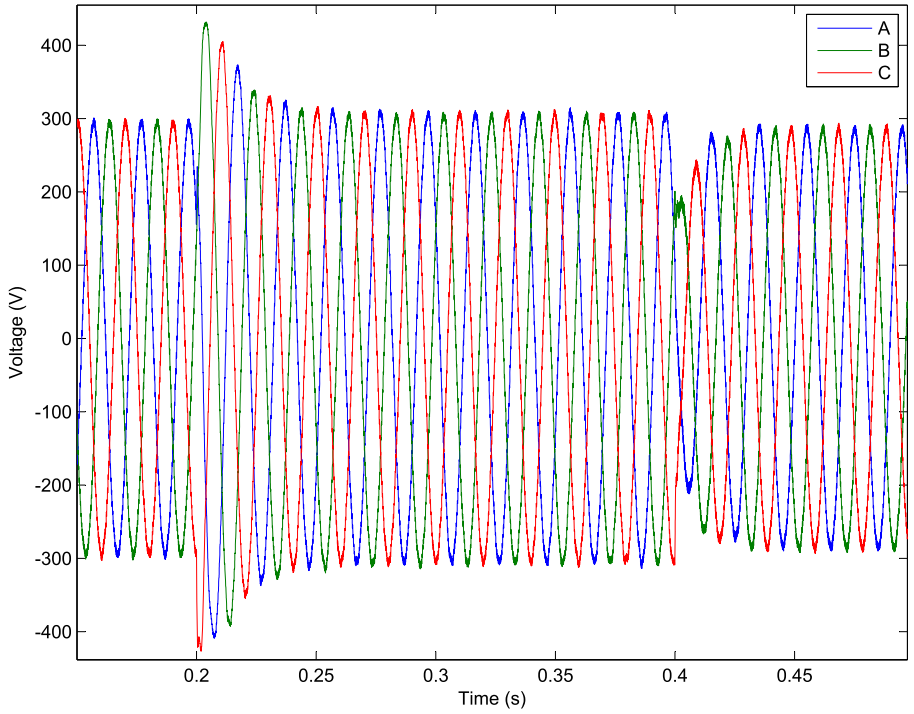

FIGURE 3.15: Autonomous Control Verification – IIEG_1 Voltage Waveform

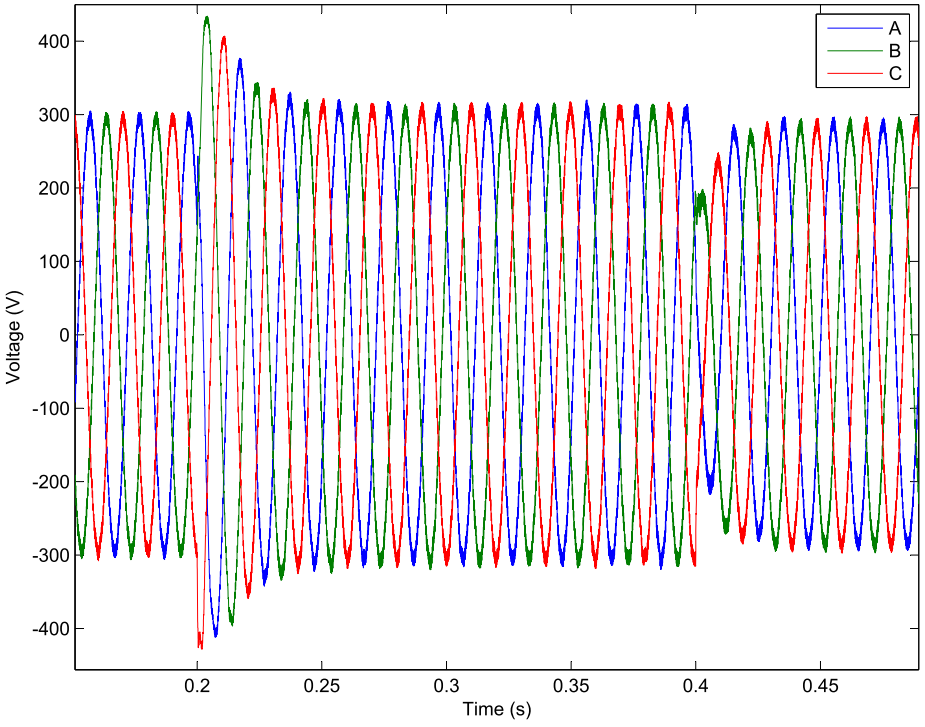

FIGURE 3.16: Autonomous Control Verification – IIEG_2 Voltage Waveform

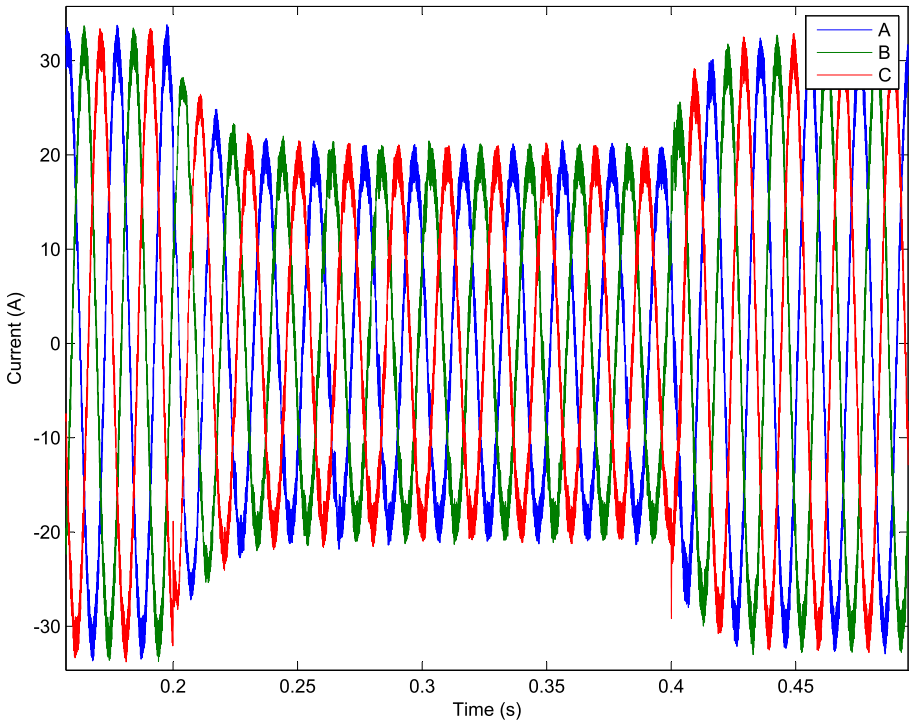

FIGURE 3.17: Autonomous Control Verification – IIEG_1 Current Waveform

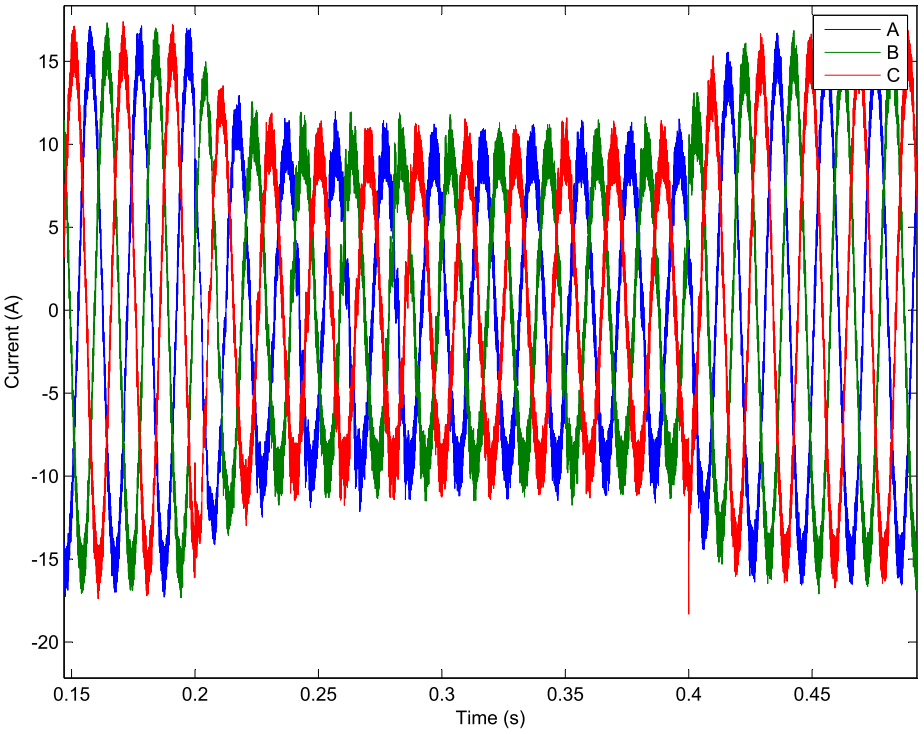

FIGURE 3.18: Autonomous Control Verification – IIEG_2 Current Waveform

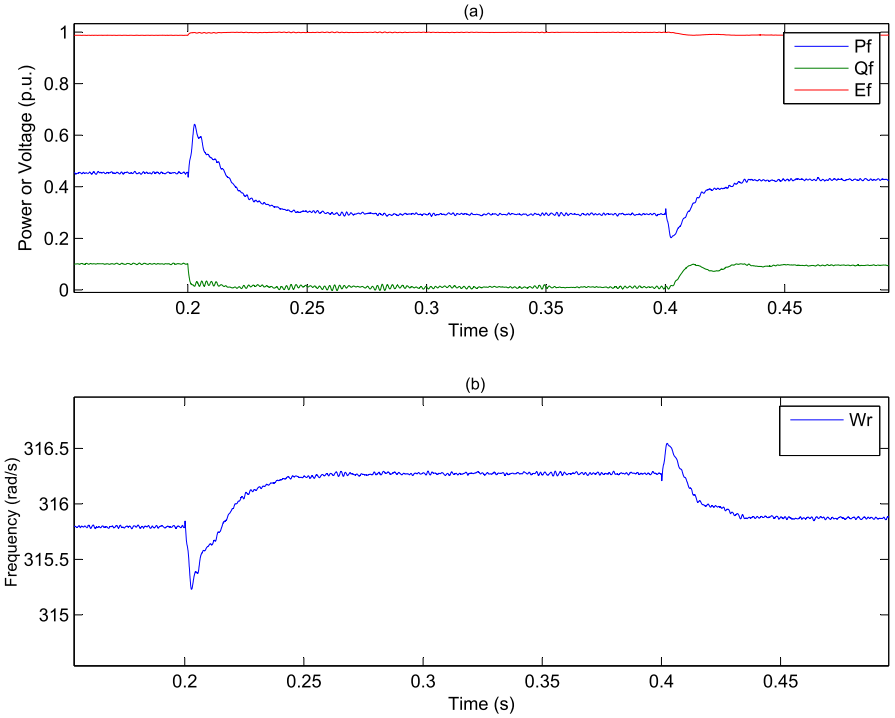

FIGURE 3.19: Autonomous Control Verification – (a) IIEG_1 Real and Reactive Power, Voltage (p.u.) and (b) Angular Velocity (rad/sec)

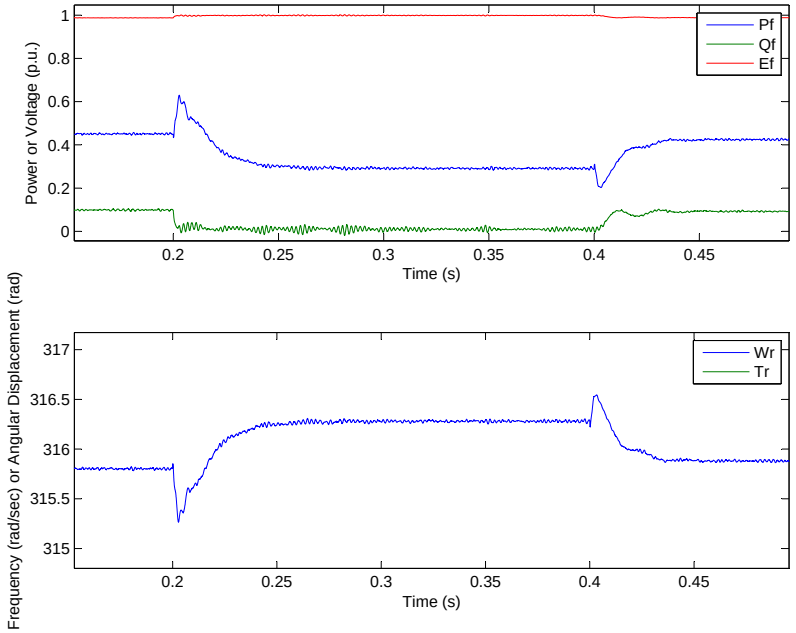

FIGURE 3.20: Autonomous Control Verification – (a) IIEG_2 Real and Reactive Power, Voltage (p.u.) and (b) Angular Velocity (rad/sec)

oscillate across phases during instances of low impedance faults. The fault response of the autonomous controller offers significant benefits from a fault protection perspective, which will be explored in greater detail in Chapter 7.

3.4.8 Justification of Inverter Models

A comprehensive and detailed verification of the IIEG model presented in this Chapter is prohibitively difficult and beyond the scope of this Thesis. Each manufacturers inverter will behave differently due to small variations in control and power electronics components. Irrespective, the adopted controllers are not designed to perfectly simulate a particular IIEG unit, rather provide a preferable control scheme for IIEG in future networks.

In order to establish a comprehensive model, significant experimental data would be required to establish a range of dynamic behaviour of each IIEG unit. The anticipated failure of power electronics devices when subjected to over-voltages or over-currents is virtually impossible to model precisely. However, catastrophic failure modelling is not required if protective devices are selected appropriately for detection of faults on a DN. Hence, the modelling presented in this Thesis is predicated on adequate protection of IIEG units.

IGBTs have a low thermal capability and can generally only sustain a short circuit for approximately 10 μs before destruction [84, 85]. However, inverters are equipped with heat sinks which will increase an IGBT's thermal tolerance and I^2t protection which will isolate the inverter before the IGBT's tolerance is exceeded, preventing damage to the power electronics. Furthermore, the impedance and control of the overall IIEG unit can reduce the short circuit current flowing through the IGBT during fault conditions, increasing the likelihood of inverter isolation before IGBT destruction. The authors of [29] present the fault response of a 1 kW single-phase IIEG and a 500 kVA three-phase IIEG. The single-phase inverter supplied a peak current of approximately five times the rated peak current for 1.6 ms. After repeated testing, the three-phase inverter supplied between two and three times the rated peak current for a duration of 1 to 4.25 ms. The duration of fault response is dictated by the protection characteristics of the inverter-interfaces which are not specified.

The actual destruction time of an inverter is dependent on the fault current magnitude, the voltage magnitude, the gate voltage, the ambient temperature of the inverter and the condition of the IGBTs. It is outside the scope of this Thesis to provide a model encompassing all possible operational variations. When developing an inverter for power applications, a design engineer has to perform a trade-off between the cost of components and the requirements of the overall system. For instance, in contemporary applications, grid-connected IIEG is not required to provide fault ride-through during disturbances in the DN. Hence, control schemes and IGBT do not need to provide excess current to maintain the voltage during reflected faults. Each IGBT simply needs to be able to sustain the current drawn due to a bolted fault at the EG terminals without destruction until the protection system operates. Empirically, the trip time for low impedance faults is in the order of 1-4.25 ms for medium-scale generators [29]. Hence, the assumption that power electronics failure will not occur before protection operation for modelling purposes can be justified.

Many authors propose the use of current limiters for IIEG fault modelling [28, 77, 86, 87]. Each of these papers contains an underlying assumption that the inverter will be able to support the current limit. This assumption can be achieved by rating power electronics switches appropriately. There exists a point of contention regarding imposing fault current limitations above rated current. Rated current can be defined as the export current at which the reliability or functionality of a device may be impaired [88]. From the power electronics' perspective, the rated current I_C is based on the ability of a device to remove heat when conducting current as shown in (3.41). T_C is the nominal ambient temperature, $T_{J(\max)}$ is the maximum junction temperature, $R_{\Theta JC}$ is the thermal resistance and $V_{CE(\text{on})}$ is the voltage across the collector and emitter of the IGBT. Ignoring factors such as junction temperature, if a fault current exceeding rated current is drawn from an IIEG unit, damage will be incurred and I^2t protection should isolate the fault.

$$I_C = \frac{T_{J(\max)} - T_C}{R_{\Theta JC} V_{CE(\text{on})}} \tag{3.41}$$

It is important to note that over voltage will also cause the breakdown of IGBT cells creating leakage current and high temperatures [70]. Over-voltage protection is mandatory

in grid-connected IIEG applications by AS4777.3 [16] and is adopted within all models; hence, IGBT failure due to over-voltage does not require modelling.

Future networks may consist of applications where sustained operation of IIEG units to achieve fault ride-through is desirable. In microgrid applications, Loix et al. in [28] suggest that the inverter output current should be limited to a value which the inverter is able to provide protective devices adequate information to isolate the fault. The over-rating of inverters for microgrid application in explored in detail in Chapter 7. For the purposes of simulation, the imposition of current limitations is not deemed essential for microgrid applications as fault ride-through is not required. Applications of FCLs in grid-connected only operation may prove unfeasible as the over-rating of power electronics may be considered an unjustifiable expense. However, Tang and Iravani in [87] propose use of current limiters to prevent the flow of excessive fault current that would compromise traditional DN line protection efficacy. Synchronous machines are used as the EG interface connected through a hybrid solid-state/mechanical switch current limiter.

In conclusion, the proposed controllers are not intended to represent an ideal case for the 'future of Australian DNs'. Rather, the controllers are designed to satisfy the envisaged requirements of future networks. In particular, to provide a level of predictability in fault response that does not require an advanced understanding of every grid-connected IIEG unit nor time-intensive small signal modelling. The controller is also designed to simplify high-impedance fault detection in microgrids which will be explored in detail in Chapter 7. The controllers are also flexible in terms of changing set points, use of a FCL and response time.

3.5 Line Protection Modelling

The line protection of contemporary Australian DNs consists of OC, EF and sensitive earth fault relays. Distance protection is usually reserved for transmission and sub-transmission networks which are considered outside the scope of this Thesis.

All line protection devices must take voltage and/or current measurements from VTs and/or CTs connected to the network. Each line protection device automatically compensates for the turns ratio of each CT and VT. The voltage and current waveforms are then filtered by a cosine filter before further analysis is taken (with the exception of frequency-based protection).

3.5.1 Cosine Filters

Modern protection devices are generally solid-state and analyse the voltage and current waveforms using digital signal processing. Sampling and filtering of the measured waveforms is necessary to maintain the integrity of the captured signal. Cosine filters have the ability to significantly attenuate DC offsets and harmonic components whilst maintaining the fundamental frequency [89]. Cosine filters are common in many protection device applications and are adopted as the filtering method used by protection devices in this Thesis [69]. The cosine filter can be determined by (3.42).

$$IX_{\text{smpl+spc}} = \frac{2}{N} \sum_{n=0}^{N-1} I_{\text{smpl+spc}-n} CFC_n \tag{3.42}$$

where:

$$CFC_n = \cos\left(\frac{2\pi n}{\text{spc}}\right)$$

spc is the number of samples per cycle and is set to 16, N is the number of samples per cycle (spc) minus one, $n = 0, 1, 2, \ldots, N$, smpl is the set of non-negative integers, I is a sample from the waveform and IX is the filter output.

The phasor output I_o can then be determined by (3.43).

$$I_{o_{\text{smpl+spc}}} = IX_{\text{smpl+spc}} + jIX_{\text{smpl+spc}-\frac{\text{spc}}{4}} \tag{3.43}$$

TABLE 3.3: OC and EF Standard Constants [4]

Characteristic	A	B	p
Standard Inverse	0.0515	0.1140	0.02
Very Inverse	19.61	0.491	2
Extremely Inverse	28.2	0.1217	2

Voltage and current amplitudes, phases and sequence components can then be calculated and interpreted by the relay in order to determine whether a trip is necessary.

3.5.2 OC, EF and SEF Protection

OC, EF and SEF protection has been essential for effective fault detection in Australian DNs. Under the premise of radial power flow, it can be assumed that the current flowing through each protection device upstream of a fault is almost equal. Hence, protection devices can be graded to ensure selectivity within the DN without requiring a communications medium. The IDMT curve which governs the trip time of an OC or EF relay can be expressed as in (3.44).

$$t = TD\Big(\frac{A}{M^p - 1} + B\Big) \tag{3.44}$$

where: t is the time to trip, TD is the time dial setting and M is the ratio of input current to the pick-up current $M = |I|/I_{pu}$. Constants A, B and p determine the relay type, which are defined to emulate the induction relays that were employed historically in DN protection schemes [4]. There are three characteristics of IDMT curves used in DNs: the standard inverse, very inverse and extremely inverse curves. The standard values for these characteristics are given in Table 3.3.

All OC, EF protection devices in DNs employ the same IDMT curve constants. When the detected fault current exceeds the time threshold defined by (3.44), a trip signal is sent to the corresponding CB, completing the trip sequence and isolating the fault. SEF relays are designed to detect high impedance single-line to earth faults and hence require high sensitivity. A large time delay of several seconds is also employed to prevent

nuisance tripping due to circulating zero sequence currents. The most likely reason for zero sequence current flow (other than a single-line to earth fault) is a parallel connection of two adjacent feeders during switching, particularly if a high impedance joint is present in the resultant ring network.

3.5.3 Sequence Component Protection

EF and SEF protection is identical to zero sequence OC protection. The three-phase currents are summated and the resulting zero sequence current is subjected to a time delayed threshold to identify whether a trip signal is warranted. Negative sequence OC protection is also a useful tool for back-up protection and is a common option in modern protection relays [69]. Negative sequence OC is particularly useful for identifying line-to-line faults. The sequence component of parameter F can be calculated through the transform (3.45).

$$\begin{bmatrix} F_0 \\ F_1 \\ F_2 \end{bmatrix} = \frac{1}{3} \begin{bmatrix} 1 & 1 & 1 \\ 1 & a & a^2 \\ 1 & a^2 & a \end{bmatrix} \begin{bmatrix} F_a \\ F_b \\ F_c \end{bmatrix} \tag{3.45}$$

Voltage sequence protection is not implemented in Australian DNs, but forms an important part of the proposed protection scheme presented in Chapter 7. Within the scope of the microgrid concept, the most difficult fault event to detect is a high-impedance single-phase to earth fault within an island. Various authors have proposed several protection schemes to identify high impedance faults, many of which are complicated or ignore effects such as transformer connections [50, 62, 63]. Through a combination of transformer and earthing connection stipulations, IIEG control modifications and the use of voltage sequence protection, a simple solution to the high-impedance fault detection problem is presented in Chapter 7.

3.5.4 Anti-Islanding Protection

3.5.4.1 Passive Anti-Islanding

Within the scope of the proposed microgrid structure, contemporary anti-islanding protection is implemented whenever communications failure occurs. All grid-connected only EG must be equipped with anti-islanding protection as defined by the Australian Standard 4777.3 [16].

The Australian Standard 4777.3 states that each EG unit must incorporate passive anti-islanding technology including under and over voltage (UOV) as well as under and over frequency (UOF) protection [16].

The Australian Standard 4777.3 indicates that tripping must always take place within two seconds once an island is detected. The IEEE 929 standard indicates the same maximum delay for most voltage deviations, but requires a much faster trip time for extreme UOVs. IEEE 929 also states that UOF protection should operate within six cycles. Accordingly, the small-signal model will incorporate multiple time-delayed trip settings for UOV and UOF protection.

The voltage magnitude is gathered using the voltage waveform gathered at the PCC passed through the cosine filter shown in (3.42). The frequency is gathered using a zero crossover method. An optional rate of change of frequency (ROCOF) passive anti-islanding protection is also available. The ROCOF model adopted in this Thesis was presented by Ten and Crossley in [90]. A window of five cycles is used as shown in (3.46).

$$\frac{df}{dt} = \frac{1}{5}\sum_{i=1}^{5}\frac{\Delta f_i}{\Delta t_i} \tag{3.46}$$

The ROCOF is then passed through a low pass filter and compared to a pre-defined value to determine if a trip is necessary. Passive anti-islanding protection is very effective at identifying LOM when a significant power discrepancy between an island's load and available generation is present. In modern Australian DNs, the risk of failure to detect LOM is very low as EG penetration levels are very small and contemporary grid-connected

EG does not offer reactive power support. Irrespective, the Australian Standard 4777.3 mandates one form of active anti-islanding protection.

3.5.4.2 Active Anti-Islanding

Each EG must contain at least one form of active anti-islanding protection; however, there is no preference towards any particular type of anti-islanding protection. Active anti-islanding protection will generally never be essential to island detection in contemporary networks as the disparity between the load and supply within an island is always large enough to create a significant voltage and/or frequency deviation. In DNs where the local load and supply are similar, this Thesis will assume that intentional islanding is advantageous and active anti-islanding techniques will be considered unnecessary. Hence, active islanding will not be modelled within this Thesis.

3.6 Conclusion

The modelling work presented in this Thesis does not provide an exhaustively accurate representation of the behaviour of modern nor future Australian DNs. The simulation platform and inherent models aim to provide a reasonable approximation for the fault and protection response of DNs with a high EG penetration to gain a conceptual understanding and verification of protection strategies that may prove useful as the DNs evolve into a decentralised entity. The proposed IIEG control schemes have never been implemented in practice and similar schemes, such as the Consortium for Electric Reliability Technology Solutions (CERTS) microgrid concept, employ control schemes and transformer configurations which are incompatible with the protection schemes proposed in Chapter 7. Hence, the conclusions drawn based on the simulation work presented in this Chapter require further investigation to verify that the concepts explored within this Thesis also apply in the field.

Chapter 4

Over Voltage Mitigation Scheme

4.1 Introduction

The principal technical constraint that is preventing connection of high levels of EG to DNs is instances of OV. EG units are not permitted to regulate the voltage at the PCC by the IEEE Standard 1547-2003 [21]. The resultant voltage at the PCC is determined by the EG power export as well as the electrical proximity of the EG to load and points of voltage regulation (such as the zone substation transformer or voltage regulator). In order to mitigate the risk of OV, utilities have imposed various policies regarding the sizing and connection restrictions of EG before a technical assessment is necessary [13]. It is important to note that there exists little consensus on how much EG penetration is tolerable before instances of OV become a likelihood. The electrical characteristics of feeders differ significantly across Australia. Line topology, line impedances and load behaviour significantly affect voltage profiles. An independent study is necessary to ensure that each EG connection will not cause OV; however, for small EG connections, the cost of an independent study is prohibitively expensive. A generalised policy is necessary to perpetuate the business case for small-scale EG connections.

Whilst an OV mitigation scheme does not explicitly pertain to protection studies, control schemes play an important part in analysing the protection response of IIEG. Empirically, OV issues have arisen at relatively low penetration levels; instances of OV have always

arisen before protection miscoordination in DNs could be incurred. Hence, it is imprudent to analyse EG penetration protection efficacy before imposing an OV mitigation scheme.

4.2 Review of OV Mitigation Schemes in DNs with a High IIEG Penetration

The simplest way to avoid OV in DNs with IIEG penetration is to place restrictions on IIEG size and location within the planning process. Australian utilities can impose a restriction on the size of a proposed IIEG unit upon application [91]. The current philosophy of IIEG control stipulates fixed power at unity power factor – a paradigm which suppresses the growth of IIEG penetration in Australian DNs. The worst case voltage profile can be determined by approximating the low load condition of a DN and running continuous load flow analyses for IIEG sizes until the voltage limit is breached. Such an exercise is time intensive and shown to be unnecessary through voltage sensitivity analysis as shown by Ayres et al. in [92].

Voltage sensitivity analysis manipulates a Jacobian matrix in order to predict the maximum IIEG size permissible before an OV is likely to arise. The Jacobian matrix is an array of the linearised rates of change tangential about a given operating point. For small deviations, linearisation can yield a reasonably accurate representation of a network's expected performance. Ayres's work is extended upon in [93] where the loadability of a line is also considered to ensure the thermal limits of a distribution network are not exceeded under low load conditions. However, these papers do not explore the plausibility of an OV management scheme which could allow for a greater IIEG penetration. The authors in [94] use the sensitivity matrix to approximate the appropriate power factor for a IIEG unit in a worst case low load scenario. The sensitivity analysis is useful for determining a fair method for allocating the reactive power license of each IIEG unit with respect to that IIEG unit's position in a DN. Various reactive power control methods are outlined in [94] and [95] including: constant power factor control, real power-dependent power factor control and voltage-dependent reactive power control. The principal weakness of these

control strategies is the necessary reconfiguration whenever a network upgrade occurs or a new IIEG unit is installed.

Consider the scenario where each IIEG unit is to be coupled with an energy storage device such as batteries. In such a case, any surplus power produced by the distributed energy resources shall be diverted into the battery bank, thus eliminating the risk of producing an OV caused by exporting more power than is being absorbed locally. Under continuous low load conditions, it may be possible that the batteries may be filled to capacity. The power set points of the inverter interface must then be altered or the IIEG unit will trip due to the OV anti-islanding protection. Such a problem can be mitigated through the appropriate sizing and control of the battery bank. However, it is important to note that the most significant deterrence of the installation of battery banks remains the exorbitant cost and slow return rate. It is unlikely that most customers would invest in energy storage unless either the cost of storage is reduced, a mandate for storage is legislated or significant benefits were to arise such as the possibility of intentional islanding. Intentional islanding is forbidden by Australian Standard 4777.3 [16] and, as such, shall not be further considered within this Chapter.

Another possible technique for OV mitigation is demand-side load management. If load behaviour could be configured to coincide with times of maximum generation, the risk of OV could be greatly diminished. However, customer and load coordination can be particularly challenging as maximum IIEG availability can be unpredictable. Even in the case of solar irradiation being somewhat predictable due to the quotidian nature of our planet's rotation, the maximum solar irradiance tends to occur when people are at work. In a commercial site, this coincidence is fortunate, but for residential premises, there exists a disparity between load and generation availability. It is generally accepted that variable tariffs and consumer awareness can be used to curb power usage during peak times [96]. However, under low load conditions where OV instances are most likely, there may be little extraneous load that customers are willing to forfeit. The notable exception is the off-peak power usage of hot water systems; hot water water systems are capable of storing heat for large periods of time. While demand-side management can be implemented to ease the disparity between generation availability and demand during times of peak load, off-peak demand-side load management schemes will likely coalesce

into an energy storage problem, yielding a situation similar to that explored previously with power diversion into battery banks. For similar reasons, demand-side management schemes shall not be considered within this Chapter.

Assuming that most customers do not invest in energy storage, the next most viable option for OV mitigation whilst maximising return is reactive power absorption. Currently, Australian IIEG unit proprietors are paid for real power injection only. There is a strong case that eventually reactive power may become a marketable commodity within DNs [97]; however, the notion of reactive power remuneration is unlikely to be prevalent in Australian DNs in the near future; hence, the notion shall not be included in this Chapter. Without reactive power remuneration, it makes financial sense for a IIEG unit to absorb reactive power during OV in order to maintain the voltage within acceptable levels rather than solely reducing the real power export. A small amount of real power output capacity is lost when reactive power is injected or absorbed by an inverter. However, the net real power export is increased through use of reactive power absorption if an OV condition is deemed unacceptable.

The capability curve of an IIEG unit can be expressed as a function of the rated current. Assuming the inverter is operating at rated voltage, a current restriction is implemented to prevent damage to the power electronic switches of the inverter interface. The utility imposes strict boundaries on the power factor produced by any IIEG unit; for example, 0.85 leading or lagging according to the standard IEEE 929 [33]. An OV mitigation scheme's configuration must be commensurate with these boundaries.

If the limitations of reactive power absorption are met, then the real power set point of the inverter interface must be limited as proposed by Calderaro et al. [98]. Calderaro et al. builds on the sensitivity matrix work presented by Ayres et al. in [92] to provide an OV mitigation algorithm. The algorithm accounts for both the voltage and current limitations of the IIEG unit. There are two main drawbacks to Calderaro et al.'s algorithm. Firstly, an off-line knowledge of the sensitivity of the network is required; the control scheme needs to be reconfigured whenever a significant alteration occurs in the DN. Hence, the Calderaro system cannot be considered as plug-and-play. Secondly, the perturbation and observation nature of the control scheme can make convergence to a preferred set point for

each IIEG unit difficult and potentially produce disproportionate power flow allocations between IIEG units. In comparison, the OV mitigation protection scheme proposed within this Thesis requires only local readings and converges to a power set point that ensures fair power flow within a DN.

Other voltage control schemes for DNs with a large EG penetration are proposed by Caldon et al. in [99] and Conti in [100]. The schemes makes use of a centralised controller located at the zone substation of a given feeder. Coordinated regulation is achieved through disseminating voltage set point instructions to the on-load tap-changer in the zone substation and reactive power instructions to EG units within the feeder. Sensitivity matrices are used to determine reactive power export of EG units in [100] as a function of voltage magnitude. Historical data is used to determine the empirical relationship between voltage magnitudes and reactive power export in [99]; hence a significant amount of trial and error may be necessary after a new EG unit is installed. The advantage of the proposed schemes is that existing technology is adopted where possible. However, the addition of a centralised controller and communications scheme is costly and a controller that uses only locally avaiable data is preferable.

4.2.1 Novel OV Mitigation Algorithm

The proposed OV mitigation algorithm is designed to ensure a fair power flow allocation using only locally sourced data. The algorithm incorporates the capabilities of the inverter interface, the available power from the distributed energy source as well as the stipulated requirements of the DN.

In order to express the power export capability of each IIEG, the same power convention as traditional machine generators such be adopted. Hence, a positive real power and reactive power shall indicate an export of real power and capacitive power of the IIEG unit, respectively.

Firstly, a voltage limit shall be imposed as in (4.1).

$$|\vec{V}_{\text{IIEG}}| \leq V_{\text{limit}} \tag{4.1}$$

Where $|\vec{V}_{\text{IIEG}}|$ is the voltage magnitude at a IIEG unit's PCC and V_{limit} is the voltage magnitude limit imposed by the OV mitigation algorithm. The voltage limit should be chosen to be below the OV threshold of the anti-islanding protection system to avoid nuisance tripping.

A power factor limit, $\text{p.f.}_{\text{limit}}$, is also imposed in order to abide by standards such as the IEEE Standard 929 [33]. Note that the power factor is always either lagging and the power angle limit, θ_{limit}, is always non-positive. Both of these restrictions are necessary as reactive power injection is not permitted by the proposed OV mitigation scheme.

$$\text{p.f.}_{\text{limit}} = \cos(\theta_{\text{limit}}) \leq \frac{P}{|\vec{S}|} \tag{4.2}$$

Finally, the power capability curve of the inverter interface is represented as a semicircle which is considered a reasonable approximation within the tolerable power factor domain bounded by (4.2). The capability curve is implemented by the control scheme to prevent damage to the power electronic switches. The domain of complex power operation is expressed in (4.3).

$$\vec{S}\epsilon\{\vec{x} = \mathbb{C} : |\vec{x}| \leq |S_{\text{rated}}|, \theta_{\text{limit}} \leq \arg(\vec{x}) \leq 0\} \tag{4.3}$$

Reactive power injection is forbidden within the scope of the proposed OV mitigation scheme. Ergo, the imaginary component of the complex power $\vec{S}$ will always be non-positive.

Beyond the constraints defined in (4.1), (4.2) and (4.3), the control scheme must provide a fair and equitable solution to avoid OV and maximise real power output. Firstly, it must be understood that it is preferable to absorb reactive power before reducing real power below the value defined on the outermost limit of the power capability domain. It is only when the power factor limit is reached that the apparent power $|\vec{S}|$ should be deliberately curtailed. The power factor limit is maintained during apparent power curtailment, again with the purpose of maximising real power output.

Given that the available apparent power $S_{\text{available}}$ is known, the domain of steady-state operation can be reduced to (4.4):

$$\vec{S}\epsilon\{\vec{x} = \mathbb{C} : |\vec{x}| = S_{\text{available}}, \theta_{\text{limit}} \leq \arg(\vec{x}) < 0\} \tag{4.4}$$

until real power curtailment is necessary to reduce the voltage when the domain changes to (4.5).

$$\vec{S}\epsilon\{\vec{x} = \mathbb{C} : 0 \leq |\vec{x}| \leq S_{\text{available}}, \arg(\vec{x}) = \theta_{\text{limit}}\} \tag{4.5}$$

The available apparent power $S_{\text{available}}$ is capped at the rated apparent power of the system S_{rated}. Without some form of energy storage coupled to the DC side of the inverter, the available power may drop below the rated power of the inverter. In such a case, the value of available power can be sourced from the maximum power-point tracker (MPPT).

If a single IIEG unit is present within a grid, the control scheme could utilise a constant voltage magnitude limit. Reactive power absorption would begin once the voltage magnitude threshold was reached. The controller would operate in a perturb and observe fashion, where the maximum real power in achieved using the domains of (4.4) and (4.5) where the voltage limit is not exceeded satisfying (4.1). If the power factor limit was met and the voltage still exceeded the voltage magnitude threshold, then apparent power curtailment would begin until the voltage condition was satisfied. However, when multiple IIEG units are connected to a DN, a constant voltage threshold can incite power export contests. Without some form of communication medium, there is no way to prevent a set of IIEG units from inadvertently and needlessly forcing other IIEG units into apparent power curtailment submission. There would also be an inherent stability problem with no clear point of convergence throughout this perturb and observe control scheme.

The proposed OV mitigation scheme uses piecewise equations to define the real and reactive power set points based on the voltage magnitude $|\vec{V}|$ at the PCC and the available apparent power $S_{\text{available}}$ sourced from the MPPT. The piecewise equations are defined in (4.6) and (4.7). The piecewise equations are segregated by three voltage magnitude

TABLE 4.1: Example Values

Parameter	Set Point
V_1	1.01 p.u.
V_2	1.02 p.u.
V_3	1.03 p.u.
$\text{p.f.}_{\text{limit}}$	0.85
$\lvert\vec{S}\rvert$	1 p.u.

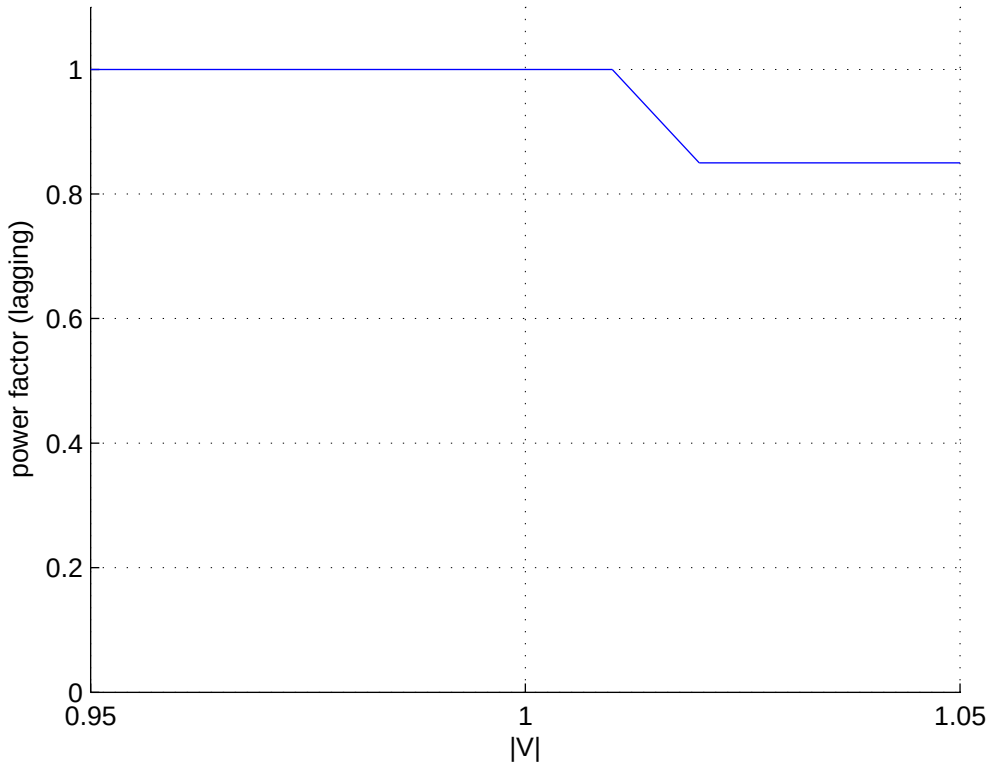

FIGURE 4.1: Proposed OV Mitigation Scheme: Power Factor and Voltage Magnitude Relationship

threshold tiers V_1, V_2 and V_3. Example plots are shown in Figs. 4.1 and 4.2 using the data in Table 4.1.

$$\text{p.f.} = \begin{cases} 1 & \text{if } |\vec{V}| \leq V_1, \\ \frac{1-\text{p.f.}_{\text{limit}}}{V_1-V_2}(|\vec{V}| - V_1) + 1 & \text{if } V_1 \leq |\vec{V}| \leq V_2, \\ \text{p.f.}_{\text{limit}} & \text{otherwise.} \end{cases} \tag{4.6}$$

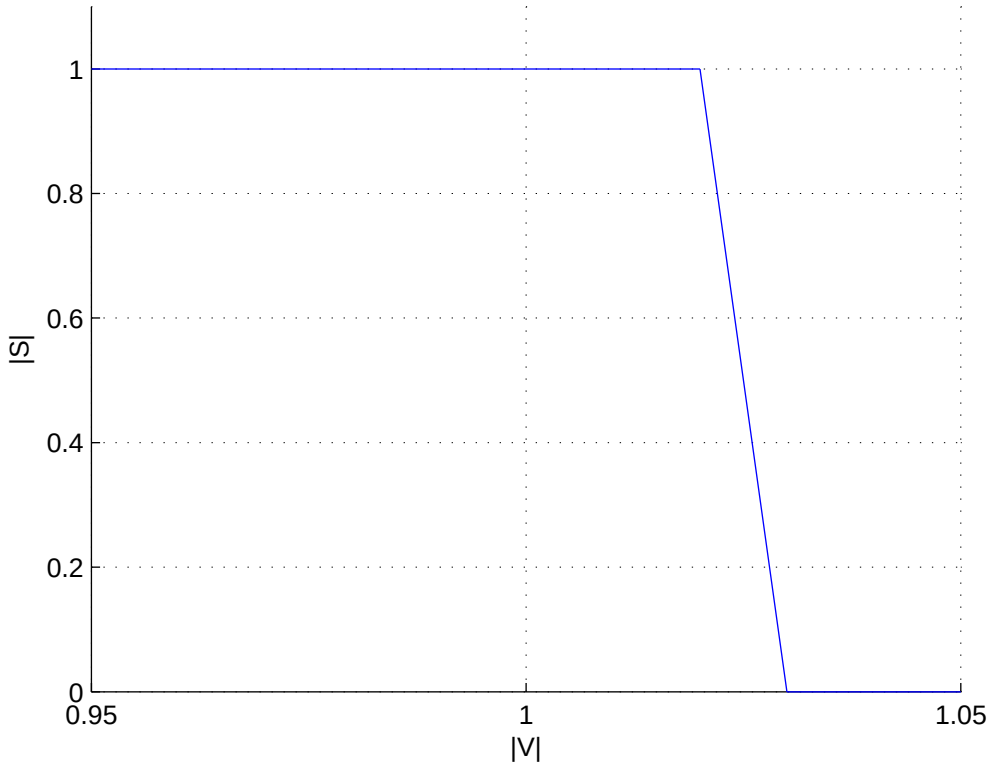

FIGURE 4.2: Proposed OV Mitigation Scheme: Apparent Power and Voltage Magnitude Relationship

$$|\vec{S}| = \begin{cases} S_{\text{available}} & \text{if } |\vec{V}| \leq V_2, \\ \frac{S_{\text{available}}}{V_2 - V_3}(|\vec{V}| - V_3) & \text{if } V_2 \leq |\vec{V}| \leq V_3, \\ 0 & \text{otherwise.} \end{cases} \tag{4.7}$$

The voltage thresholds V_1, V_2 and V_3 are predefined and common to all generators. The relationship $V_{\text{nominal}} < V_1 < V_2 < V_3 <= V_{\text{limit}}$ must be satisfied, but there is a considerable degree of freedom otherwise. The real and reactive set points can be determined from (4.8) and (4.9).

$$P = |\vec{S}|\text{p.f.} \tag{4.8}$$

$$Q = |\vec{S}|\sqrt{1 - \text{p.f.}^2} \tag{4.9}$$

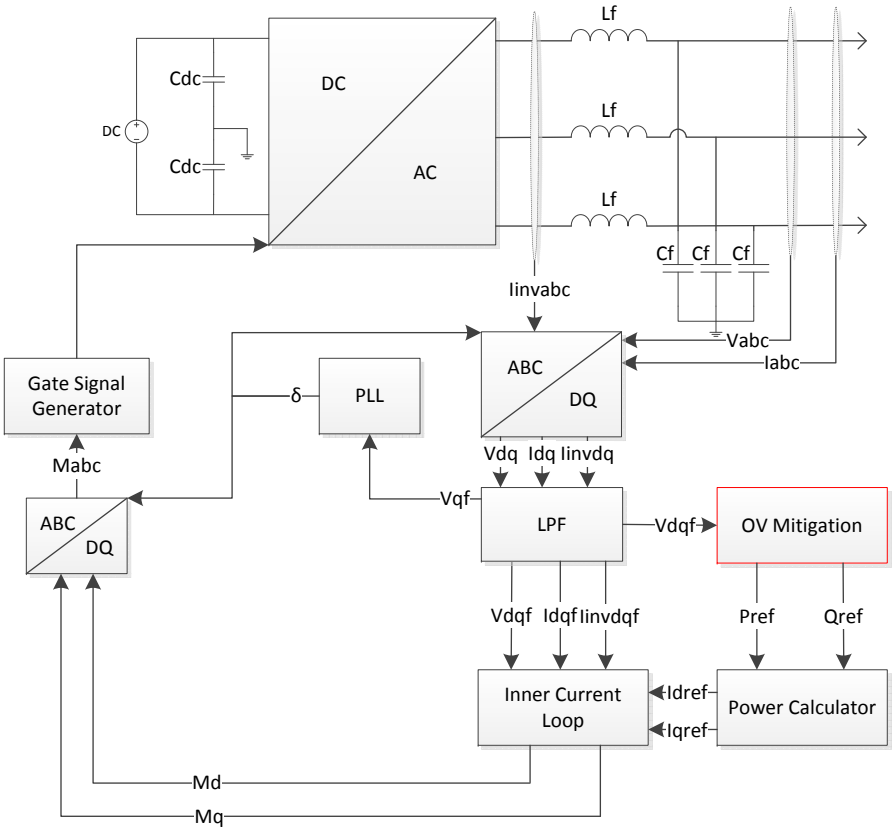

FIGURE 4.3: Grid-Connected Controller with OV Mitigation

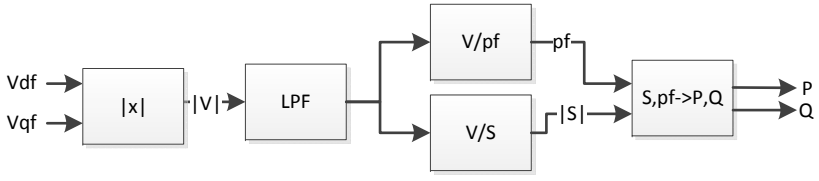

FIGURE 4.4: OV Mitigation Control Block

These power set points are then exported to a typical constant power inverter control system to determine the gating signals for the power electronic switches. The modified grid connected controller is shown in Fig. 4.3. The contents of the OV mitigation block are shown in Fig. 4.4.

The $|x|$ block computes the voltage magnitude using (4.10).

$$|V| = \sqrt{\frac{3}{2}} \frac{\sqrt{V_{df}^2 + V_{qf}^2}}{V_{\text{base}}} \tag{4.10}$$

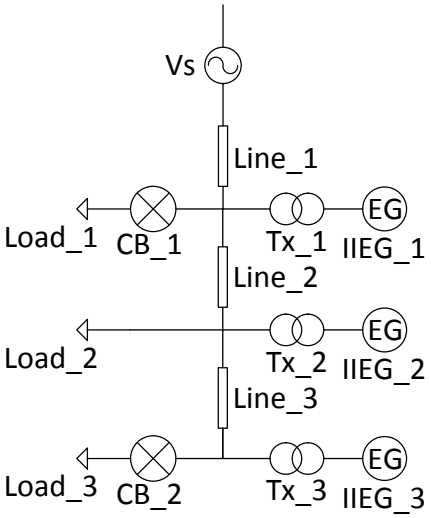

FIGURE 4.5: OV Mitigation Example

The voltage magnitude signal is then passed through a LPF to ensure that any changes in power set points are gradual and unaffected by short term voltage ripples and disturbances in the DN. The power factor, apparent power, real power and reactive powers are then calculated by (4.6), (4.7), (4.8) and (4.9), respectively. The remainder of the controller is identical to the grid-connected controller outlined in Chapter 3, emphasising the minimal alterations of the controller required to employ the proposed OV mitigation scheme.

4.2.2 OV Mitigation Simulation

An example network as shown in Fig. 4.5 has been constructed to demonstrate in principle how the OV mitigation scheme should operate. The network data is given in Table 4.2.

Transformers Tx_2 and Tx_3 are tapped up to exaggerate the problem in a small network. In practice, transformers are tapped up in rural locations where a significant voltage drop is present in the network. When lightly loaded and a significant grid-connected EG penetration is present, considerable OV can arise. The OV mitigation scheme aims to alleviate instances of OV without penalising EG proprietors connected to strong segments of the network. The chosen thresholds are used for demonstration purposes only and do not reflect the preferred voltage thresholds. In Australian DNs, the acceptable low voltage

TABLE 4.2: OV Mitigation Example Data

Infinite Bus Data			
Voltage l-l rms (kV)	11000		
Frequency (Hz)	50		
Line Data			
Line No.	1	2	3
Resistance (Ω)	1	5	10
Inductance (mH)	0.01	0.05	0.1
Transformer Data			
Transformer No.	1	2	3
Primary Voltage l-l rms (V)	11000	11000	11000
Primary Winding Resistance (Ω)	0.1	0.1	0.1
Primary Winding Inductance (mH)	0.1	0.1	0.1
Primary Connection	Delta	Delta	Delta
Secondary Voltage l-l rms (V)	400	404	408
Secondary Winding Resistance (Ω)	0.1	0.1	0.1
Secondary Winding Inductance (mH)	0.1	0.1	0.1
Secondary Connection	Wye-earthed	Wye-earthed	Wye-earthed
Load Data			
Load No.	1	2	3
Real Power (kW)	20	15	50
IIEG Data			
IIEG No.	1	2	3
DC Voltage (V)	1000	1000	1000
Switching Frequency (kHz)	4	4	4
Filter Inductance (mH)	20.41	20.41	20.41
Filter Capacitance (μF)	3.316	3.316	3.316
Power Setpoint (kVA)	10	10	10
Low Pass Filter Cut-Off Frequency (Hz)	10	10	10
OV Mitigation Voltage Thresholds	V1=1.01	V2=1.02	V3=1.03
$\text{p.f.}_{\text{limit}}$	0.85		
$\lvert\vec{S}\rvert$	1 p.u.		

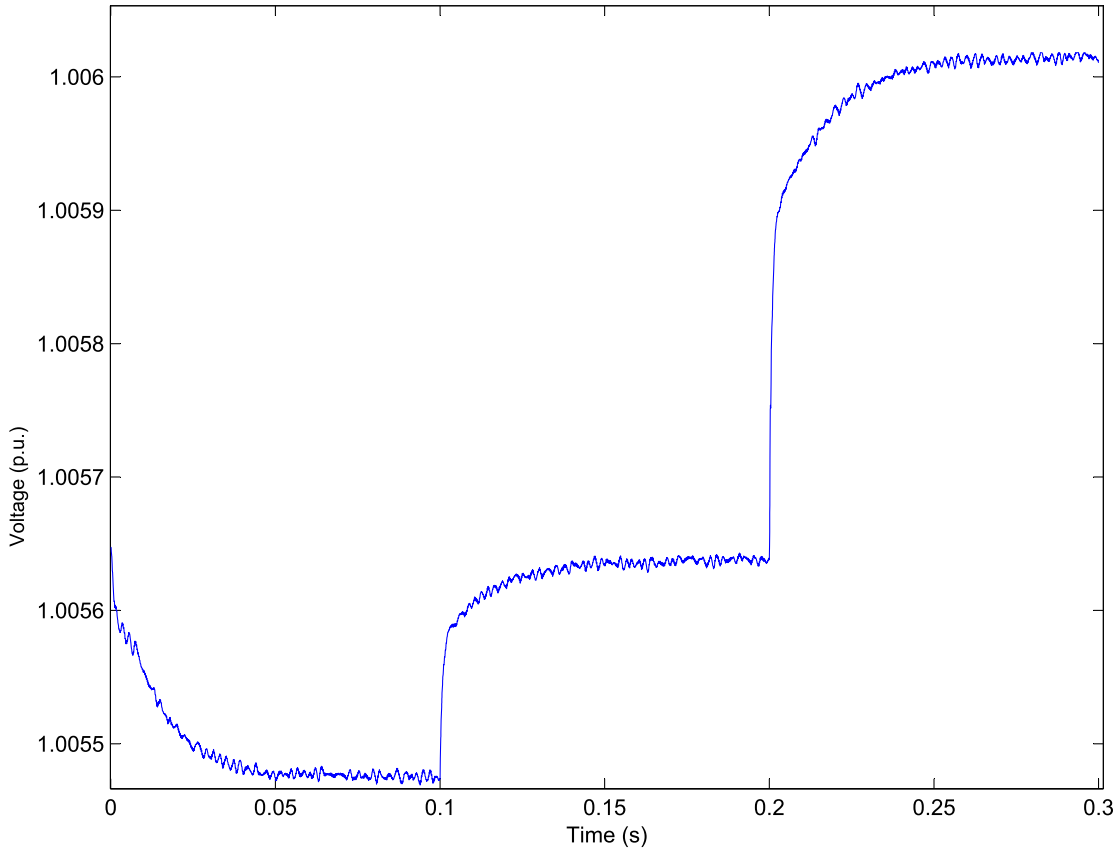

FIGURE 4.6: OV Mitigation Example – IIEG_1 Voltage

range is 230 V (+10 % -6 %) [101]. Hence, a more reasonable range of voltage curtailment might be $V1 = 1.08$ p.u., $V2 = 1.09$ p.u. and $V3 = 1.1$ p.u..

Load 1 is isolated at t=0.1 seconds and Load 3 is isolated at t=0.2 seconds. The voltage magnitude and power export of IIEG_1 are given in Fig. 4.6 and Fig. 4.7, respectively. The voltage magnitude of at the POC of IIEG_1 does not exceed the first voltage threshold of 1.01 p.u.; hence no reactive power absorption nor apparent power curtailment is necessary. The real power and reactive power set points are fixed at 10 kW and 0 kVAr, respectively. The controller maintains the power export as desired. The ripple is a consequence of the imperfect attenuation of the harmonics induced by the power electronics interface. The ripple shown is further reduced by the inductance of the transformer before the power is exported into the network.

The voltage magnitude and power export of IIEG_2 are given in Fig. 4.8 and Fig. 4.9, respectively. The voltage magnitude of IIEG_2 remains within the first two thresholds

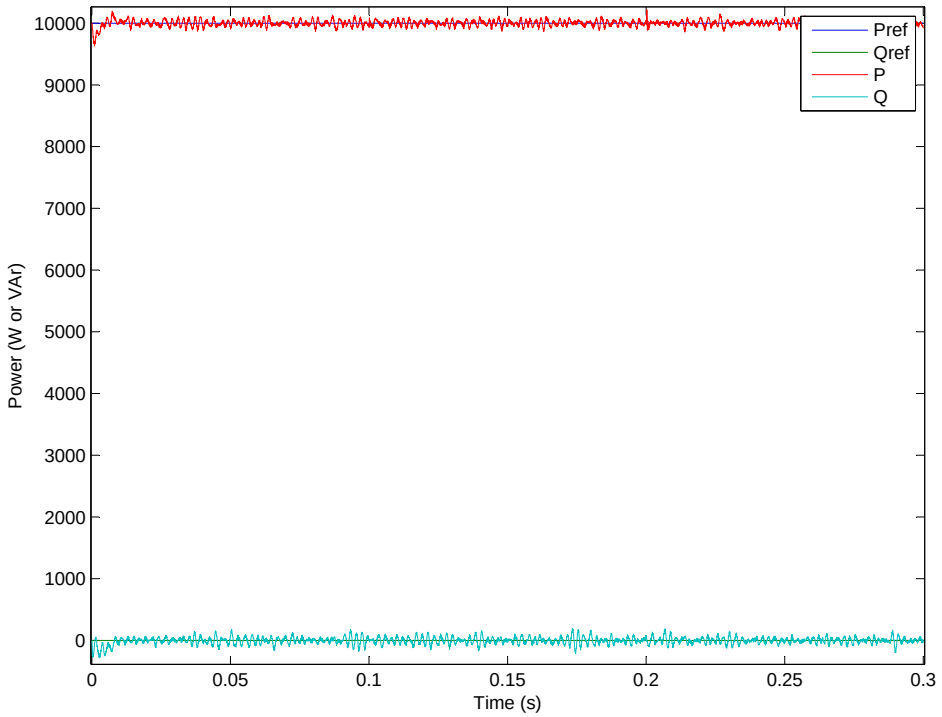

FIGURE 4.7: OV Mitigation Example – IIEG_1 Power

$V1$ and $V2$ throughout all disturbances. Hence, the real and reactive power set points are governed by (4.11) and (4.12). The response to changes in load is consistent the expectations of the OV mitigation scheme. The power export of IIEG_2 follows the power reference set points with significant accuracy.

$$|\vec{S}| = S_{\text{available}} \tag{4.11}$$

$$\text{p.f.} = \frac{1 - \text{p.f.}_{\text{limit}}}{V_1 - V_2}(|\vec{V}| - V_1) + 1 \tag{4.12}$$

The voltage magnitude and power exports of IIEG_3 are given in Fig. 4.10 and Fig. 4.11, respectively. The voltage magnitude remains between thresholds $V1$ and $V2$ for the first two loading states and then extends beyond $V2$ for the final loading state. Therefore, for the first two loading conditions, the real and reactive power set points are governed by (4.11) and (4.12) as with IIEG_2. However, after load 3 is isolated, the real and reactive power set points are governed by (4.13) and (4.14). The power set points follow these

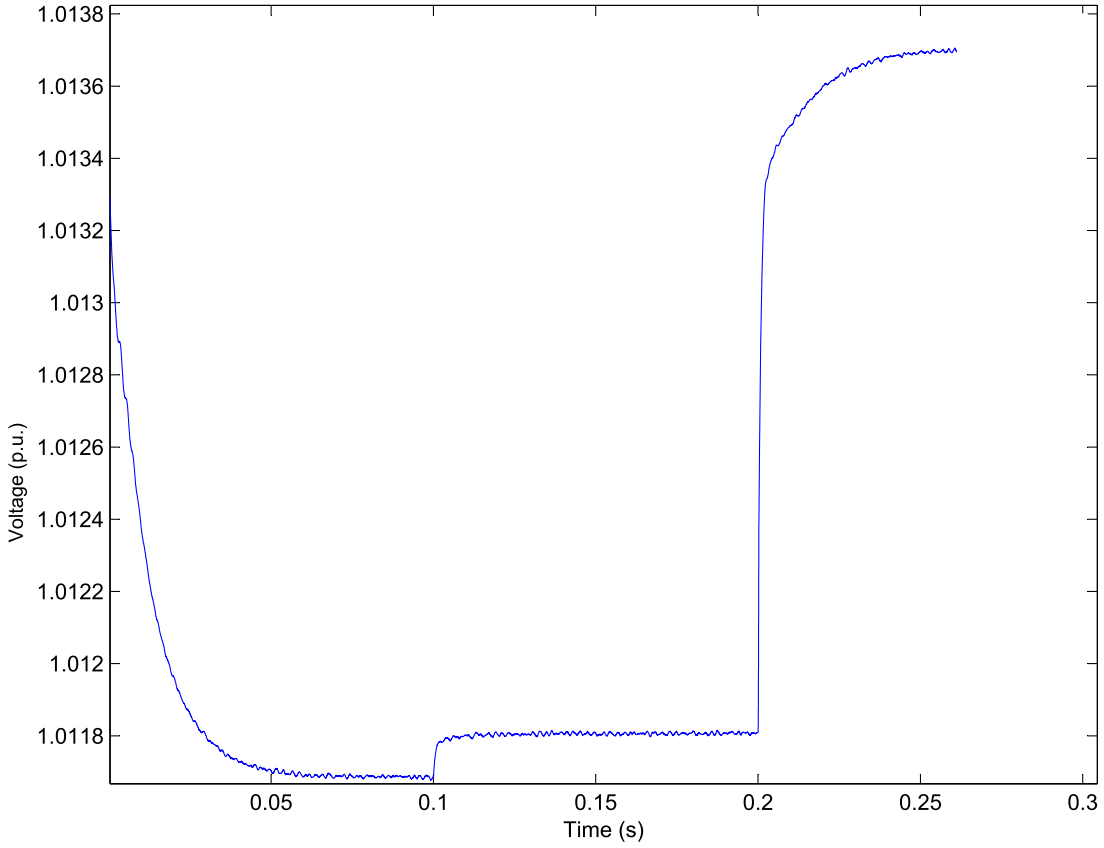

FIGURE 4.8: OV Mitigation Example – IIEG_2 Voltage

governing equations as expected. Further, the power export of IIEG_3 closely matches the power set points. Hence, the IIEG unit's controller provides reactive power absorption and apparent power curtailment consistent with the OV mitigation scheme.

$$\text{p.f.} = \text{p.f.}_{\text{limit}} \tag{4.13}$$

$$|\vec{S}| = \frac{S_{\text{available}}}{V_2 - V_3}(|\vec{V}| - V_3) \tag{4.14}$$

The same network was simulated with the OV mitigation scheme turned off. The voltage magnitudes at IIEG_1, IIEG_2 and IIEG_3 are shown in Fig. 4.12, Fig. 4.13 and Fig. 4.14. The power set points of each IIEG unit are fixed where the customer is exporting the maximum allowable real power and no reactive power irrespective of the voltage magnitude.

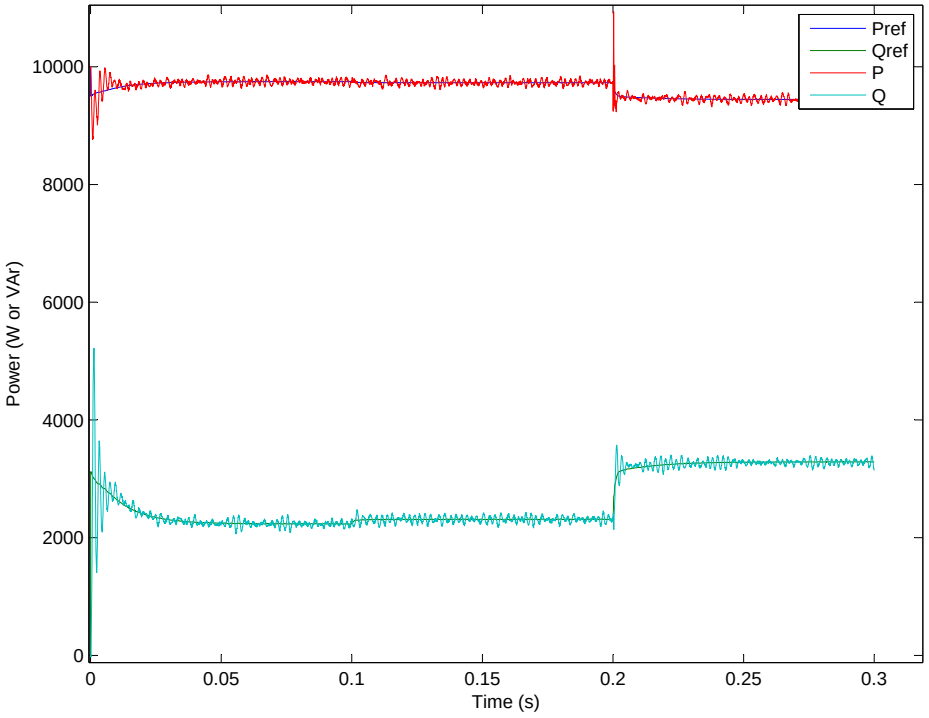

FIGURE 4.9: OV Mitigation Example – IIEG_2 Power

The voltage magnitude increases when the OV mitigation scheme is turned off because IIEG_2 and IIEG_3 are exporting more real power (and absorbing no reactive power) than in the previous case, raising the voltage profile of the entire feeder. Hence, implementation of the OV mitigation scheme has reduced the voltage profile of the DN. All IIEG units must implement the proposed OV mitigation scheme to ensure power exports are fair and the voltage remains within acceptable bounds. The scheme will naturally permit a greater power export and therefore greater financial remuneration for IIEG unit's connected to stronger segments of a DN. Hence, the scheme also encourages IIEG connection at stronger segments of a feeder and an increased financial incentive for upgrades of power lines.

4.2.3 Conclusion

The proposed OV mitigation scheme has been shown to operate effectively within the simulation environment. The are a wide array of advantages of the proposed scheme, including:

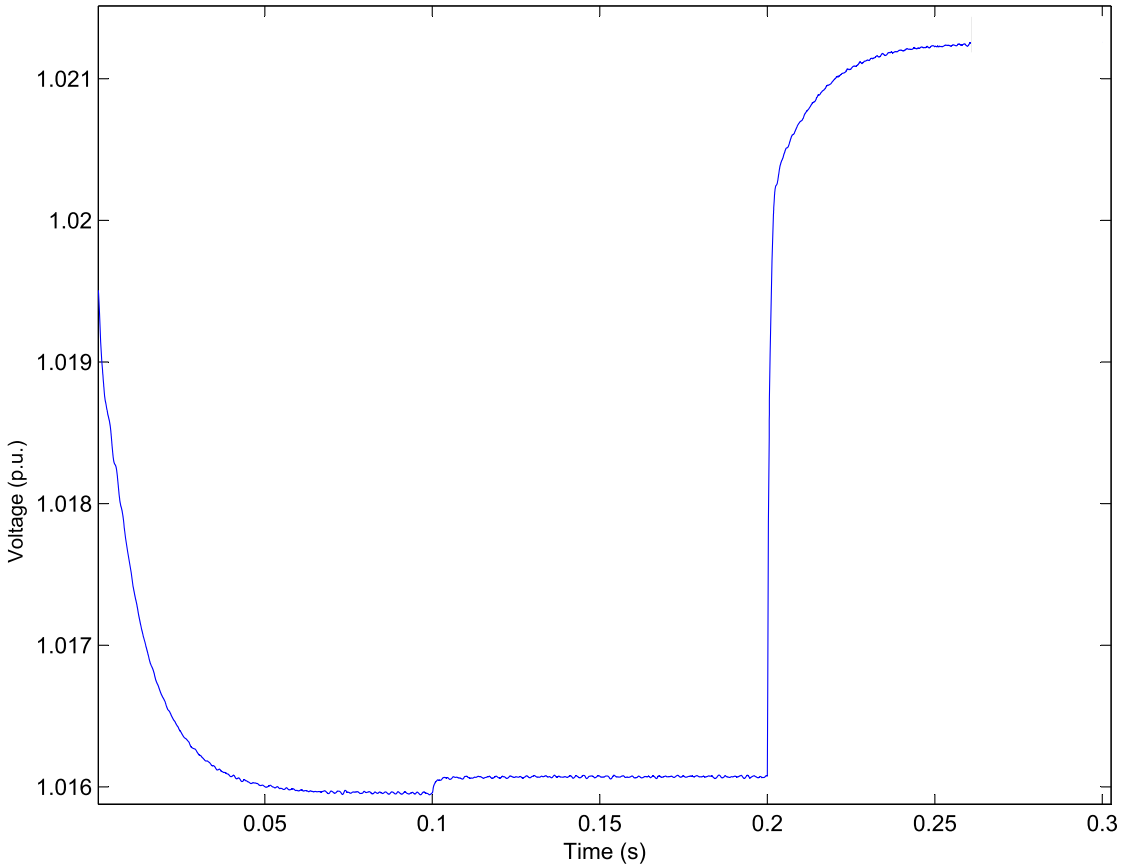

FIGURE 4.10: OV Mitigation Example – IIEG_3 Voltage

- the scheme requires only a small modification of contemporary IIEG unit controllers.
- there exists no reliance of communications infrastructure for the scheme to operate correctly.
- a knowledge of sensitivity matrices or network data is not required.
- each IIEG unit can be installed in a plug-and play fashion. No recalibration is necessary upon modifications of the overall DN.
- the scheme automatically restricts power export based on local load availability and the short circuit impedance of the POC. The voltage thresholds must be common to all EG units to ensure the scheme is fair for all proprietors.

The suitability of the proposed scheme in practical applications requires further exploration. In particular, the effects of the scheme on the economic suitability of IIEG requires

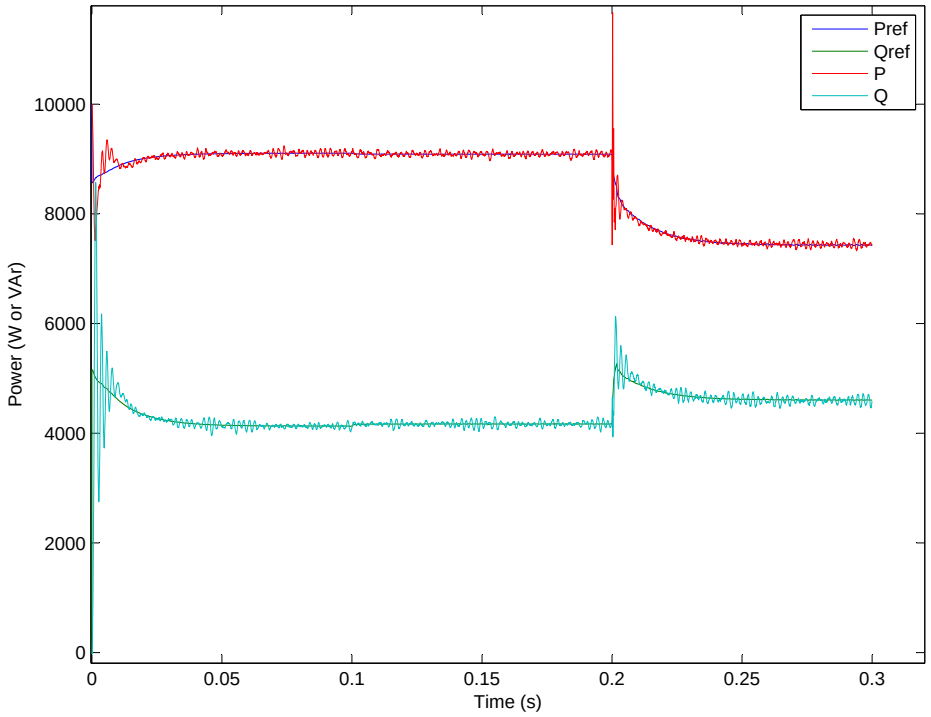

FIGURE 4.11: OV Mitigation Example – IIEG_3 Power

further exploration. Furthermore, the proposed scheme may have a negative impact on the efficacy of anti-islanding protection. However, since the controller is incapable of exporting reactive power, it is very unlikely that the available generation will exactly match the demands of a load which normally absorbs reactive power. A sufficient frequency deviation that will active passive anti-islanding protection is very likely. The small non-detection zone of the passive anti-islanding protection scheme can be eliminated through use of an appropriate frequency-based active anti-islanding protection selection.

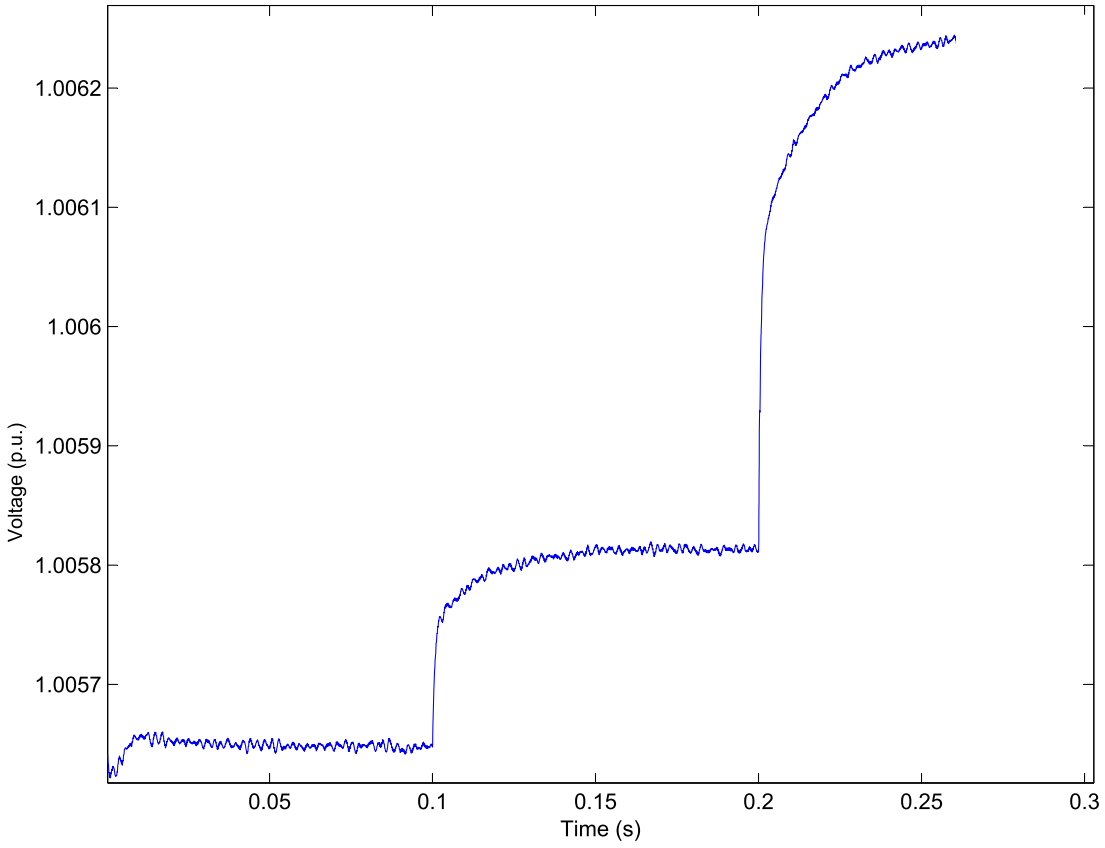

FIGURE 4.12: OV Mitigation Example – IIEG_1 Voltage with OV Mitigation Turned Off

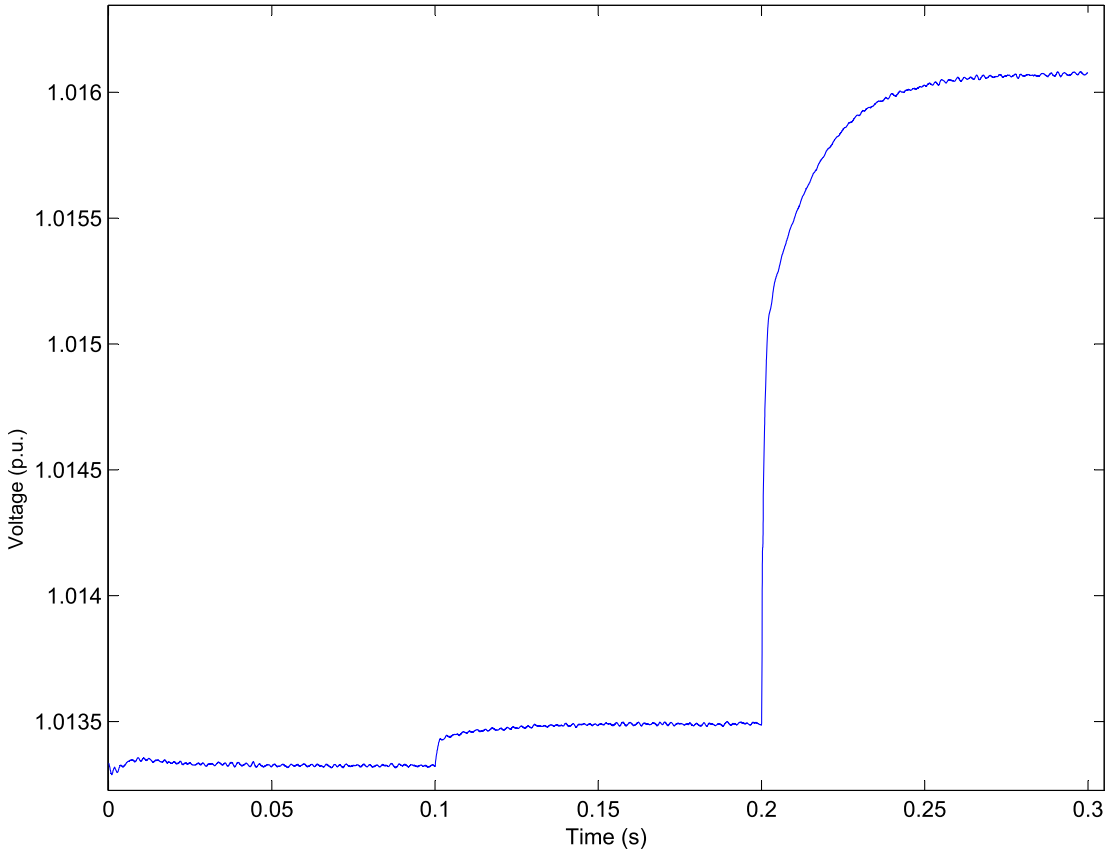

FIGURE 4.13: OV Mitigation Example – IIEG_2 Voltage with OV Mitigation Turned Off

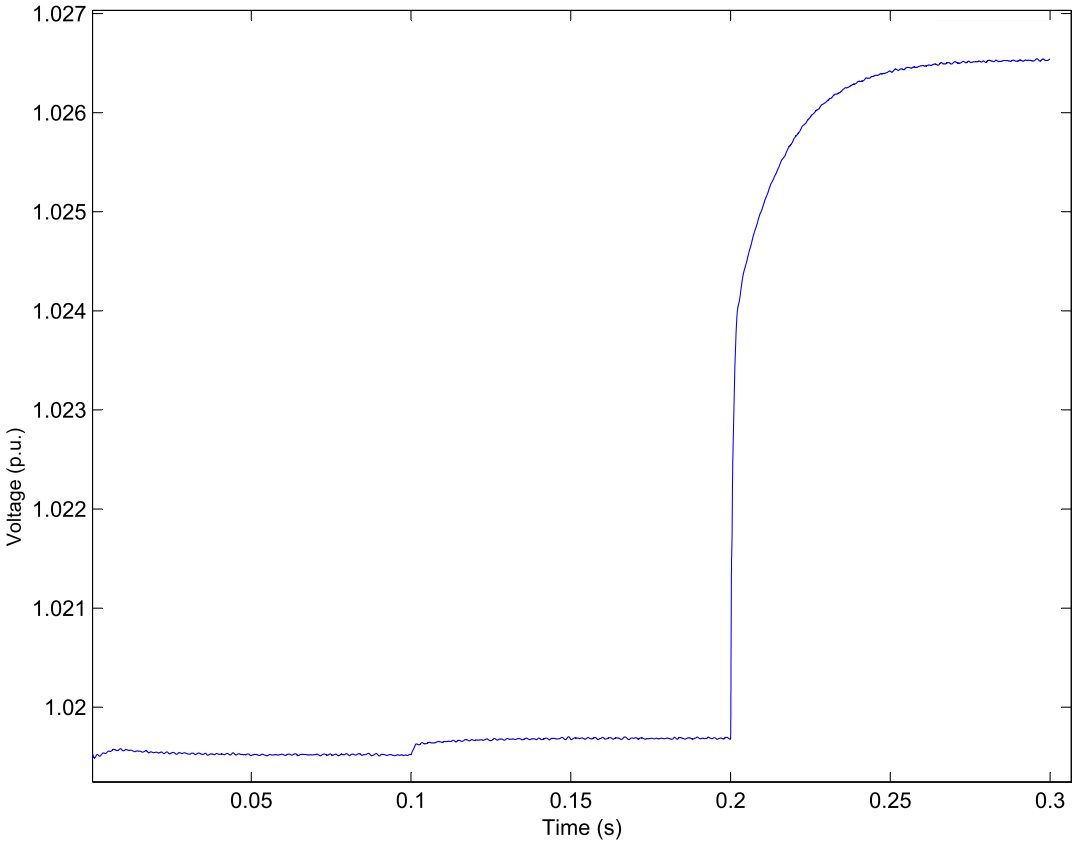

FIGURE 4.14: OV Mitigation Example – IIEG_3 Voltage with OV Mitigation Turned Off

Chapter 5

Fault Analysis Tools

5.1 Introduction

One of the significant contributions of this Thesis is the development of a fault analysis platform suitable for DNs with a high EG penetration. Traditional fault analysis techniques were predicated on the notion of radial power flow from large-scale synchronous generators. The application of fault analysis techniques is common practice in modern protection design. Presently, the low EG penetration levels in DNs are insufficient to adversely affect protection setting practices using radial techniques. In fact, the IEEE Standard [21] states that EG must not impact the normal operation of protective devices, which implies that EG must not invalidate the efficacy of traditional fault analysis techniques. However, as EG penetrations rise, international standard reform will be required to sustain the proliferation of small and medium-scale renewable energy resources. In such a case, improved fault analysis techniques that encompass EG fault response will be required.

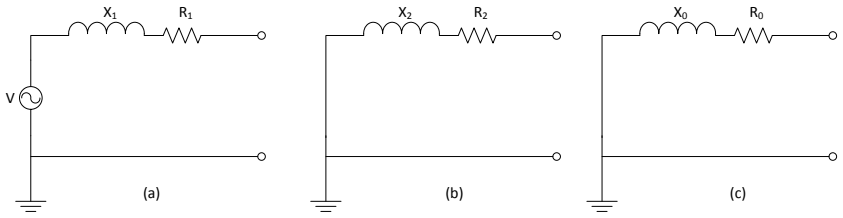

FIGURE 5.1: (a) Positive Sequence Equivalent Circuit (b) Negative Sequence Equivalent Circuit (c) Zero Sequence Equivalent Circuit

5.2 Traditional Fault Analysis Techniques

Traditional fault analysis techniques of DNs typically employ sequence component Thévenin equivalent circuits for all power infrastructure upstream of the analysed feeder. The equivalent circuits are shown in Fig. 5.1.

Sequence components allow the parameters of three-phase networks to be expressed as a set of three sequence parameters. The transformation between phase and sequence components can be achieved using (5.1) and (5.2).

$$\begin{bmatrix} F_a \\ F_b \\ F_c \end{bmatrix} = \begin{bmatrix} 1 & 1 & 1 \\ 1 & a^2 & a \\ 1 & a & a^2 \end{bmatrix} \begin{bmatrix} F_0 \\ F_1 \\ F_2 \end{bmatrix} \tag{5.1}$$

$$\begin{bmatrix} F_0 \\ F_1 \\ F_2 \end{bmatrix} = \frac{1}{3} \begin{bmatrix} 1 & 1 & 1 \\ 1 & a & a^2 \\ 1 & a^2 & a \end{bmatrix} \begin{bmatrix} F_a \\ F_b \\ F_c \end{bmatrix} \tag{5.2}$$

The character a is the unit vector at 120^o, that is $a = 1\angle 120^o$ and F can be replaced by any three-phase vector quantity such as voltage and current. The equivalent sequence component circuits can then be concatenated according to the fault type [102]. The use of sequence components greatly simplifies the process of approximating the fault current drawn for any given fault type and location.

Adjacent feeders are generally omitted when determining the Thévenin equivalent circuit upstream of a feeder for two reasons. Firstly, there exists no reverse fault current flow in traditional radial DNs. Secondly, the current drawn by the adjacent feeder during a fault is negligible compared to the fault current. The reactance of the Thévenin equivalent circuit is generally determined by (5.3).

$$X = \frac{S_b}{SCC} \tag{5.3}$$

Where X is the equivalent per unit reactance of a bolted three-phase fault, SCC is the short circuit capacity in MVA and S_b is the apparent power base in MVA, typically 100 MVA. The assumptions made in (5.3) are:

- The prefault voltage is 1 p.u. and;
- Voltage bases are equal to voltage ratings.

Generally, the reactance X is adopted as the positive and negative sequence impedance for the Thévenin equivalent circuit upstream of the DN for fault analysis. Assuming the zone substation transformer is wye-earth connected, upstream zero sequence data is not required for earth fault analysis in DNs.

The inclusion of EG subverts the premise of radiality implemented in fault analysis within DNs. In order to gain an understanding of the fault response of a DN with a high EG penetration using sequence components, a sequence component representation of each component within the DN is required. The derivations of sequence component representations of synchronous generators, power lines, transformers and loads are well established and are commonly used within protection design practice.

5.2.1 Sequence Representation of Earth Impedances

Generators, transformers and loads can be connected in multiple configurations including delta, wye and zig-zag. Furthermore, the earthing connection can have a significant

impact from a protection perspective. Generally speaking, the connection type of power infrastructure does not have an effect on positive and negative sequence representations of that power infrastructure. However, zero sequence currents are significantly affected by phase and earth connections.

Zero sequence currents are in-phase and therefore do not cancel out when connected to an earth-connected star point. The sum of the three zero sequence currents will flow through to earth if an earth connection is available. Given that a star point is connected to earth through impedance Z_e, the total zero sequence impedance $Z_0(\text{total})$ can be expressed as (5.4).

$$Z_0(\text{total}) = Z_0(\text{phase}) + 3Z_e \tag{5.4}$$

Where $Z_0(\text{phase})$ is the zero sequence impedance of each phase connection. If no earthing impedance is used, $Z_e = 0$. If there is no connection to earth at the star point or the power infrastructure is delta-connected, the zero sequence equivalent circuit can be represented as an open circuit.

5.2.2 Synchronous Generators

During three-phase balanced faults, the transient synchronous machine fault current can be calculated by (5.5).

$$i_{ac}(t) = \sqrt{2}E_0[(\frac{1}{X''_d} - \frac{1}{X'_d})e^{-t/\tau''_d} + (\frac{1}{X'_d} - \frac{1}{X_d})e^{-t/\tau'_d} + \frac{1}{X_d}]\sin(\omega t + \delta) + \sqrt{2}\frac{E_0}{X''_d}\sin(\delta e^{-t/\tau_0}) \tag{5.5}$$

X''_d, X'_d and X_d are the direct axis subtransient, transient and steady-state reactances respectively. τ''_d, τ'_d and τ_d are the direct axis subtransient, transient and steady-state time constants respectively. E_0 and δ are the prefault voltage magnitude and angle respectively.

The reactances X''_d, X'_d and X_d can be employed as the positive sequence impedances in a fault analysis. It is often acceptable to choose the direct axis subtransient reactance as the

positive sequence Thèvenin Impedance to simulate fault response as protection systems normally operate within the few cycles [26].

The negative sequence reactance is largely determined by the damper windings of the rotor [3, 26]. The negative sequence impedance is constant throughout subtransient, transient and steady-state response of a synchronous machine. The constant negative sequence impedance is presumed to be close to the positive sequence subtransient reactance in [3], but is chosen to be the average between the direct and quadrature axes subtransient impedance in [26].

The zero sequence impedance of a synchronous machine is approximated to be equal to the leakage reactance X_l. The zero sequence impedance of a synchronous machine is generally very small. In fact, many synchronous generators are unearthed or earthed through an impedance to prevent damage incurred during a single-phase to earth faults at the generator terminals. An unearthed synchronous generator has an infinite zero sequence impedance, represented as an open circuit. A synchronous generator with an earthing impedance Z_e must pass the zero sequence current of each line through the earthing impedance; therefore, the total zero sequence impedance can be expressed as in (5.4).

The decoupling of machines from the grid via a power electronics interface can offer significant flexibility of the transient response of the overall generation system. The proposed controllers chosen in Chapter 3 implement a LPF to determine the transient response on each IIEG. The proposed fault analysis tool presented in this Chapter assumes that the proposed IIEG controllers are employed and are standard across all IIEG units. This assumption greatly simplifies the fault determination process including the transient response without computationally expensive small-signal models.

5.2.3 Power Line Sequence Representation

Most 11 kV three-phase power lines in Australia can be approximated to be balanced. If the power line geometry is consistent irrespective of the phase rotation, the positive

and sequence impedances can be considered equal. The zero sequence impedance can be approximated by (5.6) [3].

$$Z_0 = X_1 + 3\omega(0.2\ln(\frac{D_n}{D}))\text{m}\Omega/\text{km} \tag{5.6}$$

Where D_n is the average distance of the earth of the three phases and D is the average distance of each phase conductor to the other phase conductors.

5.2.4 Power Transformer Sequence Representation

The windings of power transformers can be configured in multiple forms. Winding and earth connections can have a significant impact on the fault response of a DN. Delta-wye transformers yield a 30^o phase shift which does not impact the fault current magnitude and, hence, can be neglected in some analyses where phase is unimportant. The core losses and magnetisation current are in the order of one percent of the rated value and are usually ignored in fault analysis [3]. If there is no earth impedance and the transformer allows the flow of zero sequence current, all sequence component impedances can be approximated to be equal to the leakage impedance Z_l as shown in (5.7) [3].

$$Z_0 = Z_1 = Z_2 = Z_l \tag{5.7}$$

The phase shift of the positive sequence is the complement of the negative sequence phase shift. For example, if the positive sequence HV leads the LV winding by 30^o, the negative sequence HV will lag the LV winding by 30^o. The zero sequence equivalent circuits for each transformer configuration are dependent on the winding and earthing configurations and are shown in Fig. 5.2.

For current to flow in a transformer, there must be a magneto-motive force (mmf) balance between the primary and secondary windings. With the exception of core reluctance, the mmf of the primary winding is equal to the mmf of the secondary winding. The mmf is measured in Ampere-turns and can be expressed as shown in (5.8).

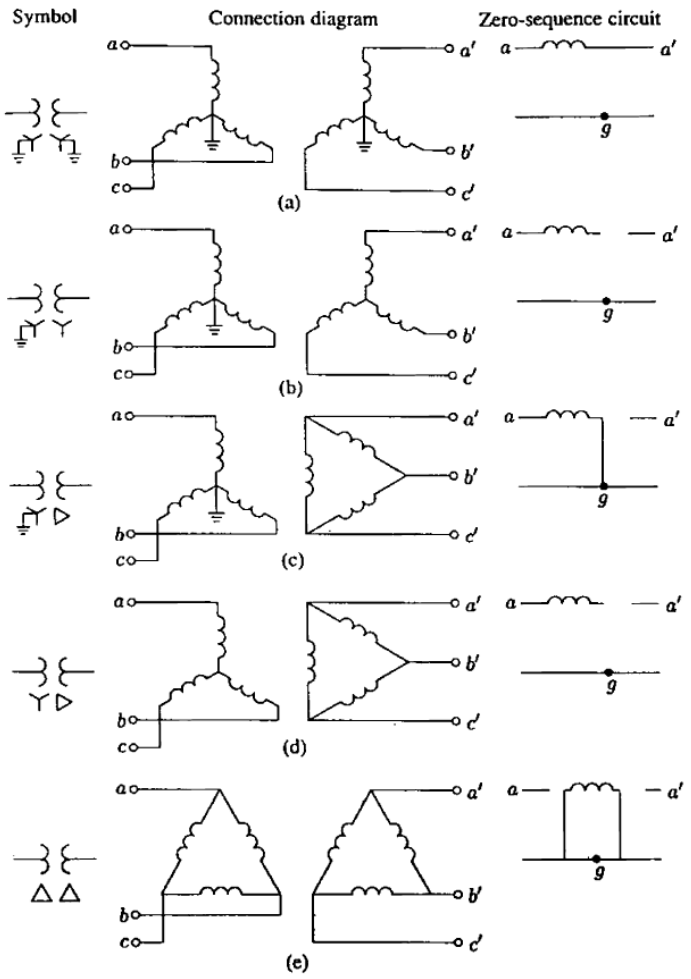

FIGURE 5.2: Zero Sequence Equivalent Circuits of Various Transformer Configurations [3]

$$\text{mmf} = NI \tag{5.8}$$

Where N is the number of turns in a coil and I is the current passing through a coil in amperes. The turns ratios can be accounted for using the per unit system. Ignoring core losses and phase shifts, the per unit current entering the transformer is equal to the per unit current leaving the transformer. Hence, if zero sequence current cannot flow through one winding, no zero sequence current can flow through the other winding irrespective of

winding connection and earthing. By (5.2), the zero sequence current can be calculated as the residual unbalance of phase currents. Hence, the zero sequence equivalent circuits as shown in Fig. 5.2 can be explained as follows:

(a) Wye-earthed to Wye-earthed – Both windings have a path for unbalanced current to flow; therefore, zero sequence current can flow. The mmf of the transformer will ensure that the per unit zero sequence current entering the HV side will leave the LV side. The zero sequence impedance is equal to the leakage impedance as stated in (5.7).

(b) Wye to Wye with one star point earthed or neither – If a wye-connection is not earthed, the sum of all currents must equal zero; therefore, there can be no zero sequence current. As a result, there will be no zero sequence mmf in either winding which suggests that the zero sequence impedance is infinite and best represented as an open circuit.

(c) Wye-earthed to Delta – Zero sequence current may flow in the form of a circulating current in a delta winding as a result of zero sequence mmf from the magnetically-coupled winding. However, no zero sequence current will flow into or out of a delta connection. Hence, an earth path is available to the wye-earthed connection that will allow the flow of zero sequence current as zero sequence mmf can be induced in the delta winding.

(d) Wye to Delta with no earthing point – If a wye-connection is not earthed, the sum of all currents must equal zero; there can be no zero sequence current and no zero sequence mmf. The equivalent circuit is identical to part (b).

(e) Delta to Delta – Both delta windings contain a path for circulating zero sequence current to flow. However, the sum of current flowing into a delta connection must be zero as there is no return path; therefore, the zero sequence current must also be zero by (5.2). Zero sequence current may not enter nor leave a delta-to-delta connected power transformer; subsequently, there is no path for zero sequence current flow from the perspective of the DN.

Transformer connections have a significant impact on the flow of zero sequence current. The transformer connection must be noted when coordinating protection devices across transmission and DNs. However, most power transformers in zone substations in Australia are connected in a Delta to Wye-earthed configuration; a configuration which possesses

two important attributes from a protection perspective. Firstly, zero sequence current cannot flow from the HV line to the LV line across a transformer; hence, the EF protection does not need to be coordinated across the zone substation transformer. Secondly, zero sequence current can flow from the earth connection of the Wye winding to a DN earth fault, allowing EF and SEF protection to detect earth faults within the DN. Therefore, a knowledge of the zero sequence impedance upstream of the Wye-earth winding of the zone substation power transformer is not necessary for DN fault analysis.

Thévenin equivalent circuits are adequate to approximate fault response in traditional DNs as the response time of OC and EF protective devices is usually very fast, typically within the subtransient domain of generator response. Hence, the subtransient reactance of synchronous generators is implemented to define the positive and negative sequence components for fault analysis.

5.2.5 Load Sequence Representation

Positive and negative sequence representations of balanced loads are identical. The zero sequence impedance of a load depends on how the load is connected. If a load is delta or unearthed-wye connected, no zero sequence current will flow as there is no return path for unbalanced currents. Otherwise, the zero sequence impedance can be calculated as in (5.4).

5.2.6 Conclusion

An outline of sequence component analysis is given as a precursor to analysing the behaviour of DNs with a high EG. The contemporary fault analysis techniques used in DNs are heavily standardised and are predicated on assumptions that may not apply in future DNs with significant EG penetration levels. Small-signal models are popular within research when investigating the impacts of IIEG on DNs [53, 61, 82, 103]. However, small-signal models are computationally expensive, require a significant amount of data and are time consuming. The proposed fault approximation tool aims to simplify the fault analysis process with significant accuracy and speed.

5.3 Novel Fault Approximation Tool

5.3.1 Introduction

The increasing prevalence of IIEG in DNs has progressively undermined the efficacy of traditional line protection design philosophy. Many dynamic models have been developed in order to better understand the effects of IIEG on traditional protection design philosophy. However, the development of dynamic models is a time consuming process and IIEG unit design differs significantly across manufacturers. Utilities usually do not possess the time and resources to build a model for each different IIEG unit that is connected to a DN. To simplify to modelling process, this Thesis presents a fault approximation tool (FAT) that utilities may adopt to ease the fault analysis of DNs with a high penetration of IIEG.

The development of dynamic models is a common topic within research. Authors of [74, 104–107] have presented different control diagrams with the common goal of simulating a constant-power, grid-connected IIEG. An accurate representation of the control scheme of an IIEG is of particular importance as there are no innate machine dynamics to govern the fault response. However, utilities may not have access to a detailed representation of an IIEG unit's control scheme and control data may be unavailable. Hence, from the utility perspective, the preferred modelling tool for a grid embedded with IIEG would require minimal IIEG behavioural information yet yield a reasonable representation of the behaviour of the IIEG when exposed to a disturbance.

A simplified modelling tool is presented by [105] using Gauss-Seidel load flow. All phases are investigated independently; hence, it can be inferred that all neutral points are assumed to be earthed. The effect of loads are ignored which may prove problematic when accurate representations of high-impedance faults required. There may also arise convergence issues for significant disturbances within the DN due to a poor selection of initial conditions. A similar tool is proposed by Tu in [86] using minor alterations to Newton-Raphson load flow, which will likely yield similar convergence issues to the tool proposed by [105]. Tu claims that Newton-Raphson solvers are less likely to have divergence issues for fault analysis than Gauss-Seidel solvers. Both authors use sequence components to

simplify the solution process. However, consideration of transformer windings and earthing connections have not been included. The proposed FAT scheme contains allowances for floating neutral points by using KVL in addition to KCL. Convergence issues are also much less likely using the proposed FAT as IIEG current outputs are used as the iterated variable; the initial values can be calculated using fault-instant data without the need of an iterative process.

The EG model in [65] uses a series of approximation methods to determine the sub-transient and transient response of IIEG. The adopted control scheme used to govern the IIDG unit is voltage based and prone to large current deviations between phases during disturbances. The absence of current regulation removes the possibility of fault current limitation and increases the likelihood of nuisance tripping. When deriving the dynamic response of IIEG, a knowledge of the equivalent grid impedance is necessary which may prove complex in a system with many IIEG units and a topologically varying network. The errors observed in the simulations conducted by [65] are much more significant than the results found using the proposed FAT.

IIEG is generally not designed to sustain fault current continuously due to the low thermal inertia of the power electronic switches within the inverter [28]. The fault current capability of an inverter is dependent on the ability of the inverter to draw heat away from the power electronics during a sustained fault. Most contemporary IIEG units are not designed with the explicit intention of providing fault ride-through; hence, fault currents tend to be limited in magnitude and brief in duration. The authors of [29] find that fault current peak magnitudes can vary from 2 to 5 times rated current for 1 to 4.25 milliseconds. The magnitude of the fault current is determined by the grid conditions as well as the characteristics of the IIEG unit. The duration of a significant fault current response is largely governed by the thermal protection of the IIEG unit. A single unified representation of the fault response for the short term transient of an IIEG unit is difficult as the thermal dynamics of the inverter must be accurately modelled in addition to the control and power dynamics of the IIEG and grid. The variety of fault current data gathered by [29] and the range of control schemes presented by authors [74, 104–107] is testament to the impracticality of deriving a unified detailed model for short term transients. The FAT provides a means of approximating the fault response of IIEG for use in analysing DN

line protection schemes without the prerequisite of an in-depth understanding of an IIEG unit's control structure.

5.3.2 Underlying Assumptions within the FAT

The FAT is predicated on the implementation of the grid-connected IIEG control characteristics defined in Chapter 3. The controller includes a feed-forward voltage which is used to ensure fast voltage commutation of the IIEG unit. The control scheme contains a PR controller which has two important advantages over commonly implemented PI controllers: PR controllers have zero steady state error at nominal frequency and do not require knowledge of the AC side filter circuit parameters of the IIEG unit [76]. The control scheme also contains a PLL which determines the phase of the voltage at the IIEG unit's PCC. Both the PR and PLL controllers have very fast tracking capabilities; thus the time delay effects of these controllers are omitted when analysing the transient response of an IIEG in the FAT.

There are two features of the control scheme that dominate the dynamics of the FAT: an LPF after the current controller and the feed-forward voltage signal. The LPF slows the response of the current reference, which implies that the power exported by the IIEG at the instant of a fault will not necessarily be equal to the power set points during the transient response. The use of a feed-forward voltage signal suggests that the voltage commutation of the IIEG is almost instantaneous. From the perspective of DN line protection device operation, the assumption of an instantaneous voltage shift is suitable as the anti-aliasing filters within protection devices attenuate high frequency transients [108].

The algorithm is based on a concatenation of the linearised solver presented in Chapter 3 and a solver based on Newton's method to find the roots of non-linear equations. Convergence issues are less likely to arise using the proposed algorithm than traditional load flow techniques for fault simulation. The key differences between the proposed algorithm and traditional load flow techniques are:

- All loads are modelled as constant impedances rather than constant loads.

- IIEG is treated as a constant current source within the inner loop of the algorithm. The current is manipulated each iteration of the outer loop until the desired power export is present.
- KCL and KVL matrices are employed rather than a Y-bus matrix.
- The variables altered each iteration are the current magnitude and angle, rather than the voltage magnitude and angle.

The benefit of the KVL and KCL matrices is that no reduction to a single line diagram is necessary. All transformer windings and earthing connections are inbuilt in the model; no artificial phase shifting nor reference voltage is necessary anywhere in the network. The alteration of current instead of voltage was chosen as the IIEG controller maintains a balanced current with equal current magnitude across all three phases of the IIEG unit; whereas the voltage across the phases of an IIEG may float. The loads were treated as impedances to reduces the number of iterative variables in the network. However, the loads may be treated as constant power with some minor alterations to the programming. The FAT implements a novel, iterative solver that converges upon IIEG currents instead of all non-slack node voltages as used in the Newton-Raphson load flow solver.

5.3.3 FAT Algorithm

The complete FAT algorithm is expressed as a logic diagram in Fig. 5.3. All IIEG units are allocated an identifying constant. Then, the iterative variable k is reserved as a reference indicating the IIEG unit where the partial differential operator is currently being applied. For example, the partial derivative with respect to $|I_k|$ will yield the partial derivative of all element parameters with respect to the current magnitude of the IIEG unit designated with the same identifier as k. Similarly, the partial derivative with respect to δ_k will yield the partial derivative of all element parameters with respect to the current angle of IIEG unit k.

IIEG units do not possess an inherent inertia. The dynamics of the inverter are therefore governed by the control and protection of the IIEG unit. Within the controller, the voltage

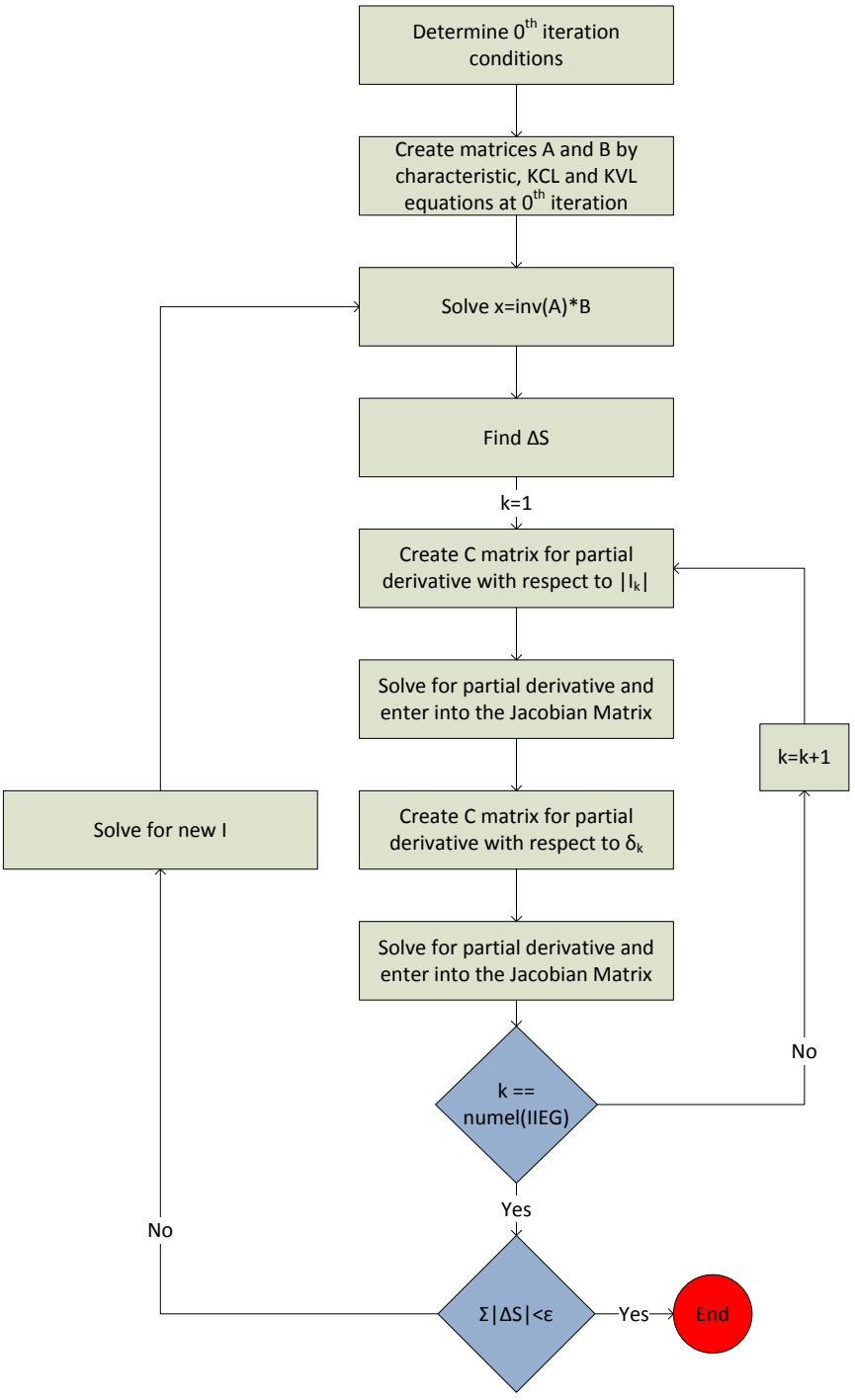

FIGURE 5.3: FAT Flow Chart

signal is passed ahead of the current controller through a feed-forward channel. The feed-forward filter has a much faster response time than the current controller; hence, the IIEG unit will response to changes in voltage must faster than changes in current. From a DN protection perspective, the change in voltage as a result of a fault can be assumed to be instantaneous. The current injected by an IIEG unit will gradually change until the power reference set points allocated within the control scheme are realised. The output of the FAT is an envelope of the transient and steady-state responses of any grid-connected DN. Assuming that the IIEG voltage does not change significantly as the current controller regulates the power export by the IIEG and the protection does not operate, the fault response of an IIEG and envelope generated by the FAT can be accurately represented by (5.9).

$$i(t) = \frac{S^*_{\text{ref}}}{3V^*_{LN_{\text{post-fault}}}} + (I_{\text{IIEG}_{\text{fault-instant}}} - \frac{S^*_{\text{ref}}}{3V^*_{LN_{\text{post-fault}}}}) \exp^{-\omega_c t} \tag{5.9}$$

Where ω_c is the cut-off frequency of the LPF and S_{ref} is the complex power set-point of an IIEG controller. $V_{LN_{\text{post-fault}}}$ is the line-to-neutral post-fault voltage at the PCC of the IIEG unit. $I_{\text{IIEG}_{\text{fault-instant}}}$ is the current supplied by the IIEG at the fault-instant.

In order to utilise (5.9) to approximate the fault response, the pre-fault voltage, $V_{LN_{\text{pre-fault}}}$, of each IIEG unit must be known as well as the steady-state current supplied by each IIEG unit. In order to find the voltage at the fault-instant, each IIEG unit behaves as a constant current source where the current is defined by (5.10); the current can be assumed to be fixed due to the slow nature of the LPF within the IIEG unit's controller. The fault-instant data is a function of the pre-fault data. All three operating states (pre-fault, fault-instant and steady-state) are determined using the FAT.

$$I_{\text{IIEG}_{\text{fault-instant}}} = \frac{S^*_{\text{ref}}}{3V^*_{LN_{\text{pre-fault}}}} \tag{5.10}$$

5.3.3.1 Determination of 0th Iteration Conditions

The algorithm is run twice to solve for the pre-fault condition and steady-state post-fault condition. The 0th iteration variables for the pre-fault condition are selected based on the ratings of each IIEG unit with a current phase angle of 0 degrees. The 0th iteration variables for the steady-state post-fault condition are taken from the fault-instant data. The fault-instant solver does not contain any non-linear functions and, hence, does not require an iterative solver.

5.3.3.2 Characteristic Equations

The network model of N elements is represented as a set of characteristic, KVL and KCL equations as shown in (5.11). The method for deriving the KCL and KVL equations was given in Chapter 3. A network element is defined as one phase of a source, line, load or transformer winding.

$$Ax = B \tag{5.11}$$

Where:

$$A = \begin{bmatrix} \text{characteristic} \\ \text{KCL} \\ \text{KVL} \end{bmatrix}$$

$$x = \begin{bmatrix} V_1 & I_1 & V_2 & I_2 & \dots & V_N & I_N \end{bmatrix}'$$

$$B = \begin{bmatrix} \text{constants} \end{bmatrix}$$

All matrix elements contain vectors unless otherwise specified. The voltages in the x matrix V_1, V_2, ..., V_N are the potential differences across each element (there is no need

for an absolute reference as used in the Newton-Raphson solver). The currents in the x matrix I_1, I_2, ..., I_N are the currents passing through each element. Each line of the characteristic, KCL and KVL matrices are of sizes $\mathbb{C}^{1\times 2N}$ and the constants matrix is of size $\mathbb{C}^{2N\times 1}$.

The characteristic and constant matrices of lines and loads are simple arrangements of Ohm's Law, (5.12).

$$\begin{bmatrix} -1 & Z \end{bmatrix} \begin{bmatrix} V \\ I \end{bmatrix} = \begin{bmatrix} 0 \end{bmatrix} \tag{5.12}$$

Where Z is the impedance of the line or load. An infinite slack bus at element p is represented as a constant voltage, (5.13).

$$\begin{bmatrix} 1 & 0 \end{bmatrix} \begin{bmatrix} V \\ I \end{bmatrix} = \begin{bmatrix} V \end{bmatrix} \tag{5.13}$$

Transformer windings can be connected in any desired configuration. The characteristic equation does not require a knowledge of external winding connections; rather, a three-phase transformer is represented as three single-phase transformers. The determination of the winding connections and subsequent phase shifting is achieved through the KCL and KVL equations. Each of the transformer single-phase equivalents are treated as two separate elements 1 and 2 and, hence, requires two characteristic equations.

$$\begin{bmatrix} -1/Z_m & 1+Z_1/Z_m & 0 & 1/a \\ 1 & -Z_1 & a & aZ_2 \end{bmatrix} \begin{bmatrix} V_1 \\ I_1 \\ V_2 \\ I_2 \end{bmatrix} = \begin{bmatrix} 0 \\ 0 \end{bmatrix} \tag{5.14}$$

Where Z_1 and Z_2 are the primary and secondary winding impedances respectively, Z_m is the magnetising impedance and a is the turns ratio.

The characteristic equation of the IIEG can be determined by (5.15). The value for I_{IIEG} is iterative. For the pre-fault condition, the ratings of each IIEG unit and a 0^o current phase angle are adopted. For the post-fault steady-state condition, the fault-instant data is employed instead.

$$\begin{bmatrix} 0 & 1 \end{bmatrix} \begin{bmatrix} V \\ I \end{bmatrix} = \begin{bmatrix} I_{IIEG} \end{bmatrix} \tag{5.15}$$

5.3.3.3 FAT Outer Loop

Upon concatenating the characteristic equations with KCL and KVL equations, the matrix x as shown in (5.11) can be determined. Once solved, the matrix x contains the voltage and current vectors of all elements for the 0th iterative condition. The next step in determining the steady state currents of the IIEG is finding the error in the power export of each IIEG unit which is calculated by (5.16).

$$\Delta S = \Delta P + j\Delta Q = -S_{\text{ref}} + \sum_{\alpha=a,b,c} V_\alpha I_\alpha^* \tag{5.16}$$

Where $\alpha = a, b, c$ is used as a partial sum iterative variable across all three phases. An application of (5.16) is undertaken for every IIEG unit; each application is concatenated to form the complete ΔS. Each successive iteration of the FAT will correct the output current vector of each IIEG until the total apparent power error $\Sigma|\Delta S|$ is acceptably small.

When the differences between the power exports by the IIEG and the specified set points are acceptably small, the FAT can be terminated. The maximum tolerable gross error is designated ϵ and has been chosen arbitrarily to be 10^{-6}.

If the condition $\Sigma|S| < \epsilon$ is not satisfied, a new value for the current vectors of each IIEG unit must be determined. The complete Jacobian matrix can then be constructed as shown in (5.17). The partial derivatives within the Jacobian matrix are determined within the inner loop of the FAT.

$$\begin{bmatrix} \Delta|I| \\ \Delta\delta_I \end{bmatrix} = \begin{bmatrix} \mathfrak{Re}(\frac{\partial \Delta S}{\partial |I|}) & \mathfrak{Re}(\frac{\partial \Delta S}{\partial \delta_I}) \\ \mathfrak{Im}(\frac{\partial \Delta S}{\partial |I|}) & \mathfrak{Im}(\frac{\partial \Delta S}{\partial \delta_I}) \end{bmatrix}^{-1} \begin{bmatrix} \Delta P \\ \Delta Q \end{bmatrix} \tag{5.17}$$

Given the grid-connected control scheme in Chapter 3 is employed, the current magnitude must be common across all three phases of an IIEG unit and the current phase difference must be 120^o across all phases. Hence, the new IIEG unit's current vectors can be grouped into one reference vector I representing the A phase current. This reference vector is calculated by (5.18). The subscript n refers to the iteration number of the outer loop within the FAT.

$$I_n = (|I_{n-1}| - \Delta|I|) \exp^{j(\delta_{n-1} - \Delta\delta_I)} \tag{5.18}$$

5.3.3.4 FAT Inner Loop

The A and x matrices constructed for (5.11) will be reused for determination of the partial derivatives of x with respect to each IIEG unit current magnitude and phase. However, the matrix of constants will require alteration as the partial derivatives of constants are all equal to zero, with the exception of the elements denoted by k which specify the IIEG currents. The altered matrix of constants is designated as C. When finding the partial derivative with respect to the IIEG current magnitude, the corresponding non-zero constant matrix elements can be calculated as shown in (5.19).

$$C_k = \frac{I_k}{|I_k|} \tag{5.19}$$

The partial derivatives of the network voltage and currents with respect to the IIEG current magnitudes can then be calculated by (5.20).

$$A\frac{\partial x}{\partial |I_k|} = C \tag{5.20}$$

The Jacobian elements can then be calculated by (5.21).

$$\frac{\partial \Delta S_k}{\partial |I_k|} = \sum_{\alpha=a,b,c} \frac{I^*_{k\alpha}}{|I_{k\alpha}|} V_{k\alpha}(I_k) + \sum_{\alpha=a,b,c} I^*_{k\alpha} \frac{\partial V_{k\alpha}(I_k)}{\partial |I_k|} \tag{5.21}$$

All non-diagonal elements are equal to zero. The same method can be used to determine the partial derivatives of the network voltages and currents with respect to the current phase using (5.22), (5.23) and (5.24).

$$C_k = jI_k \tag{5.22}$$

$$A\frac{\partial x}{\partial \delta_k} = C \tag{5.23}$$

$$\frac{\partial \Delta S_k}{\partial \delta_{Ik}} = \sum_{\alpha=a,b,c} -jI^*_{k\alpha} V_{k\alpha}(I_k) + \sum_{\alpha=a,b,c} I^*_{k\alpha} \frac{\partial V_{k\alpha}(I_k)}{\partial \delta_k} \tag{5.24}$$

A set of partial derivatives with respect to all IIEG current magnitude and current angle must be applied. The inner loop iterates k from 1 to the total number of IIEG units, thus satisfying the condition $k == \text{numel}(IIEG)$, before terminating the inner loop.

5.3.3.5 Terminating

Upon the tolerance requirement of the FAT algorithm being satisfied, the gathered data can then be used to extrapolate the pre-fault, transient and steady-state response of each IIEG unit using (5.9). Provisions should be made for an escape sequence if convergence is not achieved within a set number of iterations.

Upon terminating, the FAT produces an envelope to be superimposed with small-signal analysis. The following simulations shall demonstrate the strengths and limitations of the FAT.

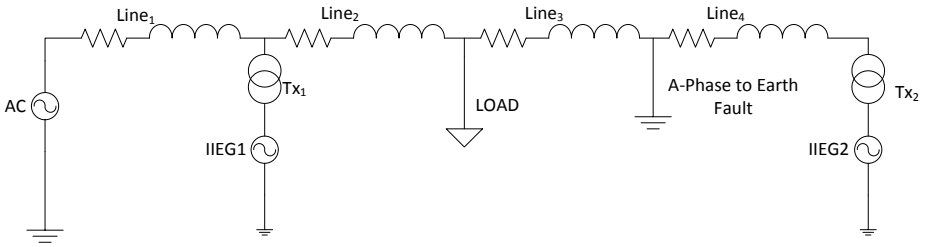

FIGURE 5.4: Example Network

5.3.4 Simulation

A simulation of an example network shown in Fig. 5.4 was implemented to verify the FAT against an equivalent small-signal model. Fig. 5.4 is a single line diagram of a three-phase system. The details of the example network are given in Table 5.1. The details are chosen to represent plausible conditions for a simple system with a high EG penetration but are otherwise arbitrary.

All plots employing the FAT contain a small-signal waveform and corresponding envelope for each parameter. All envelope colours match the colour of the corresponding small-signal waveform. Note that in cases on balanced networks, envelopes may overlap as only the parameter magnitude are considered in each plot.

5.3.4.1 Simulation I

The first simulation involved a single-phase to earth fault on phase A as indicated in Fig 5.4 at 0.15 s. The current and voltage waveforms of IIEG1 are given in Figs. 5.5 and 5.6. The current and voltage waveforms of IIEG2 are given in Figs. 5.7 and 5.8. The sinusoidal waveforms are the results of the small-signal model and the enveloping curves are the voltage and current magnitude outputs of the FAT. The plot measurement points are located at the PCC of IIEG1 and IIEG2. All voltages are measured in a line-to-line fashion.

TABLE 5.1: Example Network Data

Infinite Bus Data				
Voltage l-l rms (kV)	11000			
Frequency (Hz)	50			
Line Data				
Line No.	1	2	3	4
Resistance (Ω)	0.3	0.3	0.3	0.003
Inductance (mH)	3	3	3	0.3
Transformer Data				
Transformer No.	1		2	
Primary Voltage l-l rms (V)	11000		11000	
Primary Winding Resistance (Ω)	0.003		0.0003	
Primary Winding Inductance (mH)	1		0.5	
Primary Connection	Delta		Delta	
Secondary Voltage l-l rms (V)	400		400	
Secondary Winding Resistance (Ω)	0.003		0.0001	
Secondary Winding Inductance (mH)	1		0.2	
Secondary Connection	Wye-earthed		Wye-earthed	
Load Data				
Real Power (kW)	200			
Reactive Power (kVAr)	10			
Note: The resistance and inductance of the load are connected in parallel.				
IIEG Data				
IIEG No.	1		2	
DC Voltage (V)	800		800	
Switching Frequency (kHz)	4		4	
Filter Inductance (mH)	16.33		16.33	
Filter Capacitance (μF)	3		3	
Power Setpoint (kVA)	10+j0		10+j0	
Low Pass Filter Cut-Off Frequency (Hz)	10		10	
Fault Data				
Simulation No.	I		II	
Fault time (s)	0.15		0.15	
Fault type	A phase to earth		A phase to B phase	
Fault impedance (Ω)	0.0001+j0		0.001+j0	

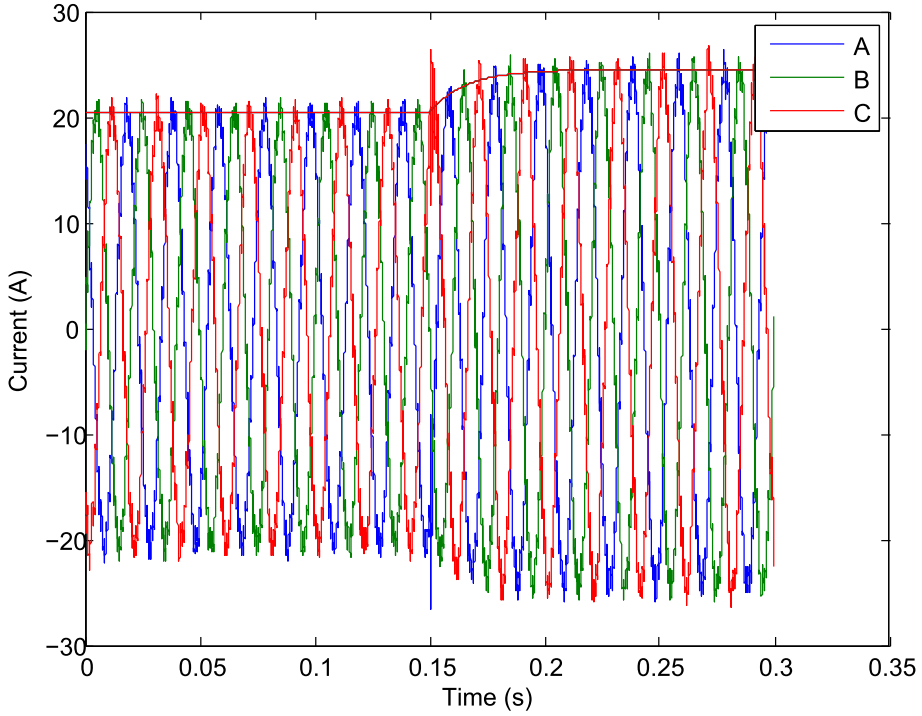

FIGURE 5.5: FAT Simulation I: Single-phase to Earth Fault – IIEG1 Current Comparison

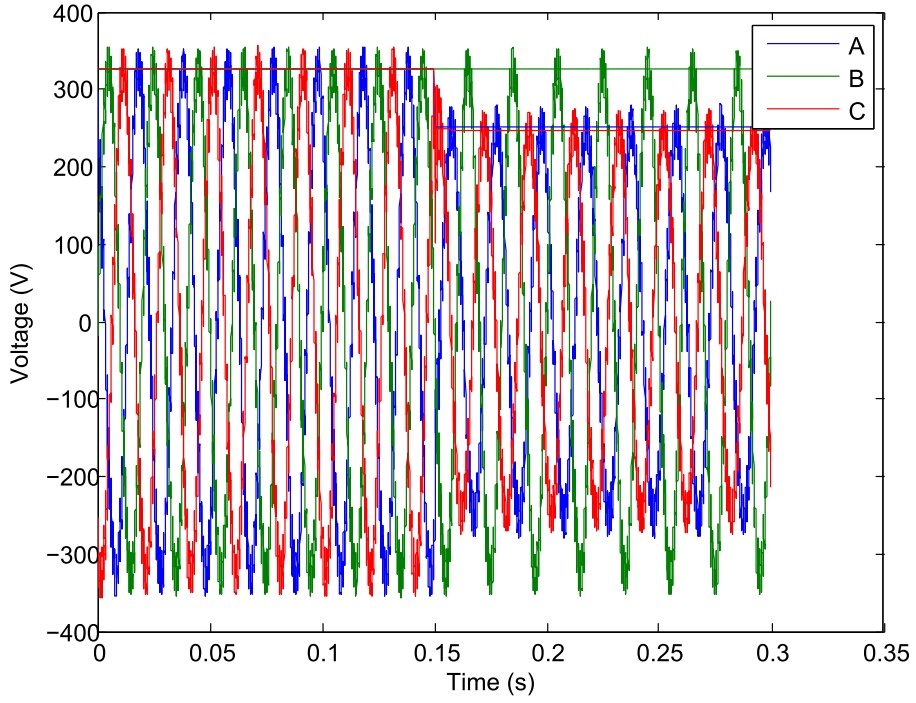

FIGURE 5.6: FAT Simulation I: Single-phase to Earth Fault – IIEG1 Voltage (Line-to-Line) Comparison

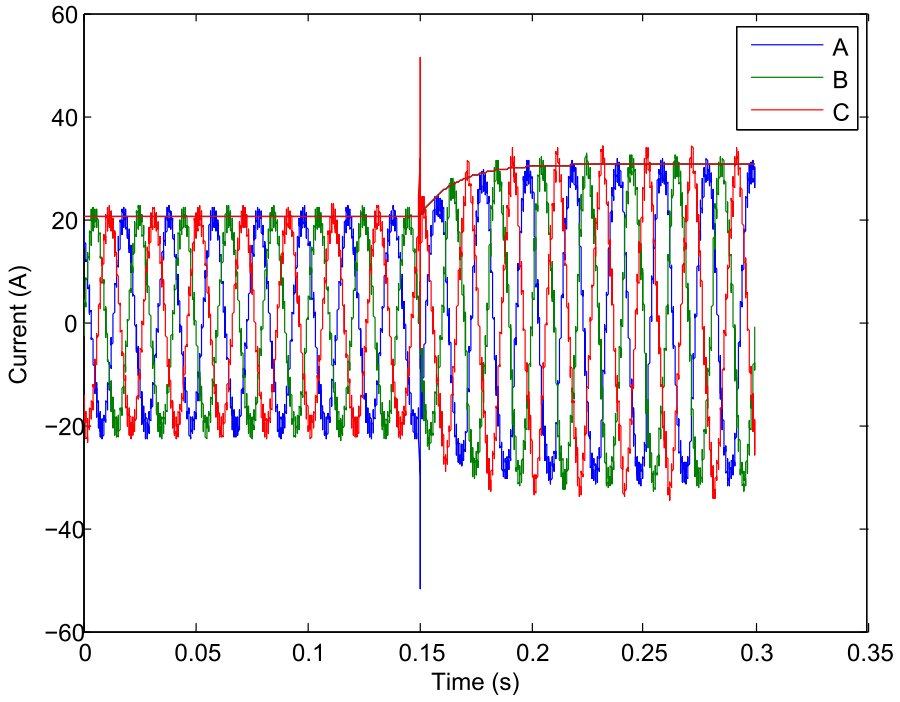

FIGURE 5.7: FAT Simulation I: Single-phase to Earth Fault – IIEG2 Current Comparison

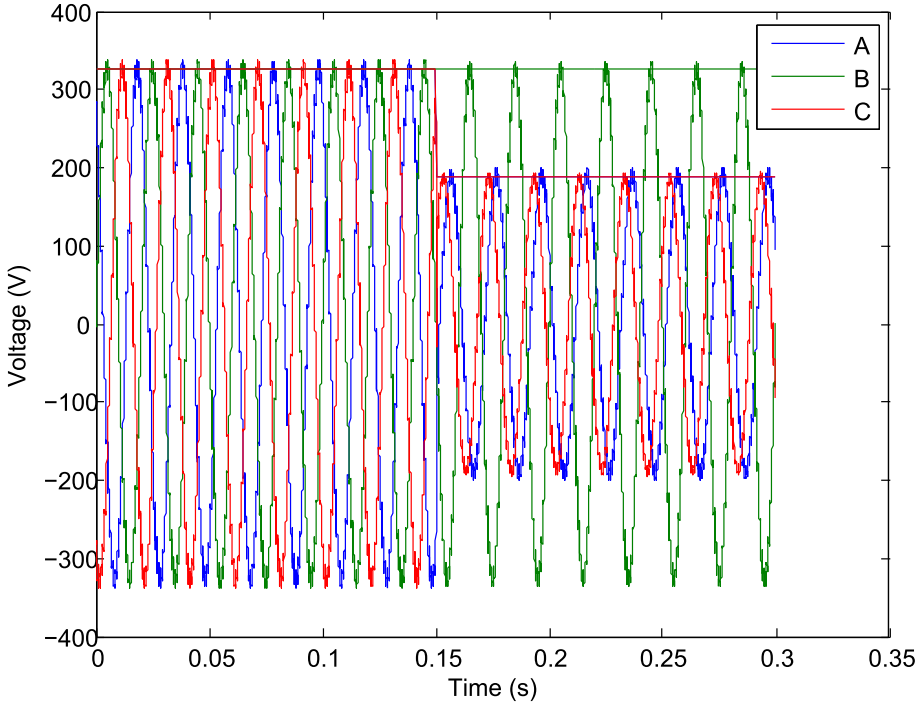

FIGURE 5.8: FAT Simulation I: Single-phase to Earth Fault – IIEG2 Voltage (Line-to-Line) Comparison

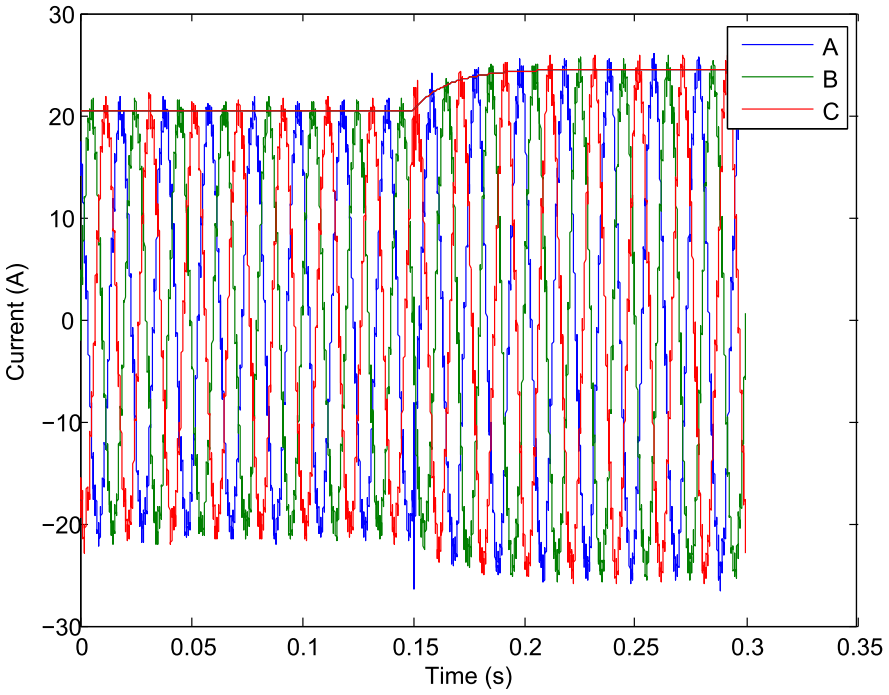

FIGURE 5.9: FAT Simulation II: Line-to-Line Fault – IIEG1 Current Comparison

5.3.4.2 Simulation II

The second simulation involved a line-to-line fault at the same location between phases A and B at 0.15 s. The current and voltage waveforms of IIEG1 are given in Fig. 5.9 and Fig. 5.10. The current and voltage waveforms of IIEG2 are given in Fig. 5.11 and Fig. 5.12.

5.3.4.3 Analysis

The results of the simulations show that the FAT data envelope closely matches the corresponding small-signal waveforms in both steady-state and transient responses. The consistency of the small-signal waveforms and FAT envelopes suggests that the FAT is accurately calculating the pre-fault, fault-instant and post-fault data and the transient response can be accurately represented by (5.9). Hence, the transient response is dominated by the LPF.

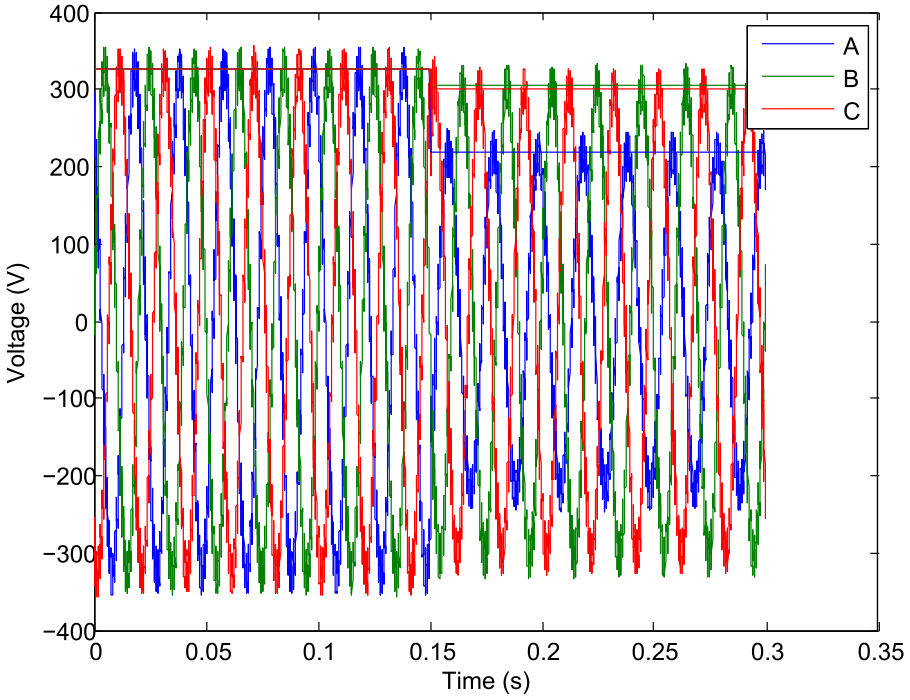

FIGURE 5.10: FAT Simulation II: Line-to-Line Fault – IIEG1 Voltage (Line-to-Line) Comparison

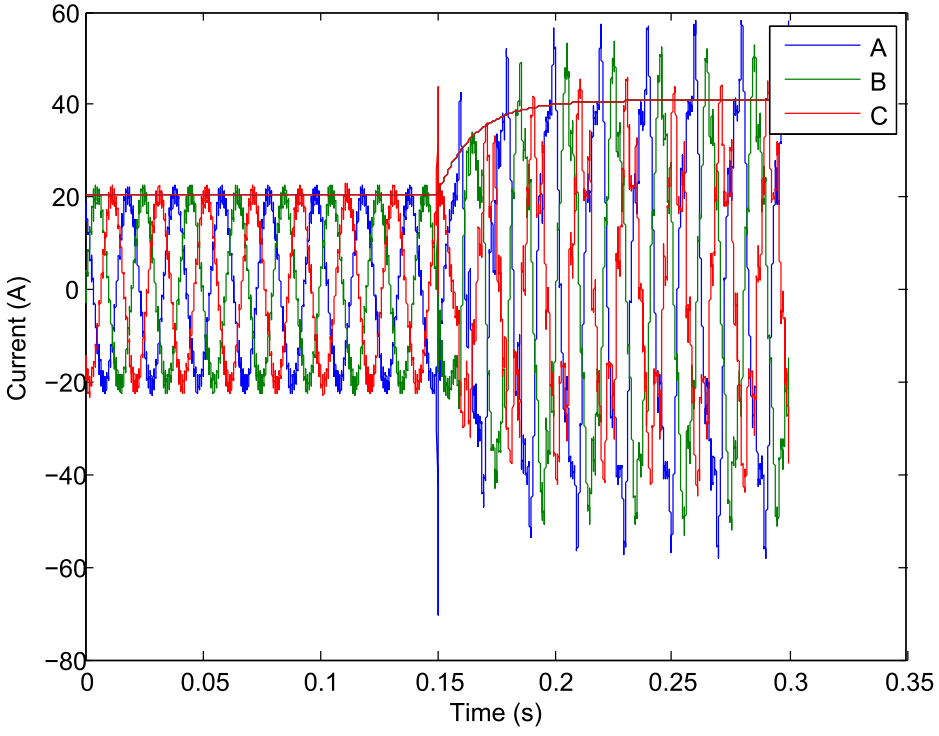

FIGURE 5.11: FAT Simulation II: Line-to-Line Fault – IIEG2 Current Comparison

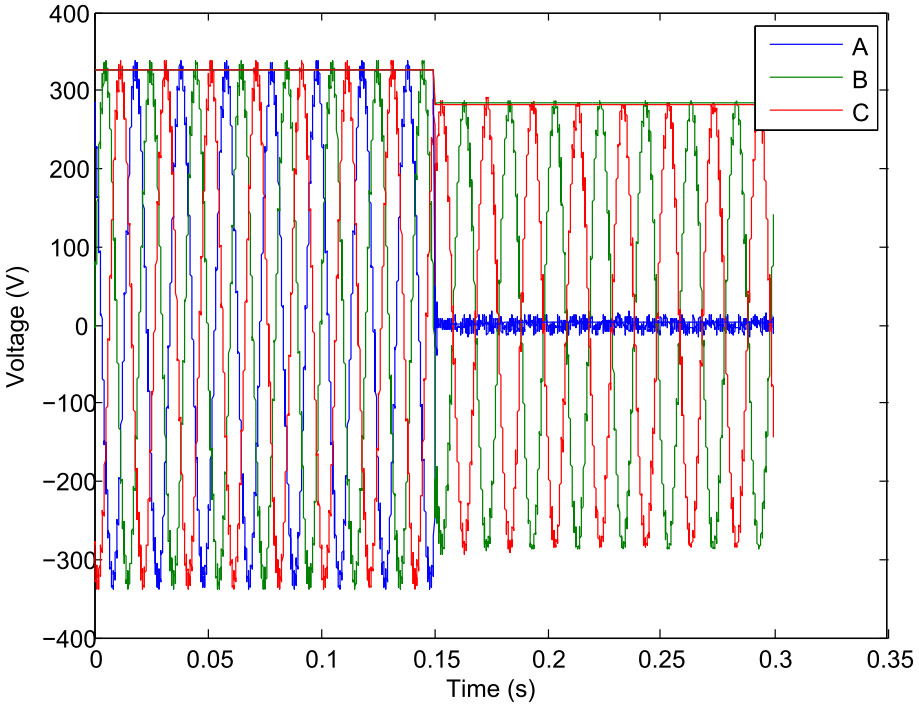

FIGURE 5.12: FAT Simulation II: Line-to-Line Fault – IIEG2 Voltage (Line-to-Line) Comparison

The small-signal model shows a very short term fault current excursion for IIEG2 in both simulations that is not observed by the FAT. The sub-transient response is not observed by IIEG1 due to the increased electrical distance between the IIEG1 and the fault. The most notable anomaly is the fault current response of IIEG2 during simulation II. Line commutation can only be achieved through the C phase connected through the delta-wye transformer. The result is a heavily distorted signal; however, the FAT still provides a reasonable approximation for the fundamental component of the resultant current waveform.

The peak current excursion of IIEG2 is approximately 2.5 times the peak rated current and has a duration of approximately 1 millisecond. The observed results are commensurate with the data published in [29] under laboratory conditions. The fault current observed within the first millisecond can be likened to the sub-transient response of a synchronous machine. The sub-transient response of an IIEG is important for the protection of the power electronics within the inverter. Hence, the FAT is inappropriate as an analysis tool for thermal protection of IIEG devices unless an IIEG contains a significant thermal

inertia where the transient and steady-state responses become important. However, the primary function of the FAT is to approximate the fault response for the purpose of DN line protection design.

Modern DN protection devices pass fault current data through an anti-aliasing filter, often a cosine filter, before analysing the waveform [108]. Cosine filters effectively eliminate high frequency transients. Therefore, the sub-transient response of an inverter will not be observed by DN protection devices. Hence, the omission of the sub-transient response of an IIEG unit is acceptable from the perspective of DN protection analysis.

The fault current and voltage of an IIEG unit calculated by the FAT is determined by the response of the control system. IIEG units are incapable of sustaining over-current and over-voltage; protection systems are designed such that an IIEG unit will be isolated before thermal breakdown of the power electronics switches occurs. The FAT can be linked with protection settings such that the fault response of a network is recalculated each time a protection device operates. The fault current contribution of an IIEG can be removed by simply setting the output current and power set points to zero or by removing the IIEG from the characteristics, KVL and KCL equations.

5.3.5 Application of OC protection and Fault Current Limiting

The IIEG simulations presented in this Chapter thus far have assumed that each inverter-interface is capable of exporting an unlimited fault current. In practice, the fault current contribution of an IIEG unit is restricted by the ratings of the power electronics within the inverter, which are generally IGBTs. In order to make the FAT simulations more accurate during significant fault conditions, three possible simulation types are offered.

1. All inverters are designed with a significant thermal inertia such that an IIEG unit can sustain a large fault current long enough for DN OC protection devices to operate. Under this assumption, the simulations presented thus far in this Chapter can be considered reasonable representations of what would happen in practice. However, increasing the thermal inertia is expensive and presents little benefit for DN customers. In future networks where EG penetrations reach 100% of subsections

of the network, there may be reason to increase the thermal capacity of inverters due to the plausibility of intentional islanding. The increased thermal capacity of IIEG would help maintain stability and provide fault ride-through. While the first option may be reasonable for research purposes within the context of microgrid research, the ratings of contemporary grid-connection IIEG render the first option impractical for fault studies.

2. An effective OC instantaneous trip of IIEG units from the perspective of DN OC protection analysis is employed. Most contemporary IIEG units do not have a significant thermal inertia, nor are equipped with fault current limiters. Isolation of IIEG units via anti-islanding protection can take as long as two seconds whilst OC and EF protection can operate in the range of tens of microseconds for a low impedance fault and up to several seconds for high impedance sensitive earth fault detection. Hence, both the connected and disconnected state of each IIEG unit must be considered within the context of anti-islanding protection and DN line protection coordination. However, if a significant fault current is drawn from the IIEG unit, the inverter's OC protection will trip the IIEG unit in the order of one to five milliseconds [29]. In such a case, the fault current supplied by the IIEG unit would not exist long enough to create a significant deviation in the fault current passing through DN line protection units.

3. A fault current limiter is installed at each IIEG unit which mitigates the need for OC protection to operate. If the current exported by an IIEG unit exceeds the fault current limit, the FAT is rerun with that IIEG unit's current export fixed at the fault current limit. The fixed current is controlled to be purely reactive, lagging the voltage at the PCC by 90 degrees.

Irrespective of the application of an effective OC instantaneous trip or FCL, the first application of the FAT will assume each IIEG is capable of exporting any voltage or current necessary to satisfy the power export requirement of that IIEG. Once convergence is achieved, the results will be assessed to see if any fault current limitations or instantaneous trip thresholds have been exceeded. If an anomaly is observed, the simulation will rerun where:

- All IIEG units that do not exceed a current threshold (or are without a current threshold) will be unchanged.
- All IIEG units that exceed an instantaneous current threshold will be removed.
- All IIEG units that exceed an FCL threshold are set to constant current devices with an angle ninety degrees out of phase (reactive) with the voltage angle at the fault-instant.

The FAT may have to be rerun several times as the inclusion of the FCL of one IIEG unit may require the subsequent implementation of another FCL. Once again, a Newtonian solver is implemented to find the roots of a non-linear system of equations. In the case of a fault current limiter which exports a fixed reactive current, the power export must be equal to zero. As the current magnitude is fixed, only the current angle δ_I will be implemented as an iterative variable.

Let S_k be the complex power export of a three-phase IIEG unit k. Given:

$$S_k = P_k + jQ_k = \sum_{\alpha=a,b,c} V_{\alpha_k} I^*_{\alpha_k} \tag{5.25}$$

Setting the real part to zero yields:

$$0 = P_k = \sum_{\alpha=a,b,c} |V_{\alpha_k}||I_{\alpha_k}| \cos\left(\delta_{V_{\alpha_k}} - \delta_{I_{\alpha_k}}\right) \tag{5.26}$$

The IIEG controller ensures that $|I_{\alpha_k}|$ is equal across all phases. Hence, both sides of (5.26) may be divided by $|I_{\alpha_k}|$, reducing the complexity of the equation to (5.27).

$$0 = P_k = \sum_{\alpha=a,b,c} |V_{\alpha_k}| \cos\left(\delta_{V_{\alpha_k}} - \delta_{I_{\alpha_k}}\right) \tag{5.27}$$

For balanced networks, the equation may be further reduced to (5.28).

$$0 = \delta_I - \delta_V - \frac{\pi}{2} \tag{5.28}$$

The IIEG current angles are fixed at $\frac{2\pi}{3}$ radians out of phase. Let $\delta_{I_k} = \delta_{I_{a_k}} = \delta_{I_{b_k}} + \frac{2\pi}{3} = \delta_{I_{c_k}} - \frac{2\pi}{3}$. For unbalanced networks, the partial derivative of (5.27) with respect to the iterative variable δ_I can then be calculated as (5.29).

$$\frac{\partial \Delta P_k}{\partial \delta_{I_k}} = \sum_{\alpha=a,b,c} \frac{\partial |V_{\alpha_k}|}{\partial \delta_I} \cos\left(\delta_{V_{\alpha_k}} - \delta_{I_{\alpha_k}}\right) + |V_{\alpha_k}|\left(1 - \frac{\partial \delta_{V_{\alpha_k}}}{\partial \delta_I}\right) \sin\left(\delta_{V_{\alpha_k}} - \delta_{I_{\alpha_k}}\right) \tag{5.29}$$

For balanced networks, (5.30) is sufficient.

$$\frac{\partial \Delta P_k}{\partial \delta_{I_k}} = 1 - \frac{\partial \delta_V}{\partial \delta_I} \tag{5.30}$$

The FAT calculates (5.29) and (5.30) in almost exactly the same fashion as in Section 5.3.3. The only significant differences are: only one iterative variable exists for an IIEG unit employing the FCL and all non-diagonal elements of the Jacobian matrix that correspond to an IIEG employing a FCL are set to zero. The constant power and FCL equations may be concatenated together and solved simultaneously.

In order to explore the implications of an FCL and the efficacy of the FAT in approximating the response of the FCL, an example using the same network shown in Fig. 5.4 is given. A single-phase to earth fault at phase A of the load is applied at t=0.1 seconds. The threshold for the FCL implementation and execution are $k_1 = 1.2$ and $k_2 = 1.32$, respectively. Hence, the FCL will not be applied unless the current magnitude exceeds 1.2 per unit and when the FCL is triggered, the constant current export will be 1.32 per unit. These values where chosen such that the FCL would not oscillate between constant-current fault current limitation and constant-power control. The choice of constants also assumes that the inverter can safely export 1.32 times the nominal current until the protection isolates the fault. The results for IIEG1 are presented in Figs. 5.13, 5.14 and 5.15.

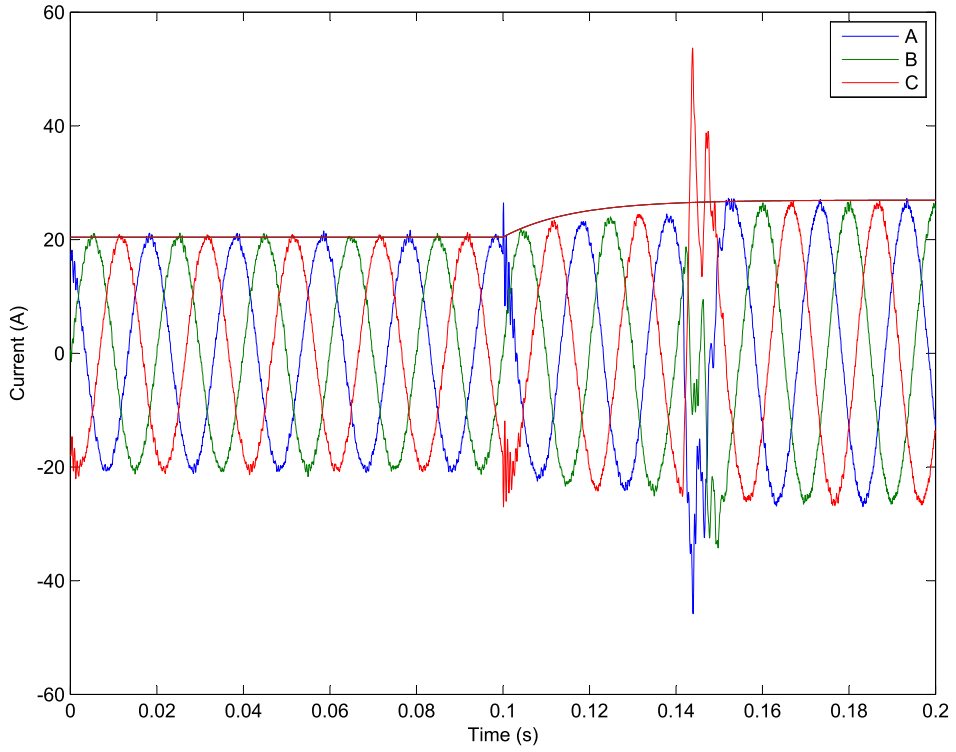

FIGURE 5.13: FCL Application: IIEG1 Current Waveform

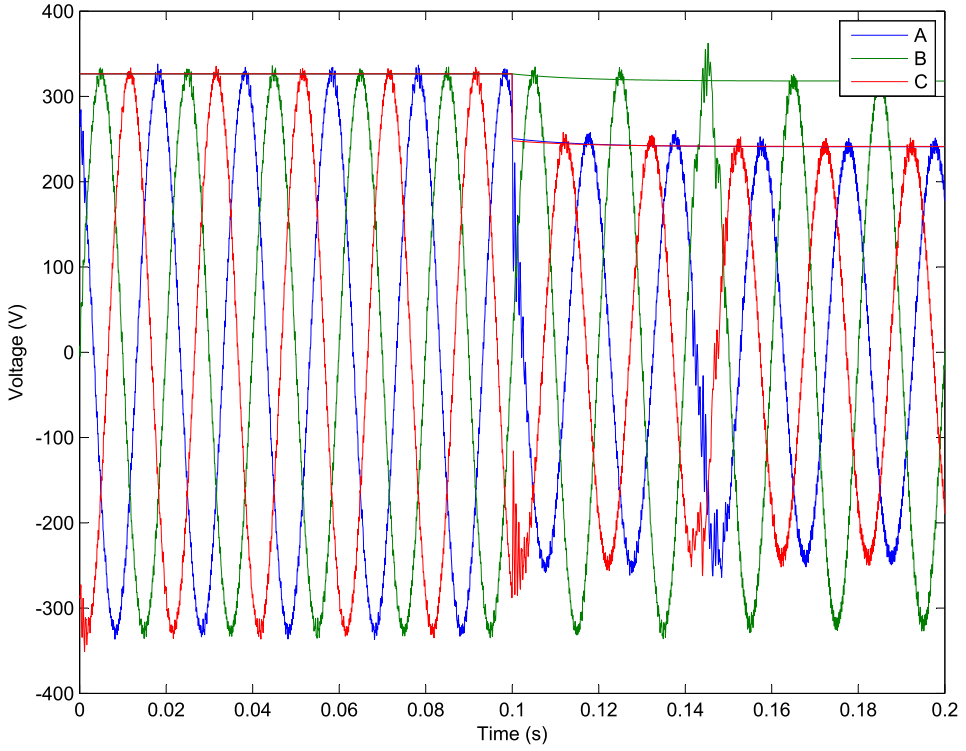

FIGURE 5.14: FCL Application: IIEG1 Voltage Waveform

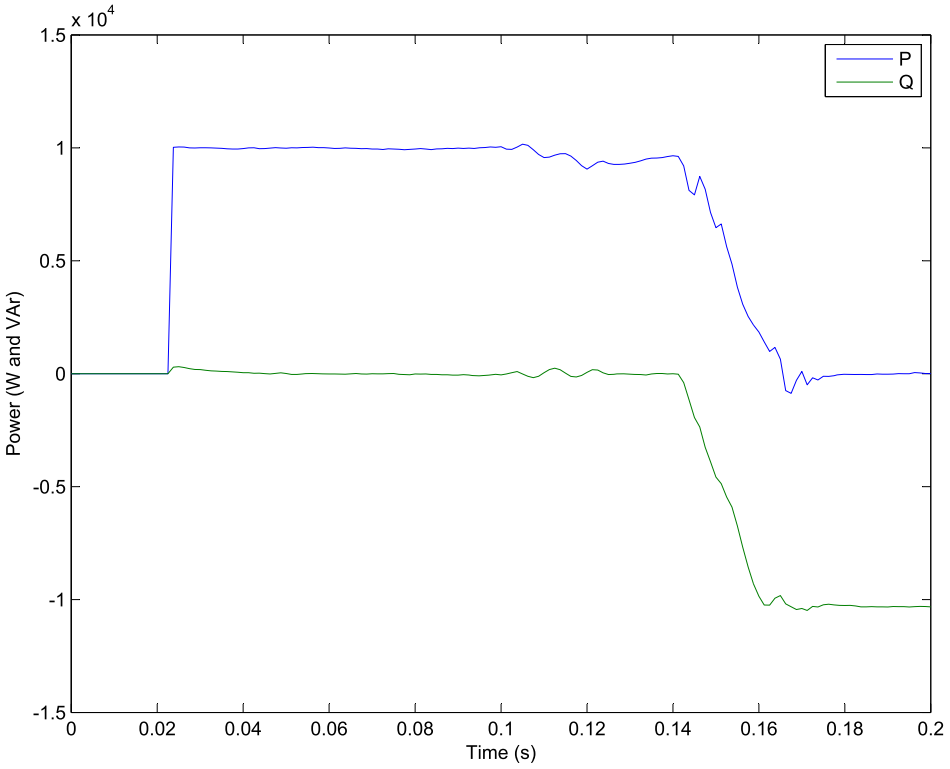

FIGURE 5.15: FCL Application: IIEG1 Power Waveforms

The FAT had to be run three times to find the the final steady-state solution. Once with no FCL implementation which found that the FCL threshold of IIEG2 was exceeded. The second iteration fixed the current export of IIEG2 which, in turn, cased the FCL threshold of IIEG1 to be exceeded. The third iteration gave the current and voltage magnitudes which have been superimposed onto the figures shown for comparison with the small signal model.

The FCL threshold of IIEG1 was exceeded just after t=0.14 seconds. The shift to constant reactive current output causes a significant current distortion which can be observed in Fig. 5.13, lasting about half a cycle. Fig. 5.14 shows that the effect of the current distortion on the voltage waveform distortion is minimal and should not significantly impact the fault ride-through capability nor the integrity of the DN. However, a significant voltage unbalance is present during the fault that shall be alleviated once the fault is isolated. The power plots shown in Fig. 5.15 show that no real power export is present after the FCL comes into effect. Furthermore, the reactive power present is absorbed by the IIEG

as expected.

The transient response of the current waveform predicted by the FAT does not match the small signal model until the FCL threshold is exceeded. The error is acceptable from the perspective of fault studies which are only interested in the prefault and steady-state post-fault conditions. However, if desired, the complete envelope can be derived and implemented using (5.31).

$$i(t) = \begin{cases} I_0 & \text{if } t < t_{\text{fault}}, \\ I_\infty + (I_0 - I_\infty)\exp^{-\omega_c t} & \text{if } t_{\text{fault}} \leq t \leq t_{\text{FCL}}, \\ I_{\text{FCL}} & \text{if } t > t_{\text{FCL}}. \end{cases} \tag{5.31}$$

Where $i(t)$ is the instantaneous current export, I_0 is the pre-fault current export, I_∞ is the steady-state post-fault current excluding the FCL and I_{FCL} is the current output once the FCL threshold is exceeded. The times t_{fault} and t_{FCL} refer to the time of the fault-instant and the time when the FCL threshold is exceeded, respectively. The value of t_{FCL} can be derived by (5.32) and ω_c is the cut-off angular frequency of the IIEG unit's current control LPF.

$$t_{\text{FCL}} = -\frac{1}{\omega_c}\ln\left[\frac{I_{\text{FCL}} - I_\infty}{I_0 - I_\infty}\right] \tag{5.32}$$

The results for IIEG2 are presented in Figs. 5.16, 5.17 and 5.18. The FCL threshold of IIEG2 is exceeded at approximately t=0.11 seconds. Again, a visible current and voltage distortion are present for about half a cycle whilst the constant reactive current reference is initiated. Again, the voltage distortion is limited and unlikely to negatively impact DN infrastructure or the fault ride-through ability of the DN. Once again, only reactive power is absorbed from the IIEG whilst the FCL is operating.

5.3.6 Conclusion

The FAT is an effective means of approximating the fault response of IIEG in DNs from the perspective of DN line protection. The envelopes produced by the FAT closely matched

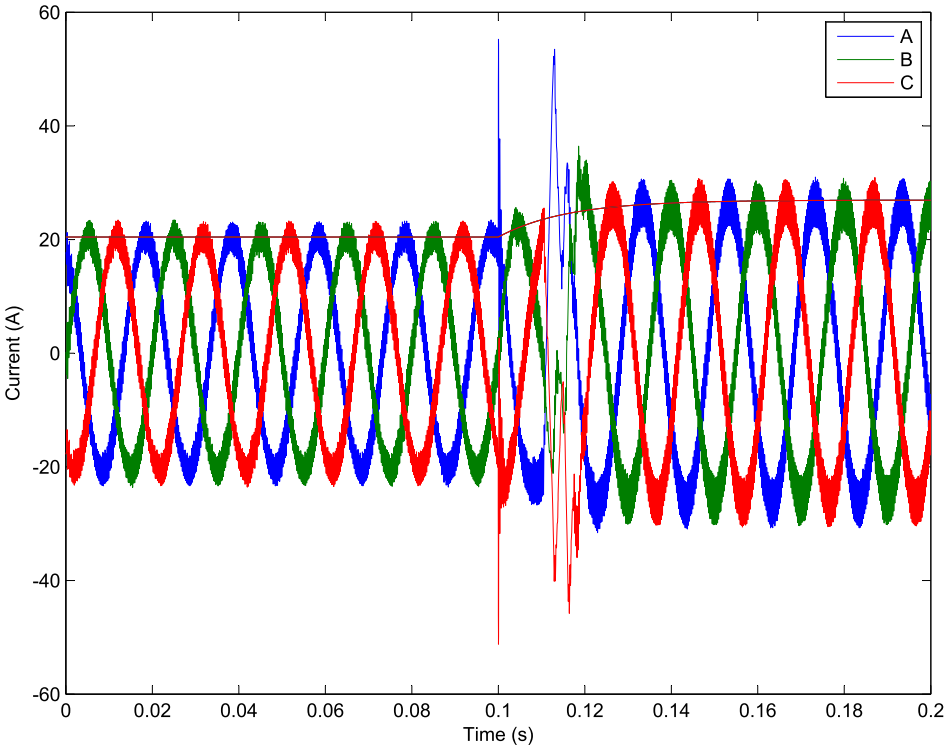

FIGURE 5.16: FCL Application: IIEG2 Current Waveform

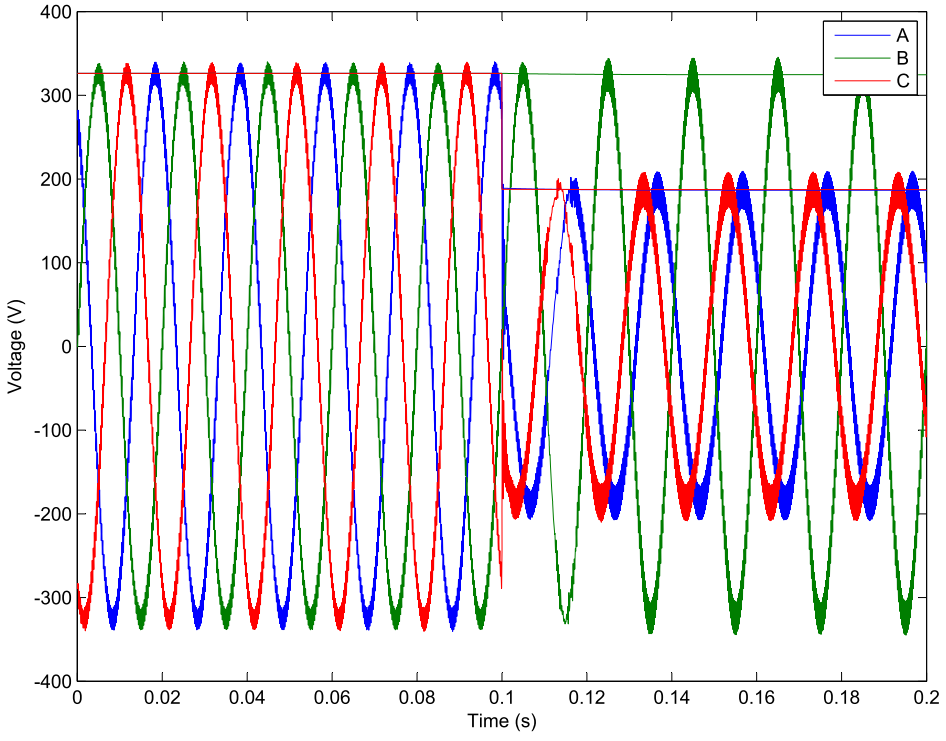

FIGURE 5.17: FCL Application: IIEG2 Voltage Waveform

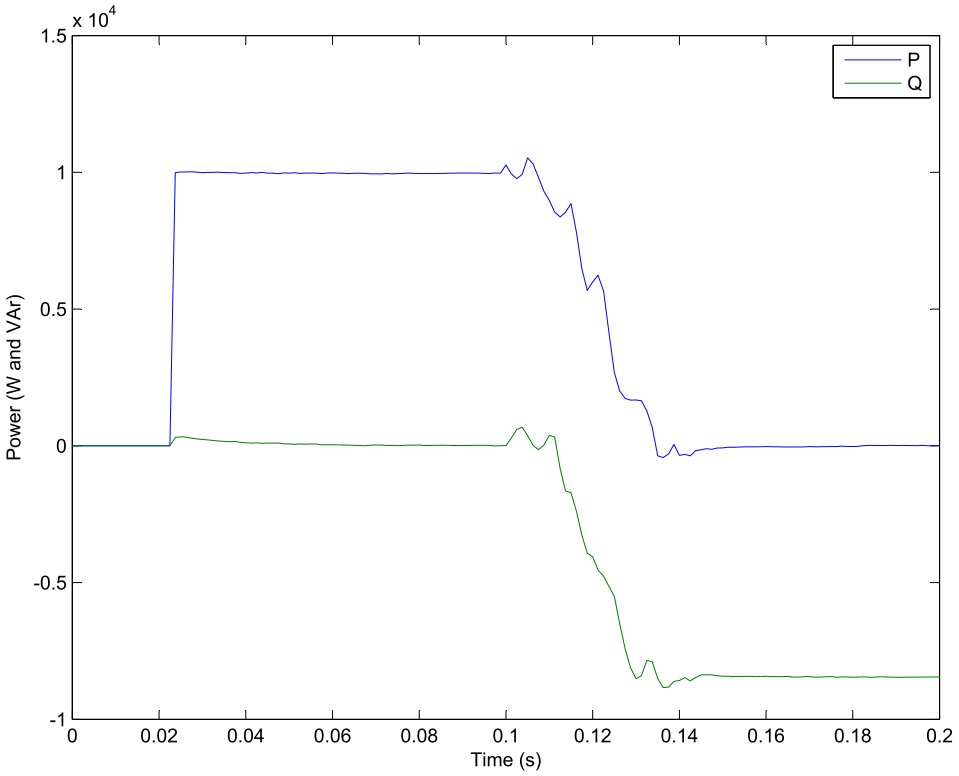

FIGURE 5.18: FCL Application: IIEG2 Power Waveforms

the small-signal modelling of faulted DNs with a high EG penetration. The FAT is much less computationally expensive when compared with small signal modelling, yet provides an accurate representation of the steady-state and transient responses of IIEG units. It must be emphasised that FAT may not be appropriate for analysing the efficacy of IIEG protection, in particular the effects of the 'sub-transient' response and islanded modes of operation on local protection. Future work will involve incorporating the protection settings of DN protection devices into the FAT. Also, an investigation into the possibility of modelling the sub-transient response of the IIEG without requiring a significant knowledge of the control dynamics of the IIEG would be of significant value.

Chapter 6

Protection Analysis Tool

6.1 Introduction

The presence of EG in DNs has, to date, not incurred an appreciable adverse effect on distribution line protection systems in Australia. The present EG penetration levels and fault current limiting nature of IIEG are insufficient to compromise fault discrimination practices. Empirically, the utility has observed problems due to OV at EG levels too small to concurrently cause protection problems. However, if an OV mitigation scheme is implemented, protection failure due to EG may become plausible and a reality in future networks.

Additional limiting factors of EG connection may be physical constraints such as siting (physical space or proximity to energy resource such as cogeneration), the business case for connecting the EG and the thermal loading of distribution line infrastructure. For the purposes of this Chapter, these limiting factors are assumed to have been considered separately. The proposed OV mitigation scheme and protection analysis do not preclude further constraint analysis encompassing these limiting factors.

The impacts of EG penetration on protection are dependent on a large number of variables:

- The topology of the network.

- The distribution line impedances.
- Load locations and sizes.
- EG location, interface, control and size.
- DN protection device locations and settings.
- EG protection settings.
- Transformer location, size, impedance and winding connections.
- Fault location, configuration (three-phase, line-to-line, single-phase to earth) and impedance.
- The earthing configuration of the distribution network.

Due to the variability and range of the characteristics of a DN containing a significant EG penetration, a generalised expression for fault efficaciousness is imprudent. Hence, this Thesis proposes an analysis tool for the protection integrity of a given DN. Note that the proposed tool is specifically designed for applications of IIEG rather than machine-interfaced EG.

6.2 Protection Analysis Tool Overview

The protection analysis tool (PAT) is designed to investigate the worst case scenarios of loading and EG connection from the protection perspective. The end result of the PAT is a report which outlines the extremities of the normal and faulted operation for a given DN. A separate section for each protection device is allocated within the report. The results of the following conditions are given for all sections:

- The current flowing through each protection device during peak loading.
- The minimum pick-up current for OC and EF relays.
- The maximum possible fault current flowing through each protection device.

- The maximum out-of-zone (OOZ) fault currents observable by OC and EF relays.

The results of each condition are calculated using the FAT (as introduced in Chapter 5) for all IIEG connection combinations. Hence, the FAT may be thought of as the engine within the PAT. The PAT provides all IIEG connection combinations and relevant DN operating conditions to the FAT. Subsequently, the FAT calculates and returns the current measured by all protection devices to the PAT. Once all simulation data is gathered, the PAT filters through the data in order to identify the conditions pertinent to protection efficacy; these pertinent conditions constitute the generated report.

The motivation for the FAT was to provide a fast method of providing fault simulations for DNs with a high IIEG penetration. In order to understand the benefits the of PAT, it is important to understand the high volume of simulations required to develop a full analysis of a DN protection scheme.

Given any network containing OC and EF protection devices, the total number of FAT simulations required can be expressed by (6.1).

$$\text{No. simulations} = 2^{\text{EG}} \sum_{a=1}^{\text{RELAYS}} \left[7 + 4\text{EOZ}_a + 3\text{EOZEF}_a + 4\text{EOZS}_a + 3\text{EOZEFS}_a\right] \quad (6.1)$$

Where:

- EG is the number of IIEG units.
- RELAYS is the number of protection devices in the network under consideration.
- EOZ_a is the number of primary OC end of zone nodes corresponding to protection device a.
- EOZEF_a is the number of primary EF end of zone nodes corresponding to protection device a.
- EOZS_a is the number of secondary OC end of zone nodes corresponding to protection device a.

- EOZEFS_a is the number of secondary EF end of zone nodes corresponding to protection device a.

Evidently, a DN containing several IIEG units and protection devices requires a large number of simulations. If all simulations were completed using small-signal analysis, developing a complete report of the impacts of IIEG on protection efficacy would be a very time-intensive process. The PAT not only significantly reduces the analysis time, but automates much of the analysis process.

A simple flow diagram of the PAT algorithm is shown in Fig. 6.1. The flow diagram is designed to give a general overview of the PAT and does not provide a detailed mapping of the PAT algorithm.

The PAT begins by identifying the slack bus within the simulated DN. A single slack bus is needed as the algorithm is predicated on radial power flow for protection assessment. If the number of buses in the DN does not equal one, the PAT algorithm shall terminate. The user is then prompted to nominate any protection devices to be excluded from consideration within the PAT algorithm. Devices that do not constitute part of the DN line protection scheme should be omitted, such as protection devices used for busbar or transformer protection in zone substations.

The PAT algorithm continues by locating and identifying the protection devices and zones of protection. Primary and secondary zones of protection are both required such that the N-1 redundancy criteria of DN protection can be validated by the PAT. OC and EF zones of protection are identified separately to account for transformer winding connections. Zero sequence current cannot enter nor leave a three-phase delta-connected transformer winding in a DN. Distribution transformers are typically delta-wye connected to ensure all zero sequence current flows from the zone substation transformer during an earth fault. Zone substation transformers are also often delta-wye connected. Hence, the connection of transformers must be taken into consideration when assessing the fault discrimination and selectivity of an EF protection device.

The PAT sequentially constructs the DN cases containing three-phase bolted, line-to-line and single-phase to earth fault types for all start of zone (SOZ) and end of zone (EOZ)

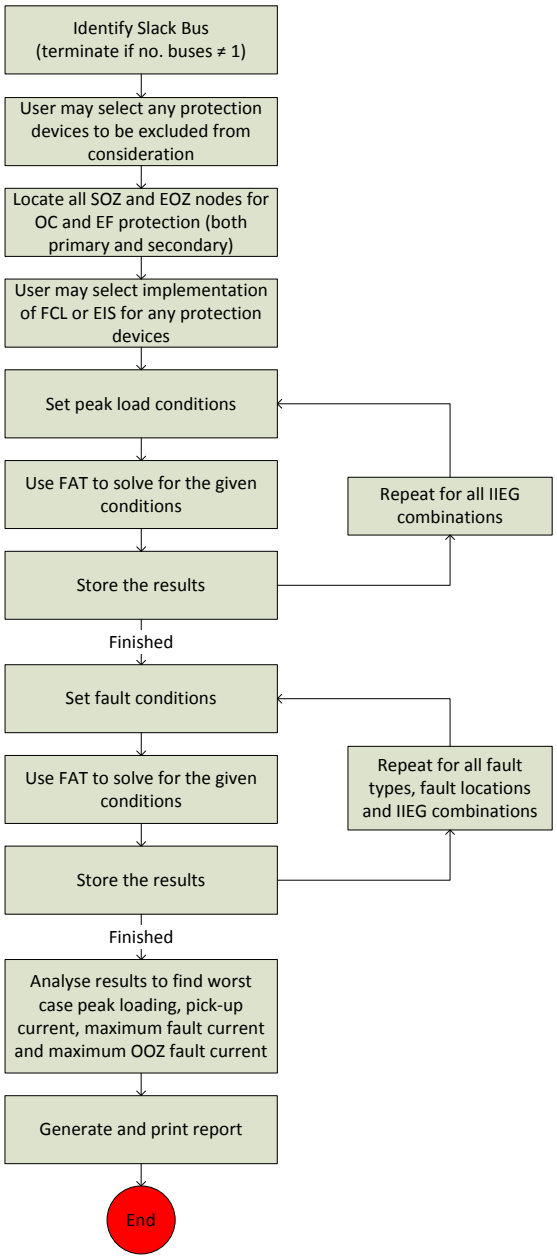

FIGURE 6.1: Flow Diagram of PAT Algorithm

locations, before employing the FAT to simulate the data. Furthermore, each case is reassessed for every IIEG connection configuration. Each IIEG is represented in two possibles states: full rated power export and isolated mode. Hence, for N IIEG units, 2^N assessments are necessary. All fault and EG combinations variations are automatically applied to the DN by the PAT, greatly reducing the workload of the user. Upon completion of all simulations, a significant amount of data is gathered which must be filtered to

discern which information is useful from the perspective of a utility protection engineer. This filtering process is automated by the PAT. A report is then generated outlining the 'worst case scenario' fault response data which may be used to simplify protection setting determinations.

The PAT is also capable of incorporating FCLs and an effective instantaneous trip (EIT) which may be implemented at the user's discretion. The EIT allows an IIEG connection to be omitted from consideration if the fault current drawn by an IIEG unit during a simulation exceeds a predefined multiple of that IIEG unit's rated current. The EIT is a simple tool that may be implemented to better represent the impacts of actual IIEG applications on DN line protection efficacy. If neither FCL nor an assumed EIT are chosen, the PAT ignores the ratings of power electronics devices and assumes that the power set points of each device will be realised in every case where convergence to a solution can be achieved by the FAT.

There exists no general consensus on how a FCL should be applied to grid-connected IIEG units. The FCL can: absorb reactive power only, inject reactive power only, export real power only or any desirable power factor. Due to the variability in plausible FCL application and the lack of contemporary practical application with grid-connected IIEG units, FCL is excluded from the PAT study in this Thesis. However, if a consensus can be reached as to how FCLs are applied and constant power and positive sequence current can be achieved across all phases, the PAT can incorporate the effects of FCLs for protection studies.

6.3 Employing the PAT Report Data

An understanding of the protection requirements within DNs is necessary in order to correctly interpret a PAT report. The report does not specifically determine the best protection settings of relays: the choice of protection settings is an inexact practice as a range of values may provide effective protection (or none at all). However, the report can be used as an aid when determining which protection settings are appropriate for a given

case. Preferably, the user would also have some understanding of the subtle impacts of a high IIEG penetration within DNs from the protection perspective.

There are two OC protection issues that can arise from EG penetration which were discussed in Chapter 2 and are reiterated here. Firstly, the current ratings of protection devices may be exceeded. Assuming that the largest fault current is supplied from the main grid during faults in a close proximity to an OC line protection device, the maximum fault current condition will occur for a fault located immediately downstream of that OC line protection device. The nodes located immediately downstream of a protection device are known as the SOZ nodes. Generally the largest fault current is drawn during a low impedance single-line to earth fault or three-phase bolted fault. The PAT simulates all single-phase, line-to-line and three-phase bolted faults at each SOZ and records each corresponding fault current to form the set $I_{\text{SOZ fault}}$. Each CB must be capable of interrupting the maximum fault current. Hence, the reported maximum current is the minimum admissible CB rating $I_{\text{CB rating}}$ and can be calculated to be the maximum of all recorded fault currents measured at the protection device as shown in (6.2). Every IIEG connection combination is investigated to account for fault current increases and decreases incurred through IIEG connection.

$$I_{\text{CB rating}} > \max[I_{\text{SOZ faults}}] \tag{6.2}$$

The second OC protection complication involves compromising the discrimination of a protection scheme. There are two ways that discrimination failure can be achieved. Firstly, a protection device can fail to detect a fault within that protection device's zone of protection. Secondly, a protection device can trip unnecessarily for a fault outside of that protection device's zone of protection. Both forms of discrimination failure must be taken into consideration when choosing pick-up currents.

Contemporary OC protection settings are determined using peak load and line data. The maximum permissible pick-up current is calculated by simulating EOZ fault responses ignoring the presence of loads. The minimum permissible pick up current is the forecasted

peak load current $I_{\text{forecasted peak}}$. The range acceptable for a pick-up current, $I_{\text{p.u.}}$, setting can be expressed as in (6.3).

$$I_{\text{forecasted peak}} < I_{\text{p.u.}} < k \cdot \min[I_{\text{faults}}] \tag{6.3}$$

Where k is an error factor multiplier used to ensure higher impedance faults are detected. The matrix I_{faults} is the set of fault currents at all EOZ nodes corresponding to a protection device. Values for k can vary: this Thesis employs $k = 0.5$ for primary protection and $k = 0.67$ for secondary protection.

The proposed PAT incorporates traditional OC and EF protection requirements, but is expanded to include protection discrimination issues that arise due to IIEG connection. Note that OC protection is designed to detect three-phase and line-to-line faults whilst EF protection is designed to detect single-phase to earth faults. Hence, the PAT only analyses the fault types relevant to the protection type. The set I_{fault} includes each IIEG connection combination to gain the entire range of possible fault currents within the designated zone of protection. Furthermore, all fault currents for OOZ faults, $I_{\text{out of zone faults}}$, are gathered to ensure a nuisance trip does not occur. The range for an acceptable OC pick-up current can now be expressed as in (6.4). The value $I_{\text{in-zone faults}}$ contains the set of all fault currents simulated within a protection device's zone of protection. Note that an OOZ fault is generally only included for instances of reverse current flow.

$$\max[I_{\text{forecasted peak}}, I_{\text{out of zone faults}}] < I_{\text{p.u.}} < k \cdot \min[I_{\text{in-zone faults}}] \tag{6.4}$$

The domain for an acceptable EF pick-up current can be expressed as in (6.5). The process for calculation is the same, except single-phase to earth faults are analysed instead of line-to-line and three-phase faults. Furthermore, an EF relay does not detect peak current, rather the current unbalance $I_{\text{unbalance}}$. Hence, $I_{\text{unbalance}}$ contains the maximum current unbalance during healthy operation of the DN. The calculation of $I_{\text{unbalance}}$ is not included in the PAT report as the simulations within this Chapter are all balanced. In practical application, many distribution feeders, particularly in remote locations, may have two or

single phase spurs. Customers are generally connected in a manner designed to minimise load unbalance; a pick up current of 30-40% of peak current is considered acceptable [109]. Alternatively, unbalance data can be captured by protection devices and accessed via system control and data acquisition (SCADA).

$$\max[I_{\text{unbalance}}, I_{\text{out of zone faults}}] < I_{\text{p.u.}} < k \cdot \min[I_{\text{in-zone faults}}] \tag{6.5}$$

If there is no acceptable domain for the pick-up current, protection discrimination cannot be achieved. There are a few techniques that can be taken to remedy poor protection discrimination due to IIEG connection:

- If the issue is caused by protection misoperation during OOZ faults, directional current elements could be installed to block nuisance trips.
- Installing FCLs on each IIEG device may reduce the risk of fault under-reach.
- Otherwise, an upgrade of DN cable is most likely necessary.

6.4 Convergence Issues

The FAT is based on Newton's method of finding the roots of an equation. Newtonian iterative solvers can be prone to conditions of divergence where a solution cannot be found. Empirically, the author has identified two situations where FAT convergence is not achieved:

- When a three-phase bolted fault is located upstream of a IIEG unit.
- When a three-phase bolted fault causes a significant voltage drop ($|V| < 0.1V_{\text{nominal}}$) at the terminals of an IIEG unit.

To reduce instances of FAT divergence, if an IIEG unit is downstream of a three-phase fault, that IIEG unit is excluded from simulation as no voltage or frequency commutation

is possible. It is assumed that the IIEG unit will be isolated by I^2t or anti-islanding protection. Irrespective of successful isolation, the IIEG downstream of the fault will not have a significant adverse effect on the fault current flowing through protection devices upstream of the fault. In the unlikely event that a protection device downstream of the fault is subject to a nuisance trip due to reverse power flow before anti-islanding protection operation, a reclose attempt after IIEG isolation will ensure that the feeder reaches the same switching state as if the IIEG unit had not caused the nuisance trip. The nuisance trip does not pose a negative impact on the overall reliability of the grid: any downstream customers will lose power due to the upstream fault irrespective of nuisance tripping.

There may be cases where the voltage drop at the IIEG unit's PCC due to a three-phase bolted fault is too significant for convergence of the FAT. The effects of subjecting a three-phase IIEG unit to a bolted three-phase fault was explored in [29]. The thermal I^2t protection trip time was only a fraction of a cycle, ranging from approximately one to four milliseconds. The fastest anti-islanding trip time defined within IEEE recommended practice due to voltage or frequency deviation is six cycles (100 ms in USA) [33]. The anti-islanding trip delay is implemented for fault ride-through purposes and is designed to protect the grid rather than an IIEG unit. The IGBTs within the inverter cannot sustain a significant OC for six cycles without over-rating the IGBTs. Hence, fast thermal protection is essential is providing protection of the inverter. Ergo, it is reasonable to assume that an inverter is likely to be isolated by thermal protection during three-phase bolted faults at or near the inverter's PCC rather than isolation via anti-islanding protection.

DN line protection relays commonly utilise cosine filters which are ideal for protection applications [69]. The cosine filter attenuates all harmonics and any DC component in an AC current waveform [89]. The cosine filter's analogue to digital converter samples at a rate of sixteen samples per cycle. Hence, the sampling period is 1.25 ms within Australian power networks.

Consider the reflected fault scenario shown in Fig. 6.2 with the IIEG unit possessing the fault and protection characteristics of the IIEG studies in [29]. A three-phase bolted fault is implemented within CB_2's zone of protection.

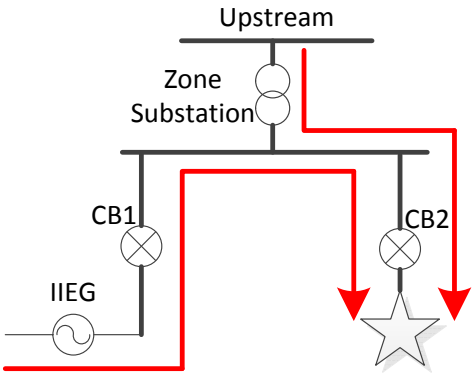

FIGURE 6.2: Low Impedance Three-Phase Bolted Reflected Fault

A significant fault current of 2-3 times rated current will be drawn from the IIEG unit for less than five milliseconds (generally around one millisecond) before the thermal protection of the IIEG unit will initiate a trip, isolating the IIEG unit. Hence, a maximum of four samples of fault current supplied by the IIEG will be captured by the protection relays of CB_1 and CB_2 before the IIEG will be isolated. The current waveform is normally passed through a LPF, further attenuating the OC waveform over the short time frame where the IIEG is still supplying fault current. Hence, the IIEG fault current observed by a line protection device will be minimal and short-lived.

The fault is within CB_2's zone of protection. The trip time for a three-phase bolted fault is variable and depends on the fault level and protection settings of devices upstream of the zone substation. However, due to grading restrictions, the trip time is generally going to be greater than the maximum five millisecond trip time of IIEG. Hence, one can assume that the IIEG has been isolated before CB_1 is opened. Therefore, consideration for increasing the rating of the CB to interrupt the aggregate fault current during a three-phase bolted fault is unnecessary.

Furthermore, the trip time of CB_1 will be considerably slower than CB_2 as CB_2 will measure a significantly greater fault current than CB_1. Hence, all IIEG thermal trip times are shorter than CB_1's trip time. The inception of the fault creates a significant voltage drop across the adjacent feeder. Because IIEG units are constant power controlled, a voltage drop induces an increase in IIEG current export. A reflected fault creating a significant voltage drop shall cause an increase in the current export from all IIEG units

sufficient to trigger thermal tripping of all IIEG units on the adjacent feeder. Ergo, it is reasonable to conclude that for a low impedance three-phase fault, the thermal protection of all IIEG units will operate before the DN line protection devices will attempt to isolate an OOZ three-phase bolted fault. Hence, the failure of the FAT to converge during bolted faults does not significant impact the integrity of the proposed PAT.

6.5 Tolerances in PAT Data

In order to illustrate the tolerances of the reports generated by the PAT, the limitations of the accuracy of the FAT must be understood. The anomalies introduced by the FAT are highlighted via the juxtaposition of results generated by the FAT and small-signal modelling. The comparison was applied to the DN represented by the single line diagram shown in Fig. 6.3 with data as presented in Table 6.1.

Some interesting anomalies occurred when comparing FAT results to small-signal simulations in instances of low impedance faults. In some cases, the FAT was able to converge to a solution during disturbances too significant for the IIEG unit to operate as expected. Generally, the cause is the IIEG unit's controller being unable to maintain a constant current (or in extreme cases, power) when a significant voltage unbalance occurs due to a non-symmetrical low impedance fault.

Consider the case study where a zero impedance single-phase to earth fault is placed immediately downstream of CT_1 on phase A at t=0.05 s. The voltage and current waveforms of IIEG_1 are shown in Figs. 6.4 and 6.5, respectively. The magnitude of the voltage waveforms is predicted by the FAT with great accuracy. The current waveforms, however, are prone to a significant total harmonic distortion once the DN is exposed to the fault. The IIEG constant power controller attempts to maintain the same current across all three phases. The rms current is shown in Fig. 6.6. The rms current clearly shows that $I_c > I_a > I_b$. The rms current predicted by the FAT is 3.935 A which is approximately the mean current magnitude across the three phases. However, I_c is greater than the expected rms current ($I_c \approx 4.1$ A) and I_b is less than the expected rms current ($I_b \approx 3.7$ A).

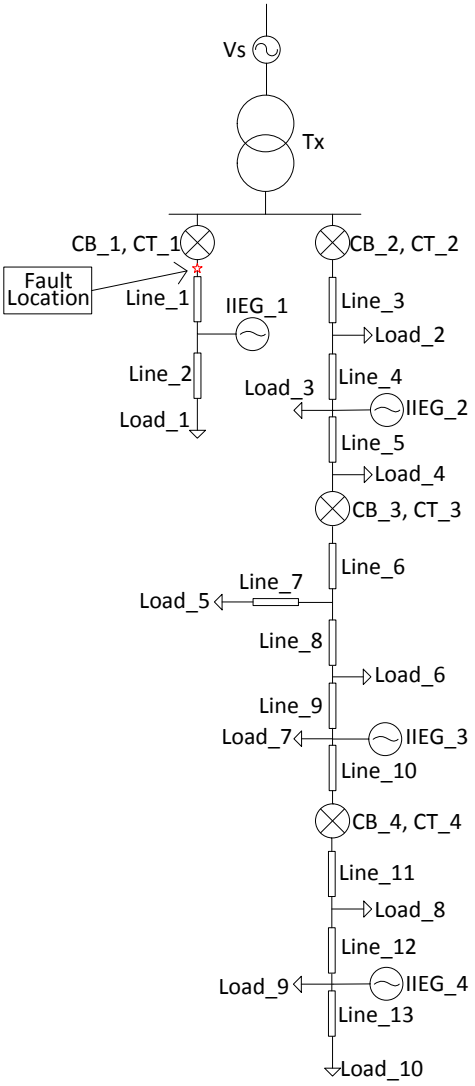

FIGURE 6.3: Single Line Diagram

The current response is oscillatory and is a response to the fluctuating dq voltage and current calculated by the controller. The fluctuating dq signals are a result of unbalance in the measured waveforms. In order to capture the maximum expected current reference signal deviation, the projected worst case scenario single-phase to earth reflected fault was simulated using the code shown in Appendix B. The three-phase voltage and current waveforms are converted into the dq axis and the reference angle is assumed to be regulated such that $V_q = 0$. To illustrate the control response of the current reference signal, all LPFs were simulated and the current reference was then calculated (by (3.22) in Chapter 3). The A phase voltage was set to zero to simulate a low impedance single-phase to earth

TABLE 6.1: Single Line Diagram Data

Infinite Bus Data	
Voltage l-l rms (kV)	33000
Frequency (Hz)	50
Line Data	
Resistance (Ω)	0.5
Inductance (mH)	5
Transformer Data	
Primary Voltage l-l rms (V)	33000
Primary Winding Resistance (Ω)	0.01
Primary Winding Inductance (mH)	1
Primary Connection	Delta
Secondary Voltage l-l rms (V)	11000
Secondary Winding Resistance (Ω)	0.01
Secondary Winding Inductance (mH)	1
Secondary Connection	Wye-earthed
Load Data	
Real Power (kW)	25
Reactive Power (kVAr)	0.5
Note: The equivalent resistance and inductance are connected in parallel.	
IIEG Data	
DC Voltage (V)	20000
Switching Frequency (kHz)	4
Filter Inductance (mH)	2245.37
Filter Capacitance (μF)	0.022
Power Setpoint (kVA)	50+j0
Low Pass Filter Cut-Off Frequency (Hz)	10

fault. The output plot is given in the Appendix B. The plot compares the current error signal peaks with the voltage peaks. As most IIEG units export real power only, the peaks of the current waveforms match the peaks of the voltage waveforms. The FAT predicts a current export assuming that all three-phase currents are of equal magnitude and $\frac{2\pi}{3}$ radians out of phase to be consistent with the expect operation of the constant power defined in Chapter 3. Hence, the FAT assumes that V_d is constant and equal to the mean value of the actual oscillatory V_d.

By matching the phase voltage peaks and troughs to the positions of the oscillatory current error signal, the phase error percentages can be calculated to be: $\Delta I_a = -2.57\%$, $\Delta I_b = -4.67\%$ and $\Delta I_c = 6.22\%$. These errors are not attenuated by cosine filters as the resultant

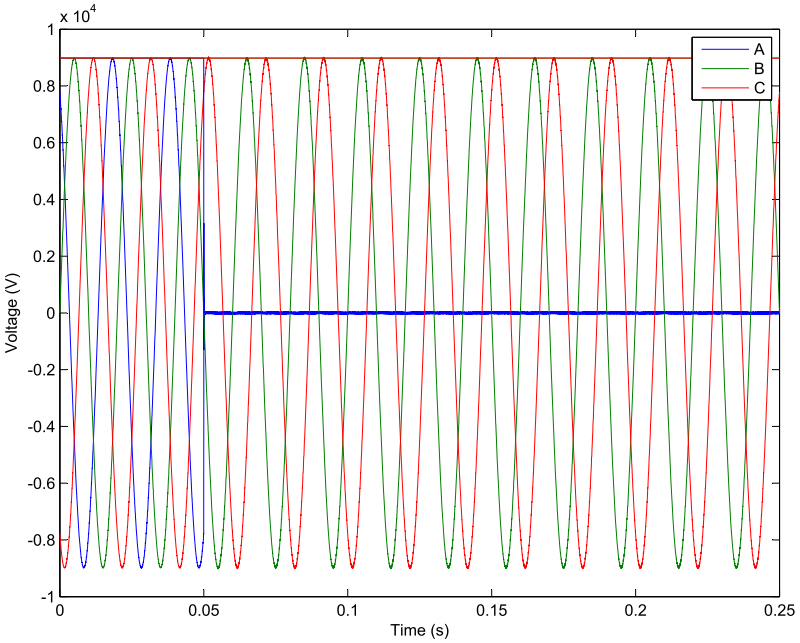

FIGURE 6.4: Voltage waveform of IIEG_1 Exposed to Close Proximity Single-Phase Fault

error manifests in the fundamental frequency. However, the errors are prone to the phase shift caused by the PR controller (as well as errors induced by higher order harmonics). Hence, the aforementioned percentage errors may be considered approximations of the expected deviations in phase current magnitude during a single-phase to earth fault.

The results of Fig. 6.6 show errors of $\Delta I_a = -0.84\%$, $\Delta I_b = -5.75\%$ and $\Delta I_c = 4.25\%$ which suggests that the effect of the PR is a slight negative phase shift at 100 Hz. The peak current reference error due to the oscillatory V_d signal is 7.3%. Empirically, the aforementioned simulations have shown that fundamental current magnitude differs by no more than 7% as a result of extreme unbalance and the dynamics of the overall control scheme. A heuristical rule is thus proposed that a tolerance of 7% is required for FAT simulations of current response of IIEG implementing the constant power controller proposed in Chapter 3 when exposed to low impedance single-phase to earth faults.

The same test was repeated for a zero impedance line-to-line fault immediately downstream of CB_1 across phases A and B. As shown in Appendix B, the predicted current error signal deviation during a line-to-line fault was shown to be 21.26 %. Upon running

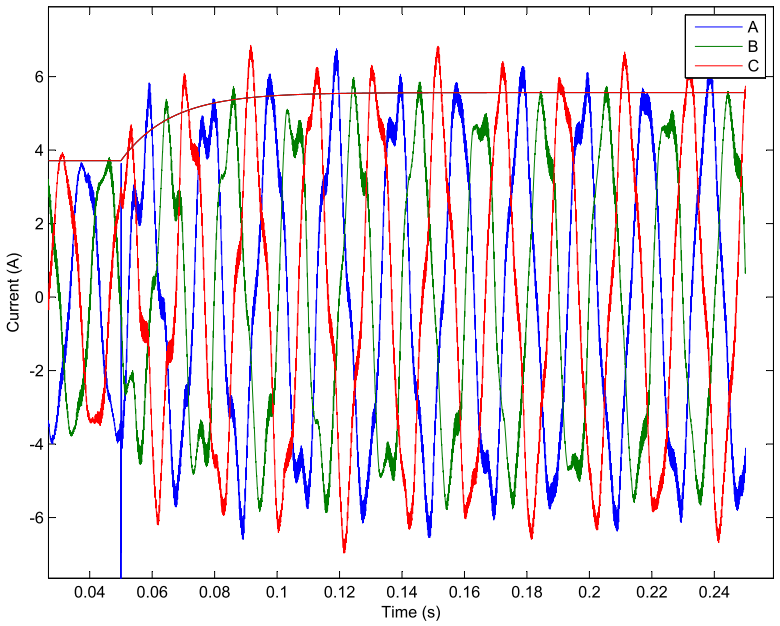

FIGURE 6.5: Current waveform of IIEG_1 Exposed to Close Proximity Single-Phase Fault

an equivalent small-signal model, IIEG_2's controller was unable to regulate real and reactive power as the current export signal calculated by the controller was too volatile for normal operation. The power export of IIEG_2 is shown in Fig. 6.7.

In cases of a large voltage drop caused by a three-phase bolted fault, errors are not induced through an unbalance of signal. Rather, the current set point calculated within the controller cannot be physically exported by the IIEG unit under such a significant fault condition. Even if over-rating of the power electronics is employed within the inverter, a greater DC voltage is required to export the desired current. The resultant waveform contains heavy clipping as shown in Fig. 6.8.

Under such extreme fault circumstances, the results of the FAT are unreliable. It must be stressed that the controllers are not designed to provide a smooth sinusoidal output for extreme fault conditions. In practice, exposure to extreme faults will result in fast tripping via I^2t thermal protection. However, as shown in Chapter 5, the results of the FAT are very accurate for higher impedance faults. The aforementioned errors can be eliminated by employing an EIT current threshold that will nullify all fault conditions where the IIEG controller is incapable of maintaining constant power and/or constant

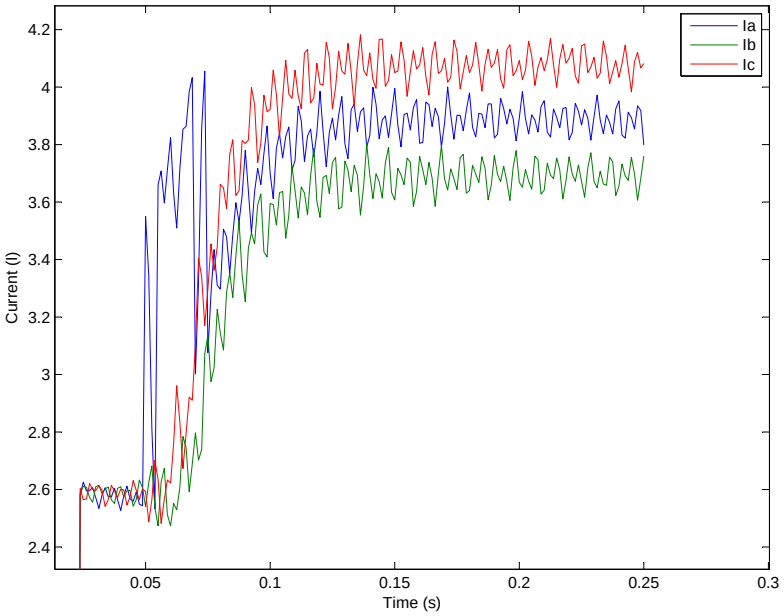

FIGURE 6.6: rms Current of IIEG_1 Exposed to Close Proximity Single-Phase Fault

current conditions. The FAT and PAT are predicated on both conditions being met when an IIEG unit is exposed to a fault.

The FAT is incapable of simulating sub-transient responses within a DN. However, the small-signal simulation platform passes all rms and sequence plots through a cosine filter of sixteen samples per cycle in order to be commensurate with protective relay devices. Hence, any brief sub-transient responses to disturbance in the grid are attenuated by protection devices and have little or no effect on the protection response. Therefore, the omission of short-term sub-transients does not negatively impact the integrity of the FAT nor PAT.

The PAT attempts to capture the worst case scenario fault instances for protection integrity analysis. The PAT takes into account the possibility of over-rated power electronic switches within IIEG units for fault ride-through purposes. The FAT assumes that the power set points of the control system can be realised during steady-state operation. In instances where an IIEG unit's control scheme and AC filter are subjected to a condition that does not allow the power set points to be realised, the resultant steady-state current will likely exceed the rated current of the inverter. The implementation of FCL or EIT can aid in providing a more realistic evaluation of a contemporary DN's protection scheme.

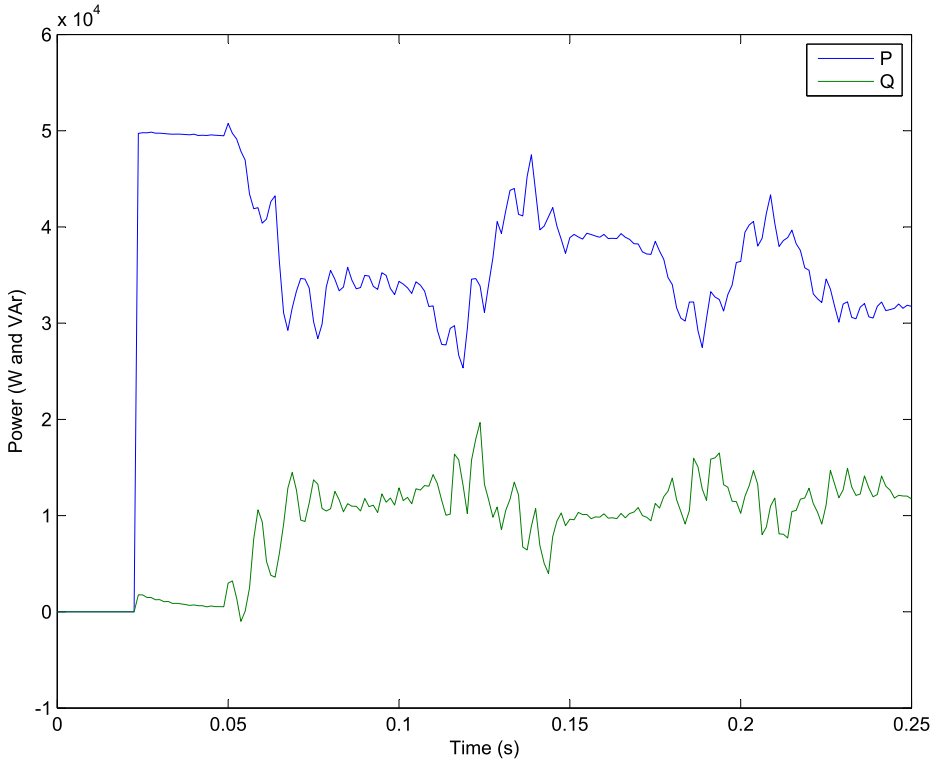

FIGURE 6.7: Power Set-Point Failure During Reflected Line-to-Line Fault

Various simulations showed that convergence is achieved for all single-phase to earth and line-to-line faults as at least one phase voltage remains at approximately the nominal value, irrespective of transformer winding connections and fault locations. However, the predicted fault response may not provide an accurate representation of the true fault response of an IIEG unit. Hence, to mitigate misleading data, an EIT should be implemented in accordance with the capability of IIEG units.

6.6 PAT Case Study

The PAT has been applied to the circuit shown in Fig. 6.9. The network data is given in Table 6.1. The generated reports of the following cases are shown in Appendix C:

- No FCL nor EIT implemented.
- EIT threshold of 1.2 is implemented.

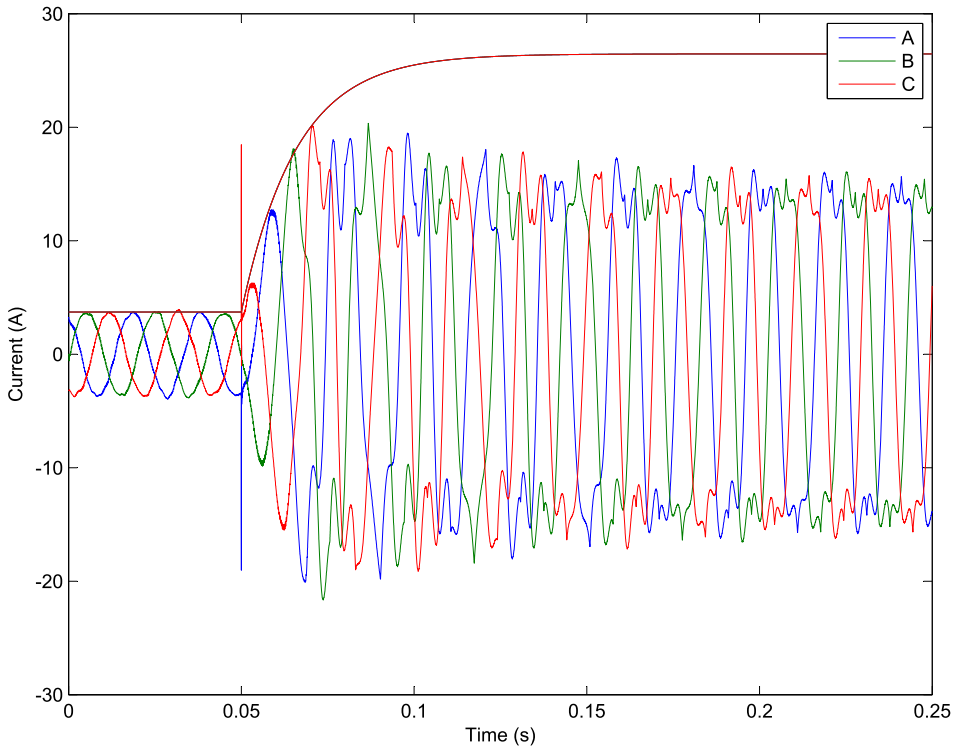

FIGURE 6.8: Current Export of IIEG_3

Both reports contain 22 cases of convergence error. The errors are reported within the MATLAB command window but are not explicitly included within the report. An analysis of the errors showed that all were instances of three-phase bolted faults immediately downstream of CT_1 and CT_2. For every fault location and type, every IIEG combination is considered. As there are four IIEG units, there are 2^4 simulations for every fault case in the example network. Consider the sixteen simulations for a three-phase fault immediately downstream of CT_1. Eight of the simulations will contain IIEG_1 which is incapable of convergence (when connected) as IIEG_1 is completely devoid of voltage and frequency regulation. Secondly, consider the sixteen simulations with a three-phase fault at CT_2. Fourteen of the simulations will contain IIEG_2, IIEG_3 or IIEG_4 which are similarly incapable of convergence without frequency and voltage regulation. Hence, there are a total of 22 cases of convergence error which are unavoidable using the PAT, but are also non-essential from a protection analysis perspective as explained in Section 6.4.

The reports show subtle differences in expected minimum, maximum and OOZ fault currents when the EIT is implemented. The peak load is unchanged as EIT thresholds

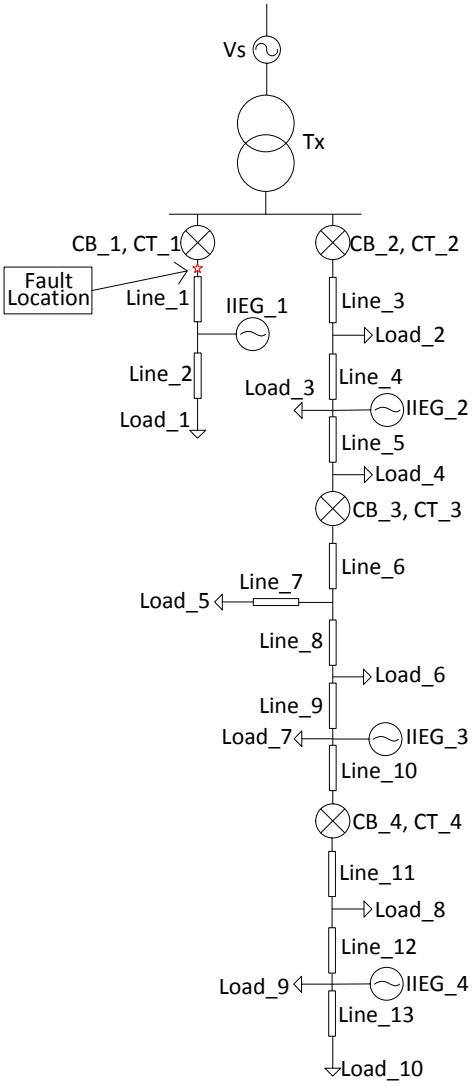

FIGURE 6.9: Single Line Diagram

are not met during healthy conditions. In order to provide a partial verification for the presented reports, a few cases were chosen to compare the small-signal modelling with the results of the generated report. Examples for PAT report interpretation for the following cases are also included. The chosen cases were:

- the peak current at CT_1.
- the OOZ current at CT_2.
- the pick-up current at CT_3.

- the maximum current at CT_4.

6.6.1 Peak Current at CT_1

In a DN with a high EG penetration, there are two possible peak current conditions for every protection device that may occur during healthy conditions:

- Forward flowing current: peak loading downstream of a protection device with no local IIEG availability.
- Reverse flowing current: low loading downstream of a protection device with maximum local IIEG availability.

The presence of upstream IIEG (or IIEG on adjacent feeders) can both increase and decrease the peak current flowing through a CT and therefore must be taken into consideration. The PAT considers all combinations of IIEG connection to determine the peak current for every protection device under healthy conditions.

A small-signal analysis of the network in Fig. 6.9 was simulated with IIEG_1 disconnected and all other IIEG units connected. This simulation represents the forward flowing current condition. The rms currents observed after passing through the cosine filter are shown in Fig. 6.10. All rms currents overlap as the DN is balanced.

The current passing through CT_1 under peak conditions as observed by the cosine filter during the small-signal analysis is 1.3121 A, which is below the value generated by the report 1.3123 A, which was determined by the PAT (see Appendix C). The discrepancy exists because the forward flowing condition did not provide the peak current for CT_1 in the PAT's analysis.

A second small-signal analysis of the network in Fig. 6.9 was simulated with IIEG_1 connected and all other IIEG units disconnected. This simulation represents the reverse flowing current condition. The rms currents observed after passing through the cosine filter are shown in Fig. 6.11.

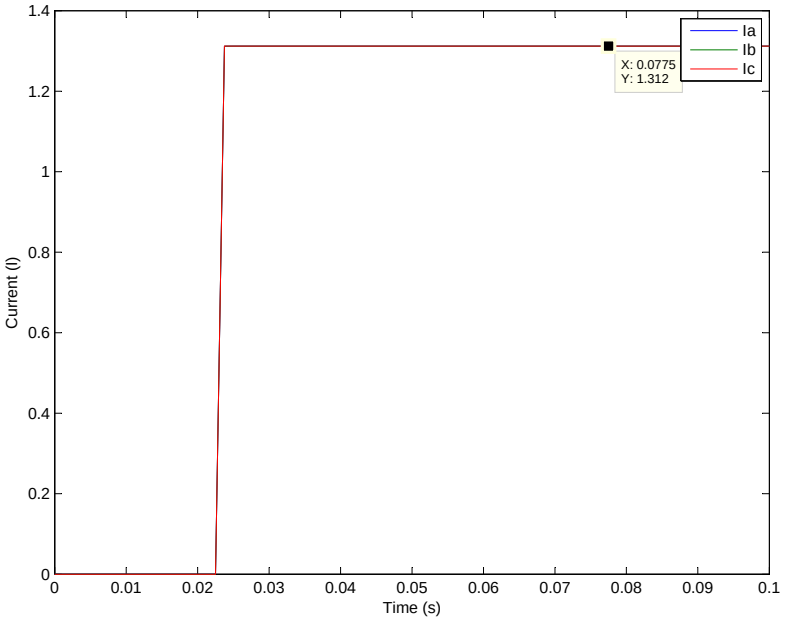

FIGURE 6.10: CT_1 rms Current under Peak Load Condition I

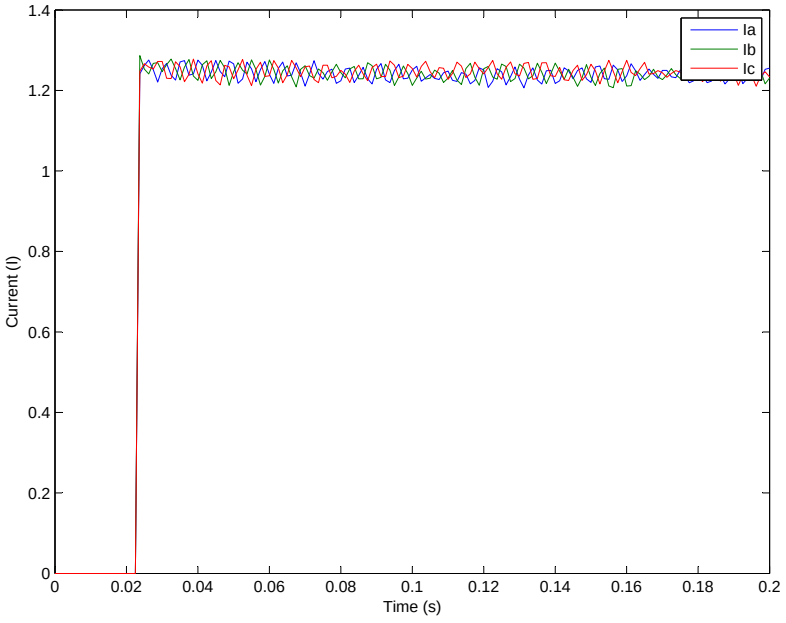

FIGURE 6.11: CT_1 rms Current under Peak Load Condition II

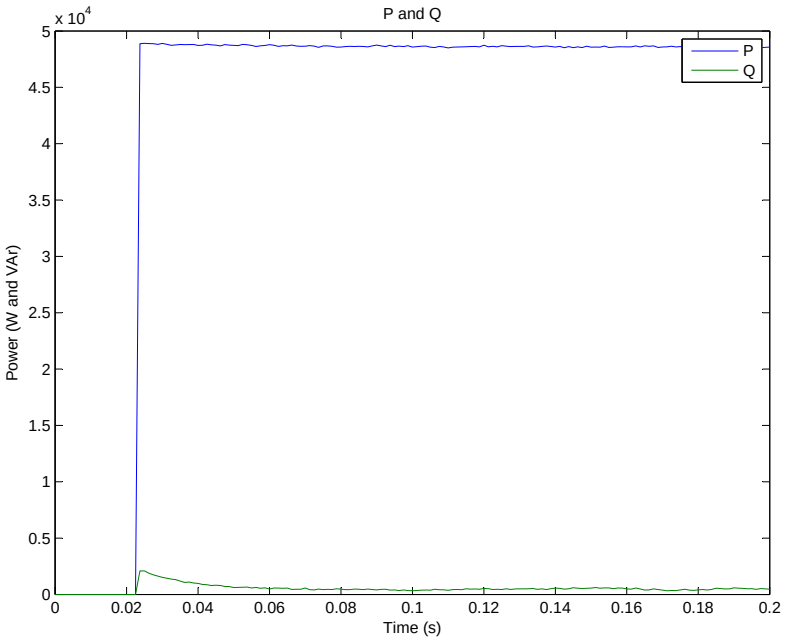

FIGURE 6.12: CT_1 rms Current under Peak Load Condition II

The theoretical current flowing through CT_1 according to the FAT is 1.312349 A, which is consistent with the PAT's peak loading value. However, the rms current measured by the cosine filter is approximately 1.24 A, well below the current observed in the forward flowing current condition. The discrepancy between the small-signal simulation and FAT results can be attributed to the large impedance between IIEG_1 and equivalent load. Each IIEG unit's control scheme was designed under the assumption that the power export would be consumed locally. This assumption is not satisfied during the reverse flowing current case. The power export of IIEG_1 is shown in Fig. 6.12 and is not operating at 50 kW unity power factor as assumed by the FAT.

A small discrepancy in the predicted peak current arose during the reverse flowing current condition. Whilst the error is in an order of magnitude that shall not negatively impact a protection scheme, it is essential to recognise that the PAT assumes that each IIEG unit is capable of exporting the desired power for all conditions. The reverse flowing current condition represents an extreme case where the IIEG power export on a feeder was double the local load. Such a condition could be eliminated through use of storage devices or careful DN planning.

The presence of IIEG on the adjacent feeder reduces the current demand of the zone substation, raising the voltage at the zone substation busbar (ignoring voltage regulation via tap-changers). Depending on the load, the voltage rise could increase or reduce the current passing through CT_1. In the simulations presented in this Thesis, all loads are constant impedance. Hence, a higher voltage usually implies a higher current drawn by a load. However, a constant power load may have an inverse relationship between voltage and the current drawn by a load. Ergo, every IIEG combination should be examined and compared to capture the true peak load situation from the perspective of any protective device.

The EIT thresholds were not exceeded by any IIEG unit during peak conditions. Therefore, the reported peak current is common across both reports. Hence, when the protection engineer is selecting the pick-up current setting, the peak current of the relevant CT within the PAT report may be used as a reliable source. The peak current is then increased to compensate for forecasted peak load and may then be used in (6.4).

6.6.2 OOZ Current at CT_2

Referring to the PAT report for CT_2 in Appendix C, there exist two OOZ cases for OC and EF protection. There exist are four protection zones in total, each corresponding to the CT immediately upstream of each zone (the CT corresponding to the CB that should trip first for a fault within a designated protection zone). The protection zones are illustrated in Fig. 6.13 for clarity. The primary and secondary zones of CT_2 correspond to zones of protection 2 and 3, respectively. Hence. the zones of protection 2 and 3 are considered to be in-zone and are excluded from OOZ protection analysis.

The purpose of OOZ analysis is to identify instances of possible nuisance tripping. The presence of IIEG can provide reverse fault current through a protective device which may instigate an unnecessary trip for a fault outside of a protection device's zone of protection. The identification of the plausibility of such a loss of discrimination may be easily remedied through either a change in pick-up protection settings or installation of a directional element with OC protection.

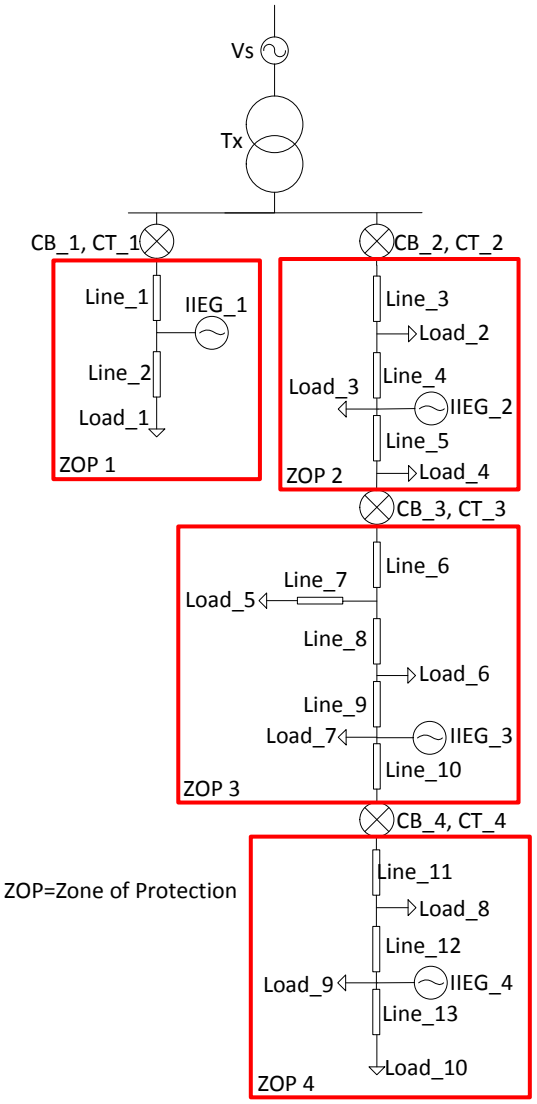

FIGURE 6.13: Single Line Diagram with Zones of Protection

Consider the case where no EIT is used in the PAT. The OC and EF OOZ fault currents of zone of protection 4 are significantly higher than the fault currents of zone of protection 1. However, as zone of protection 4 is downstream of CT_2, no discrimination problems will arise provided the IDMT curves between zone CT_2, CT_3 and CT_4 are graded properly.

A small-signal model of the example network was run with a single-phase to earth fault placed immediately downstream of CT_1, representing the worst case scenario for an OOZ fault from CT_2's perspective. The rms current and current waveform flowing through

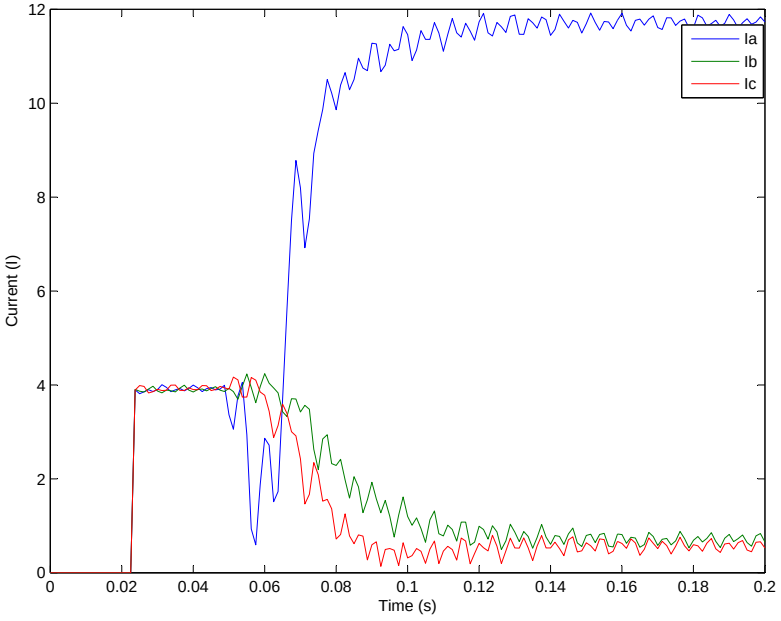

FIGURE 6.14: CT_2 rms Current with Reverse Current Flow

CT_2 are shown in Figs. 6.14 and 6.15, respectively. Note that the small-signal current waveform is superimposed with the FAT approximation. The current waveform is heavily distorted due to the significant voltage unbalance at the IIEG unit's PCC. The control dynamics of the inverter and the AC filter are not designed to provide a smooth sinusoidal waveform during such significant disturbances. The steady-state rms current is 11.71 ± 0.14 A which closely matches the predicted OOZ EF current of the PAT which was 11.742 A. Hence, the PAT result has accurately capture the worst case scenario EF condition for CT_2.

A three-phase fault immediately downstream of CT_2 rendered the FAT unsolvable as the voltage drop on the adjacent feeder was too significant to allow voltage commutation. Hence, the results from such a situation are excluded. However, as explained in Section 6.4, the significant voltage drop at each IIEG unit's PCC will likely result in a fast thermal trip, isolating the IIEG prior to the operation of any line protection devices. Hence, the three-phase fault case may be ignored without compromising the integrity of the PAT.

A line-to-line fault was placed immediately downstream of CT_2 across phases A and B at $t = 0.05$ s. The fault response predicted by the FAT proved to be significantly different from the small-signal simulation. The controller of each IIEG was unable to maintain

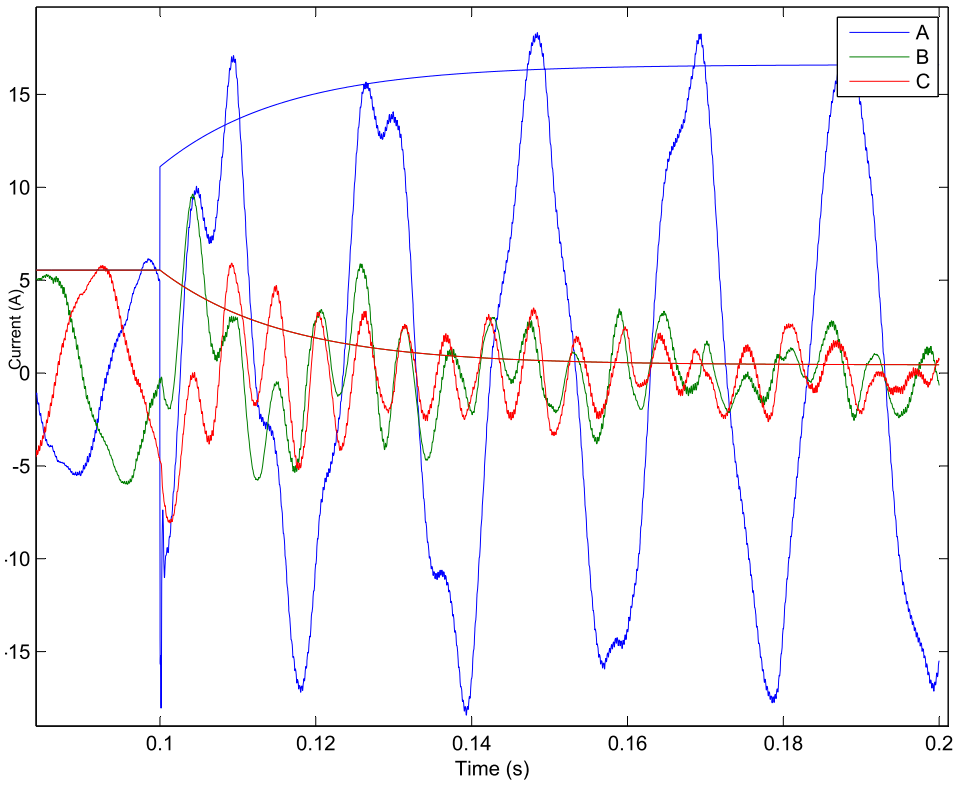

FIGURE 6.15: CT_2 Current Waveform with Reverse Current Flow

the specified power set points 50,000+j0 VA. The power export of IIEG_2 is shown in Fig. 6.16. The power calculation within the small-signal environment requires a cycle of voltage and current data before plotting the real and reactive powers. Hence, the first 0.02 seconds of power data are omitted.

In practice, all IIEG would be isolated via thermal protection due to large fault current drawn from each IIEG unit; failure to quickly isolate the IIEG would result in fast destruction of the inverter interface. Hence, the fault contribution of IIEG does not significantly affect the protection efficacy of the DN line protection and can be ignored from consideration in the PAT using the EIT.

The PAT report employing EIT in Appendix C shows that the maximum fault current flowing through CT_2 during any fault in CT_1's zone of protection is less than the peak current. However, the PAT examines only SOZ and EOZ faults. There may exist a point within CT_1's zone of protection which defines the threshold where the fault current of IIEG_2 does not exceed the EIT threshold. The true maximum OOZ fault current flowing

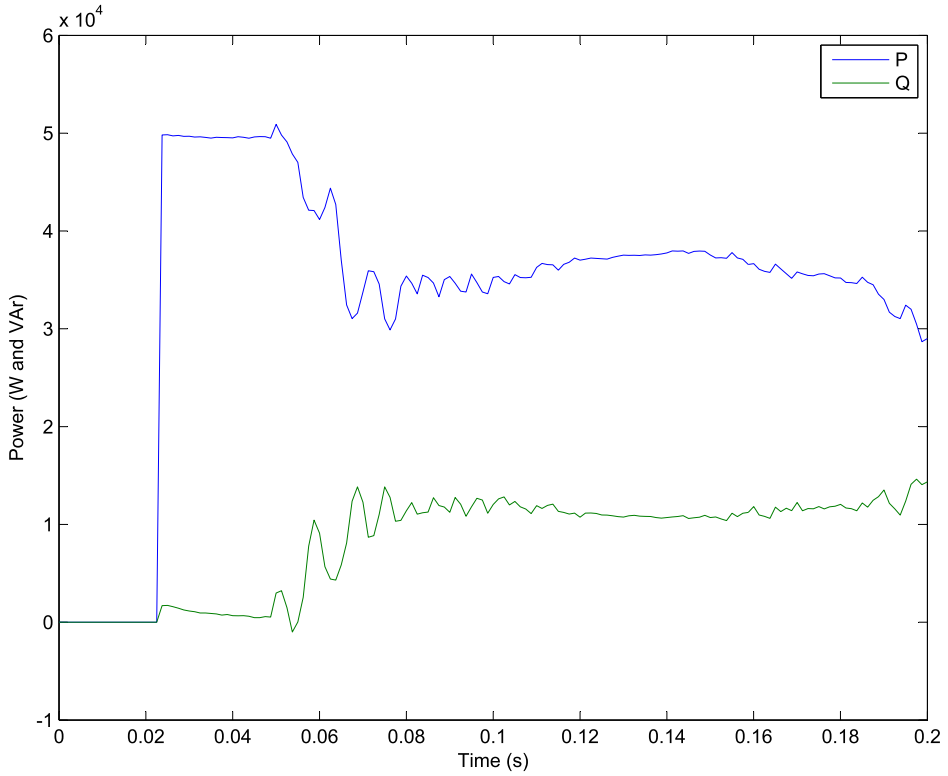

FIGURE 6.16: IIEG_2 Power Export during Low Impedance Line-to-Line Fault

through CT_2 for a fault in CT_1 lies between the values indicated by the two reports. If the worst case report can be satisfied within the scope of (6.4), then no further exploration is necessary. However, if tolerances on the pick-up current do not satisfy the worst case scenario, supplementary FAT or small-signal simulations will be necessary to capture the true OOZ fault current in this case.

Supplementary simulations will explore faults midway through a zone of protection, rather than the extremities. The desired fault location will incite the maximum fault current through CT_2 without IIEG_2 from tripping due to thermal tripping. An algorithm to automate the desired fault location is outside the scope of the PAT, but represents an opportunity for future work.

6.6.3 Pick-up current at CT_3.

Pick up currents are determined through an analysis of forecasted peak load, OOZ fault events and the minimum expected fault current for a given zone of protection. EOZ faults will generally not necessitate fast tripping of IIEG units upstream of the fault unless an IIEG unit is in very close proximity to the fault.

Consider the case where a low impedance single-phase to earth fault is placed at CT_3's EOZ. IIEG_3 and IIEG_4 both exceed the threshold for an EIT. The PAT report predicts a primary earth fault pick-up current of 535.49 A without the EIT and 535.65 A with the EIT. The implementation of an EIT generally offers only a minor change in pick-up settings. The increased predicted fault current of the EIT case compared to the non-EIT case can be attributed to the effect of IIEG_3 on the fault current. A decrease in the fault current flowing through a protection device occurs whenever an IIEG unit is exporting real power in between that protection device and a fault. The discrepancy in the PAT report is caused by the EIT case omitting the connection of IIEG_3 during the fault as the current threshold of IIEG_3 is exceeded; the non-EIT case does not exclude the connection of IIEG_3.

Two cases of the observed fault current of CT_3 during the single-phase to earth fault are shown in Figs. 6.17 and 6.18. Fig. 6.17 is the rms current when IIEG_3 is connected; Fig. 6.18 is the rms current when IIEG_3 is disconnected.

The PAT predicted fault currents of 535.49 A when IIEG_3 is connected and 535.65 A when IIEG_3 is disconnected. The small-signal results yield a fault current of 535.50 A when IIEG_3 is connected and 535.65 A when IIEG is disconnected. Hence, the PAT is capable of discerning the subtle effects of IIEG connection (and disconnection) on the required pick-up currents within a tolerance reasonable for DN line protection devices.

The minimum fault current is the final piece of information required for determination of an acceptable pick-up EF current, which is redefined in (6.6).

$$\max[I_{\text{unbalance}}, I_{\text{out of zone faults}}] < I_{\text{p.u.}} < k \cdot \min[I_{\text{in-zone faults}}] \tag{6.6}$$

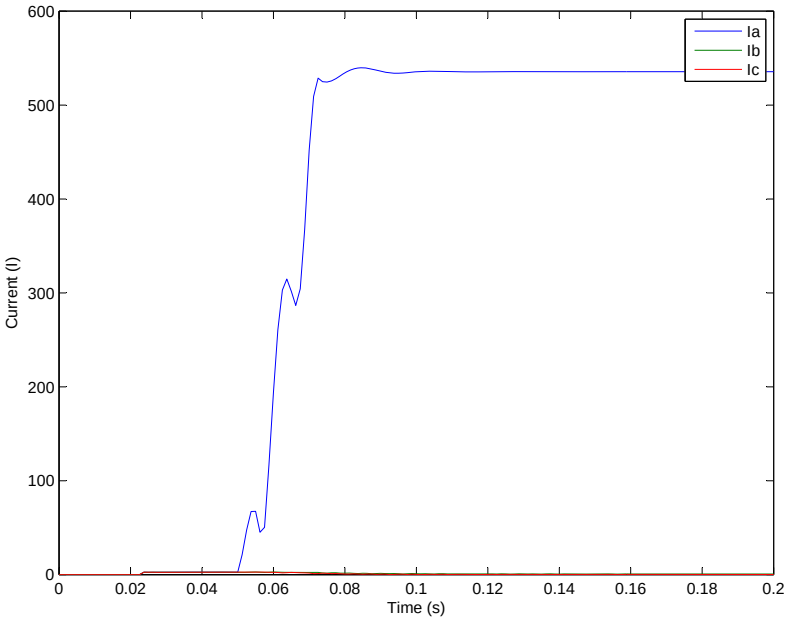

FIGURE 6.17: CT_3 rms Current with IIEG_3 Connected

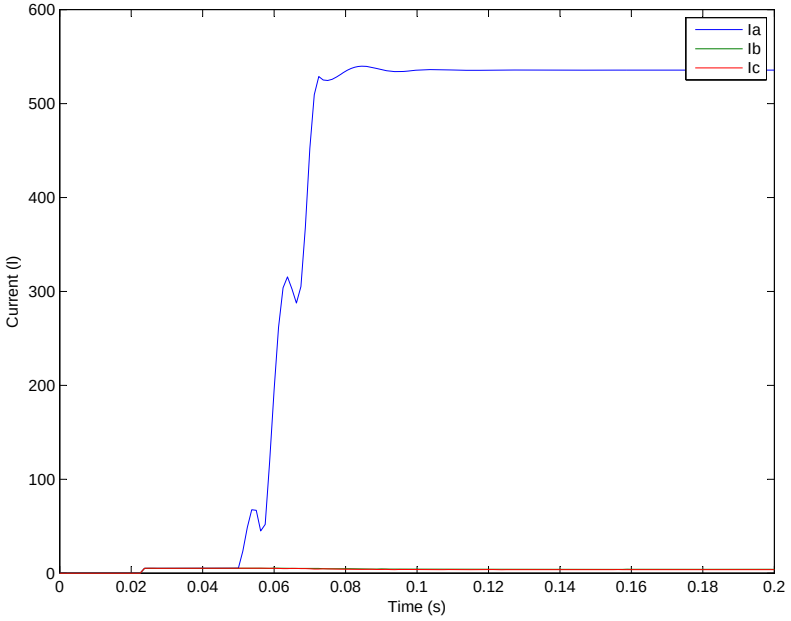

FIGURE 6.18: CT_3 rms Current without IIEG_3 Connected

The aforementioned results found a minimum in-zone EF current of 535.49 A. Hence, $\min[I_{\text{in-zone faults}}] = 535.49$ A. Using the information in the PAT reports found in Appendix C, and OOZ cases can be found. The PAT report without the EIT has a maximum OOZ EF current of $I_{\text{out of zone faults}} = 7.84$ A. The PAT report with the EIT has only a slight variation in OOZ EF. There is no unbalance within the simulated networks; hence, $I_{\text{unbalance}} = 0$ A. A FAT tolerance error does not need to be included as only high impedance faults are assessed in pick-up current determination. Choosing a hypothetical forecasted peak load of 2 times the current peak load and $k = 0.5$, the range of acceptable EF pick-up currents can be expressed as (6.7).

$$15.68 < I_{\text{p.u.}} < 267.75 \tag{6.7}$$

The process can be repeated similarly for the OC pick-up settings by employing (6.4). The peak current is available in the PAT; however, forecasting is necessary to determine the value of $I_{\text{forecasted peak}}$.

6.6.4 Maximum current at CT_4.

The maximum current reported in Appendix C by the PAT is 540.27 A which occurs during a three-phase bolted fault immediately downstream of CT_4. When the EIT option is employed, the maximum anticipated fault current is reduced to 535.28 A. IIEG_4 is excluded from the simulation as all IIEG downstream of a three-phase bolted fault are incapable of voltage and frequency regulation. IIEG_2 and IIEG_3 both exceed the EIT current threshold and are therefore excluded during the EIT case.

A small-signal model of the same DN with a three-phase bolted fault placed immediately downstream of CT_4 was simulated. The rms currents and voltages measured by CT_4 are shown in Fig. 6.19 with all IIEG connected (reflecting the non-EIT case) and Fig. 6.20 with IIEG_2 and IIEG_3 disconnected (reflecting the EIT case). Note that the voltages across the CTs are very small due to the low impedance of the CTs and overlap the time axis.

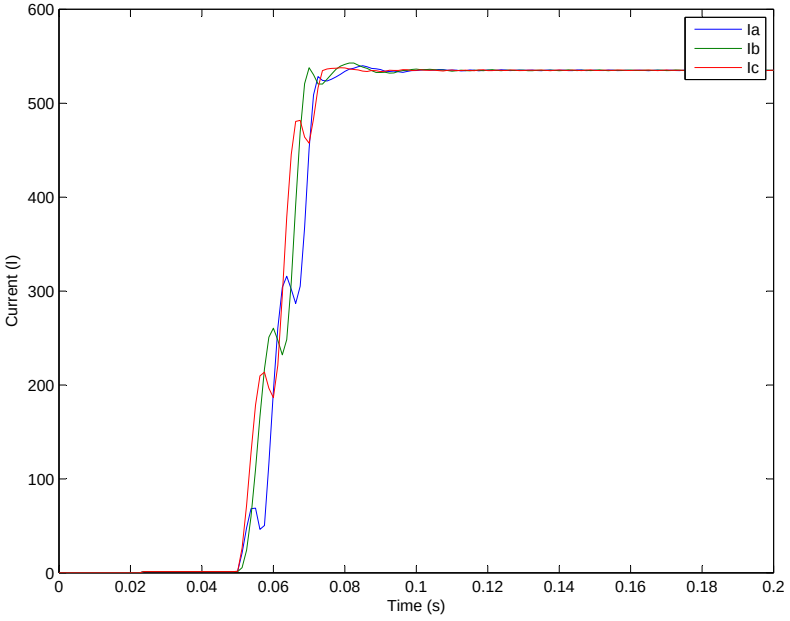

FIGURE 6.19: CT_4 rms Current with IIEG_2 and IIEG_3 Connected

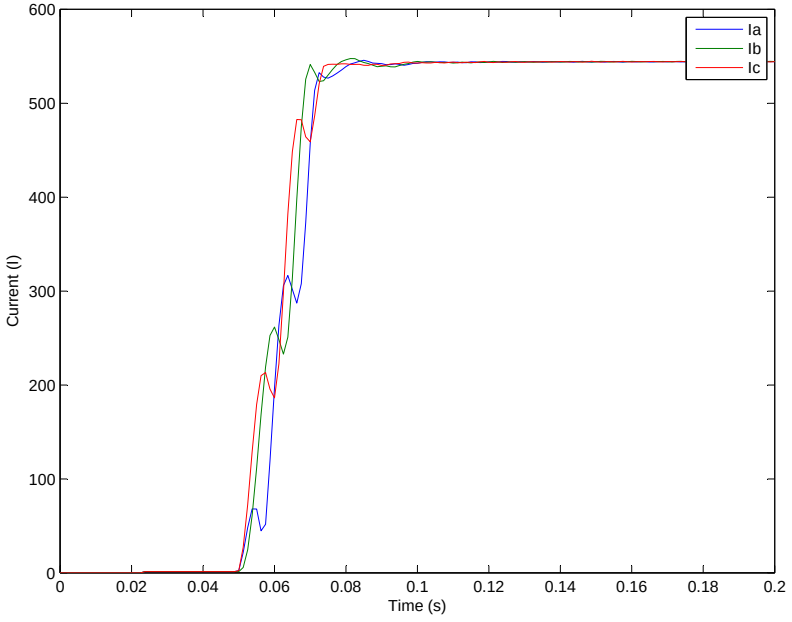

FIGURE 6.20: CT_4 rms Current with IIEG_2 and IIEG_3 Disconnected

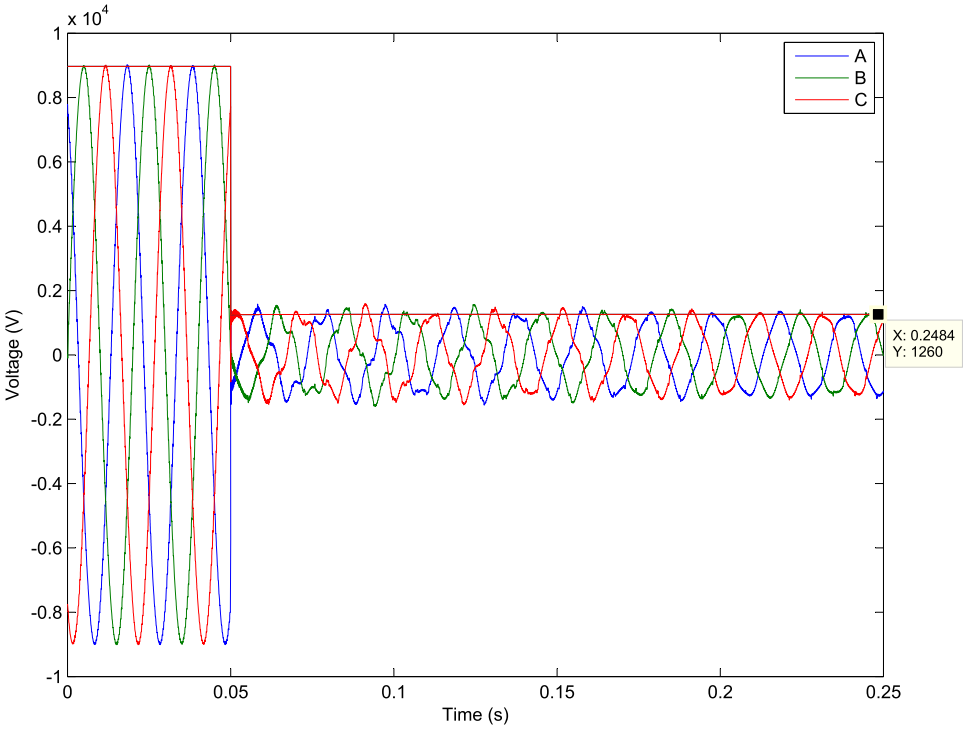

FIGURE 6.21: Voltage at Terminals of IIEG_3

The rms current measured by the small-signal simulation with all IIEG connected is 544.4 ± 0.3 A which is significantly higher than the maximum fault current predicted by the PAT (540.27 A). Once again, the error is a result of an IIEG unit's inability to provide the constant power and constant current on which the PAT scheme is predicated. The most extreme case is IIEG_3 where the voltage drops to approximately 14% of the prefault voltage as shown in Fig. 6.21. The current exported by IIEG_3 and the current predicted by the FAT are shown in Fig. 6.22. The current waveform is clearly prone to clipping as the IIEG unit is incapable of exporting such a high current.

The rms current measured by the small-signal simulation with IIEG_2 and IIEG_3 disconnected is 535.1 ± 0.3 A which is within range of the maximum fault current predicted by the PAT (535.28 A). Once again, the results of the PAT for extreme faults are unreliable without the application of an EIT. An appropriate setting for EIT is pivotal to the integrity of the PAT scheme unless IIEG units are over-rated and designed such that the desired constant power and constant current output is achieved.

The results within the PAT predicting the maximum current flowing through a CT can

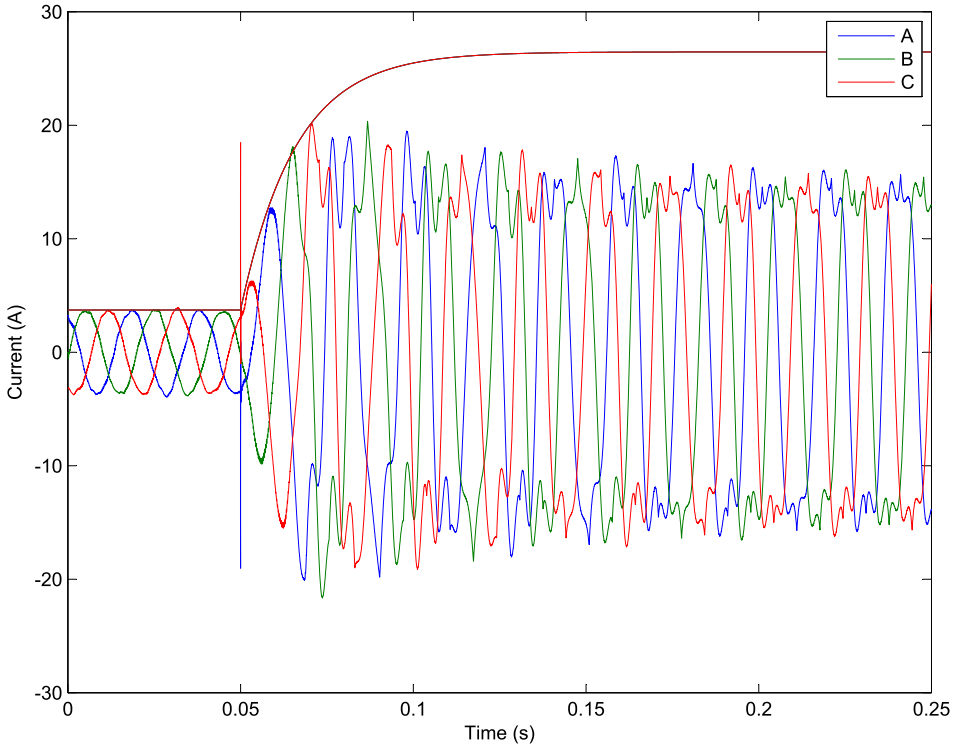

FIGURE 6.22: Current Export of IIEG_3

aid in the appropriate selection of CBs. The PAT data in Appendix C reveals the impacts of IIEG connection on fault currents with and without the application of an EIT. The EIT option reveals a more realistic requirement of the maximum fault current that will flow through a CB assuming IIEG units will trip due to thermal overloading for low impedance faults. However, if the CB is rated higher than the maximum fault current predicted without application of the EIT, then the CB is correctly selected such that all faults can be cleared in instances of IIEG protection failure and significant inverter over-rating.

Maximum fault currents are the most likely candidate for errors in calculations within the FAT. If the EIT is incorporated into the PAT, then this error should be minimised. For single-phase to earth faults, an error of 7% should be added to the contribution of IIEG fault current. For all other fault types, it may be assumed that either a thermal trip will isolated the IIEG unit or the voltage drop at the PCC of the IIEG unit is insufficient to create a significant error in the IIEG unit's fault current.

6.7 Conclusion

The PAT has proven to be an effective means of analysing the protection adequacy of a DN with a high IIEG penetration if the tolerances of the tool and IIEG unit's are taken into consideration. The constant power control scheme adopted in the small-signal modelling (which was introduced in Chapter 3) was shown to be ineffective in achieving the desired output for extreme fault conditions. In all cases of significant voltage drop at the terminals of an IIEG, the controller was unable to maintain the desired constant power export and/or a balanced current export. Hence, for the adopted controller, implementation of an EIT is essential in maintaining the accuracy of the results generated by the PAT. Alternatively, an FCL could be utilised thus removing the risk of excessive fault current be drawn from IIEG units under fault conditions.

The limitations of the PAT to adequately represent the actual fault response of an IIEG unit are generally made redundant by the thermal tripping feature of IIEG units. For the IIEG unit's controller to be unable to export the desired power set points, a significant fault current will always be drawn, triggering the thermal trip.

Examples of how the PAT may be applied to a DN have been included. The PAT is simply an aid is the process of determining appropriate CB ratings and OC/EF relay protection settings. The PAT must in practice be supplemented with data captured by SCADA, DN line data as well as expectations of demand growth. The connection of a large IIEG unit may preclude DN protection adequacy; the PAT is a very useful tool for this purpose. If the proliferation of IIEG continued in Australian DNs, the applications for the PAT will become apparent.

Future work involves verifying the application of FCLs to the PAT and defining the power factor utilised when the FCL is applied. Furthermore, the ability for the threshold fault locations where a maximum OOZ fault event occurs without triggering an EIT could be of significant value in DNs where protection discrimination is difficult to achieve.

Chapter 7

Proposed Microgrid Design Philosophy

7.1 Introduction

Chapters 3 through 6 have focused on methods allowing for the increased presence of IIEG in DNs. If IIEG penetration levels grow past 100% of local load, an opportunity for isolated and autonomous segments of DNs arises. The concept of autonomous segments of DNs is otherwise known as the microgrid.

This chapter proposes a microgrid control and design philosophy that will ensure adequate fault discrimination during intentional islanding. Fault discrimination is assured through a novel autonomous IIEG controller, alterations to transformer winding connections within microgrids and the voltage sequence detection protection scheme. Small signal modelling results within the MATLAB environment yield a proof of concept for the proposed controller, microgrid design philosophy and protection scheme. Further research is required to prototype the proposed microgrid design philosophy.

The proposed microgrid design philosophy is not intended to assimilate the various microgrid design philosophies asserted by other authors as outlined in Chapter 2. Rather, the proposed microgrid design philosophy simply adopts the preferred microgrid attributes

and applies these attributes to an envisaged microgrid deployment that is retrofitted with Australian distribution networks. Hence, minimal changes to existing distribution network design philosophy are recommended – the most significant change exists in the installation of reliable medium-scale IIEGs coupled to distribution networks. Medium scale IIEG units are defined to be three-phase, over 30 kW in size, highly reliable and must be galvanically isolated from all loads through a wye-wye transformer. The presence of reliable medium-scale IIEGs is vital to ensure sufficient local generation is available to meet the demand of an island and adequate power quality can be maintained.

7.2 The Motivation for Microgrids

The contemporary microgrid concept is a vision for maximising reliability in DNs. The renewable nature of most small and medium-scale IIEG is attractive from an environmental perspective and possesses the potential to be lucrative through carbon pricing (if such a scheme is permanently implemented). However, due to the intermittent behaviour of IIEG energy resources, a significant storage capacity is an essential segment of any network. These large storage units constitute an important part of medium-scale IIEG. The presence of storage negates issues concerned with steady state voltage levels and can provide superior stability, protection discrimination and reliability properties if well designed.

Medium-scale generation is presently incapable of satisfactory operation when in autonomous mode. Hence, pre-existing systems will require a significant investment in control, storage and protection systems in order to render microgrid operation permissible. Furthermore, new systems would have to be added to bolster the EG penetration level of a microgrid in excess of 100% of peak demand. The implementation of the proposed microgrid philosophy is primarily the deployment of new infrastructure with limited manipulations of older infrastructure.

Due to the sizing and location of medium scale EG, much of the cost is borne by investors, rather than the government bodies. A highly capitalistic economic structure such as the Australian economy would thrive if adequate returns could be achieved. The most

significant cost to the utility would be the deployment of communications infrastructure between medium scale IIEG units and microgrid DN devices. A cost-benefit analysis is beyond the scope of this Thesis; however, if DN reliability decreases due to deregulation and the increase in the frequency of natural disasters, microgrids may become the only viable alternative for many customers whom cannot sacrifice supply and for the utility that wants to defer infrastructure upgrades.

The focus of this Chapter is the development of a microgrid philosophy which allows for adequate fault discrimination. IIEG are used instead of traditional synchronous machine-based generation; hence, traditional OC and EF techniques are insufficient for fault identification. Protection is only one of several technical challenges that must be overcome within microgrid design philosophy. Islanded microgrid stability is an important issue that will require further research before this design philosophy can be accepted. Voltage, frequency and reactive power support can all be achieved in principle using the droop controller defined in Chapter 3 and through EG coordination as elaborated within this Chapter. Disconnection and reconnection with the grid is explored in this Chapter briefly, but again requires significant investigation before the proposed microgrid design philosophy can be accepted. Furthermore, the proposed earthing and transformer connection is a topic of controversy: the balance between cost, electrical safety and robustness of microgrid operation a topic requiring further debate.

7.3 Microgrid Components

7.3.1 Static Transfer Switch

A static transfer switch (STS) is a microgrid component implemented to separate and reconnect a microgrid with a larger grid. However, when considering a more modular microgrid, each STS defines a point of modularity: a point where any segment of a network can be divided or adjoined to any other segment of a network where intentional islanding is permitted. The functionality of a STS must include:

- the ability to communicate with all other local STSs and IIEG units;

- the ability to deliberate whether intentional islanding of a microgrid meets certain requirements;
- the ability to detect LOM;
- the ability to disconnect and resynchronise with the grid, which requires:
  - the ability to measure the voltage difference across the circuit breaker when open, and;
  - the standard protection and fault isolation capabilities of contemporary reclosers.

The envisaged STS is essentially an advanced form of recloser that has been modified to allow for grid resynchronisation and advanced coordination with other protection devices and IIEG units. Grid resynchronisation can be achieved via zero voltage difference detection across the open terminals of the STS. The voltage waveforms on each side of the STS will eventually reach zero phase difference due to slight frequency discrepancies between the segregated networks [44]. Islanded microgrids are controlled using a droop control scheme; a very slight real power deviation from nominal will result in a non-nominal island frequency. The impacts of resynchronising the proposed microgrid on network stability are beyond the scope of this Thesis, yet are an important topic for future research. It is envisaged that, if the microgrid becomes commonplace, eventually every DN recloser will have the ability to behave as a STS to allow for any future upgrades of a network segment.

7.3.2 Transformers

Each load and small-scale IIEG unit must be interfaced with the grid through a three-phase delta-wye transformer. The wye side must be solidly earthed to be commensurate with AS/NZS 3000:2007 [64]. In urban locations in Australia, the use of three-phase delta-wye transformers is wide-spread; hence, little modification of existing infrastructure would be necessary. In rural applications, there exists many single phase transformers. However, rural applications tend to have significant impedances between loads. It is uneconomical

to design and implement a microgrid when exporting power to any neighbours requires a significant upgrade of power lines. In the case where high reliability is necessary, the most economical solution is an uninterruptable power supply, usually a diesel generator and flywheel. Hence, the assumption that all customers in a microgrid are connected through a three-phase delta-wye transformer can be considered reasonable.

All medium-scale IIEG units within the proposed microgrid design philosophy must be interfaced within the grid through a wye-wye transformer. Both star points of the transformer must be solidly earthed. The use of wye-wye transformers in distribution networks has been avoided, mainly due to the impacts of multiple zero sequence paths on sensitive earth fault protection and power quality. Consequently, an analysis of sensitive earth fault reach must be conducted for a proposed microgrid before the proposed microgrid design philosophy can be adopted. Furthermore, the use of wye-wye transformers will preclude the zero sequence harmonic attenuation normally associated with delta connected transformer windings. Where harmonics are considered to be a problem, harmonic compensation can be achieved through IIEG control [74].

From a microgrid perspective, there are significant benefits of having an IIEG unit connected through a wye-wye transformer. The rated voltage of an inverter interface is not necessarily the grid voltage; hence, a transformer can be useful in stepping up the voltage. The transformer also behaves similarly to a series connected inductor providing a filtering function which is useful when attenuating voltage waveform distortion. Finally, a wye-wye transformer allows measurable zero sequence voltage at the terminal of an IIEG unit. Since all loads are connected through delta-wye transformers, no zero sequence voltage will be present at any load terminals. Hence, all zero sequence voltage can only be instigated by shunt elements such as capacitances between lines and earth and earth faults. Given that the lengths of lines in a microgrid are in the order of only a few kilometres, the shunt reactances between power lines and the earth are very large and can generally be neglected during fault calculations. Hence, the use of wye-wye connected transformers is beneficial for the detection of high-impedance single-phase to earth faults without resorting to complicated energy spectral methods such as those proposed by [62].

It is important to note that zero sequence current flow can also be achieved if a wye earthed-delta transformer is installed at each IIEG unit (where the delta connection is on the IIEG side). Furthermore, triplen harmonic attenuation can be achieved through use of a wye-delta transformer. However, the current and voltage measurements would need to be made on the high voltage side for zero sequence current and voltage detection which would likely necessitate extra expenditure on CTs and VTs. There would be little benefit from a the line protection's SEF adequacy perspective. Hence, the use of wye-wye connected transformers for medium-scale IIEG interconnection is preferred and adopted within this Thesis.

7.3.3 Embedded Generation

All EG units are to be coupled to a microgrid via an inverter interface. The inverter interface provides decoupling of the energy resource dynamics from the grid [18]. The inverter interface can be controlled to provide significant versatility regarding control characteristics given the voltage and current ratings of the internal power electronics are not exceeded. The block diagram of the control scheme was given in Chapter 3. In order to prevent damage to IGBTs, voltage protection is provided as well the option of a fault current limiter which is included within the control scheme. The inverter control scheme employs droop control and maintains an equal current magnitude and 120^o phase shift across all three phases. Maintaining the current across all three phases can induce a significant over-voltage during unbalanced faults. The inverter and AC filter must be designed to withstand short term over-voltages; in particular, the AC filter capacitors and inverter IGBTs should be selected such that an over voltage can be sustained until the voltage sequence protection isolates the IIEG.

Instances of over voltage are already possible in existing distribution networks during single-phase to earth faults as IIEG units are coupled to the grid through a delta-wye transformer. The voltage may rise to 173% of nominal on the grid side of the transformer [26]. A single-phase to earth fault using the proposed control scheme connected through a wye-wye transformer can yield a maximum theoretical voltage rise of 150% on the grid side of the transformer; hence, the proposed microgrid design philosophy is preferable

to contemporary IIEG unit control and transformer connection from the grid's voltage profile perspective. In theory, if the proposed autonomous controller was exposed to a line-to-line fault, an even higher voltage would arise; however, the proposed autonomous controller is incapable of providing a balanced current output when two phase voltages are subject to a significant voltage drop. The IIEG unit's voltages will not exceed 150% of the nominal voltage during fault conditions. The over-rating of IIEG units and DN infrastructure is critical to the adequacy of the autonomous controller and protection scheme for intentional islanding operation.

The proposed control scheme of the IIEG unit ensures that the positive sequence voltage is maintained within a certain range as determined by the droop controller. Whilst the phase-to-earth voltages may be significantly unbalanced during a single-phase to earth fault on an HV line, the line-to-line voltages remain near balanced and provide a near nominal voltage. Hence, no extra losses attributable to zero sequence unbalance are present in the delta-wye connected distribution transformers. Furthermore, due to all loads being interfaced to the microgrid through a delta-wye connected transformer, no significant voltage unbalance will occur at the terminals of the load. Hence, the only important considerations are the voltage ratings of the IIEG and the line-to-earth insulation of the HV infrastructure within the microgrid.

7.4 Communications

A communications medium must exist between line protection devices, STSs and medium-scale IIEG. Under the proposed scheme, communications failure between devices will preclude autonomous operation of the microgrid. Intentional islanding can only be permitted when communications are healthy, sufficient generation is present and the island is protectable. The communications protocol and medium are considered outside the scope of this Thesis. Rather, the necessary information between devices is asserted and the transmission time of signals is assumed to be in the order of hundreds of milliseconds [110]. It is important to note that the communications medium is not necessary for fault detection. Rather, the communications medium is used to advise the STS of the presence and state

of each protection device and IIEG to disseminate permission for intentional islanding of a microgrid.

A failure in the communications medium will void permission for intentional islanding. The microgrid will operate in grid-connected mode only commensurate with contemporary IIEG control and protection. Anti-islanding protection will isolate each IIEG when LOM is detected.

The transmitted data shall be sent in packets. The general format of a single packet is:

- Packet ID Number (PXXX)
- From Device ID Number (STSXXX, RECXXX or IIEGXXX)
- To Device ID Number (STSXXX, RECXXX or IIEGXXX)
- From Device Type (STS, REC or IIEG)
- From Device CB State (0=open, 1=closed)
- Trip Request (0=open, 1=close or N/A if type==IIEG or REC as these do not dispatch trip request)
- From Device Mode (0=grid-connected, 1=autonomous or N/A if type==STS)
- Mode Shift Request (0=grid-connected, 1=autonomous or N/A if type==REC or IIEG)
- From Device Complex Power Availability (X+jY or N/A if type==REC or IIEG)
- Last Received Packet ID Number from To Device (PXXX)

Consider the case where Device STS001 is sending a packet with ID No. P002 to Device IIEG003 after receiving packet ID No. P001. The STS has just opened and is requesting all IIEG units to shift to islanding mode. The packet P002 shall contain the following information:

- Packet ID Number (P002)

- From Device ID Number (STS001)
- To Device ID Number (IIEG003)
- From Device Type (STS)
- From Device CB State (0)
- Trip Request (0)
- From Device Mode (N/A)
- Mode Shift Request (1)
- From Device Complex Power Availability (N/A)
- Last Received Packet ID Number from To Device (P001)

Upon Device IIEG003 receiving the data, the IIEG will shift to autonomous mode and send the following packet:

- Packet ID Number (P003)
- From Device ID Number (IIEG003)
- To Device ID Number (STS001)
- From Device Type (IIEG)
- From Device CB State (1)
- Trip Request (N/A)
- From Device Mode (1)
- Mode Shift Request (N/A)
- From Device Complex Power Availability (10000+j4000)
- Last Received Packet ID Number from To Device (P002)

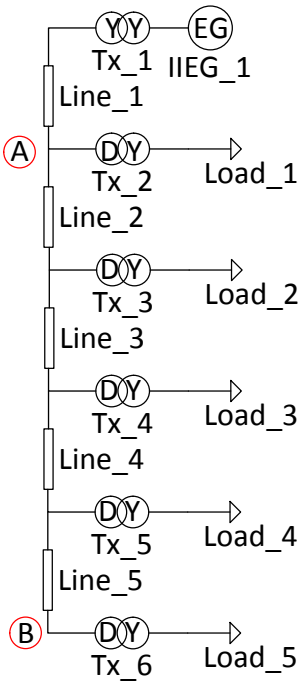

FIGURE 7.1: Example Island

7.5 Protection

All medium-scale EG units are to be fitted with anti-islanding protection commensurate with AS 4777.3 [16]. In the event of communications failure or insufficient generation within an island, IIEG protection should operate exactly as contemporary Australian Standards require. However, anti-islanding protection shall be by-passed if an intentional island is formed, constituting autonomous operation of IIEG units.

A common complication identified within microgrid protection research is the discrimination of high impedance single-phase to earth faults [48, 50]. Consider the intentional island shown in Fig. 7.1.

The proposed microgrid design philosophy provides galvanic isolation of unbalanced loads through delta-wye connected transformers. The delta connection prevents the flow of zero sequence current through the high voltage side of a transformer irrespective of any loading unbalance. Furthermore, each autonomously controlled IIEG unit exports only positive sequence current; hence, ideally no zero sequence current is drawn during single phase to

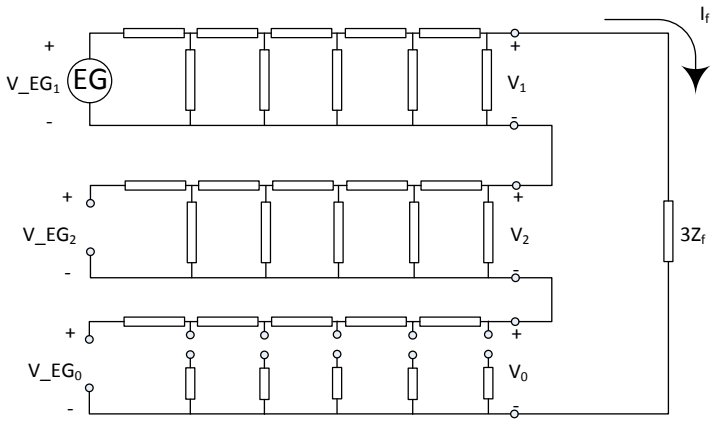

FIGURE 7.2: Sequence Component Circuit for Single-Phase to Earth Fault

earth faults on the high voltage line. Hence, the symmetrical component representation of the circuit with a single-phase to earth fault can be constructed as in Fig. 7.2.

The transformer connections and IIEG unit controller ensure that no fault current flows ($I_f = 0$). Kirchoff's Voltage Law yields $V_0 + V_1 + V_2 = 0$. $V_2 = I_f Z_2 = 0$ by Ohm's Law. Hence, $V_0 = -V_1$. There exists a positive sequence voltage drop between the IIEG unit's positive sequence voltage V_{EG1} and V_1, but no zero sequence voltage drop between the IIEG unit's zero sequence voltage V_{EG0} and V_0. The positive sequence voltage drop is unchanged by the faulted condition; hence, the end of line voltage magnitude will remain within normal voltage bounds. Subsequently, the magnitude of the zero sequence voltage measurable at the IIEG unit's PCC must also be within normal positive sequence voltage bounds. Therefore, single-phase to earth faults will always be detectable under the proposed microgrid design philosophy irrespective of the fault impedance.

In practice, a small zero sequence and negative sequence current will be drawn from the IIEG unit under fault conditions. However, the magnitudes of these undesirable sequence components are acceptably small (as shown in Chapter 5) and will yield no discrimination issues with the proposed protection scheme.

A block diagram of the proposed protection relay is shown in Fig. 7.3. A voltage transformer is unnecessary for low voltage applications, but may be required in some higher voltage applications. A cosine filter is common in modern protection applications and is

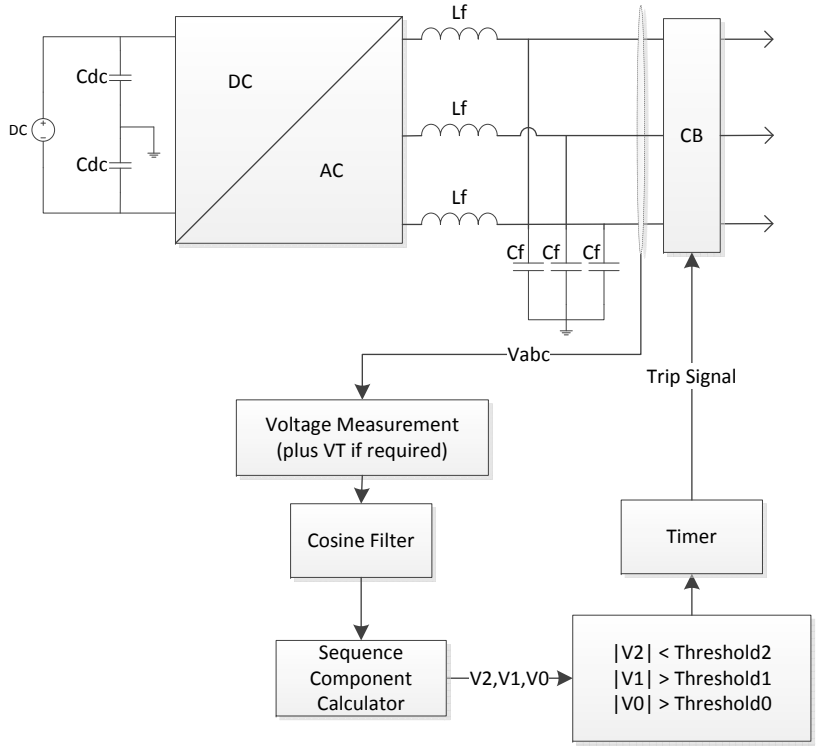

FIGURE 7.3: Voltage Sequence Protection

implemented to attenuate any DC components or harmonics that may be present in the measured voltage waveform [108]. The output of the cosine filter contains three-phase vector representations of the voltage waveforms. These vectors are transformed into sequence components by (7.1). The modulus of the sequence components is then compared with a set of thresholds; if any threshold condition is violated for a predetermined amount of time, a signal is sent to the trip coil instigating the isolation of the IIEG unit.

$$\begin{bmatrix} F_0 \\ F_1 \\ F_2 \end{bmatrix} = \frac{1}{3} \begin{bmatrix} 1 & 1 & 1 \\ 1 & a & a^2 \\ 1 & a^2 & a \end{bmatrix} \begin{bmatrix} F_a \\ F_b \\ F_c \end{bmatrix} \tag{7.1}$$

The use of the island protection scheme does not preclude the necessity for rating IIEG technology and microgrid infrastructure to sustain an over voltage. The efficacy of the proposed island protection scheme is predicated on the presence of under/over voltages and voltage unbalance during faults within an island.

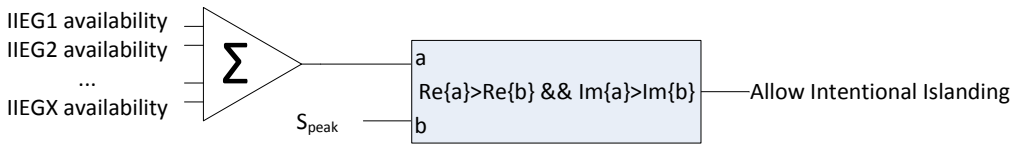

FIGURE 7.4: Logic for Intentional Islanding

7.6 Modes of Microgrid Operation

7.6.1 Grid Connected Mode

During grid connected operation, the DN should possess all control and protection features of contemporary DNs. Hence, constant power control and anti-islanding protection commensurate with AS4777.3 is employed [16]. Throughout all modes of operation, packets of information are transmitted between devices. Hence, when in grid connected mode, the STS is determining whether intentional islanding of the microgrid should be permitted if an island is formed.

7.6.2 Shift from Grid Connected to Autonomous Mode

A communications medium is necessary to coordinate control and protection during autonomous operation of a microgrid. Without communications, intentional islanding is forbidden under the proposed microgrid scheme. The shift to autonomous mode is instigated by either an advisory trip signal from an upstream protection device or detection of LOM by the STS. Furthermore, for intentional islanding to the permissible, the STS logic must be satisfied that sufficient supply is available in the island. The logic diagram for intentional islanding is shown in Fig. 7.4.

The STS controller must ensure that both the real and reactive power demand of an island is met. The Σ block adds the complex power availabilities which are part of the communicated packets as defined in Section 7.3. The value S_{peak} can be determined using historical data and will be variable throughout the day. An arbitrary time step may be imposed for the updating of power availability and demand. A significant amount of storage must be present in the microgrid if renewable energy resources are to be employed.

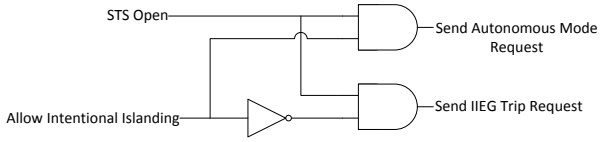

FIGURE 7.5: Logic for Inter-Trip or Autonomous Mode Shift

The availability value may be determined using the maximum real and reactive power capabilities programmed into the autonomous controller if sufficient energy storage is present for a dedicated time period. If communications to an IIEG unit are lost or if an IIEG unit has tripped, the power availability will be set to zero.

Once the STS is open, either a shift to intentional island signal or an inter-trip signal is dispatched to all IIEG units as shown in Fig. 7.5.

All IIEG units are equipped with anti-islanding protection. Consider the case where some generators have lost the ability to communicate with the STS. If sufficient generation is deemed to be present by the STS, intentional islanding is permissible. All IIEG with failed communications will export constant power whilst the frequency, voltage and load following requirements of the island are be met by the IIEG with a functional communications link. If insufficient generation is identified by the STS, all IIEG with healthy communications will trip and all other generators will still be isolated via anti-islanding protection.

Traditional reclose attempts are not employed with the proposed controller. Reconnection to the mains is achieved through implementation of a synchronisation module once mains supply has returned.

7.6.3 Autonomous Mode

Whilst in autonomous mode, the STS continues to monitor the available power and will dispatch an inter-trip signal if insufficient generation is available. All IIEG with healthy communications are operating in droop control mode. Voltage sequence protection shall be employed by all IIEG units with healthy communications.

7.6.4 Shift from Autonomous Mode to Grid Connected

When the STS has established that mains supply has been reconnected, the synchronisation module may be used to close the STS. The synchronisation module monitors the phase shift between the voltage waveform on either side of the STS. The instant that the STS closes should be chosen such that both voltage waveforms are approximately in-phase and at a zero crossing. The transient response of the network upon reclosure must also be considered before reconnection. A detailed study of reconnection to the grid is outside the scope of this Thesis. Some proposed strategies are available in literature [44, 111, 112]. Upon reconnection to the mains, all IIEG units shall be instructed to return to constant power control and employ anti-islanding protection by the STS.

7.7 Predicting the Fault Response of the Microgrid

The fault response of a microgrid is dependent on the state of the microgrid: grid-connected or islanded. The FAT and PAT presented in Chapters 4 and 5 are excellent tools for predicting the fault response of a grid-connected microgrid as all IIEG devices are constant power controlled. However, when a microgrid is operating in autonomous mode, the fault response is governed by the droop controllers and inverter interface capabilities of the IIEG within the microgrid. Assuming that the droop controller detailed in Chapter 3 is employed, IIEG units are incapable of providing a sinusoidal voltage waveform and sustained fault current required for fault ride-through purposes. However, fault ride-through is not a requisite for autonomous operation of a microgrid.

Whenever a fault is detected in a microgrid, all IIEG units must detect the fault based on voltage sequence measurements and trip. During low impedance faults, a significant voltage drop will always be observable at all IIEG units. For high impedance single-phase to earth faults, the positive sequence voltage deviation at many IIEG units may not exceed the voltage range during healthy operation. However, as all loads are connected through delta-wye transformers, the zero sequence voltage difference observable by all IIEG units between healthy and faulted conditions is easily discernible. In order to verify that a

microgrid is capable of identifying faults, the author proposes the Fault Analysis Tool: Microgrid Version (FATM).

7.7.1 The Fault Analysis Tool: Microgrid Version

The key differences between the FAT and the FATM are the lack of an absolute frequency and the implementation of droop control. The FATM assumes that the autonomous controller defined in Chapter 3 is employed. All nomenclature used to describe the FATM's iterative solver is consistent with that defined in Chapter 3. Nomenclature describing the iterative solving process of the FATM is consistent with the description of the FAT in Chapter 5.

The FATM begins by selecting a single IIEG unit as a reference. The reference IIEG unit provides the absolute current phase reference. Hence, the reference IIEG unit does not require the current angle δ_I iterative variable. Instead, the reference IIEG unit is allocated an iterative variable for the angular frequency of the entire island ω. All IIEG units are treated as constant current devices within each iteration; the IIEG currents are altered between each iteration to achieve $\Delta S_k = 0$ as expressed in (7.2).

$$\Delta S_k = \Delta P_k + j\Delta Q_k = -(P_{ref} - \frac{\omega - \omega_{\text{ref}}}{m_P} + j\frac{V_{\text{ref}} - |V_k|}{m_Q})S_{\text{base}} + \sum_{\alpha=a,b,c} V_{k\alpha} I^*_{k\alpha} \tag{7.2}$$

Where:

$$V_k = \frac{\sqrt{3}}{V_{\text{base}}} \frac{V_{ka} + V_{kb}\exp^{j\frac{2\pi}{3}} + V_{kc}\exp^{-j\frac{2\pi}{3}}}{3} \tag{7.3}$$

The steady-state condition of the autonomous controller defined in Chapter 3 is implemented to derive (7.2). The voltage magnitude is determined using a positive sequence calculation as shown in (7.3).

The process for determination of partial derivatives is similar to the FAT's method outlined in Chapter 5. In order formulate the elements of the Jacobian matrix pertaining to the

angular frequency of the microgrid ω, significant alteration of the constant matrix B is necessary.

Recall the format of the characteristic, constant and parameter matrices outlined in Chapter 4 and shown in (7.4).

$$Ax = B \tag{7.4}$$

Where:

$$A = \begin{bmatrix} \text{characteristic} \\ \text{KCL} \\ \text{KVL} \end{bmatrix}$$

$$x = \begin{bmatrix} V_1 & I_1 & V_2 & I_2 & \dots & V_N & I_N \end{bmatrix}'$$

$$B = \begin{bmatrix} \text{constants} \end{bmatrix}$$

When taking the partial derivative of the system expressed in (7.4) with respect to the microgrid frequency ω, the characteristic and constant matrices of series impedances such as lines must be modified as in (7.5).

$$\begin{bmatrix} -1 & R + j\omega L \end{bmatrix} \begin{bmatrix} \frac{\partial V}{\partial \omega} \\ \frac{\partial I}{\partial \omega} \end{bmatrix} = \begin{bmatrix} -jI_p L_p \end{bmatrix} \tag{7.5}$$

For parallel connected RLC loads, the system is modified as in (7.6).

$$\begin{bmatrix} \frac{1}{R} + \frac{1}{j\omega L} + j\omega C & -1 \end{bmatrix} \begin{bmatrix} \frac{\partial V}{\partial \omega} \\ \frac{\partial I}{\partial \omega} \end{bmatrix} = \begin{bmatrix} V(-jC + \frac{1}{j\omega^2 L}) \end{bmatrix} \tag{7.6}$$

Transformers are also frequency dependent as must be modified accordingly as in (7.7).

$$\begin{bmatrix} -1/Z_m & 1+Z_1/Z_m & 0 & 1/a \\ 1 & -Z_1 & a & aZ_2 \end{bmatrix} \begin{bmatrix} \frac{\partial V_1}{\partial \omega} \\ \frac{\partial I_1}{\partial \omega} \\ \frac{\partial V_2}{\partial \omega} \\ \frac{\partial I_2}{\partial \omega} \end{bmatrix} = \begin{bmatrix} I_1(\frac{R_1}{j\omega^2 L_m} - \frac{jL_1}{R_m}) - V_1(\frac{1}{j\omega^2 L_m}) \\ jI_1 jL_1 - jI_2 L_2 \end{bmatrix} \tag{7.7}$$

Where $Z_m = \frac{1}{\frac{1}{R_m}+\frac{1}{j\omega L_m}}$, $Z_1 = R_1 + j\omega L_1$ and $Z_2 = R_2 + j\omega L_2$.

All sources behave as constant current sources exporting zero current as in (7.8)

$$\begin{bmatrix} 0 & 1 \end{bmatrix} \begin{bmatrix} \frac{\partial V_p}{\partial \omega} \\ \frac{\partial I_p}{\partial \omega} \end{bmatrix} = \begin{bmatrix} 0 \end{bmatrix} \tag{7.8}$$

After employing the aforementioned alterations, the linearised system can be solved to yield the linearised voltage and current deviations with respect to ω. These linearised deviations can be substituted into (7.9), (7.10), (7.11) and (7.12) to determine the final Jacobian elements pertaining to the angular frequency of the microgrid.

$$\begin{aligned} A_k = {} & \frac{\partial V_{ka}}{\partial \omega}\cos(\delta_{Ika}) - V_{ka}\sin(\delta_{Ika})\frac{\partial \delta_{Ika}}{\partial \omega} \\ & + \frac{\partial V_{kb}}{\partial \omega}\cos(\delta_{Ikb}+\frac{2\pi}{3}) - V_{kb}\sin(\delta_{Ikb}+\frac{2\pi}{3})\frac{\partial \delta_{Ikb}}{\partial \omega} \\ & + \frac{\partial V_{kc}}{\partial \omega}\cos(\delta_{Ikc}-\frac{2\pi}{3}) - V_{kc}\sin(\delta_{Ikc}-\frac{2\pi}{3})\frac{\partial \delta_{Ikc}}{\partial \omega} \end{aligned} \tag{7.9}$$

$$\begin{aligned} B_k = {} & \frac{\partial V_{ka}}{\partial \omega}\sin(\delta_{Ika}) + V_{ka}\cos(\delta_{Ika})\frac{\partial \delta_{Ika}}{\partial \omega} \\ & + \frac{\partial V_{kb}}{\partial \omega}\sin(\delta_{Ikb}+\frac{2\pi}{3}) + V_{kb}\cos(\delta_{Ikb}+\frac{2\pi}{3})\frac{\partial \delta_{Ikb}}{\partial \omega} \\ & + \frac{\partial V_{kc}}{\partial \omega}\sin(\delta_{Ikc}-\frac{2\pi}{3}) + V_{kc}\cos(\delta_{Ikc}-\frac{2\pi}{3})\frac{\partial \delta_{Ikc}}{\partial \omega} \end{aligned} \tag{7.10}$$

$$dV_k = \frac{\mathfrak{Re}(V_k)A_k + \mathfrak{Im}(V_k)B_k}{3|V_k|} \tag{7.11}$$

$$\frac{\partial \Delta S_k}{\partial \omega} = \frac{S_{\text{base}}}{m_P} + \sum_{\alpha=a,b,c} I^*_{k\alpha} \frac{\partial V_{k\alpha}(I_k)}{\partial \omega} \tag{7.12}$$

The calculation of the partial derivative of IIEG power export with respect to angular frequency is only required for the reference IIEG. For any further IIEG present within the microgrid, the power export must be linearised with respect to the angular position of the current vector $\frac{\partial \Delta S_k}{\partial \delta_{Ik}}$. The determination of $\frac{\partial \Delta S_k}{\partial \delta_{Ik}}$ may be achieved using a similar technique as in the FAT presented in Chapter 4. The constant matrix B is once again replaced with constant matrix C which is an array of zero elements with the exception of the elements corresponding to the relevant IIEG unit denoted k. The non-zero elements are equal to (7.13).

$$C_k = jI_k \tag{7.13}$$

The linearised system the becomes (7.14).

$$A\frac{\partial x}{\partial \delta_{Ik}} = C \tag{7.14}$$

The solution to the array of partial derivatives $\frac{\partial x}{\partial \delta_{Ik}}$ is then inputted into (7.15), (7.16) and (7.17) to yield the Jacobian elements shown in (7.18).

$$\begin{aligned} A_k = \frac{\partial V_{ka}}{\partial \delta_{Ik}} \cos\left(\delta_{Ika}\right) - V_{ka} \sin\left(\delta_{Ika}\right) \frac{\partial \delta_{Ika}}{\partial \delta_{Ik}} \\ + \frac{\partial V_{kb}}{\partial \delta_{Ik}} \cos\left(\delta_{Ikb} + \frac{2\pi}{3}\right) - V_{kb} \sin\left(\delta_{Ikb} + \frac{2\pi}{3}\right) \frac{\partial \delta_{Ikb}}{\partial \delta_{Ik}} \\ + \frac{\partial V_{kc}}{\partial \delta_{Ik}} \cos\left(\delta_{Ikc} - \frac{2\pi}{3}\right) - V_{kc} \sin\left(\delta_{Ikc} - \frac{2\pi}{3}\right) \frac{\partial \delta_{Ikc}}{\partial \delta_{Ik}} \end{aligned} \tag{7.15}$$

$$B_k = \frac{\partial V_{ka}}{\partial \delta_{Ik}} \sin\left(\delta_{Ika}\right) + V_{ka} \cos\left(\delta_{Ika}\right) \frac{\partial \delta_{Ika}}{\partial \delta_{Ik}} + \frac{\partial V_{kb}}{\partial \delta_{Ik}} \sin\left(\delta_{Ikb} + \frac{2\pi}{3}\right) + V_{kb} \cos\left(\delta_{Ikb} + \frac{2\pi}{3}\right) \frac{\partial \delta_{Ikb}}{\partial \delta_{Ik}} + \frac{\partial V_{kc}}{\partial \delta_{Ik}} \sin\left(\delta_{Ikc} - \frac{2\pi}{3}\right) + V_{kc} \cos\left(\delta_{Ikc} - \frac{2\pi}{3}\right) \frac{\partial \delta_{Ikc}}{\partial \delta_{Ik}} \tag{7.16}$$

$$dV_k = \frac{\mathfrak{Re}(V_k) A_k + \mathfrak{Im}(V_k) B_k}{3|V_k|} \tag{7.17}$$

$$\frac{\partial \Delta S_k}{\partial \delta_{Ik}} = \frac{j\sqrt{3} S_{\text{base}} dV_k}{m_Q V_{\text{base}}} + \sum_{\alpha=a,b,c} -j I^*_{k\alpha} V_{k\alpha}(I_k) + \sum_{\alpha=a,b,c} I^*_{k\alpha} \frac{\partial V_{k\alpha}(I_k)}{\partial \delta_k} \tag{7.18}$$

Finally, the partial derivatives with respect to the current magnitude may be calculated similarly through a modification of the C matrix as shown in (7.19). The current magnitude partial derivatives are required for all IIEG units.

$$C_k = \frac{I_k}{|I_k|} \tag{7.19}$$

The Jacobian elements can then be determined via (7.20), (7.21), (7.22) and (7.23).

$$A_k = \frac{\partial V_{ka}}{\partial |I_k|} \cos\left(\delta_{Ika}\right) - V_{ka} \sin\left(\delta_{Ika}\right) \frac{\partial \delta_{Ika}}{\partial |I_k|} + \frac{\partial V_{kb}}{\partial |I_k|} \cos\left(\delta_{Ikb} + \frac{2\pi}{3}\right) - V_{kb} \sin\left(\delta_{Ikb} + \frac{2\pi}{3}\right) \frac{\partial \delta_{Ikb}}{\partial |I_k|} + \frac{\partial V_{kc}}{\partial |I_k|} \cos\left(\delta_{Ikc} - \frac{2\pi}{3}\right) - V_{kc} \sin\left(\delta_{Ikc} - \frac{2\pi}{3}\right) \frac{\partial \delta_{Ikc}}{\partial |I_k|} \tag{7.20}$$

$$B_k = \frac{\partial V_{ka}}{\partial |I_k|}\sin\left(\delta_{Ika}\right) + V_{ka}\cos\left(\delta_{Ika}\right)\frac{\partial \delta_{Ika}}{\partial |I_k|} + \frac{\partial V_{kb}}{\partial |I_k|}\sin\left(\delta_{Ikb} + \frac{2\pi}{3}\right) + V_{kb}\cos\left(\delta_{Ikb} + \frac{2\pi}{3}\right)\frac{\partial \delta_{Ikb}}{\partial |I_k|} + \frac{\partial V_{kc}}{\partial |I_k|}\sin\left(\delta_{Ikc} - \frac{2\pi}{3}\right) + V_{kc}\cos\left(\delta_{Ikc} - \frac{2\pi}{3}\right)\frac{\partial \delta_{Ikc}}{\partial |I_k|} \tag{7.21}$$

$$dV_k = \frac{\mathfrak{Re}(V_k)A_k + \mathfrak{Im}(V_k)B_k}{3|V_k|} \tag{7.22}$$

$$\frac{\partial \Delta S_k}{\partial \omega} = \frac{j\sqrt{3}S_{\text{base}}dV_k}{m_Q V_{\text{base}}} + \sum_{\alpha=a,b,c}\frac{I^*_{k\alpha}}{|I_{k\alpha}|}V_{k\alpha}(I_k) + \sum_{\alpha=a,b,c} I^*_{k\alpha}\frac{\partial V_{k\alpha}(I_k)}{\partial |I_k|} \tag{7.23}$$

The Jacobian elements may then be concatenated to form the complete Jacobian matrix shown in (7.24) which may be implemented to linearise the system as shown in (7.25).

$$J = \begin{bmatrix} \mathfrak{Re}(\frac{\partial \Delta S_1}{\partial |I_1|}) & \mathfrak{Re}(\frac{\partial \Delta S_1}{\partial |I_2|}) & \cdots & \mathfrak{Re}(\frac{\partial \Delta S_1}{\partial |I_N|}) & \mathfrak{Re}(\frac{\partial \Delta S_1}{\partial \omega}) & \mathfrak{Re}(\frac{\partial \Delta S_1}{\partial \delta_{I2}}) & \cdots & \mathfrak{Re}(\frac{\partial \Delta S_1}{\partial \delta_{IN}}) \\ \mathfrak{Re}(\frac{\partial \Delta S_2}{\partial |I_1|}) & \mathfrak{Re}(\frac{\partial \Delta S_2}{\partial |I_2|}) & \cdots & \mathfrak{Re}(\frac{\partial \Delta S_2}{\partial |I_N|}) & \mathfrak{Re}(\frac{\partial \Delta S_2}{\partial \omega}) & \mathfrak{Re}(\frac{\partial \Delta S_2}{\partial \delta_{I2}}) & \cdots & \mathfrak{Re}(\frac{\partial \Delta S_2}{\partial \delta_{IN}}) \\ \vdots & \vdots & \ddots & \vdots & \vdots & \vdots & \ddots & \vdots \\ \mathfrak{Re}(\frac{\partial \Delta S_N}{\partial |I_1|}) & \mathfrak{Re}(\frac{\partial \Delta S_N}{\partial |I_2|}) & \cdots & \mathfrak{Re}(\frac{\partial \Delta S_N}{\partial |I_N|}) & \mathfrak{Re}(\frac{\partial \Delta S_N}{\partial \omega}) & \mathfrak{Re}(\frac{\partial \Delta S_N}{\partial \delta_{I2}}) & \cdots & \mathfrak{Re}(\frac{\partial \Delta S_N}{\partial \delta_{IN}}) \\ \mathfrak{Im}(\frac{\partial \Delta S_1}{\partial |I_1|}) & \mathfrak{Im}(\frac{\partial \Delta S_1}{\partial |I_2|}) & \cdots & \mathfrak{Im}(\frac{\partial \Delta S_1}{\partial |I_N|}) & \mathfrak{Im}(\frac{\partial \Delta S_1}{\partial \omega}) & \mathfrak{Im}(\frac{\partial \Delta S_1}{\partial \delta_{I2}}) & \cdots & \mathfrak{Im}(\frac{\partial \Delta S_1}{\partial \delta_{IN}}) \\ \mathfrak{Im}(\frac{\partial \Delta S_2}{\partial |I_1|}) & \mathfrak{Im}(\frac{\partial \Delta S_2}{\partial |I_2|}) & \cdots & \mathfrak{Im}(\frac{\partial \Delta S_2}{\partial |I_N|}) & \mathfrak{Im}(\frac{\partial \Delta S_2}{\partial \omega}) & \mathfrak{Im}(\frac{\partial \Delta S_2}{\partial \delta_{I2}}) & \cdots & \mathfrak{Im}(\frac{\partial \Delta S_2}{\partial \delta_{IN}}) \\ \vdots & \vdots & \ddots & \vdots & \vdots & \vdots & \ddots & \vdots \\ \mathfrak{Im}(\frac{\partial \Delta S_N}{\partial |I_1|}) & \mathfrak{Im}(\frac{\partial \Delta S_N}{\partial |I_2|}) & \cdots & \mathfrak{Im}(\frac{\partial \Delta S_N}{\partial |I_N|}) & \mathfrak{Im}(\frac{\partial \Delta S_N}{\partial \omega}) & \mathfrak{Im}(\frac{\partial \Delta S_N}{\partial \delta_{I2}}) & \cdots & \mathfrak{Im}(\frac{\partial \Delta S_N}{\partial \delta_{IN}}) \end{bmatrix} \tag{7.24}$$

$$\begin{bmatrix} \Delta|I_1| \\ \vdots \\ \Delta|I_N| \\ \Delta\omega \\ \Delta\delta_{I2} \\ \vdots \\ \Delta\delta_{IN} \end{bmatrix} = J^{-1} \begin{bmatrix} \Delta P_1 \\ \vdots \\ \Delta P_N \\ \Delta Q \\ \vdots \\ \Delta Q_N \end{bmatrix} \tag{7.25}$$

The current export of each IIEG is updated according to (7.26). $\Delta\delta_{I_k} = 0$ for the reference IIEG unit.

$$I_{k_n} = (|I_{k_{n-1}}| - \Delta|I_k|) \exp^{j(\delta_{k_{n-1}} - \Delta\delta_{I_k})} \tag{7.26}$$

The frequency of the microgrid is updated by (7.27).

$$\omega_n = \omega_{n-1} - \Delta\omega \tag{7.27}$$

The process is iterated until either an arbitrarily large number of iterations has occurred, indicating a failed convergence, or $|\Sigma\Delta S| < \epsilon$ where ϵ is the tolerance of the FATM.

7.7.2 Simulation

7.7.2.1 Single-Phase to Earth Fault

Consider the island as shown in Fig. 7.6 with the line parameters given in Table 7.1. An A phase single-phase to earth fault of impedance 2 Ω is simulated at the marker A at t=0.1 seconds.

The IIEG unit is equipped with a voltage sequence protection device. If a zero sequence voltage of over 10% of nominal voltage is detected for two cycles (40 ms), the IIEG unit's

Table 7.1: Island Data

Line Data (1-4)	
Resistance (Ω)	0.1
Inductance (mH)	1
Line Data (5)	
Resistance (Ω)	1
Inductance (mH)	10
Transformer Data (all)	
Primary Voltage l-l rms (V)	11000
Primary Winding Resistance (Ω)	0.001
Primary Winding Inductance (mH)	1
Primary Connection	Delta (except Tx1 which is Wye-earthed)
Secondary Voltage l-l rms (V)	400
Secondary Winding Resistance (Ω)	0.001
Secondary Winding Inductance (mH)	1
Secondary Connection	Wye-earthed
Load Data(1-4)	
Real Power (kW)	20
Reactive Power (kVAr)	0.5
Note: The equivalent resistance and inductance are connected in parallel.	
Load Data(5)	
Real Power (kW)	0.1
Reactive Power (kVAr)	0
Note: The equivalent resistance and inductance are connected in parallel.	
IIEG Data	
DC Voltage (V)	1000
Switching Frequency (kHz)	4
Filter Inductance (mH)	1.36
Filter Capacitance (μF)	49.736
Power Rating (kVA)	150
Pref (p.u.)	1
Pmax (p.u.)	1.05
Pmin (p.u.)	0
Qmax (p.u.)	0.4
Vref (p.u.)	1
Vmax (p.u.)	1.05
ωref (rad/s)	314.159265
ωmin (rad/s)	311.017673
Low Pass Filter Cut-Off Frequency (Hz)	10

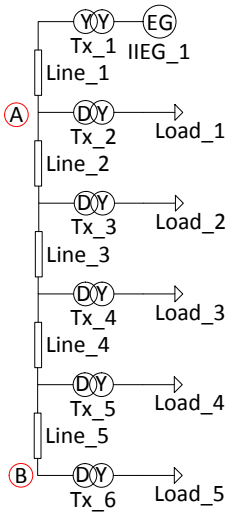

FIGURE 7.6: Example Island

circuit breaker will trip. All protection settings are chosen to ensure nuisance trips do not occur due to transient behaviour of the IIEG unit, but are otherwise arbitrary.

The small-signal voltage and current waveforms of the IIEG are given in Fig. 7.7 and Fig. 7.8. The straight horizontal lines represent the responses predicted by the FATM. The error between the predicted and small-signal models can be attributed to the oscillatory positive sequence waveform captured by the signal processing of the autonomous controller; the error was also present in the grid-connected controller. In the given case, the current magnitude error is 3.58 %, which is within the tolerances outlined in Chapter 5.

The voltage sequence component signals measured by the protection scheme are shown in Fig. 7.9. All measurements are taken between the filter capacitors and wye-wye transformer. The voltage sequence protection scheme detected a zero sequence voltage violation approximately 11 ms after the fault inception. The IIEG unit's circuit breaker opened 40 ms later as expected. The protection scheme has identified the single-phase to earth fault, satisfying the discrimination requirements of the protection scheme. The voltage sequence protection scheme will identify a single-phase to earth fault irrespective of the fault impedance as IIEG units do not allow the flow of zero sequence current. Hence, protection discrimination is assured.

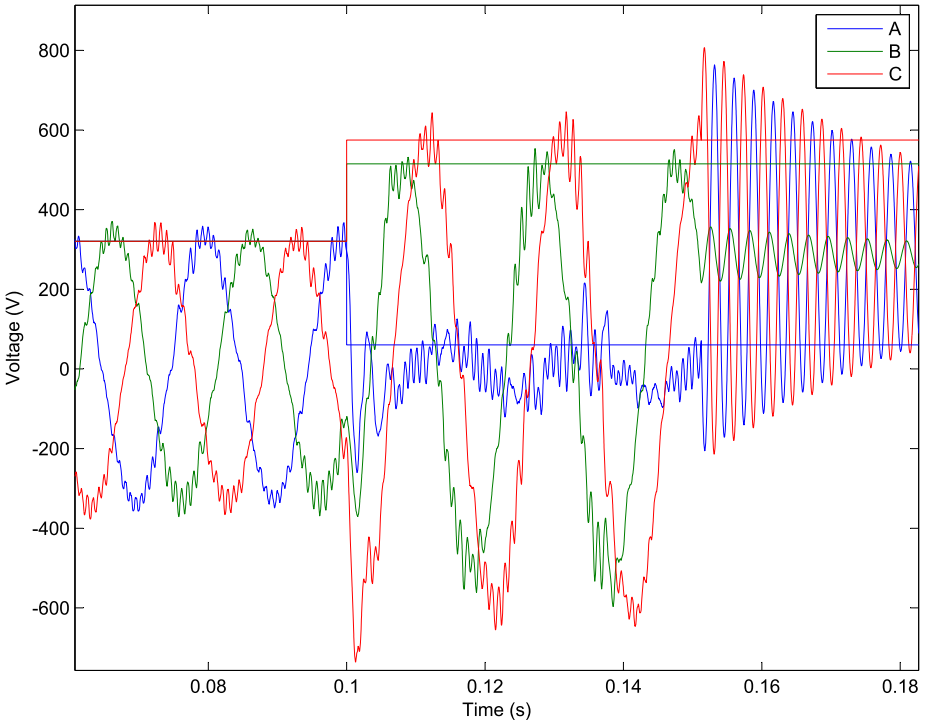

FIGURE 7.7: Single-Phase to Earth Fault Response of IIEG_1 – Voltage Waveform

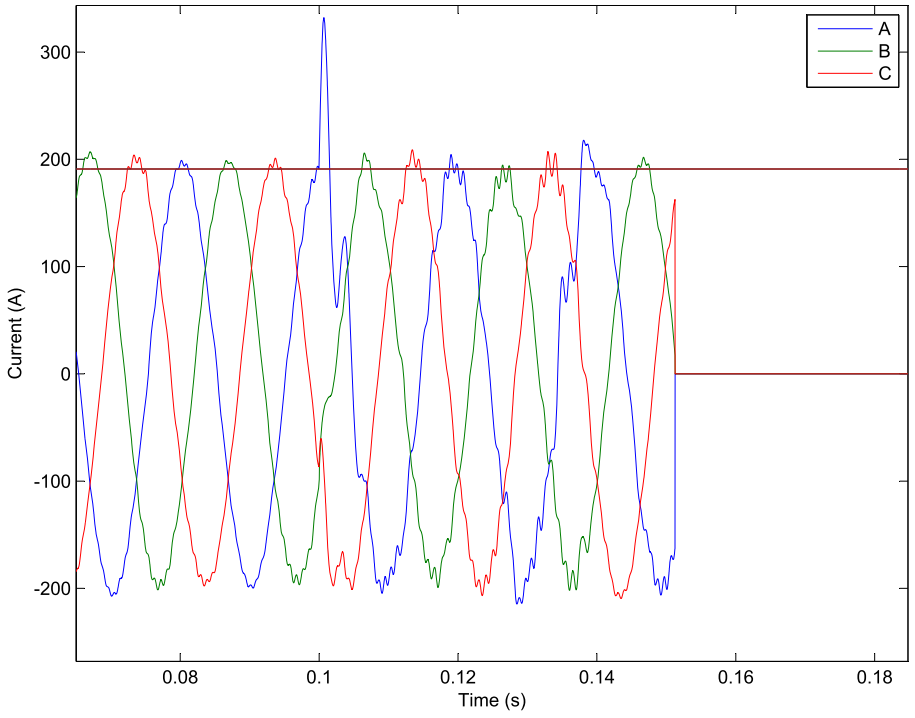

FIGURE 7.8: Single-Phase to Earth Fault Response of IIEG_1 – Current Waveform

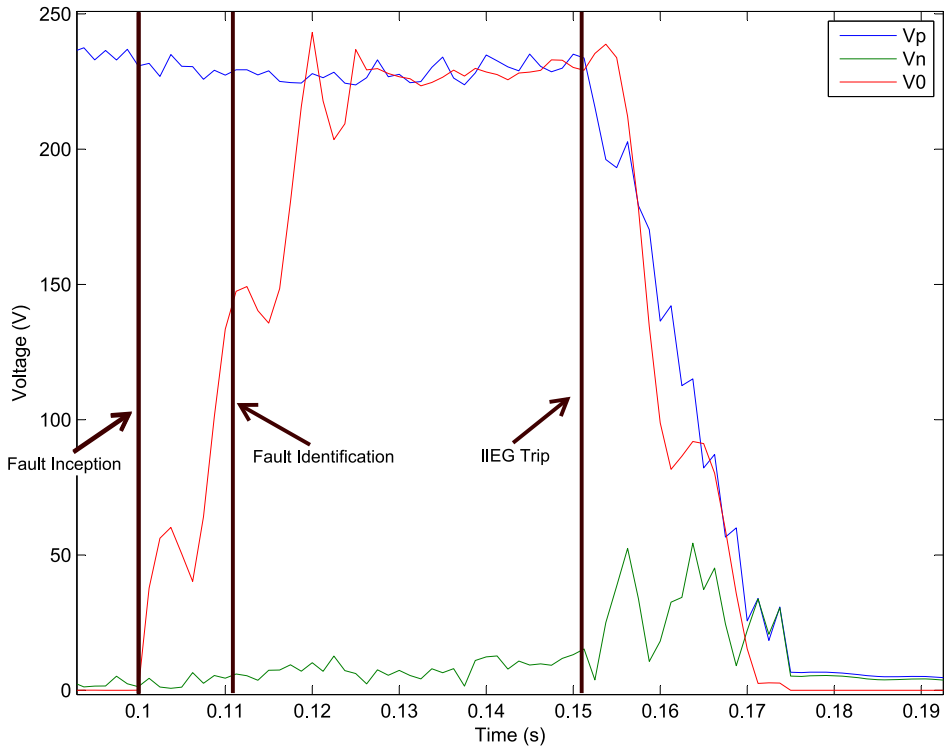

FIGURE 7.9: Single-Phase to Earth Fault Response of IIEG_1 – Voltage Sequence Component Measurement

Within the simulation platform, the IIEG unit is not turned off during a circuit breaker event, hence a voltage is still present after the fault isolation.

An excerpt from the steady state fault response generated using the FATM is shown in Appendix D. A significant voltage drop can be observed on phase A of the IIEG and Tx_1. However, the voltages across Tx_2 and Load_1 possess minimal unbalance. The unbalance present is attributable to the negative sequence current drawn from the fault which induces a negative sequence voltage at the terminals of the IIEG unit. Unlike zero sequence voltage, negative sequence voltage is passed through a delta-wye connected transformer. Hence, through use of delta-wye connected distribution transformers, the voltage unbalance caused by non-symmetrical faults is largely attenuated, preventing OV damage to customers.

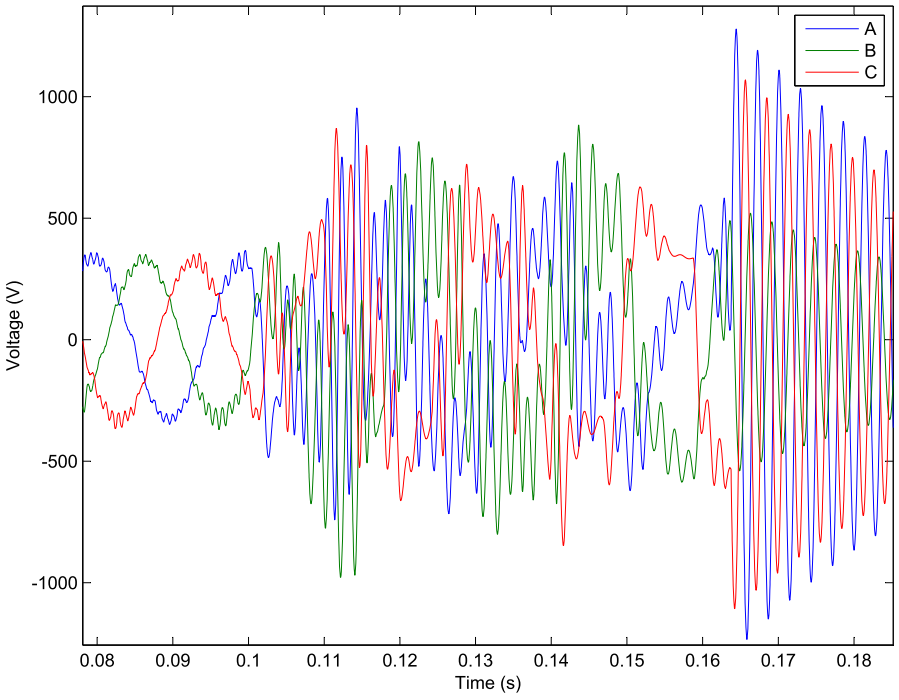

FIGURE 7.10: Line-to-Line Fault Voltage Response: Autonomous Control

7.7.2.2 Line-to-Line Fault

A simulation containing a line-to-line fault at the marker B using the same microgrid as in Fig. 7.6 was conducted. A fault impedance of 1 kΩ at t=0.1 seconds was chosen to demonstrate the effects of a high-impedance line-to-line fault. Once again, voltage sequence protection was employed. The negative sequence voltage threshold is 10% of the nominal voltage and the time delay is two cycles (40 ms). The resultant IIEG voltage and current waveforms are shown in Fig. 7.10 and 7.11 respectively. The sequence component responses are shown in Fig. 7.12.

In the event of line-to-line faults, the autonomous controller is incapable of providing the nominal positive sequence current. The resultant IIEG response is a heavily distorted waveform, but a clear negative sequence voltage is detectable. The negative sequence voltage protection identifies a fault condition approximately 23.8 ms after the fault inception and trips 40 ms later as expected. IIEG units are not designed to maintain sinusoidal waveforms during faults. Hence, the inability for the autonomous controller to provide

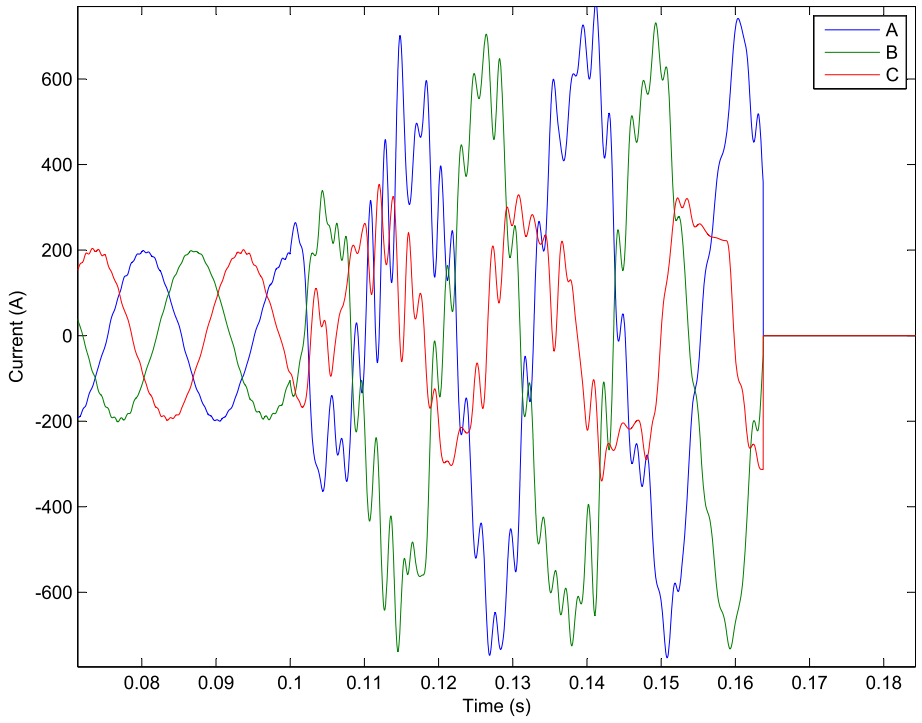

FIGURE 7.11: Line-to-Line Fault Current Response: Autonomous Control

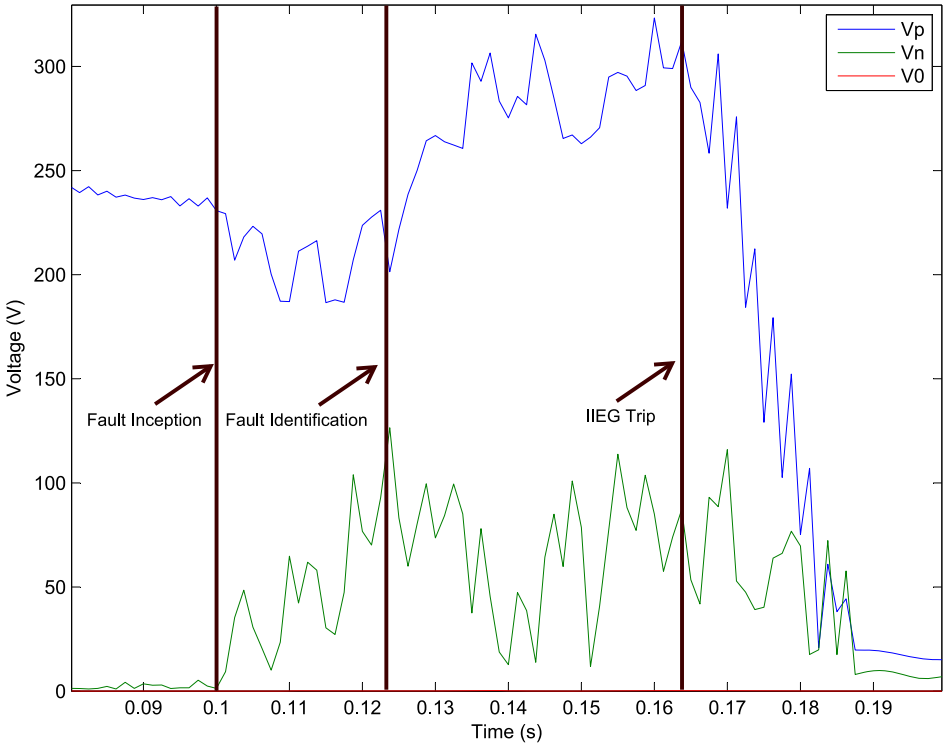

FIGURE 7.12: Line-to-Line Sequence Component Response: Autonomous Control

fault ride-through during line-to-line-faults is an acceptable limitation of the proposed controller.

7.7.2.3 Three-Phase Bolted Faults

Three-phase bolted faults are rare and have a very low impedance. A three-phase bolted fault will generally draw significantly more power than is locally available and cause a large voltage drop that will initiate an positive sequence under voltage trip. The positive sequence protection settings consist of an under voltage threshold equal to 94% of nominal voltage with a time delay of two cycles (40 ms). The proposed FATM may be used to verify that the positive sequence voltage drop is significant enough for adequate protection discrimination. The tool will provide information whether the ratings of the IIEG unit will, in an ideal case, be exceeded. If the ratings are exceeded by a significant margin, the IIEG will export a heavily distorted waveform and the predicted response will not match the actual exported voltage and current waveforms of the IIEG. The FATM was designed under the premise that a perfectly sinusoidal waveform and the ideal steady-state output according to the droop controller is achievable.

An additional line with an large impedance of $Z = 20 + j31.416\ \Omega$ was attached to the node with marker B. A three-phase bolted fault was placed at the end of the newly added line. The purpose of this case study is to demonstrate the response of an exaggerated end of line three-phase bolted fault. The network was analysed using the FATM and yielded the results shown in Fig. 7.13.

The total IIEG complex power export predicted by the FATM can be calculated by $Q = \Sigma VI*$ is $\vec{S} \approx 22 + j265$ kVA which is significantly higher than the 150 kVA rating of the IIEG unit. Furthermore, the reactive power exported by the IIEG is approximately 2.5 times the maximum reactive power deliverable by the IIEG unit. The small-signal response of the same case study yields a heavily distorted voltage and current waveform as shown in Fig. 7.14 and Fig. 7.15.

The sequence data measured by the voltage sequence protection is given in Fig. 7.16.

```
******************
Steady State data
******************
Grid Frequency: 50.406601 Hz
Element: IIEG1
Voltage: 179.867729/_85.278049
Current: 493.480508/_0.000000
Element:
Voltage: 179.867729/_-34.721951
Current: 493.480508/_-120.000000
Element:
Voltage: 179.867729/_-154.721951
Current: 493.480508/_120.000000
```

FIGURE 7.13: Three-Phase Bolted Fault Response: Autonomous Control

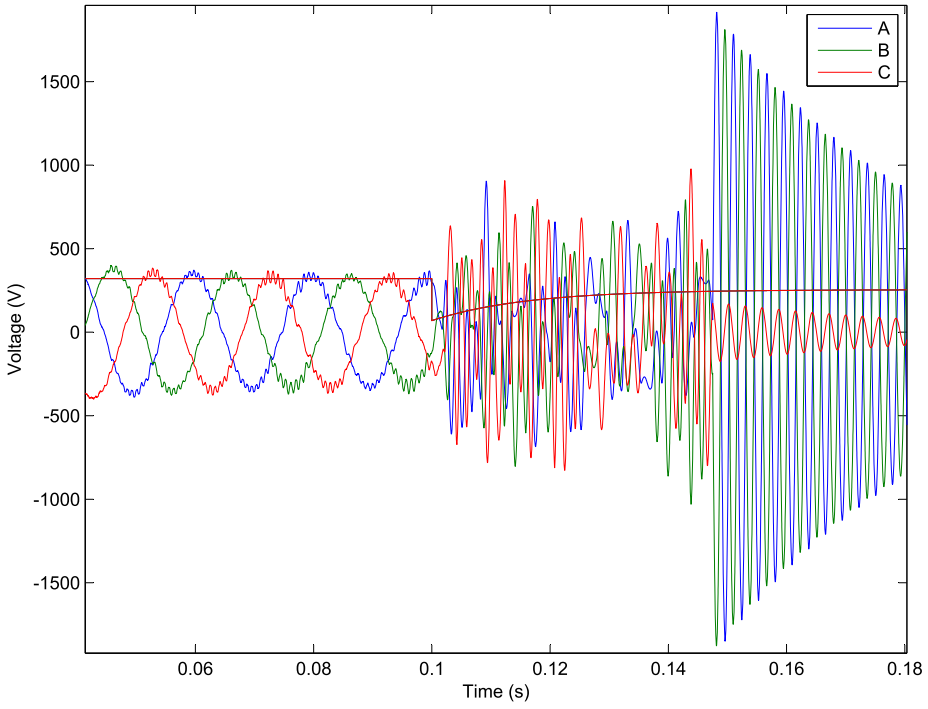

FIGURE 7.14: Three-Phase Bolted Fault Voltage Response: Autonomous Control

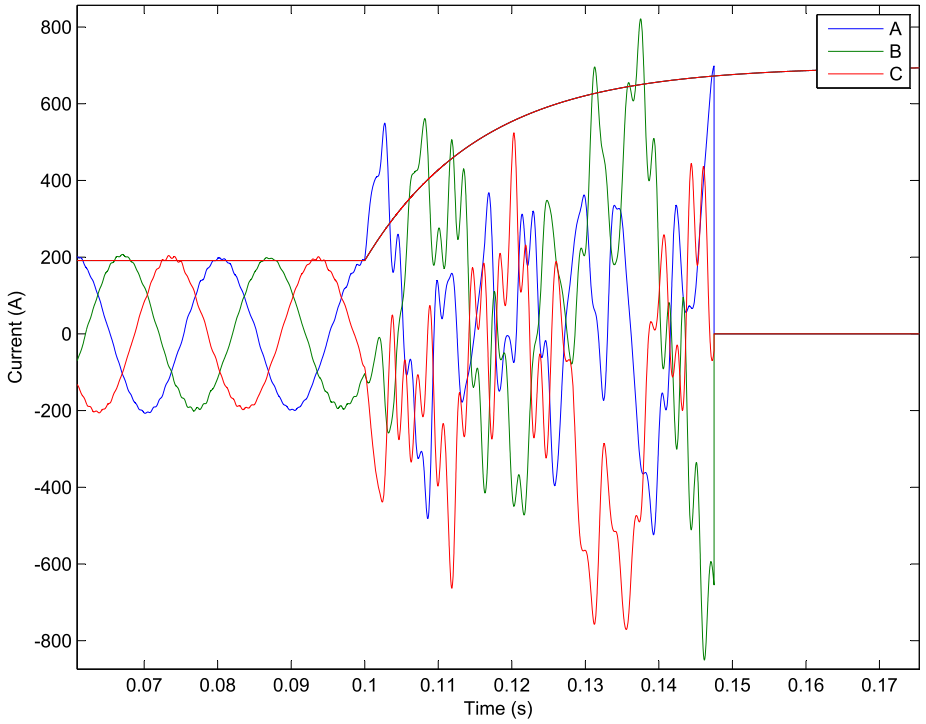

FIGURE 7.15: Three-Phase Bolted Fault Current Response: Autonomous Control

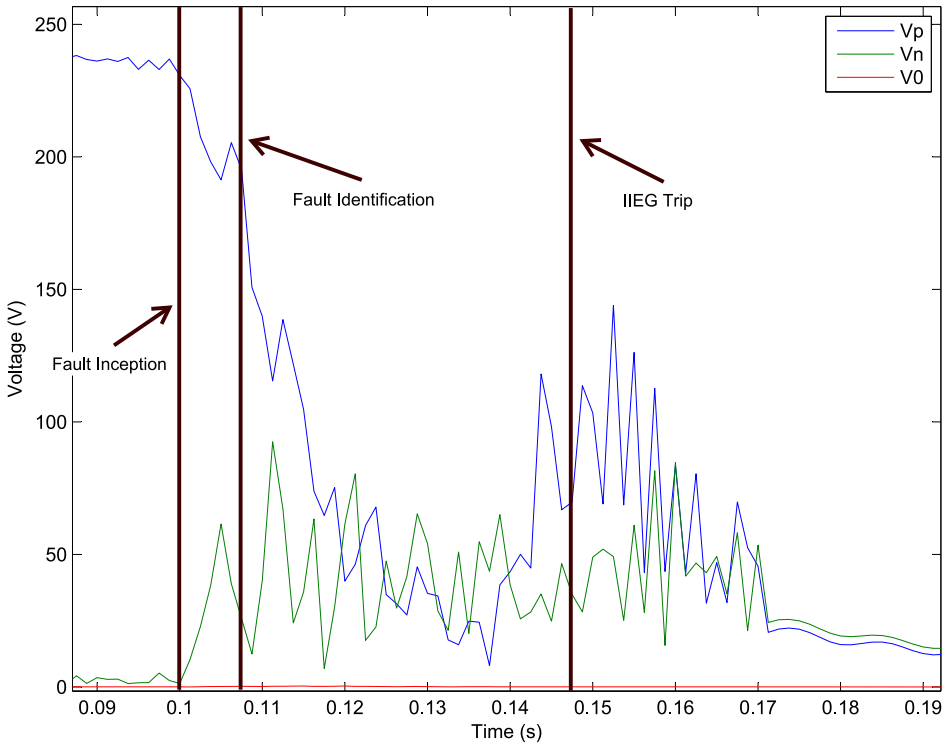

FIGURE 7.16: Three-Phase Bolted Fault Response of IIEG_1 – Voltage Sequence Component Measurement

The voltage sequence protection detects a positive sequence voltage below the threshold of 0.94 p.u. at approximately 7.5 ms after the fault inception and trips 40 ms later. A negative sequence voltage violation was also detected and may operate as a form of secondary protection for three-phase balanced faults.

In the event of an end of line fault, the reactive power absorption of the fault is too significant for the autonomous control scheme to maintain a smooth sinusoidal output predicted by the FATM. However, the presented case is arbitrary and the reactive power export from IIEG units may not necessarily exceed the rated value for all microgrid configurations when exposed to three-phase bolted faults. The line impedances of a microgrid capable of exposure to three-phase bolted faults without exceeding the maximum allowable reactive power export will likely also incur a significant voltage drop and thermal overload instances. Hence, whilst a minor study regarding the fault discrimination of three-phase bolted faults in microgrids cannot be omitted, it is unlikely that three-phase bolted fault discrimination will be an issue in the majority of microgrid cases.

7.7.2.4 Conclusion

The formation of an island precludes the voltage and frequency commutation of an effective infinite bus. IIEG units adopting the autonomous control scheme described in Chapter 3 do not ensure that the voltage magnitude is common across all three phases. The proposed protection scheme is predicated on the presence of voltage unbalance for fault discrimination purposes. As described in Chapter 2, many authors have presented fault identification techniques which are effective for low impedance faults. However, the proposed techniques for high-impedance fault detection in an island are generally complex and often do not take into account the connection of transformers within the DN.

The autonomous control scheme adopted in this Thesis cannot provide fault ride-through during low impedance line-to-line or three-phase bolted faults. The local IIEG protection will isolate an IIEG unit by detecting an abnormal positive or negative sequence voltage. Furthermore, the autonomous control scheme is incapable of producing the sinusoidal

voltage and current waveform magnitudes commensurate with the ideal steady-state line-to-line or three-phase bolted fault response upon which the FATM is predicated. Hence, a meaningful comparison of small-signal modelling analysis and the FATM cannot be drawn.

7.7.3 Determining Settings for Island Protection

Three-phase balanced faults will generally draw above the aggregate rated power of IIEG units within a microgrid. An abnormally large reactive power export shall yield a significant positive sequence voltage drop via the response of the droop controller and/or the implementation of the FCL. Hence, an appropriate protection setting would be slightly below the minimum voltage of the droop controller. If the minimum voltage threshold is reached due to a peak loading condition, insufficient generation is present and the IIEG unit should be isolated unless a load shedding scheme is implemented. However, load shedding is the responsibility of the STS and, as such, an overloading condition identified by an IIEG can be construed as a STS failure to ensure adequate supply is present. Ergo, isolation of the IIEG due to positive sequence under-voltage is an acceptable protection discrimination tool for three-phase bolted faults.

In order to verify that a significant voltage drop will occur for a three-phase bolted fault within a microgrid, the FATM places a three-phase bolted fault at all nodes. Fig. 7.13 reveals the voltage and current data considered as an exaggerated example for a high impedance three-phase fault. The reactive power export of the IIEG was shown to exceed the maximum reactive power capability as programmed into the droop controller. Hence, a significant voltage drop and total harmonic distortion is assured if such a three-phase bolted fault is present. Note that the voltage drop will not be the same as that predicted by the FATM as the ideal droop control steady-state condition cannot be met by the controller during such significant disturbances; irrespective, a significant voltage drop sll occur. The positive sequence voltage threshold should be slightly lower than the minimum voltage of an IIEG controller as shown in (7.28). The minimum voltage of the IIEG controller is 0.95 p.u.; hence, a threshold setting of 0.94 p.u. is appropriate. All IIEG devices must be isolated for any fault within a microgrid; no fault selectivity is required. As such, the

time delay of a trip needs only be long enough such that no trips are instigated due to short term transients. 40 ms or two cycles was chosen within this Thesis.

$$V_{1_{\text{threshold}}} < \min(V_{\text{min}}) \tag{7.28}$$

Line-to-line faults cause a voltage drop on two phases of the IIEG unit. The autonomous controller is unable to maintain a sinusoidal voltage and current waveform as shown in Fig. 7.10 and Fig. 7.11. However, after passing the waveforms through the cosine filter, a clear negative sequence voltage can be observed as shown in Fig. 7.12. A negative sequence voltage threshold should be chosen that is greater than the negative sequence voltage unbalance caused by loading within the island, but smaller than the minimum negative sequence voltage observed during all possible fault locations. The proposed autonomous controller is more prone to voltage unbalance than other controllers that do not maintain a balanced current export. The chosen negative sequence threshold is case dependent and cannot be applied to the simulations in this Chapter which contain perfectly balanced loading. However, the unbalance can be determined using the prefault condition FATM analysis. The negative sequence voltage threshold can then be selected within the range given by (7.29).

$$\max(V_{2_{\text{healthy}}}) < V_{2_{\text{threshold}}} < \min(V_{2_{\text{faulted}}}) \tag{7.29}$$

Single-phase to earth faults are the only fault type which can be accurately modelled using the FATM. The FATM was applied to the microgrid shown in Fig. 7.6. The FATM results pertaining to single-phase to earth faults are given in Appendix E. The fault impedance is 1000 kΩ for all cases. All single-phase to earth fault placed directly adjacent to nodes attached to loads yield no zero sequence voltage at the IIEG due to the presence of delta-wye connected transformers. For any other fault locations, the zero sequence voltage is in the order of ≈ 220 V. The zero sequence current drawn by the fault is very small due to the high impedance of the fault and the current balancing characteristic of the proposed autonomous controller. Hence, there is very little zero sequence voltage drop across the

microgrid. Subsequently, fault discrimination is very easy to achieve even in the instance of high impedance faults as predicted earlier in this Chapter.

The zero sequence voltage at all IIEG points of connection is minimal during healthy microgrid operation. The separation of loads from IIEG through delta-wye connected transformers disallows zero sequence voltage at an IIEG to be present due to unbalanced loading. Shunt impedances of the HV domain within the microgrid are generally very high impedance and near balanced. Therefore, high impedance single-phase to earth fault discrimination is easily achievable for the proposed microgrid design philosophy and protection scheme. The zero sequence voltage thresholds must be chosen such that (7.30) is satisfied.

$$\max(V_{0_{\text{healthy}}}) < V_{0_{\text{threshold}}} < \min(V_{0_{\text{faulted}}}) \tag{7.30}$$

7.8 Conclusion

The proposed microgrid design philosophy and protection scheme are not compatible with microgrid philosophies asserted by other authors [53, 55–57]. The proposed autonomous controller ensures that a significant voltage unbalance follows any fault condition within a microgrid. This chapter is not an exhaustive study of the feasibility of the nexus of balanced current export, droop control and voltage sequence protection; rather, a preliminary study of the plausibility if such a nexus is proffered. Further research investigating the stability of the control scheme, the effects of significant line impedances, negative sequence loading impedance and the robustness of the proposed protection scheme is needed. Furthermore, increasing the modularity of the microgrid concept may eventually further increase microgrid reliability and robustness.

One limitation of the proposed scheme is that whilst the LV segment of the microgrid is effectively earthed, the MV segment is technically not earthed. Irrespective of the solid earth connection of the AC filter and wye-wye connected transformer, the IIEG is not effectively earthed because an effective infinite zero sequence impedance is present due to the zero sequence current restriction of the IIEG controller. Whilst step and touch

potential problem can be avoided through appropriate designing of insulators, the shunt capacitance between the line and earth can provide a path for zero sequence current to flow, posing a safety risk to customers and personnel [113]. The effects of zero sequence shunt capacitance requires more research before the proposed microgrid design philosophy could be employed.

The FATM is an integral part for protection analysis of the microgrid. The FATM provides a high level of accuracy when predicting any healthy state of a microgrid as well as the fault response of single-phase to earth faults. The FATM is also useful for verifying whether the reactive power threshold of an IIEG unit is exceeded for a three-phase balanced fault. This verification confirms an IIEG unit's inability to maintain the voltage within the stipulated bounds and ensures a positive sequence voltage threshold violation and subsequent isolation of that IIEG unit.

Chapter 8

Conclusions and Future Work

The research within this Thesis proffers an academic study into a deterministic approach towards the plausibility of continued EG proliferation in DNs. Whilst the main focus is predicting and mitigating the impacts of large penetrations of grid-connected EG, ostensibly, the natural progression of EG proliferation is the microgrid concept. However, the contemporary definition of the microgrid concept is very much in its infancy and, as such, a significant academic license may be granted. The proposed microgrid philosophy does not reflect philosophies asserted by many other authors, particularly when considering transformer connection as well as IIEG control and protection. The proposed microgrid structure is compliant with contemporary grid-connected IIEG Australian and International Standards during grid-connected mode and is designed to ensure fault discrimination and power quality for customers.

The major contributions of this Thesis are:

- A thorough literature review that critically analyses the effects of high EG penetration on contemporary protection strategies. Furthermore, there is a detailed review on protection strategies proposed by various authors for future networks, including intentionally islanded networks.
- A small-signal simulation platform capable of simulating the fault response of IIEG units in DNs has been developed and partially verified. A further contribution

is the modification of the control of IIEG units to ensure only positive sequence current export is possible and a more consistent control operation when traversing grid-connected and autonomous operation. The contribution of these controllers is pivotal to the success of the voltage sequence protection scheme proposed in this Thesis. The development of the small-signal platform is also crucial to the verification of the FAT and FATM.

- A novel OV mitigation scheme that does not require an off-line sensitivity analysis nor communications infrastructure. The scheme requires a simple modification of the aforementioned grid-connected control scheme and operates in a plug-and-play fashion. Furthermore, the scheme naturally allows a higher power export for customers connected to a point of connection with a lower short circuit impedance or in close proximity to load. Hence, the proposed OV mitigation scheme allows the utility to bolster EG presence in DNs with a large short circuit impedance and limited load diversity.

- The FAT developed as a means for approximating the fault response of grid-connected IIEG units. The FAT is capable of determining the fault response of IIEG units with FCLs for all fault types with a high success rate of convergence. The scheme, upon verification, precludes the need for time-intensive small-signal analysis. Hence, the impact of IIEG on fault efficacy can be determined quickly and accurately without a significant amount of prior research, time or computational power.

- The PAT created to automate the protection analysis process by simulating fault conditions pertinent to the determination of protection settings, taking into consideration the impact of IIEG on protection adequacy. The PAT utilises the FAT to determine the fault data, which is subsequently compiled and analysed to generate a protection report. The report highlights the data required to understand the impacts of high IIEG penetrations on the efficacy of a DN's protection scheme. The study includes the necessary CB ratings, OOZ fault current flow and pick-up currents. Hence, the time required for a technical analysis of the effects of a large EG installation on protection efficacy may be dramatically shortened and highly automated.

- A new microgrid philosophy was proposed with the intention of improving the fault discrimination characteristics of a microgrid. Voltage sequence protection was asserted as the preferred protection type and was shown to be effective within the small-signal simulation platform. A modification of the microgrid FAT scheme, namely the FATM, was implemented to aid in the determination of the necessary protection settings and protection efficacy of a microgrid with IIEG units and the proposed microgrid structure.

The technical challenges of continued EG proliferation are generally poorly understood, even by industry personnel. A large contribution of the work proffered in this Thesis is the prediction tools addressing the impacts of high EG penetration on protection efficacy without laborious small-signal modelling analyses. The FAT is currently unnecessary for contemporary EG penetrations within Australian DNs. However, if medium-scale IIEG proliferation occurs, applications for the FAT may arise and the efficacy of the FAT can be verified and subsequently used in industry applications. From an industrial point of view, the FAT and PAT represent powerful tools for protection diagnostics without requiring a significant amount of control data and both are relatively computationally inexpensive. Such tools could instill confidence in the utility towards the aim of the continued connection of IIEG in DNs.

For IIEG proliferation to continue, the risk of OV in DNs must be mitigated. Reportedly, there already exist cases of OV in Australian DNs. Hence, practical applications of the OV mitigation scheme are already present. Implementation of the OV mitigation scheme can represent a reduction in remuneration received by an IIEG proprietor. However, instances of OV represent a cost via the loss of power quality in the DN, which represents a long term cost in equipment life reduction. The impacts of OV can be alleviated through the proposed OV mitigation scheme. Many other schemes require off-line sensitivity analysis, fixed power factors or communications infrastructure. The proposed scheme does not require a detailed study of the DN, maximises real power export within voltage limitations and utilises only locally available data for successful operation. Furthermore, the control scheme requires only a simple modification of contemporary constant power control schemes. Future work will involve justifying (or mandating) the application of OV

mitigation and verifying that the scheme works as expected in practice. Furthermore, the effects of large number of OV mitigation schemes on the utility must also be studied before a mass roll-out of the proposed scheme is conducted.

The proposed microgrid philosophy, whilst experimental in nature, offers an alternative to other microgrid concepts that may ameliorate issues concerned with the detection of high-impedance single-phase to earth faults, without complicated spectral energy protection schemes. Fault discrimination if networks dominated by IIEG has been a topic of considerable research within both grid-connected and autonomous applications. The proposed philosophy does not require a significant change to current infrastructure, but does require significant changes in transformer connections, protection philosophy, communications infrastructure and IIEG control for adequate fault discrimination.

A significant amount of future work is necessary to provide a complete verification of the proposed models and fault analysis techniques. A limitation of this Thesis is the non-existence of a practical application of the proposed control schemes, which are exorbitantly expensive and logistically difficult. However, the transient responses and steady-state values of IIEG units within the small-signal simulation platform closely match the respective theoretical responses as shown in Chapter 3. A thorough stability analysis of the proposed schemes is necessary, especially in the case of the autonomous controller. Stability analysis is outside the scope of this Thesis; however, improvement of the control response could minimise the steady state error of the controller during fault responses, or possibly reduce the risk of instability when fault ride-through is required for more modular microgrids.

Appendix A

Constant Power Control Island Response Derivation

A single phase diagram of the test circuit is given in Fig. A.1.

The power equations used to derive the voltage and frequency response of the island are shown in (A.1)

$$S = VI^* = P + jQ = \frac{|V|^2}{Z^*} \tag{A.1}$$

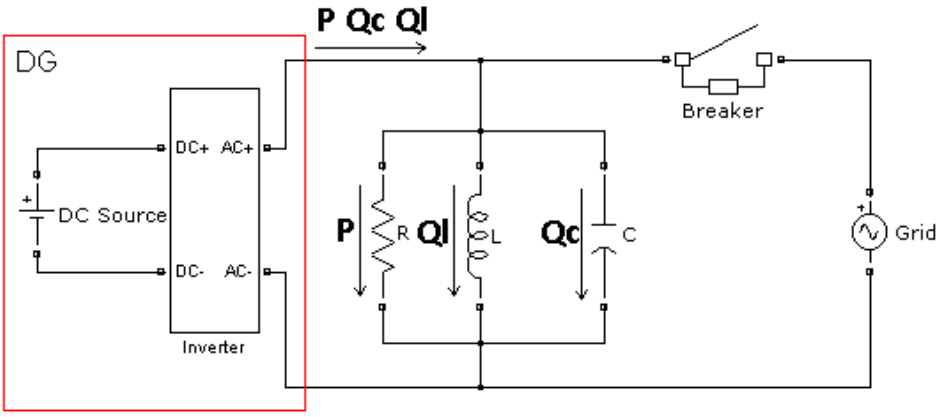

FIGURE A.1: Equivalent Circuit for Island

The load behaves as a constant impedance with parallel connected RLC elements. The rated voltage, angular frequency, real power, inductive reactive power and capacitive reactive power are denoted V_{rated}, ω_{rated}, P_{rated}, $Q_{l_{\text{rated}}}$ and $Q_{c_{\text{rated}}}$, respectively. The element resistance, inductance and capacitance may be expressed as:

$$R = \frac{V_{\text{rated}}^2}{P_{\text{rated}}} \tag{A.2}$$

$$L = \frac{V_{\text{rated}}^2}{Q_{l_{\text{rated}}}\omega_{\text{rated}}} \tag{A.3}$$

$$C = \frac{Q_{c_{\text{rated}}}}{V_{\text{rated}}^2\omega_{\text{rated}}} \tag{A.4}$$

The IIEG unit is constant power controlled and exports power set points of P_{sp} and Q_{sp}. Let ω and $|V|$ be the steady-state angular frequency and voltage magnitude after the island is formed.

$$P_{sp} + jQ_{sp} = \frac{|V|^2}{R} + j(\frac{|V|^2}{\omega L} - |V|^2\omega C) \tag{A.5}$$

Combining (A.2) and the real part of (A.5) yields:

$$\frac{|V|}{V_{\text{rated}}} = \sqrt{\frac{P_{sp}}{P_{\text{rated}}}} \tag{A.6}$$

Combining (A.3), (A.4) and the imaginary part of (A.5) yields:

$$\omega^2 Q_{c_{\text{rated}}}|V|^2 + \omega Q_{sp} V_{\text{rated}}^2\omega_{\text{rated}} - \omega_{\text{rated}}^2|V|^2 Q_{l_{\text{rated}}} = 0 \tag{A.7}$$

When applying the quadratic formula:

$$\frac{\omega}{\omega_{\text{rated}}} = \frac{Q_{sp}V_{\text{rated}}^2 \pm \sqrt{Q_{sp}^2 V_{\text{rated}}^4 + 4Q_{c_{\text{rated}}}|V|^4 Q_{l_{\text{rated}}}}}{2Q_{c_{\text{rated}}}|V|^2} \tag{A.8}$$

All terms are non-negative; thus, only the positive case shall be considered. If a per unit system is employed with V_{rated} and ω_{rated} used as bases, the equations can be reduced to (A.9) and (A.10).

$$|V| = \sqrt{\frac{P_{sp}}{P_{\text{rated}}}} \tag{A.9}$$

$$\omega = \frac{Q_{sp} + \sqrt{Q_{sp}^2 + 4Q_{c_{\text{rated}}}|V|^4 Q_{l_{\text{rated}}}}}{2Q_{c_{\text{rated}}}|V|^2} \tag{A.10}$$

Appendix B

Control Signal Deviation during Unbalanced Faults

B.1 Single-Line to Earth Phase

The code is shown in Fig. B.1 and the generated plot is shown in Fig. B.2.

Command Window Output:

Current Error Signal amplitude = 7.307324 %

B.2 Single-Line to Earth Phase

The code is shown in Fig. B.3 and the generated plot is shown in Fig. B.4.

Command Window Output:

Current Error Signal amplitude = 21.257014 %

```
Ts=0.0001; % Time step
frequency=50;
t=0:Ts:2; % time range
V=8981.46; % voltage magnitude
S=50000; % power export
%I=5.1*S/V; % current magnitude l-l fault
I=1.1268*S/V; % current magnitude l-e fault
Va=0*cos(2*pi*50*t); % PCC voltages
Vb=V*cos(2*pi*50*t-2*pi/3);
Vc=V*cos(2*pi*50*t+2*pi/3);
Ia=I*cos(2*pi*50*t); % PCC currents chosen such that delta I = 0
Ib=I*cos(2*pi*50*t-2*pi/3);
Ic=I*cos(2*pi*50*t+2*pi/3);
Vp=2/3*(Va.*cos(2*pi*50*t)+Vb.*cos(2*pi*50*t-2*pi/3)+Vc.*cos(2*pi*50*t+2*pi/3)); %↙
conversion to direct axis
Ip=2/3*(Ia.*cos(2*pi*50*t)+Ib.*cos(2*pi*50*t-2*pi/3)+Ic.*cos(2*pi*50*t+2*pi/3));

Vf(1)=0; % wc=2pi250 rad/sec LPFs
for p=2:numel(t)
    Vf(p)=(Ts*Vp(p)*2*pi*250+Vf(p-1))/(1+Ts*2*pi*250);
end

If(1)=0;% wc=2pi250 rad/sec LPFs
for p=2:numel(t)
    If(p)=(Ts*Ip(p)*2*pi*250+If(p-1))/(1+Ts*2*pi*250);
end

Iref=2/3*S./Vf-If; % current error calculator

Ireff(1)=0;% wc=2pi10 rad/sec LPFs
for p=2:numel(t)
    Ireff(p)=(Ts*Iref(p)*2*pi*10+Ireff(p-1))/(1+Ts*2*pi*10);
end

Vpeak=0.3; %l-e fault
%Vpeak=4; %l-l fault

Va=Vpeak*cos(2*pi*50*t); % voltage signals chosen to compare phase peaks with↙
oscillating current error signal
Vb=Vpeak*cos(2*pi*50*t-2*pi/3);
Vc=Vpeak*cos(2*pi*50*t+2*pi/3);
Iax=(1.1268*S/V+3/2*Ireff).*cos(2*pi*50*t); % PCC currents chosen such that delta I =↙
0
Ibx=(1.1268*S/V+3/2*Ireff).*cos(2*pi*50*t-2*pi/3);
Icx=(1.1268*S/V+3/2*Ireff).*cos(2*pi*50*t+2*pi/3);

figure(6); % plot signals l-e fault
plot(t,Ireff,t,Va,t,Vb,t,Vc);
legend('dI','Va','Vb','Vc');
grid on;

per_error=(((max(Ireff(5000:end))+abs(min(Ireff(5000:end)))))/2)/(2/3*I); % calculate↙
and plot deviation
fprintf('Current Error Signal amplitude = %f %%\n.', per_error*100);
```

FIGURE B.1: Control Signal Code Simulating Reflected Line-to-Earth Fault

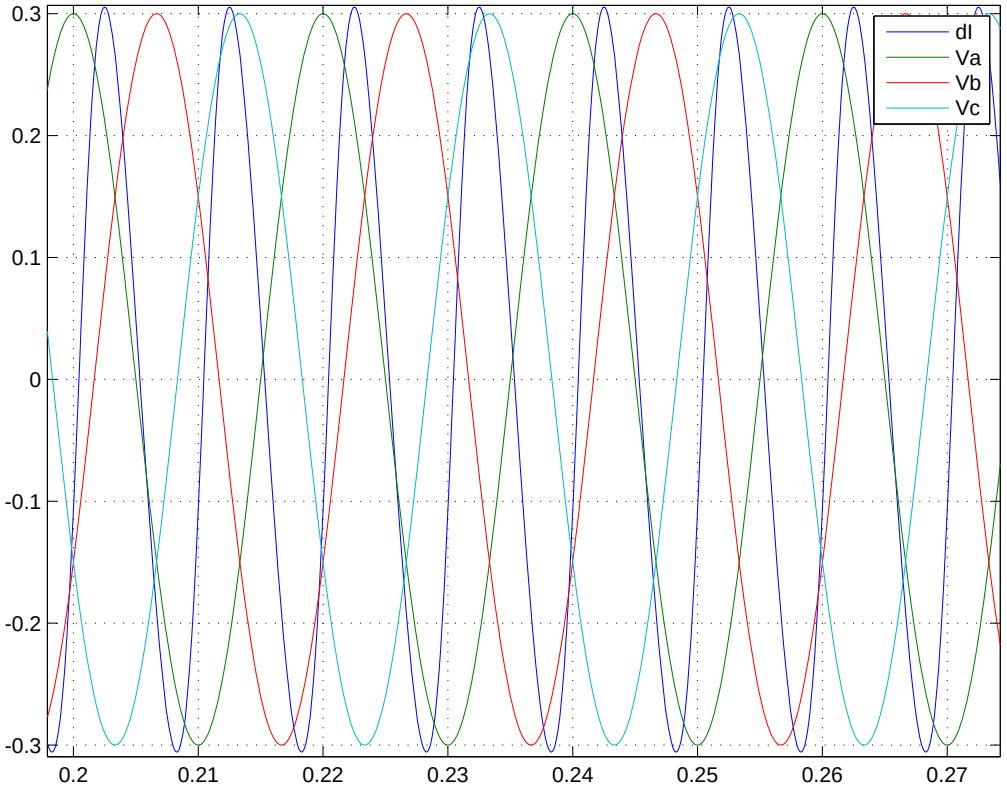

FIGURE B.2: Control Signal Plot Simulating Reflected Line-to-Earth Fault

```
Ts=0.0001; % Time step
frequency=50;
t=0:Ts:2; % time range
V=8981.46; % voltage magnitude
S=50000; % power export
I=5.1*S/V; % current magnitude l-l fault
%I=1.1268*S/V; % current magnitude l-e fault
Va=0*cos(2*pi*50*t); % PCC voltages
Vb=0*cos(2*pi*50*t-2*pi/3);
Vc=V*cos(2*pi*50*t+2*pi/3);
Ia=I*cos(2*pi*50*t); % PCC currents chosen such that delta I = 0
Ib=I*cos(2*pi*50*t-2*pi/3);
Ic=I*cos(2*pi*50*t+2*pi/3);
Vp=2/3*(Va.*cos(2*pi*50*t)+Vb.*cos(2*pi*50*t-2*pi/3)+Vc.*cos(2*pi*50*t+2*pi/3)); %↙
conversion to direct axis
Ip=2/3*(Ia.*cos(2*pi*50*t)+Ib.*cos(2*pi*50*t-2*pi/3)+Ic.*cos(2*pi*50*t+2*pi/3));

Vf(1)=0; % wc=2pi250 rad/sec LPFs
for p=2:numel(t)
    Vf(p)=(Ts*Vp(p)*2*pi*250+Vf(p-1))/(1+Ts*2*pi*250);
end

If(1)=0;% wc=2pi250 rad/sec LPFs
for p=2:numel(t)
    If(p)=(Ts*Ip(p)*2*pi*250+If(p-1))/(1+Ts*2*pi*250);
end

Iref=2/3*S./Vf-If; % current error calculator

Ireff(1)=0;% wc=2pi10 rad/sec LPFs
for p=2:numel(t)
    Ireff(p)=(Ts*Iref(p)*2*pi*10+Ireff(p-1))/(1+Ts*2*pi*10);
end

%Vpeak=0.3; %l-e fault
Vpeak=4; %l-l fault

Va=Vpeak*cos(2*pi*50*t); % voltage signals chosen to compare phase peaks with↙
oscillating current error signal
Vb=Vpeak*cos(2*pi*50*t-2*pi/3);
Vc=Vpeak*cos(2*pi*50*t+2*pi/3);
Iax=(1.1268*S/V+3/2*Ireff).*cos(2*pi*50*t); % PCC currents chosen such that delta I =↙
0
Ibx=(1.1268*S/V+3/2*Ireff).*cos(2*pi*50*t-2*pi/3);
Icx=(1.1268*S/V+3/2*Ireff).*cos(2*pi*50*t+2*pi/3);

figure(6); % plot signals l-e fault
plot(t,Ireff,t,Va,t,Vb,t,Vc);
legend('dI','Va','Vb','Vc');
grid on;

per_error=(((max(Ireff(5000:end))+abs(min(Ireff(5000:end)))))/2)/(2/3*I); % calculate↙
and plot deviation
fprintf('Current Error Signal amplitude = %f %%\n.', per_error*100);
```

FIGURE B.3: Control Signal Code Simulating Reflected Line-to-Line Fault

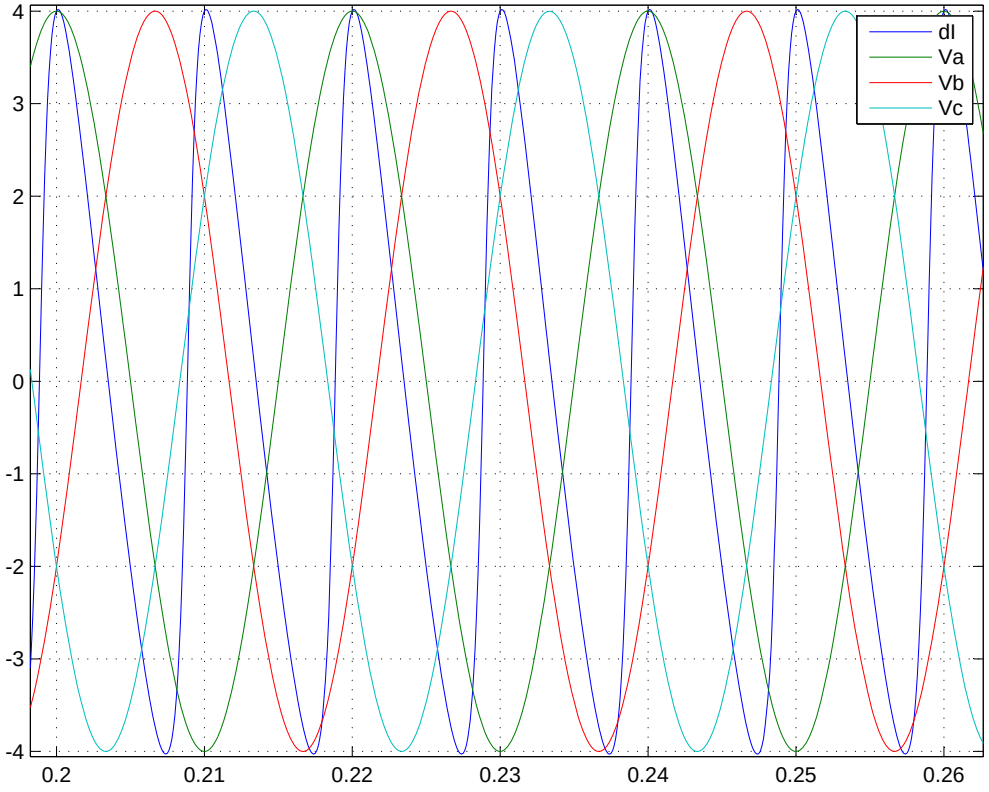

FIGURE B.4: Control Signal Plot Simulating Reflected Line-to-Line Fault

Appendix C

PAT Reports

C.1 Report of PAT – no FCL or EIT

There were 22 failures of convergence noted. All were three phase faults.

Protection Report: CT1_a

Peak current: 1.312349 amps

Primary OC pick-up minimum required: 1523.413310 amps

Primary EF pick-up minimum required: 1757.914853 amps

Maximum OC current: 19483.349758 amps

Maximum EF current: 19483.778049 amps

CT Zone: CT2_a Maximum OC out-of zone fault current: 4.958971 amps

CT Zone: CT3_a Maximum OC out-of zone fault current: 1.557184 amps

CT Zone: CT4_a Maximum OC out-of zone fault current: 1.418272 amps

CT Zone: CT2_a Maximum EF out-of zone fault current: 3.934510 amps

CT Zone: CT3_a Maximum EF out-of zone fault current: 1.444648 amps

CT Zone: CT4_a Maximum EF out-of zone fault current: 1.370636 amps

Protection Report: CT2_a

Peak current: 11.768138 amps

Primary OC pick-up minimum required: 1046.410518 amps

Primary EF pick-up minimum required: 1207.270502 amps

Secondary OC pick-up minimum required: 464.482902 amps

Secondary EF pick-up minimum required: 535.745830 amps

Maximum OC current: 19481.547370 amps

Maximum EF current: 19481.677596 amps

CT Zone: CT1_a Maximum OC out-of zone fault current: 13.869333 amps

CT Zone: CT4_a Maximum OC out-of zone fault current: 536.525732 amps

CT Zone: CT1_a Maximum EF out-of zone fault current: 11.768162 amps

CT Zone: CT4_a Maximum EF out-of zone fault current: 536.525338 amps

Protection Report: CT3_a

Peak current: 7.841797 amps

Primary OC pick-up minimum required: 464.684138 amps

Primary EF pick-up minimum required: 535.486960 amps

Secondary OC pick-up minimum required: 327.356335 amps

Secondary EF pick-up minimum required: 377.680716 amps

Maximum OC current: 1208.835522 amps

Maximum EF current: 1207.812071 amps

CT Zone: CT1_a Maximum OC out-of zone fault current: 9.251499 amps

CT Zone: CT2_a Maximum OC out-of zone fault current: 9.253091 amps

CT Zone: CT1_a Maximum EF out-of zone fault current: 7.843460 amps

CT Zone: CT2_a Maximum EF out-of zone fault current: 7.843460 amps

Protection Report: CT4_a

Peak current: 3.923409 amps

Primary OC pick-up minimum required: 327.278429 amps

Primary EF pick-up minimum required: 377.451083 amps

Maximum OC current: 540.274459 amps

Maximum EF current: 536.495479 amps

CT Zone: CT1_a Maximum OC out-of zone fault current: 4.636271 amps

CT Zone: CT2_a Maximum OC out-of zone fault current: 4.637069 amps

CT Zone: CT3_a Maximum OC out-of zone fault current: 4.638306 amps

CT Zone: CT1_a Maximum EF out-of zone fault current: 3.928990 amps

CT Zone: CT2_a Maximum EF out-of zone fault current: 3.929023 amps

CT Zone: CT3_a Maximum EF out-of zone fault current: 3.934928 amps

C.2 Report of PAT with EIT

There were 22 failures of convergence noted. All were three phase faults.

Protection Report: CT1_a

Peak current: 1.312349 amps

Primary OC pick-up minimum required: 1523.413310 amps

Primary EF pick-up minimum required: 1758.363435 amps

Maximum OC current: 19483.349758 amps

Maximum EF current: 19483.349758 amps

CT Zone: CT2_a Maximum OC out-of zone fault current: 1.312079 amps

CT Zone: CT3_a Maximum OC out-of zone fault current: 1.557184 amps

CT Zone: CT4_a Maximum OC out-of zone fault current: 1.418272 amps

CT Zone: CT2_a Maximum EF out-of zone fault current: 1.312079 amps

CT Zone: CT3_a Maximum EF out-of zone fault current: 1.444648 amps

CT Zone: CT4_a Maximum EF out-of zone fault current: 1.370636 amps

Protection Report: CT2_a

Peak current: 11.768138 amps

Primary OC pick-up minimum required: 1051.394168 amps

Primary EF pick-up minimum required: 1207.600684 amps

Secondary OC pick-up minimum required: 468.164903 amps

Secondary EF pick-up minimum required: 535.901961 amps

Maximum OC current: 19481.547370 amps

Maximum EF current: 19481.547370 amps

CT Zone: CT1_a Maximum OC out-of zone fault current: 11.768087 amps

CT Zone: CT4_a Maximum OC out-of zone fault current: 536.525732 amps

CT Zone: CT1_a Maximum EF out-of zone fault current: 11.768087 amps

CT Zone: CT4_a Maximum EF out-of zone fault current: 536.525338 amps

Protection Report: CT3_a

Peak current: 7.841797 amps

Primary OC pick-up minimum required: 467.587530 amps

Primary EF pick-up minimum required: 535.645777 amps

Secondary OC pick-up minimum required: 331.222330 amps

Secondary EF pick-up minimum required: 378.189804 amps

Maximum OC current: 1207.144640 amps

Maximum EF current: 1207.142465 amps

CT Zone: CT1_a Maximum OC out-of zone fault current: 7.838424 amps

CT Zone: CT2_a Maximum OC out-of zone fault current: 7.838424 amps

CT Zone: CT1_a Maximum EF out-of zone fault current: 7.838424 amps

CT Zone: CT2_a Maximum EF out-of zone fault current: 7.838424 amps

Protection Report: CT4_a

Peak current: 3.923409 amps

Primary OC pick-up minimum required: 328.829569 amps

Primary EF pick-up minimum required: 377.563194 amps

Maximum OC current: 535.281557 amps

Maximum EF current: 535.535398 amps

CT Zone: CT1_a Maximum OC out-of zone fault current: 3.916696 amps

CT Zone: CT2_a Maximum OC out-of zone fault current: 3.916696 amps

CT Zone: CT3_a Maximum OC out-of zone fault current: 3.916718 amps

CT Zone: CT1_a Maximum EF out-of zone fault current: 3.916696 amps

CT Zone: CT2_a Maximum EF out-of zone fault current: 3.916696 amps

CT Zone: CT3_a Maximum EF out-of zone fault current: 3.916717 amps

Appendix D

FATM Excerpt

Fig. D.1 is a print out from a FATM case study. The steady-state grid frequency is given as well as the voltage and current vectors of each element within the microgrid. The A phase current vector of IIEG1 is used as the absolute reference for all vectors.

```
******************
Steady State data
******************
Grid Frequency: 50.193201 Hz
Element: IIEG1
Voltage: 42.694002/_89.794581
Current: 135.018186/_0.000000
Element:
Voltage: 364.237327/_-140.941936
Current: 135.018186/_-120.000000
Element:
Voltage: 406.432234/_158.087645
Current: 135.018186/_120.000000
Element: Tx1_a_primary
Voltage: 42.694002/_-90.205419
Current: 135.018186/_-180.000000
Element: Tx1_b_primary
Voltage: 364.237327/_39.058064
Current: 135.018186/_60.000000
Element: Tx1_c_primary
Voltage: 406.432234/_-21.912355
Current: 135.018186/_-60.000000
Element: Tx1_a_secondary
Voltage: 1.624548/_72.391097
Current: 4.909752/_-0.000000
Element: Tx1_b_secondary
Voltage: 10489.598555/_-146.941621
Current: 4.909629/_-119.999262
Element: Tx1_c_secondary
Voltage: 10491.133264/_153.053631
Current: 4.909636/_119.999122
Element: Tx2_a_primary
Voltage: 10489.862973/_-146.950376
Current: 0.681782/_-150.097941
Element: Tx2_b_primary
Voltage: 10490.126673/_93.048885
Current: 0.681799/_89.901320
Element: Tx2_c_primary
Voltage: 10489.877693/_-26.951993
Current: 0.681783/_-30.099558
Element: Tx2_a_secondary
Voltage: 219.815942/_30.793597
Current: 27.485512/_29.367011
Element: Tx2_b_secondary
Voltage: 219.821468/_-89.207142
Current: 27.486203/_-90.633728
Element: Tx2_c_secondary
Voltage: 219.816251/_150.791980
Current: 27.485551/_149.365394
Element: Load1_a
Voltage: 219.815942/_-149.206403
Current: 27.485512/_-150.632989
Element: Load1_b
Voltage: 219.821468/_90.792858
Current: 27.486203/_89.366272
Element: Load1_c
Voltage: 219.816251/_-29.208020
Current: 27.485551/_-30.634606
Element: Line1_a
Voltage: 1.624381/_72.406977
Current: 4.909752/_-0.000000
Element: Line1_b
Voltage: 1.624340/_-47.592285
Current: 4.909629/_-119.999262
Element: Line1_c
Voltage: 1.624342/_-167.593901
Current: 4.909636/_119.999122
Element: Fault Impedance
Voltage: 0.000481/_2.846930
Current: 0.000240/_2.846930
```

FIGURE D.1: Steady State Fault Response

Appendix E

FATM Output Data

Figs. contain an excerpt of the FATM scheme applied to the microgrid detailed in Chapter 7. The excerpt contains all single-phase to earth data. The fault data may be interpretted as follows:

Node: (location of the fault)

ef (phase on which the fault is placed) fault (IIEG phase measurement): (quantity measured at IIEG unit) (units: either volts or amperes)

The node positions corresponding to Fig. 7.6 are explained in Table E.1.

```
**********
Microgrid Protection:
**********

DGconfig:
IIEG1 connected
Sensor: IIEG1

Prefault: 135.016127/_-0.000000 A
Prefault: 226.699012/_13.886284 V
Prefault Vp: 226.699012/_13.886284 V
Prefault Vn: 0.000000/_-31.607502 V
Prefault V0: 0.000000/_-169.441012 V
Node: 2
ef a fault a: 135.018266/_0.000000 amps
ef a fault b: 135.018266/_-120.000000 amps
ef a fault c: 135.018266/_120.000000 amps
ef b fault a: 135.018266/_0.000000 amps
ef b fault b: 135.018266/_-120.000000 amps
ef b fault c: 135.018266/_120.000000 amps
ef c fault a: 135.018266/_0.000000 amps
ef c fault b: 135.018266/_-120.000000 amps
ef c fault c: 135.018266/_120.000000 amps
ef a fault a: 6.602820/_13.689684 V
ef a fault b: 386.957215/_-135.621516 V
ef a fault c: 386.936886/_163.399195 V
ef b fault a: 386.936886/_43.399195 V
ef b fault b: 6.602820/_-106.310316 V
ef b fault c: 386.957215/_104.378484 V
ef c fault a: 386.957215/_-15.621516 V
ef c fault b: 386.936886/_-76.600805 V
ef c fault c: 6.602820/_133.689684 V
ef a fault Vp: 226.699012/_13.886062 V
ef a fault Vn: 0.003695/_-152.424033 V
ef a fault V0: 220.092641/_-166.108274 V
ef b fault Vp: 226.699012/_13.886062 V
ef b fault Vn: 0.003695/_-32.424033 V
ef b fault V0: 220.092641/_73.891726 V
ef c fault Vp: 226.699012/_13.886062 V
ef c fault Vn: 0.003695/_87.575967 V
ef c fault V0: 220.092641/_-46.108274 V
Node: 5
ef a fault a: 135.018187/_-0.000000 amps
ef a fault b: 135.018187/_-120.000000 amps
ef a fault c: 135.018187/_120.000000 amps
ef b fault a: 135.018187/_-0.000000 amps
ef b fault b: 135.018187/_-120.000000 amps
ef b fault c: 135.018187/_120.000000 amps
ef c fault a: 135.018187/_-0.000000 amps
ef c fault b: 135.018187/_-120.000000 amps
ef c fault c: 135.018187/_120.000000 amps
ef a fault a: 42.638100/_89.806601 V
ef a fault b: 364.279631/_-140.936019 V
ef a fault c: 406.419875/_158.095433 V
ef b fault a: 406.419875/_38.095433 V
ef b fault b: 42.638100/_-30.193399 V
ef b fault c: 364.279631/_99.063981 V
ef c fault a: 364.279631/_-20.936019 V
ef c fault b: 406.419875/_-81.904567 V
ef c fault c: 42.638100/_-150.193399 V
ef a fault Vp: 226.698912/_13.886409 V
ef a fault Vn: 0.003593/_-174.075419 V
ef a fault V0: 220.240461/_-176.936822 V
ef b fault Vp: 226.698912/_13.886409 V
ef b fault Vn: 0.003593/_-54.075419 V
ef b fault V0: 220.240461/_63.063178 V
ef c fault Vp: 226.698912/_13.886409 V
ef c fault Vn: 0.003593/_65.924581 V
ef c fault V0: 220.240461/_-56.936822 V
Node: 8
ef a fault a: 135.018186/_0.000000 amps
ef a fault b: 135.018186/_-120.000000 amps
ef a fault c: 135.018186/_120.000000 amps
ef b fault a: 135.018186/_-0.000000 amps
ef b fault b: 135.018186/_-120.000000 amps
ef b fault c: 135.018186/_120.000000 amps
ef c fault a: 135.018186/_-0.000000 amps
ef c fault b: 135.018186/_-120.000000 amps
ef c fault c: 135.018186/_120.000000 amps
ef a fault a: 42.694467/_89.782897 V
ef a fault b: 364.230292/_-140.941125 V
ef a fault c: 406.424317/_158.087130 V
ef b fault a: 406.424317/_38.087130 V
ef b fault b: 42.694467/_-30.217103 V
ef b fault c: 364.230292/_99.058875 V
ef c fault a: 364.230292/_-20.941125 V
ef c fault b: 406.424317/_-81.912870 V
ef c fault c: 42.694467/_-150.217103 V
ef a fault Vp: 226.698912/_13.886410 V
ef a fault Vn: 0.003592/_-174.104177 V
```

FIGURE E.1: FATM Output Data: pp. 1

ef a fault V0: 220.219632/_-176.951200 V
ef b fault Vp: 226.698912/_13.886410 V
ef b fault Vn: 0.003592/_-54.104177 V
ef b fault V0: 220.219632/_63.048800 V
ef c fault Vp: 226.698912/_13.886410 V
ef c fault Vn: 0.003592/_65.895823 V
ef c fault V0: 220.219632/_-56.951200 V
Node: 11
ef a fault a: 135.018186/_-0.000000 amps
ef a fault b: 135.018186/_-120.000000 amps
ef a fault c: 135.018186/_120.000000 amps
ef b fault a: 135.018186/_0.000000 amps
ef b fault b: 135.018186/_-120.000000 amps
ef b fault c: 135.018186/_120.000000 amps
ef c fault a: 135.018186/_-0.000000 amps
ef c fault b: 135.018186/_-120.000000 amps
ef c fault c: 135.018186/_120.000000 amps
ef a fault a: 42.737289/_89.764968 V
ef a fault b: 364.192836/_-140.945008 V
ef a fault c: 406.427721/_158.080825 V
ef b fault a: 406.427721/_38.080825 V
ef b fault b: 42.737289/_-30.235032 V
ef b fault c: 364.192836/_99.054992 V
ef c fault a: 364.192836/_-20.945008 V
ef c fault b: 406.427721/_-81.919175 V
ef c fault c: 42.737289/_-150.235032 V
ef a fault Vp: 226.698912/_13.886410 V
ef a fault Vn: 0.003592/_-174.126026 V
ef a fault V0: 220.203845/_-176.962125 V
ef b fault Vp: 226.698912/_13.886410 V
ef b fault Vn: 0.003592/_-54.126026 V
ef b fault V0: 220.203845/_63.037875 V
ef c fault Vp: 226.698912/_13.886410 V
ef c fault Vn: 0.003592/_65.873974 V
ef c fault V0: 220.203845/_-56.962125 V
Node: 14
ef a fault a: 135.018186/_-0.000000 amps
ef a fault b: 135.018186/_-120.000000 amps
ef a fault c: 135.018186/_120.000000 amps
ef b fault a: 135.018186/_-0.000000 amps
ef b fault b: 135.018186/_-120.000000 amps
ef b fault c: 135.018186/_120.000000 amps
ef c fault a: 135.018186/_0.000000 amps
ef c fault b: 135.018186/_-120.000000 amps
ef c fault c: 135.018186/_120.000000 amps
ef a fault a: 42.766563/_89.752782 V
ef a fault b: 364.167260/_-140.947666 V
ef a fault c: 406.430085/_158.076517 V
ef b fault a: 406.430085/_38.076517 V
ef b fault b: 42.766563/_-30.247218 V
ef b fault c: 364.167260/_99.052334 V
ef c fault a: 364.167260/_-20.947666 V
ef c fault b: 406.430085/_-81.923483 V
ef c fault c: 42.766563/_-150.247218 V
ef a fault Vp: 226.698912/_13.886410 V
ef a fault Vn: 0.003591/_-174.140964 V
ef a fault V0: 220.193094/_-176.969594 V
ef b fault Vp: 226.698912/_13.886410 V
ef b fault Vn: 0.003591/_-54.140964 V
ef b fault V0: 220.193094/_63.030406 V
ef c fault Vp: 226.698912/_13.886410 V
ef c fault Vn: 0.003591/_65.859036 V
ef c fault V0: 220.193094/_-56.969594 V
Node: 17
ef a fault a: 135.018185/_-0.000000 amps
ef a fault b: 135.018185/_-120.000000 amps
ef a fault c: 135.018185/_120.000000 amps
ef b fault a: 135.018185/_-0.000000 amps
ef b fault b: 135.018185/_-120.000000 amps
ef b fault c: 135.018185/_120.000000 amps
ef c fault a: 135.018185/_0.000000 amps
ef c fault b: 135.018185/_-120.000000 amps
ef c fault c: 135.018185/_120.000000 amps
ef a fault a: 42.782290/_89.746317 V
ef a fault b: 364.153565/_-140.949099 V
ef a fault c: 406.431407/_158.074205 V
ef b fault a: 406.431407/_38.074205 V
ef b fault b: 42.782290/_-30.253683 V
ef b fault c: 364.153565/_99.050901 V
ef c fault a: 364.153565/_-20.949099 V
ef c fault b: 406.431407/_-81.925795 V
ef c fault c: 42.782290/_-150.253683 V
ef a fault Vp: 226.698912/_13.886410 V
ef a fault Vn: 0.003591/_-174.148990 V
ef a fault V0: 220.187376/_-176.973607 V
ef b fault Vp: 226.698912/_13.886410 V
ef b fault Vn: 0.003591/_-54.148990 V
ef b fault V0: 220.187376/_63.026393 V
ef c fault Vp: 226.698912/_13.886410 V
ef c fault Vn: 0.003591/_65.851010 V

FIGURE E.2: FATM Output Data: pp. 2

ef c fault V0: 220.187376/_-56.973607 V
Node: 20
ef a fault a: 135.083128/_0.000000 amps
ef a fault b: 135.083128/_-120.000000 amps
ef a fault c: 135.083128/_120.000000 amps
ef b fault a: 135.083128/_-0.000000 amps
ef b fault b: 135.083128/_-120.000000 amps
ef b fault c: 135.083128/_120.000000 amps
ef c fault a: 135.083128/_-0.000000 amps
ef c fault b: 135.083128/_-120.000000 amps
ef c fault c: 135.083128/_120.000000 amps
ef a fault a: 226.614755/_13.870441 V
ef a fault b: 226.658985/_-106.078581 V
ef a fault c: 226.811481/_133.886256 V
ef b fault a: 226.811481/_13.886256 V
ef b fault b: 226.614755/_-106.129559 V
ef b fault c: 226.658985/_133.921419 V
ef c fault a: 226.658985/_13.921419 V
ef c fault b: 226.811481/_-106.113744 V
ef c fault c: 226.614755/_133.870441 V
ef a fault Vp: 226.695058/_13.892705 V
ef a fault Vn: 0.119188/_-118.475510 V
ef a fault V0: 0.000000/_173.262493 V
ef b fault Vp: 226.695058/_13.892705 V
ef b fault Vn: 0.119188/_1.524490 V
ef b fault V0: 0.000000/_173.343929 V
ef c fault Vp: 226.695058/_13.892705 V
ef c fault Vn: 0.119188/_121.524490 V
ef c fault V0: 0.000000/_147.745666 V
Node: 23
ef a fault a: 135.083134/_0.000000 amps
ef a fault b: 135.083134/_-120.000000 amps
ef a fault c: 135.083134/_120.000000 amps
ef b fault a: 135.083134/_0.000000 amps
ef b fault b: 135.083134/_-120.000000 amps
ef b fault c: 135.083134/_120.000000 amps
ef c fault a: 135.083134/_-0.000000 amps
ef c fault b: 135.083134/_-120.000000 amps
ef c fault c: 135.083134/_120.000000 amps
ef a fault a: 226.614765/_13.870433 V
ef a fault b: 226.658968/_-106.078585 V
ef a fault c: 226.811492/_133.886256 V
ef b fault a: 226.811492/_13.886256 V
ef b fault b: 226.614765/_-106.129567 V
ef b fault c: 226.658968/_133.921415 V
ef c fault a: 226.658968/_13.921415 V
ef c fault b: 226.811492/_-106.113744 V
ef c fault c: 226.614765/_133.870433 V
ef a fault Vp: 226.695059/_13.892702 V
ef a fault Vn: 0.119194/_-118.467478 V
ef a fault V0: 0.000000/_116.319546 V
ef b fault Vp: 226.695059/_13.892702 V
ef b fault Vn: 0.119194/_1.532522 V
ef b fault V0: 0.000000/_142.624951 V
ef c fault Vp: 226.695059/_13.892702 V
ef c fault Vn: 0.119194/_121.532522 V
ef c fault V0: 0.000000/_-103.706472 V
Node: 26
ef a fault a: 135.083163/_-0.000000 amps
ef a fault b: 135.083163/_-120.000000 amps
ef a fault c: 135.083163/_120.000000 amps
ef b fault a: 135.083163/_-0.000000 amps
ef b fault b: 135.083163/_-120.000000 amps
ef b fault c: 135.083163/_120.000000 amps
ef c fault a: 135.083163/_0.000000 amps
ef c fault b: 135.083163/_-120.000000 amps
ef c fault c: 135.083163/_120.000000 amps
ef a fault a: 226.614806/_13.870397 V
ef a fault b: 226.658891/_-106.078601 V
ef a fault c: 226.811541/_133.886256 V
ef b fault a: 226.811541/_13.886256 V
ef b fault b: 226.614806/_-106.129603 V
ef b fault c: 226.658891/_133.921399 V
ef c fault a: 226.658891/_13.921399 V
ef c fault b: 226.811541/_-106.113744 V
ef c fault c: 226.614806/_133.870397 V
ef a fault Vp: 226.695063/_13.892684 V
ef a fault Vn: 0.119223/_-118.430699 V
ef a fault V0: 0.000000/_123.664260 V
ef b fault Vp: 226.695063/_13.892684 V
ef b fault Vn: 0.119223/_1.569301 V
ef b fault V0: 0.000000/_146.686631 V
ef c fault Vp: 226.695063/_13.892684 V
ef c fault Vn: 0.119223/_121.569301 V
ef c fault V0: 0.000000/_-89.567029 V
Node: 29
ef a fault a: 135.083146/_0.000000 amps
ef a fault b: 135.083146/_-120.000000 amps
ef a fault c: 135.083146/_120.000000 amps
ef b fault a: 135.083146/_-0.000000 amps

FIGURE E.3: FATM Output Data: pp. 3

ef b fault b: 135.083146/_-120.000000 amps
ef b fault c: 135.083146/_120.000000 amps
ef c fault a: 135.083146/_-0.000000 amps
ef c fault b: 135.083146/_-120.000000 amps
ef c fault c: 135.083146/_120.000000 amps
ef a fault a: 226.614781/_13.870419 V
ef a fault b: 226.658937/_-106.078591 V
ef a fault c: 226.811512/_133.886256 V
ef b fault a: 226.811512/_13.886256 V
ef b fault b: 226.614781/_-106.129581 V
ef b fault c: 226.658937/_133.921409 V
ef c fault a: 226.658937/_13.921409 V
ef c fault b: 226.811512/_-106.113744 V
ef c fault c: 226.614781/_133.870419 V
ef a fault Vp: 226.695061/_13.892695 V
ef a fault Vn: 0.119206/_-118.452540 V
ef a fault V0: 0.000000/_-99.776083 V
ef b fault Vp: 226.695061/_13.892695 V
ef b fault Vn: 0.119206/_1.547460 V
ef b fault V0: 0.000000/_173.176323 V
ef c fault Vp: 226.695061/_13.892695 V
ef c fault Vn: 0.119206/_121.547460 V
ef c fault V0: 0.000000/_148.107331 V
Node: 32
ef a fault a: 135.018185/_-0.000000 amps
ef a fault b: 135.018185/_-120.000000 amps
ef a fault c: 135.018185/_120.000000 amps
ef b fault a: 135.018185/_-0.000000 amps
ef b fault b: 135.018185/_-120.000000 amps
ef b fault c: 135.018185/_120.000000 amps
ef c fault a: 135.018185/_-0.000000 amps
ef c fault b: 135.018185/_-120.000000 amps
ef c fault c: 135.018185/_120.000000 amps
ef a fault a: 42.804057/_89.738773 V
ef a fault b: 364.135417/_-140.951188 V
ef a fault c: 406.434208/_158.071061 V
ef b fault a: 406.434208/_38.071061 V
ef b fault b: 42.804057/_-30.261227 V
ef b fault c: 364.135417/_99.048812 V
ef c fault a: 364.135417/_-20.951188 V
ef c fault b: 406.434208/_-81.928939 V
ef c fault c: 42.804057/_-150.261227 V
ef a fault Vp: 226.698912/_13.886411 V
ef a fault Vn: 0.003591/_-174.160125 V
ef a fault V0: 220.180506/_-176.979178 V
ef b fault Vp: 226.698912/_13.886411 V
ef b fault Vn: 0.003591/_-54.160125 V
ef b fault V0: 220.180506/_63.020822 V
ef c fault Vp: 226.698912/_13.886411 V
ef c fault Vn: 0.003591/_65.839875 V
ef c fault V0: 220.180506/_-56.979178 V
Node: 35
ef a fault a: 135.084738/_-0.000000 amps
ef a fault b: 135.084738/_-120.000000 amps
ef a fault c: 135.084738/_120.000000 amps
ef b fault a: 135.084738/_-0.000000 amps
ef b fault b: 135.084738/_-120.000000 amps
ef b fault c: 135.084738/_120.000000 amps
ef c fault a: 135.084738/_0.000000 amps
ef c fault b: 135.084738/_-120.000000 amps
ef c fault c: 135.084738/_120.000000 amps
ef a fault a: 226.622228/_13.866536 V
ef a fault b: 226.650690/_-106.081576 V
ef a fault c: 226.814185/_133.886255 V
ef b fault a: 226.814185/_13.886255 V
ef b fault b: 226.622228/_-106.133464 V
ef b fault c: 226.650690/_133.918424 V
ef c fault a: 226.650690/_13.918424 V
ef c fault b: 226.814185/_-106.113745 V
ef c fault c: 226.622228/_133.866536 V
ef a fault Vp: 226.695685/_13.890405 V
ef a fault Vn: 0.119632/_-114.002620 V
ef a fault V0: 0.000000/_-150.909360 V
ef b fault Vp: 226.695685/_13.890405 V
ef b fault Vn: 0.119632/_5.997380 V
ef b fault V0: 0.000000/_127.069531 V
ef c fault Vp: 226.695685/_13.890405 V
ef c fault Vn: 0.119632/_125.997380 V
ef c fault V0: 0.000000/_141.308170 V

FIGURE E.4: FATM Output Data: pp. 4

Table E.1: Island Node Data

Element	Node Adjacencies
IIEG	2
Line_1	5,8
Line_2	8,11
Line_3	11,14
Line_4	14,17
Line_5	17,32
Tx_1	2,5
Tx_2	8,26
Tx_3	11,29
Tx_4	14,23
Tx_5	17,20
Tx_6	32,35
Load_1	26
Load_2	29
Load_3	23
Load_4	20
Load_5	35

Bibliography

[1] S. Conti, L. Raffa, and U. Vagliasindi. Innovative solutions for protection schemes in autonomous MV micro-grids. In *Clean Electrical Power, 2009 International Conference on*, pages 647–654, June 2009. doi: 10.1109/ICCEP.2009.5211985.

[2] X. Li, A. Dysko, and G. Burt. Enhanced protection for inverter dominated microgrid using transient fault information. In *Developments in Power Systems Protection, 2012. DPSP 2012. 11th International Conference on*, pages 1–5, April 2012. doi: 10.1049/cp.2012.0081.

[3] H. Saadat. *Power system analysis*, chapter 10. McGraw-Hill, New York, USA, 1999.

[4] G. Benmouyal et al. IEEE Standard Inverse-Time Characteristic Equations for Overcurrent Relays. *IEEE Transactions on Power Delivery*, 14:868–872, July 1999.

[5] S. H. Schneider. *Climate Change Science and Policy*. Island Press Washington [DC], 2010. ISBN 9781597265676.

[6] Z. Leviston, et al. Fourth annual survey of Australian attitudes to climate change: Interim report. Technical report, CSIRO, Perth, Australia, January 2014. URL http://images.smh.com.au/file/2014/02/07/5139061/CSIROCC4.pdf?rand=1391724434771.

[7] J. Gilmore and C. Giacomantonio. RET Policy Analysis. Technical Report Cec00011, Roam Consulting: Energy Modelling Expertise, Brisbane, Australia, April 2014.

[8] T. Arup. Abbott out of step on climate change, says Prof. Jeffrey Sachs. Sydney Morning Herald: available http://www.smh.com.au/federal-politics/political-news/abbott-out-of-step-on-climate-change-says-professor-jeffrey-sachs-20140520-38mmn.html, 2014. Accessed: 2014-05-23.

[9] L. Lu and H. X. Yang. Environmental payback time analysis of a roof-mounted building-integrated photovoltaic (BIPV) system in Hong Kong. *Applied Energy*, 87(12):3625–3631, 2010.

[10] B. Mountain. Electricity Prices in Australia: An International Comparison. Technical report, Carbon and Energy Markets, Melbourne, Australia, March 2012.

[11] Australian PV Institute. Australian PV Market since April 2001. http://pv-map.apvi.org.au/analyses, 2014. Accessed: 2014-05-16.

[12] A. Hepworth. Rooftop solar panels overloading electricity grid. The Australian Newspaper: available http://www.theaustralian.com.au/news/rooftop-solar-panels-overloading-electricity-grid/story-e6frg6n6-1226165360822, 2011. Accessed: 2014-05-16.

[13] B. Noone. PV Integration on Australian Distribution Networks. Technical report, Centre for Energy and Environmental Markets, University of NSW, Sydney, Australia, September 2013. URL http://apvi.org.au/wp-content/uploads/2013/12/APVA-PV-and-DNSP-Literature-review-September-2013.pdf.

[14] E. Twining and G. Holmes. Voltage profile optimisation for weak distribution networks. *Journal of Electrical and Electronics Engineering, Australia*, 22(3):179–186, 2002. ISSN 07252986.

[15] F. A. Viawan and M. Reza. The impact of synchronous distributed generation on voltage dip and overcurrent protection coordination. In *Future Power Systems, 2005 International Conference on*, pages 1–6, Nov. 2005. doi: 10.1109/FPS.2005.204298.

[16] Standards Australia. Australian Standard AS 4777.3-2005, Standard for Grid Connection of Energy Inverter Systems via Inverter, Part 3: Grid Protection Requirements. Technical report, 2005.

[17] Technical report.

[18] R. H. Lasseter. CERTS Microgrid. In *System of Systems Engineering, 2007. SoSE '07. IEEE International Conference on*, pages 1–5, April 2007. doi: 10.1109/SYSOSE.2007.4304248.

[19] IEC. Microgrids for disaster preparedness and recovery. Technical report, 2014.

[20] The Institute of Electrical and Inc. Electronics Engineers. IEEE Standards 1547.4-2011, IEEE Guide for Design, Operation and Integration of Distributed Island Systems with Electric Power Systems. Technical report, 2011.

[21] The Institute of Electrical and Inc. Electronics Engineers. IEEE Standards 1547-2003, Standard for Interconnecting Distributed Resources with Electric Power Systems. Technical report, 2003.

[22] B. Bhalja, P. Shah, N. Chothani, and N. Patel. A Novel Approach to Tackle Miscoordination of Protective Device in Radial Distribution Network during DG Interconnections. *International Journal of Emerging Electric Power Systems*, 12(4):1–21, 2011. ISSN 1553779X. URL http://search.ebscohost.com.ezproxy.uow.edu.au/login.aspx?direct=true&db=a9h&AN=63621217&site=ehost-live.

[23] A. Girgis and S. Brahma. Effect of distributed generation on protective device coordination in distribution system. In *Power Engineering, 2001. LESCOPE '01. 2001 Large Engineering Systems Conference on*, pages 115–119, 2001. doi: 10.1109/LESCPE.2001.941636.

[24] S. Conti. Analysis of distribution network protection issues in presence of dispersed generation. *Electric Power Systems Research*, 79(1):49–56, 2009. ISSN 0378-7796. doi: DOI:10.1016/j.epsr.2008.05.002. URL http://www.sciencedirect.com/science/article/B6V30-4T0800P-2/2/9f026c3eb1237d863d56b7a66fc69836.

[25] H. Al-Nasseri and M. A. Redfern. Harmonics content based protection scheme for Microgrids dominated by solid state converters. In *Power System Conference, 2008. MEPCON 2008. 12th International Middle-East*, pages 50–56, March 2008. doi: 10.1109/MEPCON.2008.4562361.

[26] T. A. Short. *Electric Distribution Systems Handbook*, pages 711–762. Taylor and Francis, New York, USA, 2003.

[27] L. Grigsby. *The Electric Power Engineering Handbook*, chapter 9. CRC Press, Florida, USA, 2001. ISBN 0-8493-8578-4.

[28] T. Loix, T. Wijnhoven, and G. Deconinck. Protection of microgrids with a high penetration of inverter-coupled energy sources. In *Integration of Wide-Scale Renewable Resources Into*

the Power Delivery System, 2009 CIGRE/IEEE PES Joint Symposium, pages 1–6, July 2009.

[29] J. Keller and B. Kroposki. Understanding Fault Characteristics of Inverter-Based Distributed Energy Resources. Technical report, 2010.

[30] W. Bower and M. Ropp. Evaluation of Islanding Detection Methods for Utility-Interactive Inverters in Photovoltaic Systems, SANDIA Report SAND2002-3591. Technical report, Albaquerque, NM: Sandia National Laboratory, November 2002.

[31] L. K. Kumpulainen and K. T. Kauhaniemi. Analysis of the impact of distributed generation on automatic reclosing. In *Power Systems Conference and Exposition, 2004. IEEE PES*, volume 1, pages 603–608, Oct 2004. doi: 10.1109/PSCE.2004.1397623.

[32] N. Cullen, J. Thornycroft, and A. Collinson. Risk analysis of islanding of photovoltaic power systems within low voltage distribution networks. *Report IEA-PVPS T5-08*, 2002, 2002. URL http://apache.solarch.ch/pdfinter/solar/pdf/PVPSTask508.pdf.

[33] The Institute of Electrical and Inc. Electronics Engineers. IEEE Standards 929-2000, Recommended Practice for Utility Interface of Photovoltaic Systems. Technical report, 2000.

[34] B. Bhalja and P. H. Shah. Miscoordination of relay in radial distribution network containing distributed generation. In *Recent Advances in Intelligent Computational Systems (RAICS), 2011 IEEE*, pages 072–075, Sept 2011. doi: 10.1109/RAICS.2011.6069275.

[35] L. Gallery, T. Martinez and D. Klopotan. Impact of distributed generation on distribution network protection. ESBI Engineering and Facility Management, Ireland, 2009. URL http://www.esbi.ie/news/pdf/white-paper-distribution-network-protection.pdf.

[36] P. P. Barker and R. W. De Mello. Determining the impact of distributed generation on power systems. i. radial distribution systems. In *Power Engineering Society Summer Meeting, 2000. IEEE*, volume 3, pages 1645–1656, 2000. doi: 10.1109/PESS.2000.868775.

[37] Z. Ye, M. Dame, and B. Kroposki. Grid Connected Inverter Anti-Islanding Test Results for General Electric Inverter-Based Interconnection Technology. Technical Report NREL/TP-560-37200, National Renewable Energy Laboratory, Colorado, USA, January 2005. URL http://www.nrel.gov/docs/fy05osti/37200.pdf.

[38] C. Joon-Ho, N. Soon-Ryul, N. Hae-Kon, and K. Jae-Chul. Adaptive protection schemes of Distributed Generation at distribution network for automatic reclosing and voltage sags. In

Sustainable Energy Technologies, 2008. ICSET 2008. IEEE International Conference on, pages 810–815, Nov 2008. doi: 10.1109/ICSET.2008.4747119.

[39] I. Chilvers, N. Jenkins, and P. Crossley. Distance relaying of 11 kV circuits to increase the installed capacity of distributed generation. *Generation, Transmission and Distribution, IEE Proceedings-*, 152(1):40–46, Jan. 2005. ISSN 1350-2360. doi: 10.1049/ip-gtd:20041205.

[40] J. H. Eto, R. Lasseter, B. Schenkman, J. Stevens, H. Volkommer, H. Klapp, E. Linton, H. Hurtado, J. Roy, and N. Lewis. CERTS Microgrid Laboratory Test Bed. Technical report, Consortium for Electric Reliability Technology Solutions (CERTS), California, USA, 2008.

[41] N. Jayawarna, M. Barnes, C. Jones, and N. Jenkins. Operating MicroGrid Energy Storage Control during Network Faults. In *System of Systems Engineering, 2007. SoSE '07. IEEE International Conference on*, pages 1–7, April 2007. doi: 10.1109/SYSOSE.2007.4304254.

[42] R. Arghandeh, M. Pipattanasomporn, and S. Rahman. Flywheel Energy Storage Systems for Ride-through Applications in a Facility Microgrid. *Smart Grid, IEEE Transactions on*, 3(4):1955–1962, Dec 2012. ISSN 1949-3053. doi: 10.1109/TSG.2012.2212468.

[43] F. Overbeeke. Fault Current Source to Ensure the Fault Level in Inverter-Dominated Networks. In *Electricity Distribution. 20th International Conference on*, pages 1–4, June 2009.

[44] R. Lasseter and P. Piagi. Control and Design of Microgrid Components - Final Report. Technical report, Power Systems Engineering Research Centre, 2006. URL http://certs.lbl.gov/certs-pubs.html.

[45] M. Dewadasa, A. Ghosh, and G. Ledwich. Dynamic response of distributed generators in a hybrid microgrid. In *Power and Energy Society General Meeting, 2011 IEEE*, pages 1–8, July 2011. doi: 10.1109/PES.2011.6039273.

[46] F. Katiraei and M. R. Iravani. Power Management Strategies for a Microgrid With Multiple Distributed Generation Units. *Power Systems, IEEE Transactions on*, 21(4):1821–1831, Nov 2006. ISSN 0885-8950. doi: 10.1109/TPWRS.2006.879260.

[47] M. A. Zamani, T. S. Sidhu, and A. Yazdani. A protection strategy and microprocessor-based relay for low-voltage microgrids. *Power Delivery, IEEE Transactions on*, 26(3):1873–1883, July 2011. ISSN 0885-8977. doi: 10.1109/TPWRD.2011.2120628.

[48] R. D. Christie, H. Zadehgol, and M. M. Habib. High impedance fault detection in low voltage networks. *Power Delivery, IEEE Transactions on*, 8(4):1829–1836, Oct 1993. ISSN 0885-8977. doi: 10.1109/61.248291.

[49] H. H. Zeineldin, E. F. El-Saadany, and M. M. A. Salama. Distributed Generation Micro-Grid Operation: Control and Protection. In *Power Systems Conference: Advanced Metering, Protection, Control, Communication, and Distributed Resources, 2006. PS '06*, pages 105–111, March 2006. doi: 10.1109/PSAMP.2006.285379.

[50] E. Sortomme, M. Venkata, and J. Mitra. Microgrid protection using communication-assisted digital relays. In *Power and Energy Society General Meeting, 2010 IEEE*, volume 25, pages 2789–2796, July 2010. doi: 10.1109/PES.2010.5588146.

[51] L. Xinyao, A. Dysko, and G. M. Burt. Application of communication based distribution protection schemes in islanded systems. In *Universities Power Engineering Conference (UPEC), 2010 45th International*, pages 1–6, Aug 2010.

[52] R. M. Tumilty, M. Brucoli, G. M. Burt, and T. C. Green. Approaches to Network Protection for Inverter Dominated Electrical Distribution Systems. In *Power Electronics, Machines and Drives, 2006. The 3rd IET International Conference on*, pages 622–626, Mar. 2006.

[53] H. Al-Nasseri, M. A. Redfern, and F. Li. A voltage based protection for micro-grids containing power electronic converters. In *Power Engineering Society General Meeting, 2006. IEEE*, pages 1–7, 2006. doi: 10.1109/PES.2006.1709423.

[54] H. Al-Nasseri, M. A. Redfern, and R. O'Gorman. Protecting micro-grid systems containing solid-state converter generation. In *Future Power Systems, 2005 International Conference on*, pages 1–5, Nov. 2005. doi: 10.1109/FPS.2005.204294.

[55] R. H. Lasseter, et al. The CERTS Microgrid Concept. In *White Paper for Transmission Reliability Program, Office of Power Technologies, U.S. Department of Energy*, April 2002. URL http://certs.lbl.gov/certs-pubs.html.

[56] F. Katiraei, M. R. Iravani, and P. W. Lehn. Small-signal dynamic model of a micro-grid including conventional and electronically interfaced distributed resources. *Generation, Transmission Distribution, IET*, 1(3):369–378, May 2007. ISSN 1751-8687. doi: 10.1049/iet-gtd:20045207.

[57] N. W. A. Lidula and A. D. Rajapakse. Microgrids research: A review of experimental microgrids and test systems. *Renewable and Sustainable Energy Reviews*, 15(1):186–202, 2011. ISSN 1364-0321. doi: http://dx.doi.org/10.1016/j.rser.2010.09.041. URL http://www.sciencedirect.com/science/article/pii/S136403211000328X.

[58] S. Voima, K. Kauhaniemi, and H. Laaksonen. Novel Protection Approach for MV Microgrid. In *Electricity Distribution. 21st International Conference on*, pages 1–4, June 2011.

[59] L. A. Kojovic. Rogowski sensor for power grid traveling wave based fault location. In *Developments in Power System Protection, 2008. DPSP 2008. IET 9th International Conference on*, pages 438–443, March 2008.

[60] A. Shafiu, T. Bopp, I. Chilvers, and G. Strbac. Active management and protection of distribution networks with distributed generation. In *Power Engineering Society General Meeting, 2004. IEEE*, volume 1, pages 1098–1103, June 2004. doi: 10.1109/PES.2004.1373011.

[61] M. Dewadasa, R. Majumder, A. Ghosh, and G. Ledwich. Control and protection of a microgrid with converter interfaced micro sources. In *Power Systems, 2009. ICPS '09. International Conference on*, pages 1–6, Dec. 2009. doi: 10.1109/ICPWS.2009.5442654.

[62] S. R. Samantaray, G. Joos, and I. Kamwa. Differential energy based microgrid protection against fault conditions. In *Innovative Smart Grid Technologies (ISGT), 2012 IEEE PES*, pages 1–7, Jan 2012. doi: 10.1109/ISGT.2012.6175532.

[63] H. Nikkhajoei and R. H. Lasseter. Microgrid Fault Protection Based on Symmetrical and Differential Current Components. Technical report, Power Systems Engineering Research Centre, 2009. URL http://certs.lbl.gov/certs-derkey-mgtb.html.

[64] Standards Australia. AS/NZS 43000-2007, Wiring Rules. Technical report, Standards Australia, 2007.

[65] M. E. Baran and I. El-Markaby. Fault analysis on distribution feeders with distributed generators. *Power Systems, IEEE Transactions on*, 20(4):1757–1764, Nov. 2005. ISSN 0885-8950. doi: 10.1109/TPWRS.2005.857940.

[66] C. Blake and C. Bull. IGBT or MOSFET: Choose Wisely. Technical report, International Rectifier, 2006. URL http://www.electroline.com.au/articles/139-IGBT-or-MOSFET-choose-wisely.

[67] Shaoyong Y., A. Bryant, P. Mawby, Dawei X., L. Ran, and P. Tavner. An industry-based survey of reliability in power electronic converters. *Industry Applications, IEEE Transactions on*, 47(3):1441–1451, May 2011. ISSN 0093-9994. doi: 10.1109/TIA.2011.2124436.

[68] M. Trivedi, V. John, T. A. Lipo, and K. Shenai. Internal dynamics of IGBT under fault current limiting gate control. In *Industry Applications Conference, 2000. Conference Record of the 2000 IEEE*, volume 5, pages 2903–2908, 2000. doi: 10.1109/IAS.2000.882578.

[69] Schweitzer Engineering Laboratories, Inc. Sel -351-5, -6, -7 directional overcurrent and reclosing relay data sheet, 2011.

[70] Rui W., F. Blaabjerg, Huai W., M. Liserre, and F. Iannuzzo. Catastrophic failure and fault-tolerant design of igbt power electronic converters - an overview. In *Industrial Electronics Society, IECON 2013 - 39th Annual Conference of the IEEE*, pages 507–513, Nov 2013. doi: 10.1109/IECON.2013.6699187.

[71] B. Ren, X. Sun, S. An, X. Cao, and Q. Zhang. Analysis and design of an LCL filter for the three-level grid-connected inverter. In *Power Electronics and Motion Control Conference (IPEMC), 2012 7th International*, volume 3, pages 2023–2027, June 2012. doi: 10.1109/IPEMC.2012.6259152.

[72] K. H. Ahmed, S. J. Finney, and B. W. Williams. Passive filter design for three-phase inverter interfacing in distributed generation. In *Compatibility in Power Electronics, 2007. CPE '07*, pages 1–9, May 2007. doi: 10.1109/CPE.2007.4296511.

[73] A. Samui and S. R. Samantaray. New active islanding detection scheme for constant power and constant current controlled inverter-based distributed generation. *Generation, Transmission Distribution, IET*, 7(7):779–789, July 2013. ISSN 1751-8687. doi: 10.1049/iet-gtd.2012.0607.

[74] A. Yazdani and R. Iravani. *Voltage-Sourced Converters in Power Systems*. John Wiley & Sons, Hoboken, New Jersey, USA, 2010. ISBN 978-0-470-52156-4.

[75] Z. Ye, R. Walling, L. Garces, R. Zhou, L. Li, and T. Wang. *Study and development of anti-islanding control for grid-connected inverters*. National Renewable Energy Laboratory, 2004. URL http://www.nrel.gov/docs/fy05osti/37200.pdf.

[76] A. R. Dash, B. C. Babu, K. B. Mohanty, and R. Dubey. Analysis of PI and PR controllers for distributed power generation system under unbalanced grid faults. In *Power and Energy Systems (ICPS), 2011 International Conference on*, pages 1–6, Dec 2011. doi: 10.1109/ICPES.2011.6156688.

[77] C. Plet and T. Green. Fault response of inverter interfaced distributed generators in grid-connected applications. *Electric Power Systems Research*, 106(0):21–28, 2014. ISSN 0378-7796. doi: http://dx.doi.org/10.1016/j.epsr.2013.07.013. URL http://www.sciencedirect.com/science/article/pii/S0378779613001946.

[78] J. Kennedy, P. Ciufo, and A. Agalgaonkar. Intelligent load management in microgrids. In *Power and Energy Society General Meeting, 2012 IEEE*, pages 1–8, July 2012. doi: 10.1109/PESGM.2012.6345729.

[79] K. De Brabandere, B. Bolsens, J. Van den Keybus, A. Woyte, J. Driesen, R. Belmans, and K. U. Leuven. A voltage and frequency droop control method for parallel inverters. In *Power Electronics Specialists Conference, 2004. PESC 04. 2004 IEEE 35th Annual*, volume 4, pages 2501–2507, 2004. doi: 10.1109/PESC.2004.1355222.

[80] D. Georgakis, S. Papathanassiou, N. Hatziargyriou, A. Engler, and C. Hardt. Operation of a prototype microgrid system based on micro-sources quipped with fast-acting power electronics interfaces. In *Power Electronics Specialists Conference, 2004. PESC 04. 2004 IEEE 35th Annual*, volume 4, pages 2521–2526, 2004. doi: 10.1109/PESC.2004.1355225.

[81] I. A. Hiskens and E. M. Fleming. Control of Inverter-Connected Sources in Autonomous Microgrids. In *American Control Conference, 2008*, pages 586–590, June 2008. doi: 10.1109/ACC.2008.4586555.

[82] M. Brucoli and T. Green. Fault response of inverter dominated microgrids. *International Journal and Distributed Energy Resources*, 3(2):157–175, Nov. 2007.

[83] Y. A. Mohamed and E. F. El-Saadany. Adaptive decentralized droop controller to preserve power sharing stability of paralleled inverters in distributed generation microgrids. *Power Electronics, IEEE Transactions on*, 23(6):2806–2816, Nov 2008. ISSN 0885-8993. doi: 10.1109/TPEL.2008.2005100.

[84] R. Chokhawala, J. Catt, and L. Kiraly. A discussion on IGBT short-circuit behavior and fault protection schemes. *Industry Applications, IEEE Transactions on*, 31(2):256–263, 1995.

[85] T. Shoji et al. Investigation of Short-circuit Capability of IGBT under High Applied Voltage Conditions, 2004. URL http://www.tytlabs.com/english/review/rev394epdf/e394_022shoji.pdf.

[86] D. Van Tu, S. Chaitusaney, and A. Yokoyama. Fault current calculation in distribution systems with inverter-based distributed generations. *IEEJ Transactions on Electrical and Electronic Engineering*, 8(5):470–477, 2013. ISSN 1931-4981. doi: 10.1002/tee.21882. URL http://dx.doi.org/10.1002/tee.21882.

[87] G. Tang and M. R. Iravani. Application of a fault current limiter to minimize distributed generation impact on coordinated relay protection. In *International Conference on Power System Transients*, 2005.

[88] Vishay Siliconix. Current rating of power semiconductors: Application note AN-949. Technical report, Vishay Siliconix, 2010. URL http://www.vishay.com/docs/91419/appnote9.pdf.

[89] S. Zocholl and G. Benmouyal. How microprocessor relays respond to harmonics, saturation and other wave distortions, 1997. URL http://www.sistemaselectricos.com/cursos/cpe2/varios/relay2.pdf.

[90] C. F. Ten and P. A. Crossley. Evaluation of ROCOF Relay Performances on Networks with Distributed Generation. In *Developments in Power System Protection, 2008. DPSP 2008. IET 9th International Conference on*, pages 523–528, March 2008.

[91] AusGrid. Requirements for connection of embedded generators, ES-1. Technical report, AusGrid, 2011. URL http://www.ausgrid.com.au/~/media/Files/Network/Documents/ES/ES1.pdf.

[92] H. M. Ayres, W. Freitas, M.C. de Almeida, and L. C. P. da Silva. Method for determining the maximum allowable penetration level of distributed generation without steady-state voltage violations. *Generation, Transmission Distribution, IET*, 4(4):495–508, April 2010. ISSN 1751-8687. doi: 10.1049/iet-gtd.2009.0317.

[93] P. Karimi-Zare and H. Seifi. Maximum allowable penetration level determination of a dg in a distribution network. In *Energy Conference and Exhibition (ENERGYCON), 2012 IEEE International*, pages 355–360, Sept 2012. doi: 10.1109/EnergyCon.2012.6347783.

[94] E. Demirok, P. Casado Gonzallez, K. H. B. Frederiksen, D. Sera, P. Rodriguez, and R. Teodorescu. Local reactive power control methods for overvoltage prevention of distributed solar inverters in low-voltage grids. *Photovoltaics, IEEE Journal of*, 1(2):174–182, Oct 2011. ISSN 2156-3381. doi: 10.1109/JPHOTOV.2011.2174821.

[95] M. Braun, T. Stetz, T. Reimann, B. Valov, and G. Arnold. Optimal reactive power supply in distribution networks-technological and economic assessment for PV-systems. In *24th European Photovoltaic Solar Energy Conference and Exhibition. Hamburg*, 2009.

[96] B. Davito, H. Tai, and R. Uhlaner. The smart grid and the promise of demand-side management. *McKinsey on Smart Grid*, 2010. URL https://www.smartgrid.gov/document/smart_grid_and_promise_demand_side_management.

[97] A. Ellis et al. Reactive Power Interconnection Requirements for PV and Wind Plants: Recommendations to NERC. 2012. URL http://renew-ne.org/wp-content/uploads/2012/05/Reactive-Power-Interconnection-Requirements.pdf.

[98] V. Calderaro, G. Conio, V. Galdi, G. Massa, and A. Piccolo. Optimal decentralized voltage control for distribution systems with inverter-based distributed generators. *Power Systems, IEEE Transactions on*, 29(1):230–241, Jan 2014. ISSN 0885-8950. doi: 10.1109/TPWRS.2013.2280276.

[99] Roberto Caldon, Silvano Spelta, Valter Prandoni, and Roberto Turri. Co-ordinated voltage regulation in distribution networks with embedded generation. In *Electricity Distribution, 2005. CIRED 2005. 18th International Conference and Exhibition on*, pages 1–4, June 2005.

[100] S. Conti. Innovative voltage regulation method for distribution networks with distributed generation. In *Electricity Distribution, 2007. CIRED 2005. 19th International Conference on*, pages 1–4, May 2007.

[101] Standards Australia. Australian Standard AS 60038-2012, Standard Voltages. Technical report, 2012.

[102] J. Glover, M. S. Sarma, and T. J. Overbye. *Power System Analysis and Design*. CENGAGE Learning, Stamford, CT, USA, 2001.

[103] N. Nimpitiwan, G. T. Heydt, R. Ayyanar, and S. Suryanarayanan. Fault current contribution from synchronous machine and inverter based distributed generators. *Power Delivery, IEEE Transactions on*, 22(1):634–641, Jan 2007. ISSN 0885-8977. doi: 10.1109/TPWRD.2006.881440.

[104] T. Wijnhoven, J. Tant, and G. Deconinck. Inverter modelling techniques for protection studies. In *Power Electronics for Distributed Generation Systems (PEDG), 2012 3rd IEEE International Symposium on*, pages 187–194, June 2012. doi: 10.1109/PEDG.2012.6253999.

[105] C. A Plet, M. Graovac, T. C. Green, and R. Iravani. Fault response of grid-connected inverter dominated networks. In *Power and Energy Society General Meeting, 2010 IEEE*, pages 1–8, July 2010. doi: 10.1109/PES.2010.5589981.

[106] N. L. Soultanis, S. A Papathanasiou, and N. D. Hatziargyriou. A Stability Algorithm for the Dynamic Analysis of Inverter Dominated Unbalanced LV Microgrids. *Power Systems, IEEE Transactions on*, 22(1):294–304, Feb 2007. ISSN 0885-8950. doi: 10.1109/TPWRS.2006.887961.

[107] A. H. K. Alaboudy, and H. H. Zeineldin. Islanding Detection for Inverter-Based DG Coupled With Frequency-Dependent Static Loads. *Power Delivery, IEEE Transactions on*, 26(2): 1053–1063, April 2011. ISSN 0885-8977. doi: 10.1109/TPWRD.2010.2087042.

[108] E. O. Schweitzer and D. Hou. Filtering for Protective Relay. Technical report, 19th Annual Western Protective Relay Conference, Spokane, Washington, October 20-22, 1992. URL https://www.selinc.com/WorkArea/DownloadAsset.aspx?id=2459.

[109] M. Bamber et al. *Network Protection and Automation Guide, 2nd ed.* Alstom Grid, 2011.

[110] L. Cheng, Z. Li, and W. Tong. Data communication and information security analysis of wide area protection system. In *Information and Automation (ICIA), 2010 IEEE International Conference on*, pages 461–465, June 2010. doi: 10.1109/ICINFA.2010.5512380.

[111] T. L. Vandoorn, B. Meersman, J. D. M. De Kooning, and L. Vandevelde. Transition from islanded to grid-connected mode of microgrids with voltage-based droop control. *Power Systems, IEEE Transactions on*, 28(3):2545–2553, Aug 2013. ISSN 0885-8950. doi: 10.1109/TPWRS.2012.2226481.

[112] T. Assis and G. Taranto. Automatic reconnection from intentional islanding based on remote sensing of voltage and frequency signals. In *Power and Energy Society General Meeting (PES), 2013 IEEE*, pages 1–8, July 2013. doi: 10.1109/PESMG.2013.6672101.

[113] J. L. Blackburn and T. J. Domin. *Protective Relaying: Principles and Applications*, chapter 7. CRC Press, Florida, USA, 2006.